Polymer-Nanocrystal Composites: Copolymers, Polymeric Particles and Hybrid Systems

Dissertation

zur Erlangung des akademischen Grades
Doktor der Naturwissenschaften
(Doctor rerum naturalium)

eingereicht im
Fachbereich Mathematik und Naturwissenschaften
der Bergischen Universität Wuppertal

von

Ioannis Kanelidis

geb. in Troisdorf,
Deutschland

Wuppertal, April 2012

Die vorliegende Arbeit wurde in der Zeit von Juni 2008 bis März 2012 in der Arbeitsgruppe für Funktionspolymere des Fachbereiches C-Mathematik und Naturwissenschaften der Bergischen Universität Wuppertal unter Anleitung von Frau Prof. Dr. Elisabeth Holder angefertigt.

Frau Prof. Dr. Elisabeth Holder gilt mein besonderer Dank für die Überlassung des interessanten Themas, ihre stete Diskussions- und Hilfsbereitschaft, sowie für die finanzielle Unterstützung. Herrn Prof. Dr. Alexander Eychmüller möchte ich für die gute Zusammenarbeit und die Übernahme des Koreferats danken.

1. Gutachter: Prof. Dr. Elisabeth Holder (Bergische Universität Wuppertal)
2. Gutachter: Prof. Dr. Alexander Eychmüller (Technische Universität Dresden)

Meinen Eltern verdanke ich das Leben und meinem Lehrer das gute Leben.

Alexander der Grosse

Um an die Quelle zu kommen, muss man gegen den Strom schwimmen.

Konfuzius

Für meine Familie in ewiger Dankbarkeit

Ioannis Kanelidis

Table of Contents

List of Symbols and Abbreviations

A	Acceptor
A^-	Negatively charged acceptor
Å	Angstrom
Abs.	Absorption
AFM	Atomic force microscopy
aliph.	Aliphatic
$Al_2(III)Te_3$	Aluminium(III) telluride
Anal.	Analytical
arom.	Aromatic
Ar	Aryl
Au(0)	Gold
a.u	Atomic units
b (NMR)	Broad
BHT	Butylated hydroxytoluene
bipy	2,2'-Bipyridine
Br	Bromine
c	Speed of light
C	Carbon
C_x	Concentration of compound X
Calcd.	Calculated
$CDCl_3$	Deuterated chloroform
$Cd(II)(OOCH_3)_2$	Cadmium(II) acetate
$Cd(II)(CH_3COO)_2 \times 2\ H_2O$	Cadmium(II) acetate dehydrate
Cd(II)S	Cadmium(II) sulfide
Cd(II)Se	Cadmium(II) selenide
Cd(II)Te	Cadmium(II) telluride
$CdTe_{red}$	Red-light emitting cadmium telluride nanocrystals
$CHCl_3$	Chloroform
Cl	Chlorine
cm	Centimeter
cm^{-1}	Reciprocal wavenumber

COD	1,5-Cyclooctadiene
d	Distance between the donor and the acceptor
d (NMR)	Doublet
dd (NMR)	Doublet of doublet
D	Donor
D*	Excited donor
D^+	Positively charged donor
Da	Dalton
DFB	2,2'-(9,9'-dioctyl-9*H*-fluorene-2,7-diyl)*bis*(1,3,2-dioxaborinane)
DFG	Deutsche Forschungsgemeinschaft
dist. d (NMR)	Distorted doublet
dist. s (NMR)	Distorted singlet
dist. t (NMR)	Distorted triplet
DLS	Dynamic light scattering
DMAA	1,3-Methylhexanamine
DMF	*N*,*N*-dimethylformamide
DMSO	Dimethyl sulfoxide
DOPO-Br	*p*-Bromobenzyl-di-*n*-octylphosphine oxide
DSC	Differential scanning calorimetry
e	Elementary electron charge
e^-	Electron
E	Efficiency of the FRET mechanism
EI	Electron impact ionization
e.g.	For example
Em.	Emission
ESI-MS	Electrospray ionization source mass spectrometry
ET	Energy transfer
eV	Electronvolt
exc.	Excitation
E_A^0	Acceptor ground energy level
E_A^1	Acceptor excited energy level
E_A^{1*}	Acceptor vibronically excited state

E_D^0	Donor ground energy level
E_D^1	Donor excited energy level
E_g	Energy band-gap
$f_D(\omega)$	Integral normalized fluorescence spectrum of a donor
F_D	Normalized donor intensity in the absence of an acceptor
F_{DA}	Normalized donor intensity in the presence of an acceptor
Fe(0)	Iron
$Fe(III)Cl_3$	Iron(III) chloride
$Fe(II)Cl_2$	Iron(II) chloride
FRET	Förster resonance energy transfer
fs	Femtosecond
FT-IR	Fourier Transform Infrared
g	Gram
Ga(III)As	Gallium(III) arsenide
Ga(III)InP2	Gallium(III) indium phosphide
Ga(III)P	Gallium(III) phosphide
GC-MS	Gas chromatography mass spectrometry
GPC	Gel permeation chromatography
h	Hour
h	Planck's constant
H	Hydrogen
H^+	Proton
HRTEM	High-resolution transmission electron microscopy
HOMO	Highest occupied molecular orbital
$HS\text{-}C_6H_4\text{-}Br$	4-Bromobenzene thiol
$HS\text{-}CH_2\text{-}COOH$	Thioglycolic acid
I	Iodine
IE	Intensity enhancement
i.e.	In other words
In(II)As	Indium(II) arsenide
In(II)P	Indium(II) phosphide

IR	Infrared
IUPAC	International Union of Pure and Applied Chemistry
J	Normalized overlap integral of the absorption and emission spectra
κ^2	Constant dependent on the mutual orientation of two dipoles
K	Experimental factor related to specific orbital interactions
K_{Dexter}	Energy transfer rate of the Dexter mechanism
kHz	Kilohertz
kJ	Kilojoule
kV	Kilovolt
L	Liter
L	Sum of van-der-Waals radius
Li(0)	Lithium
Log ε	Logarithm of the molar extinction coefficient
LUMO	Lowest unoccupied molecular orbital
m (IR)	Medium
m (NMR)	Multiplet
m_e	Effective mass of an electron
m_h	Effective mass of a hole
M	Molarity
M_n	Number average molecular weight
M_w	Weight average molecular weight
MALDI-TOFMS	Matrix-assisted laser-desorption/ionization time-of-flight mass spectrometry
mg	Milligram
min	Minute
mL	Millilitre
mm	Millimeter
mM	Millimolarity
mmol	Millimole
mol	Mole

MPs	Microparticles
m/z	Mass to charge ratio
n	Refractive index
N	Nitrogen
N (mol/L)	Normality
NaEDTA	Sodium ethylenediamine tetraacetic acid
NC(s)	Nanocrystal(s)
NC**1-3**	Nanocomposite **1-3**
$NH(CH_2CH_3)_2$	Di-*n*-propylamine
NH_2-$NH_2{\cdot}H_2O$	Hydrazine monohydrate
Ni(0)	Nickel
$Ni(II)Cl_2$	Nickel(II) chloride
$Ni(0)(COD)_2$	*Bis*(cyclooctadiene)nickel(0)
$Ni(II)(dppp)Cl_2$	Dichloro(1,3-*bis*(diphenylphosphino)propane) nickel(II)
nm	Nanometer
NMR	Nuclear magnetic resonance
OD	Optical density
P	Phosphor
Pb(II)S	Lead(II) sulfide
Pb(II)Se	Lead(II) selenide
Pb(II)Te	Lead(II) telluride
PCT	Phase-transfer catalyst
$Pd(II)(Cl_2)(Ph_3P)_2$	*Bis*(triphenylphosphine)palladium(II) chloride
PDI	Polydispersity index
$Pd(II)(OAc)_2$	Palladium(II) acetate
$Pd(0)(PPh_3)_4$	*Tetrakis*(triphenylphosphine) palladium(0)
PFs	Poly(fluorene)s
PF6	Poly(9,9'-dihexylfluorene)
PF8	Poly(9,9'-dioctylfluorene)
PFO	Fluorenone-containing poly(fluorene)s
P3HT	Poly(3-hexylthiophen-2,5-diyl)
PL	Photoluminescence

ppm	Parts per million
ps	Picosecond
PTFBDV	Poly{(5,6-*bis*(trifluoromethyl)bicyclo[2,2,2]octa-5,7-dienevinylene}
q (NMR)	Quartet
QD	Quantum dot
QE	Quenching effect
qui. (NMR)	Quintet
R	Radius of the nanoparticle
R_{DA}	Distance between donor and acceptor
R_{ET}	Energy transfer rate of the Förster mechanism
rgt	Reagent
RI	Intelligent Refractometer
rpm	Revolutions per minute
s (IR)	Strong
s (NMR)	Singlet
$Sn(II)Cl_2{\cdot}H_2O$	Tin(II) chloride
Sol	Solution
t (NMR)	Triplet
T	Transmission
$T_{d5\%}$	Decomposition temperature @ 5% weight loss
T_g	Glass transition temperature
τ_r	Radiative lifetime of a donor
TBPO	Tributylphosphine oxide
$Te(-II)H_2$	Hydrogen telluride(-II)
TEM	Transmission electron microscopy
TGA	Thermal gravimetric analysis
TGA (NCs)	Thioglycolic acid
THF	Tetrahydrofuran
$Ti(IV)Cl_4$	Titanium(IV) tetrachloride
TLC	Thin layer chromatography
TMS	Tetramethylsilane

TOP	Trioctyl phosphine
TOPO	Trioctyl phosphine oxide
UV	Ultraviolet
UV-vis	Ultraviolet-visible
V	Retention volume
v/v	Volume to volume
vw (IR)	Very weak
w (IR)	Weak
W	Molecular weight
Zn(0)	Zinc
Zn(II)O	Zinc(II) oxide
Zn(II)S	Zinc(II) sulfide
Zn(II)Se	Zinc(II) selenide
Zn(II)Te	Zinc(II) telluride
γ	Gamma
δ	Chemical shift
ε	Dielectric constant
$\lambda_{exc.}$	Excitation wavelength
λ_{max}	Absorption/Emission wavelength maximum
μL	Microliter
μm	Micrometer
$\sigma_A(\omega)$	Absorption cross section of acceptor molecules
Φ_{sol}	Quantum yield in solution
ω	Angular frequency
°C	Degree Celsius
ΔE	Change in the band-gap energies relative to a bulk solid
3d/5d	Three days/five days
3-D	Three-dimensional
@	At

~	Approximately
	The carbon at the 9-position of the fluorene-ring
&	And

1 Introduction

1.1 Conjugated Polymers

Conjugated polymers have drawn the attention of the scientific community over the last three decades. They are known as the class of polymers, which has a backbone configuration of alternating single and double bonds, whereby the delocalization of the π-electrons along the polymer chain is feasible.[1,2] The initial intension and thoughts of using the conjugated polymers as insulating materials was rapidly overrun by a wide range of other potential implementations. Applications in the fields of rechargeable batteries, electrical circuits, antistatic coatings, light-emitting diodes, biosensors or ultrathin multi-media screens have already been presented.[3] As conjugated polymers are endowed with a distinguished chain conjugation, which enables the delocalization and the distribution of the electrons between the atoms through the whole polymeric backbone, they fulfill the structural requirement for a conducting polymer. A critical point, which must however be considered, is that polymers reveal conductivity when treated by a doping process. Doping carried out by either a partial reduction or an oxidation of the polymer through charge transfer agents (dopants), allows loosely bound electrons to flow along the polymer chain producing electric current.[4] Except their ability to remove or add electrons to the conjugated systems, dopants play also the role of charge carriers between the polymer chains.[3] By means of the doping process conducting properties are passed on to the polymers and the first conjugated polymer exhibiting electrical conduction namely poly(acetylene) became reality.

1.1.1 Historical Background

The first attempts to synthesize conducting conjugated polymers have roots back to the nineteen sixties and are the merit of the work carried out by Pohl, Katon and others.[5,6] The synthesis of poly(sulfur) nitride (**Figure 1.1a**) allowed acquiring a material, where high conductivity was observed, recording a first success in the field of fabrication of viable polymeric conductors.[7,8] The research on this area was intensified in the late seventies-early eighties[9-11] when poly(acetylene) films were investigated showing enhanced conductivity upon exposure to halogen vapour. Poly(acetylene) (**Figure 1.1b**) is the simplest conjugated polymer, where the build-up of the backbone is based on three in-plane σ-orbitals. Two of the σ-orbitals are linked to the neighboring carbon atom, while the third one is bonded

to a hydrogen atom. The fourth electron is found in the p_z-orbital and can be considered as independent from the residual three orbitals due to its orthogonality to the plane. This one electron exhibits the tendency to decouple and delocalize being thus responsible for the interesting electronic properties of poly(acetylene).[12]

a)

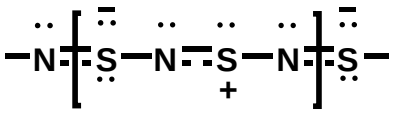

b)

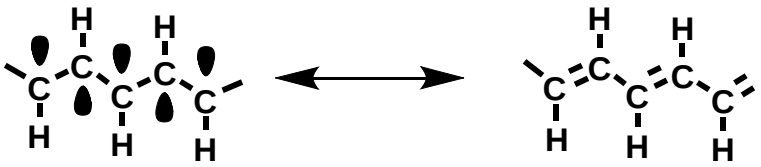

Figure 1.1: Structural configuration of poly(sulfur) nitride (a)[13] and the schematic representation of the sp^2p_z hybridization (: p_z) in poly(acetylene) (b).[12]

The endeavors of Alan J. Heeger, Alan. G. MacDiarmid and Hideki Shirakawa in order to produce conducting poly(acetylene)s ended up in 1977 with the discovery that acetylene monomers doped with bromine and iodine vapours led to polymers with ten times higher electrical conductivity compared to undoped monomers. The efforts of the three aforementioned scientists and researchers were awarded with the Nobel Prize in Chemistry 2000 indicating emphatically the significance of their work on the field of the 'development of conductive polymers'. The findings of the trio motivated scientists to investigate extensively and systematically conjugated macromolecular systems and more specifically in terms of their chemical and physical properties. These properties made conjugated polymers promising for light-emitting devices and their journey towards their implementation in commercial development started in the 1990s. It was the work of R. H. Friend and co-workers, which initiated the future of conjugated polymers in application of scientific and industrial interest giving birth to economically viable light-emitting diodes.[14] This remarkable trend is still ongoing up-to-date rendering the conjugated polymers one of most interesting classes of macromolecular materials.[15-17]

1.1.2 Synthetic Methodologies

The interesting opto-electronic properties of the conjugated polymers and their potential applications as semiconducting, light-emitting or sensing materials caused the growth of the efforts to successfully synthesize such kind of polymers. The dependence of the properties on the purity of the conjugated polymers demanded the development of synthetic procedures free of catalyst leftovers and side-products, which can deteriorate the quality of the end-products. In general, conjugated polymers can be prepared by six different types of procedures and are briefly described below[18]:

1) Coordination Polymerization[19]

The metathesis polymerization of phenylacetylene depicted in **Figure 1.2** is an example of this type of polymerization.

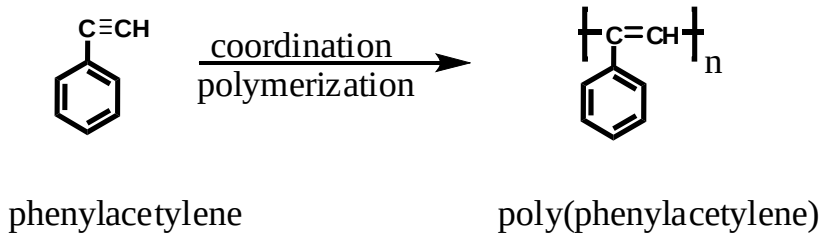

Figure 1.2: Coordination polymerization of phenylacetylene.[18]

2) Chemical (Oxidative/Dehalogenation) Polymerization[20]

Industrial production of poly(thiophene) by means of stoichiometric amounts of a chemical oxidant (**Figure 1.3**) is representative for this type of polymerization.

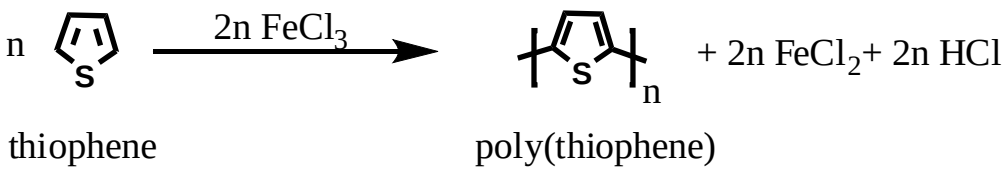

Figure 1.3: Chemical polymerization of thiophene *via* oxidation.[18]

3) Chemical (Catalytic) Polymerization[21]

The catalyst-based chemical polymerization includes couplings like the Suzuki-Miyaura coupling, the Heck, Yamamoto, Stille, Kumada, or Sonogashira ones and is in particular applied for the synthesis of poly(phenylene ethynylene)s and fluorene homo- and copolymers (**Figure 1.4**).

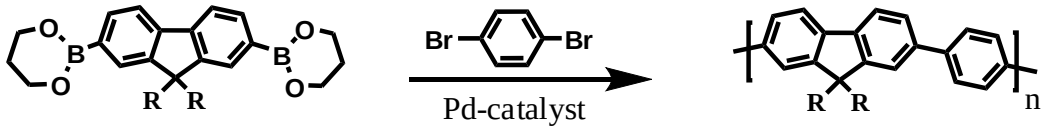

fluorene

Figure 1.4: Chemical polymerization of a fluorene *via* the Pd-mediated Suzuki-Miyaura reaction.[18]

4) Chemical Transformation of a Precursor Polymer[19]

A typical example of this procedure is the retro Diels-Alder reaction exemplarily depicted in **Figure 1.5** for poly{(5,6-*bis*(trifluoromethyl)bicyclo[2,2,2]octa-5,7-dienevinylene} abbreviated as PTFBDV.

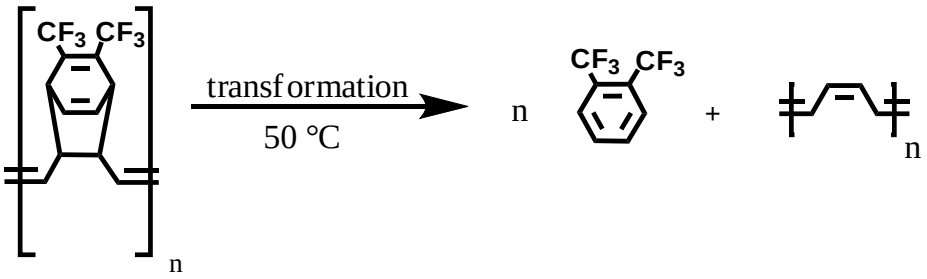

PTFBDV

Figure 1.5: Chemical transformation of the precursor PTFBDV *via* a retro Diels-Alder reaction.[18]

5) Electrochemical Polymerization[3,22]

Electrochemical polymerization is carried out by passing current through a solution, whereby oxidation at the anode and reduction at the cathode takes place resulting in polymer-film deposition in one of the electrodes. One prominent example in this category is the

electrochemical polymerization of aniline in aqueous HCl solution, while its reaction course is depicted in **Figure 1.6**.

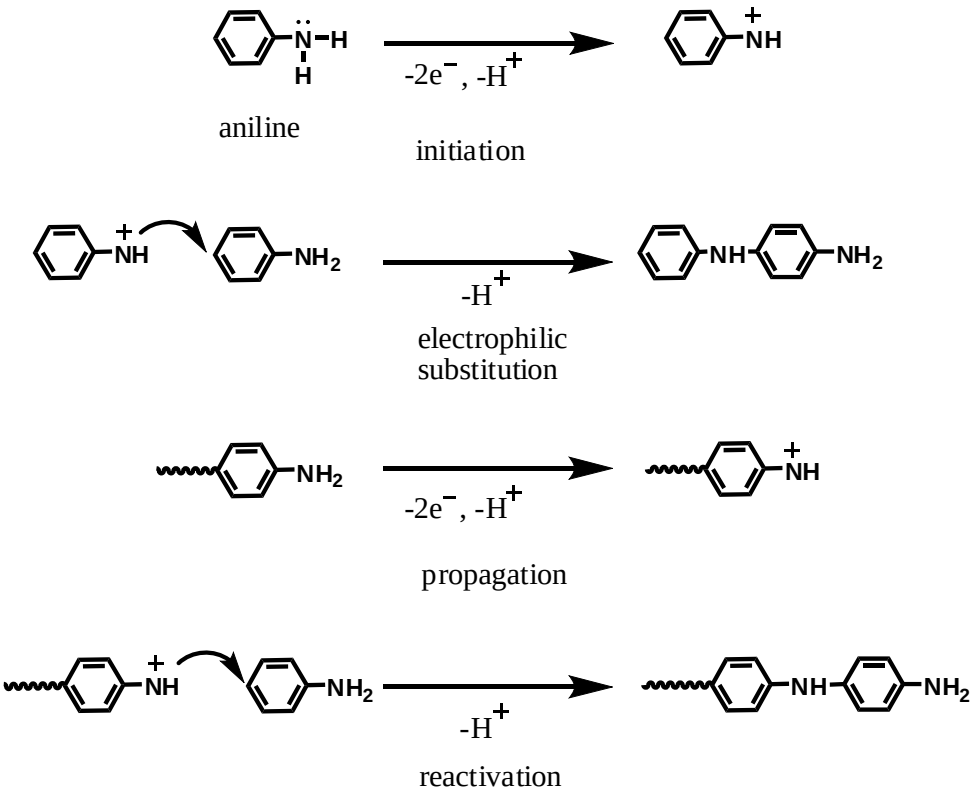

Figure 1.6: Schematic description of the electrochemical polymerization of aniline.[3]

6) Photochemical Polymerization[23]

The 1,2- or 1,4-addition polymerization of dialkynes (R_1-C≡C-C≡C-R_2) are typical examples for a photochemical polymerization and can be initiated by high UV-, X- or γ-irradiation (**Figure 1.7**). In this case, the type of addition depends significantly on the geometry of the monomer.

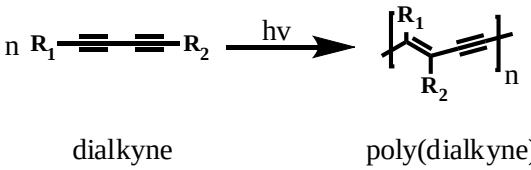

Figure 1.7: Photochemical polymerization of dialkyne proceeded *via* a 1,2-addition.[18]

1.2 Poly(fluorene)s

Conjugated polymers embrace a vast number of macromolecular compounds, whereby their structural diversity is attributed to the variety of choice when designing the backbone- and the side-chain configuration.[24] Among the many reported conjugated polymers, the family of poly(fluorene)s (PFs) has evolved as an interesting class on the basis of desirable properties like the facile synthesis, the environmental stability, their processability and their efficient blue-light emission just to mention few.[25-27] Poly(fluorene)s belong to the class of rigid-rod polymers with a rigid backbone and flexible side-chains, which can be varied or end-group-functionalized. The building block of the fluorene monomer consists of a stiff biphenyl unit, which is interconnected to a central carbon atom at the nine position as depicted in **Figure 1.8**.

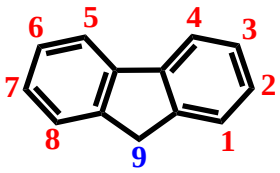

Figure 1.8: The fluorene building block.

The remote carbon at the 9-position of the fluorene-ring can participate to nucleophilic substitution reactions due to the acidity of the bridgehead protons giving the possibility to decorate the fluorene building-block with different side-chains improving in this way the solubility and processing quality of the coming-out polymers.

The discovery of electrical conductivity in poly(acetylene) was indeed a pioneering achievement in the field of developing polymeric conducting materials. However, the disadvantage of poor processabilty and instability of poly(acetylene)s turned scientists to investigate the more stable class of aromatic polymers including poly(fluorene)s. At the early 1980s electrochemical polymerization enabled the acquirement of poly(fluorene)s in the solid state (**Figure 1.9a**).[28-30] The prepared films were, however, infusible and insoluble and thus far away from the target of synthesizing polymers, which can be easily processed, combining synchronously the electronic properties of conducting materials and the mechanical characteristics of the traditional polymers. The first report of a solution-processable poly(fluorene) (**Figure 1.9b**) is attributed to Fukuda and coworkers[31] who revolutionized the synthesis-field and widespread the attempts of the researchers to control and manipulate the structures of the PFs in order to exploit their properties for advanced polymeric technologies.

a)

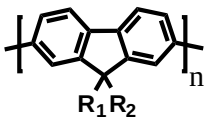

R_1:H R_2:H
R_1:CH_3 R_2:H
R_1:CH_3 R_2:CH_3
R_1:OH R_2:H
R_1:Cl R_2:H

b)

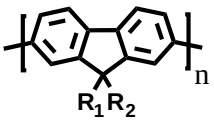

R_1:H R_2:alkyl
R_1:alkyl R_2:alkyl

Figure 1.9: Poly(fluorene)s synthesized by electrochemical polymerization (a)[29,30] and the structure of the first reported soluble analogue (b).[31]

Except the chemical polymerization by means of $FeCl_3$ as oxidative coupling agent introduced by Fukuda et al., organic chemistry provides a variety of synthetic tools in order to produce structurally defined poly(fluorene)s. Heck[32,33], Kumada[34,35], Yamamoto[36], Suzuki[37], Stille[38,39], Sonogashira[40] couplings, amongst others, are utilized for this purpose allowing significant progress in the field of synthesis of poly(fluorene)s with specific design and configuration. **Figures 1.10a-f** illustrate the synthetic pathways towards poly(fluorene)s based on the six aforementioned reactions. Most of the poly(fluorene) synthetic approaches are based on the nickel(0)-catalyzed polymerization of Yamamoto and the palladium-mediated polymerization of Suzuki. The Yamamoto step-growth polymerization requires fluorene comonomers, which possess dibromo-functionalities but chloro- or iodo-functionalities attached on the fluorene building block render the reaction feasible, as well (**Figure 1.10c**). The polymers obtained according to Yamamoto are normally of high molecular weight[41], while the operators profit also from the experimental simplicity of the method. The disadvantages, however, are the obligatory use of stoichiometric amounts of the expensive nickel reagent and the loss of control over the backbone configuration of the final products. On the other side, the Suzuki-based methodologies demand dibromo- and diboronic acid ester-functionalities of the comonomers participating in the polymerization procedure (**Figure 1.10d**). The A-B backbone configuration (A & B stand for the two comonomers) guaranteed by the Suzuki cross-coupling make the control over the backbone constitution possible.

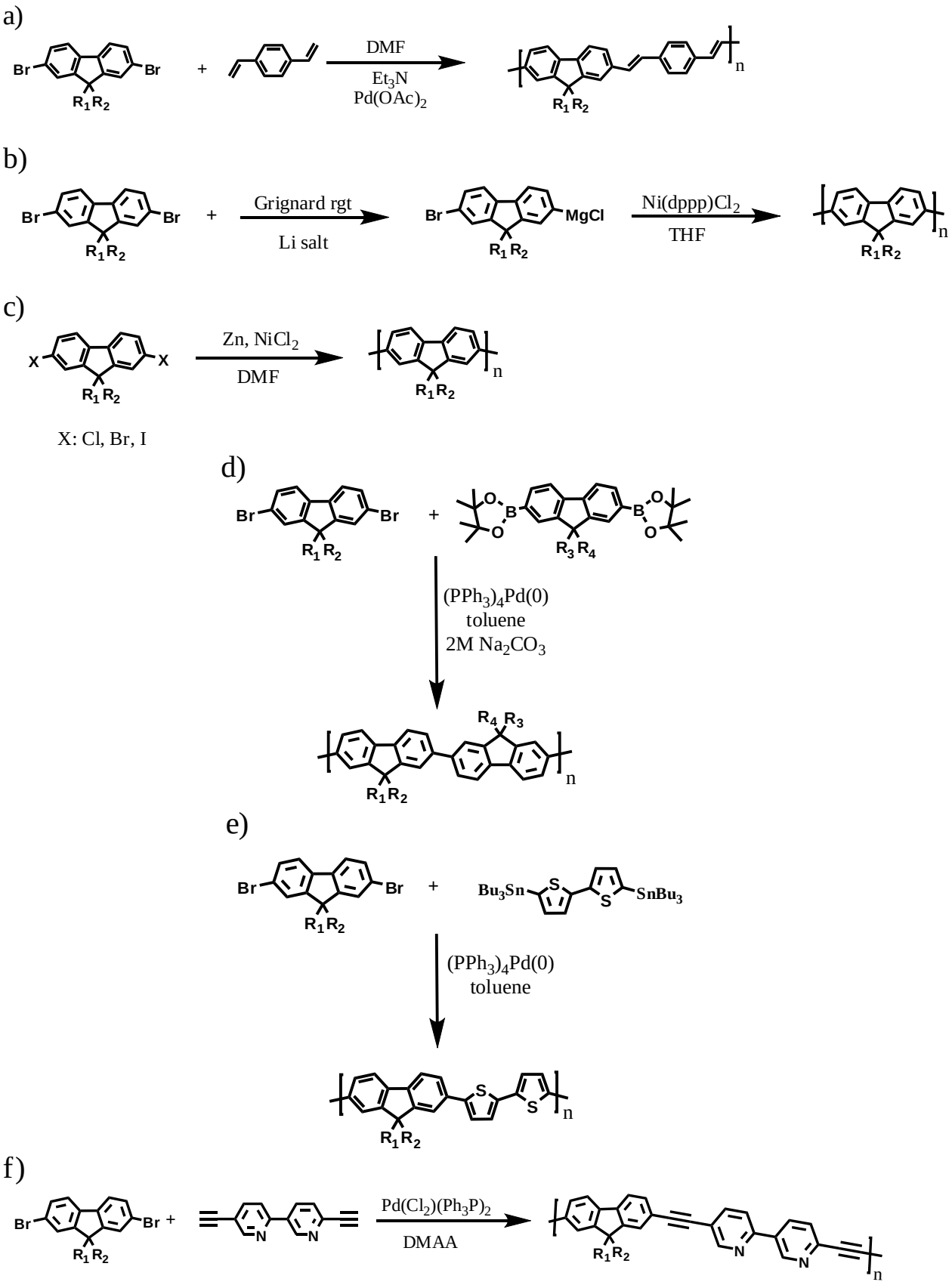

Figure 1.10: Schematic representation of the different synthetic routes for the acquirement of poly(fluorene)s by means of Heck (a)[33], Kumada (b)[35], Yamamoto (c)[36], Suzuki (d)[37] Stille (e)[39] and Sonogashira (f)[40] coupling reactions.

High molecular weights are, however, not always the case due to the strict stoichiometry required and the difficulties in purifying the boron-containing counterparts.[42] The utilization of a phase-transfer catalyst can in this case give increased molecular weights.[37] The achieved target of synthesizing solution-processable poly(fluorene)s had as logical succession the investigation of their behavior in solution. Three key factors are responsible for the polymer characteristics in solution, namely the nature of the solvent, the fraction of the polymer and the nature of the side-chains. Taking poly(9,9'-dioctylfluorene) (**PF8**) as fundamental example a chain morphology, depending on the type of solvent used, could be documented. Thus, **PF8** forms sheet-like geometries in a poor solvent like methylcyclohexane but builds an isotropic phase of rod-like polymeric chains when investigated under identical conditions in the better solvent toluene.[43,44] The same rod-like structure exhibits the tendency to aggregate forming a huge cluster-like morphology, when the polymer fraction is enhanced in the toluene solution.[45] The aggregation tendency is also influenced by the length of the side-chains and in particular an aggregation diminishment was found with increasing side-chain length at room temperature allowing the falling back of the polymer to an isotropic phase.[46] In terms of their optical properties in solution, **Figure 1.11** illustrates exemplarily the observed transitions as measured for a poly(9,9′-dioctylfluorene) (**PF8**), a Yamamoto synthesized polymer.

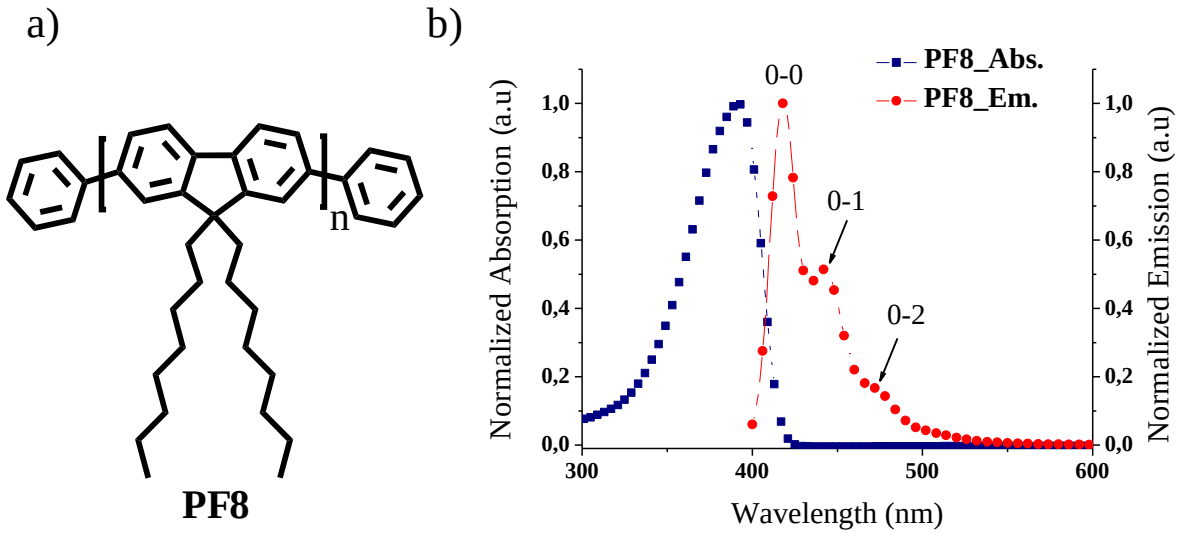

Figure 1.11: a) Poly(9,9′-dioctylfluorene) with an M_w of 321000 g/mol and polydispersity of 3.1. b) Normalized absorption and emission spectra of **PF8** in chloroform (10^{-7} mol/L).[27]

The absorption spectrum of **PF8** exhibits a maximum at 390 nm assigned to a strong π-π* transition, while the absorption onset often used for the determination of the optical band-gap is found at circa 418 nm. The featureless absorption pattern is typical for many conjugated

polymers and has its origin to the fact that polymers consist of a distribution of conjugation lengths. The distribution of polymeric chains is responsible for a distribution of energies and as the energy of the π-π* transition is associated with the conjugation lengths a broad absorption is the final outcome, whereby vibronic features of any particular segment are hidden.[27] On the other side, the emission spectrum shows three well-resolved peaks with a maximum at 418 nm and vibronic shoulders at 442 nm and 472 nm assigned to the 0-0, 0-1 and 0-2 *intra*chain singlet transitions, respectively. **PF8** and poly(fluorene)s exhibit blue photoluminescence but combination of the fluorene building block with a variety of different aromatic monomers like anthracene, biphenyl, furan, 2,1,3-benzothiadiazole, 2,2'-bithiophene, 1*H*-pyrrole, thiophene, phenylene, (*E*)-1,2-diphenylethene, triarylamine and their derivatives can expand the emission over the full range of colors (blue, green, yellow, red).[47] The photoluminescence quantum efficiencies of PFs are high in solution and remain large in films as well.[36,48,49] However, the blue emission originating from poly(fluorene)s and especially from poly(dialkylfluorene)s becomes unstable after annealing the material or implementing it in an electroluminescent device. The result is a long-wavelength emission band at around 530 nm, which is assigned to emission from fluorenone defects incorporated in the polymer backbone. The defect sites were postulated to be formed during the polymerization *via* reduction of fluorene to fluorenyl anions, which were subsequently oxidized by atmospheric oxygen to ketone during synthesis or handling.[50,51] Thus, developing stable blue emission has drawn the attention of scientists, whereby attachment of bulky groups[52], blends with hole transporting materials[53,54] and preclusion of monoalkylfluorenes from the reaction[55,56] are some of the approaches applied and improved the quality of the polymers as emitters. Moreover, PFs as wide band-gap materials can play the role of a host and serve as energy transfer donors, when used in conjunction with other smaller band-gap comonomers or phosphorescent dyes.[57,58] The design of these host-guest systems targets to an efficient Förster energy transfer from the fluorene to the chromophores, enabling emission across the whole visible spectrum. The thermal stability of homo- and copolymers of the class of PFs is excellent with decomposition temperatures at 5% weight loss exceeding 400 °C. The glass transition temperature (T_g) depends on the nature of the comonomers and the backbone composition. Nevertheless, a 'rule of thumb' concerning the dependence between comonomer backbone incorporation and T_g value could not be established.[49] Poly(dialkylfluorene)s with unbranched alkyl substituents at the C9-position like **PF8** possess two nematic liquid crystalline phases. Longer alkyl-chains exhibit the tendency to reduce the transition temperatures. Exemplarily, homopolymer **PF8** with the two

octyl-chains shows nematic phases between 80-103 °C and 108-57 °C, while **PF6**, the analogue with the two hexyl-chains, possesses nematic phases between 162-213 °C and 222-246 °C.[59,60] In contrast, polymers with branched alkyl-substituents like 2-ethylhexyl exhibit only one nematic phase.[61]

1.3 Semiconductor Nanocrystals

Semiconductor nanocrystals, known also as quantum dots (QD), are inorganic solids possessing sizes in the range of 1-100 nm. In the past three decades a raising interest regarding the exploration of the QDs behavior emerged, triggered by the work of A. Henglein[62,63] and expressed by moving from the basic nanocrystal science to the implementation of their opto-electronic characteristics in commercial areas aiming at high-tech profitable applications. Their tunable optical and electronic properties make them ideal candidates in photonic-, photovoltaic-, sensor- and light-emitting diode devices.[64] The most widespread quantum dots are the so-called II-VI semiconductor nanocrystals including CdSe, CdS, CdTe, ZnSe, ZnS, ZnTe, whereas quantum dots of the III-V (InP, GaP, GaInP2, GaAs, InAs) and IV-VI (PbS, PbSe, PbTe) groups have been synthesized and photophysically characterized, as well.[65] The dependence of their physical, chemical and electronic properties on the 'quantum confinement' effect brings the tuning of the nanocrystals qualities in direct connection to the energy band distribution in the material. Quantum dots as semiconductors possess a filled band called 'valence band' and an empty one called the 'conduction band'. The 'quantum confinement' phenomenon comes into sight when a semiconductor is irradiated with photon energy larger than the band-gap energy E_g. As a consequence, an electron will be promoted from the valence to the conduction band, whereby a hole, considered behaving as a particle, remains in the valence band. This electron-hole pair, also referred to as exciton, has a low binding energy due to the small masses of the two counterparts and its radius plays a crucial role influencing the properties of the nanocrystals.[66,67] In particular, if the Bohr radius of the nanocrystal is equal or smaller compared to the radius of the exciton, the latter can not anymore remain in the ground state. The energy level structure of the ground state including the exciton must be thus rearranged in a higher level due to the higher kinetic energy. In other words, when the dimensions of the nanocrystals are reduced, the exciton can still populate the ground state, the energy level of the latter is, however, altered by the size diminishment and shifted to a promoted level. The 'particle in a box' model, mathematically expressed by **Equation 1**, is used in order to describe the aforementioned event, where the particle walls are understood as the box.[68]

$$\Delta E = \frac{\pi^2 \cdot \hbar^2}{2 \cdot R^2}\left(\frac{1}{m_e} + \frac{1}{m_h}\right) - \frac{1.8 \cdot e^2}{4 \cdot \pi \cdot \varepsilon} \cdot \frac{1}{R} \qquad \textbf{(1)}$$

where ΔE is the change in the band-gap energies relative to a bulk solid

R is the radius of the nanoparticle

$m_{e/h}$ are the effective masses of the electron and the hole

ε is the dielectric constant

e is the elementary electron charge and

h the Planck's constant.

The first term of **Equation 1** reveals that the energy is a function of $1/R^2$, while the second term is representative for the hole-electron Coulombic interaction. As a consequence, the energy band E_g is associated with the size of the particle and more specifically an energy increase is the result of a diminishment in the particle dimensions. This correlation is schematically represented in **Figure 1.12** being, however, strong simplifications of the band structures as the actual quantum dots display surface imperfections and loosely attached bonds.

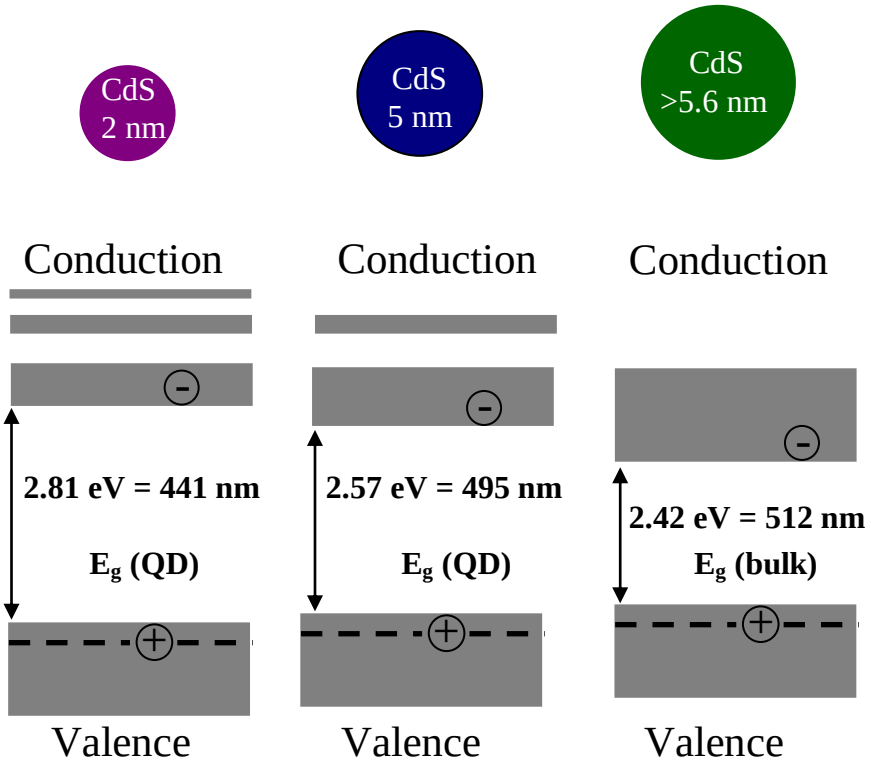

Figure 1.12: Diagram of the change in energy levels upon changing the quantum dot size, where E_g(QD) and E_g(bulk) represent the band-gap energies of the quantum dot and the bulk solid, correspondingly.[69]

Figure 1.12 shows that the bulk material with the large number of atoms possesses strong bands and a small band-gap. If the number of atoms is reduced, the density of the energy levels decreases and simultaneously the distance between the top band-edge of the valence band and the bottom band-edge of the conduction band increases. Thus, nanoparticles with a smaller number of atoms (smaller radius) possess larger energy band-gaps compared to particles, which have larger radii. In other words, the reduction of the particle size causes a division in the distribution of the band energy leading to higher band-gap energy values and size-tunable optical properties of the semiconductor quantum dots.[70-72] **Figure 1.13** represents exemplarily the optical properties in terms of absorption (blue line) and emission (red line) intensity of CdSe nanocrystals passivated by a ZnS shell in a typical core-shell quantum dot. In the absorption spectrum, two maxima can be identified at 510 nm and 620 nm. The maximum at 620 nm comes off by excitation of an electron from the top side of the valence band to the bottom layer of the conduction band. As a consequence, the energy of this transition can be assigned to the band-gap value and incorporated in **Equation 1** in order to calculate the radius of the particle. The second maximum at 510 nm is the result of an electron transition from the valance band into a higher level of the conduction band, whereas further maxima would speak for transitions in even higher levels of the conduction band.

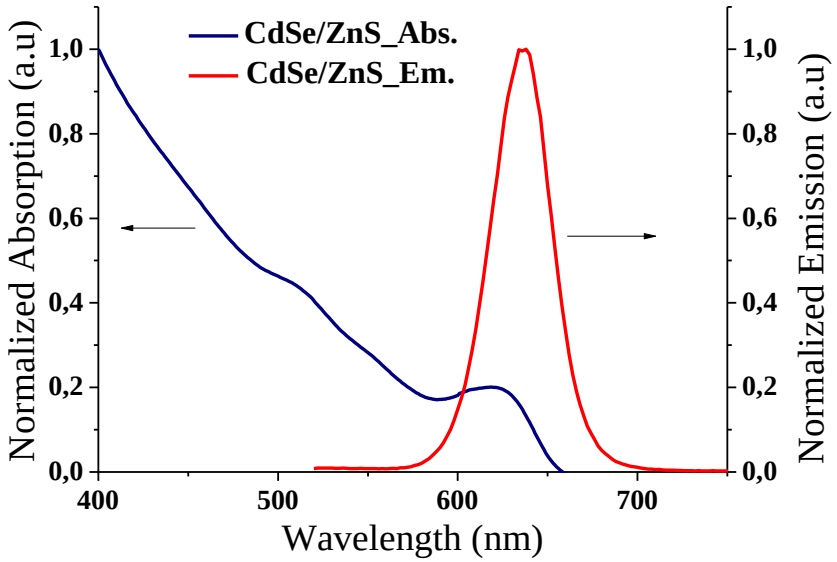

Figure 1.13: Normalized absorption and emission spectra of CdSe/ZnS Lumidots purchased from Sigma-Aldrich. Experiments performed using a concentration of 0.033 mg/mL in toluene and an excitation wavelength of 500 nm in case of the fluorescence measurement.[70]

The absorption characteristics revealed in the spectrum are signature proofs of the consequences of the 'quantum confinement' effect upon decrease of the particle's dimensions namely the increased band-gaps and the decreased density of band levels. In the emission spectrum, only one maximum at 638 nm is observed and is assigned to the radiation-emitting transition of the electron populating the lower edge of the conduction band to the upper level of the valence band. The broadness of the peak is attributed to the fact that the energy band-gap is not only dependent on the particle structure and surface functionalization but on the particle size, as well. All other transitions are not pronounced and proceed *via* release of vibrational energy.[73]

The structural build-up of quantum dots can be composed of only crystalline cores decorated with surface stabilizing ligands (core particles e.g. CdSe), cores on which an external coating is grown and increases the stability of the dots (core/shell particles e.g. CdSe/CdS)[74] and particles passivated by a multi-shell architecture (core/shell/shell e.g. CdSe/CdS/ZnS), whereby the lattice parameters and band-gap alignment must be taken into consideration, when fabricating such systems.[75] Generally, the synthesis of nanoparticles involves addition of surfactants, which play the role of surface stabilizers, preventing aggregation and controlling the particles' growth. Three strategies are applied in order to synthesize quantum dots, whereby the so-called 'bottom-up' and 'top-down' approaches are the two basic ones. According to the 'bottom-up' method, molecular or ionic precursors of the quantum dots are allowed reacting in solution in order to obtain the nanocrystals as colloids. The 'top-down' approach uses macroscopic material, which is broken down by means of laser or crushing enabling large production volumes. In the third available methodology, known as the 'hybrid route', quantum dot precursors are utilized, which are reacted in the gas phase and finally deposited as films on substrates.[69] Regardless which synthetic method is applied, the acquired quantum dots possess a large surface to volume ratio rendering them unstable in solution and inducing cluster formation (agglomeration) due to the high surface energy. Thus, stabilization of the newly fabricated nanoparticles is inevitable and must be considered as part of the synthetic route. The ligands bound to the surface of the nanoparticles ('capping ligands') can contribute to the stability and prevent collapse of the particles. Regarding their interaction with the solvent, polar or charged ligands provide solubility in polar solvents, while non-polar ligands provide solubility in apolar organic solvents like *n*-hexane or toluene. In case of the organic solvents, hydrophobic ligands prevent aggregation of the nanoparticles. Molecules belonging to this class of ligands are illustrated in **Figure 1.14**. In aqueous solutions stability is guaranteed by repulsive forces between the particles originating from

electrostatic interactions of equally-charged ligands, which are attached on the particle surface and contain most commonly carboxylic or sulfonic acid-groups. Examples of such molecules, which enable the stabilization of the nanoparticles through simultaneous transfer from the initial organic to the aqueous phase[76] are represented in **Figure 1.15**.

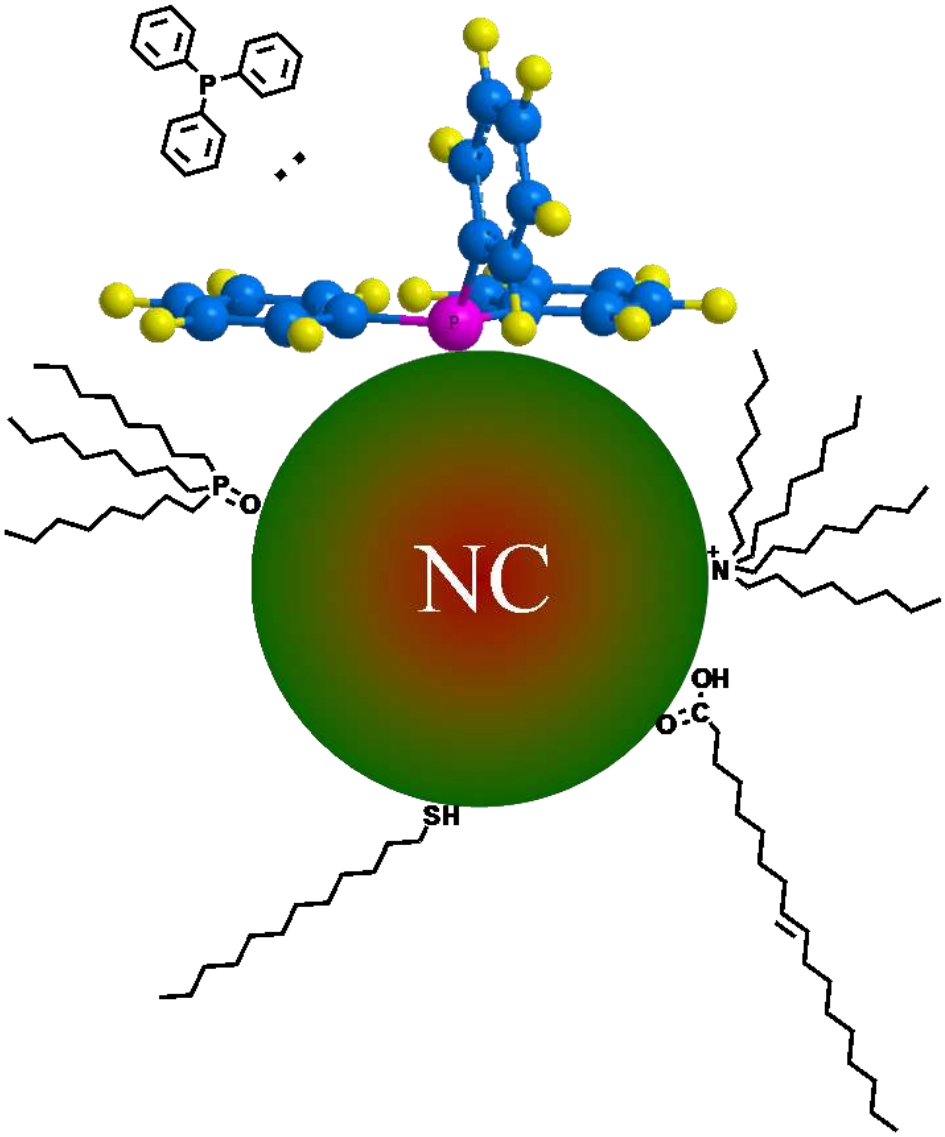

Figure 1.14: Capping ligands used for the functionalization and stabilization of a nanoparticle in organic solvents. Beginning from the top and following a clockwise direction the hydrophobic molecules represented in here are: Triphenylphosphine, tetraoctylammonium, oleic acid, dodecanethiol, trioctylphosphine oxide. The three-dimensional structural representation of the triphenylphosphine reveals the spatial conformation of the molecule on the surface of the nanocrystal and the binding *via* the phosphor atom. In the 3-D model the yellows spheres designate hydrogen atoms, the blue ones carbon atoms and the single purple sphere the phosphor atom.[77]

Generally, three capping methodologies have been developed, targeting the synthesis of water-dispersible and photochemical stable nanocrystals.[71] In the firstly described methodology of the ligand-exchange, the ligands stabilizing the particles at first point are exchanged by capping ligands, which bind more strongly to the inorganic nanoparticle surface providing colloidal stability. Typical example is the exchange of a trioctyl phosphine/trioctyl phosphine oxide mixture (TOP/TOPO) with a hydrophilic thiol-based molecule like mercamptocarboxylic acids (see **Figure 1.15**), which possess a good surface-anchoring thiol-group able to chemisorbe or covalently link on the surface of the quantum dot and a hydrophilic end-group able to facilitate water compatibility.

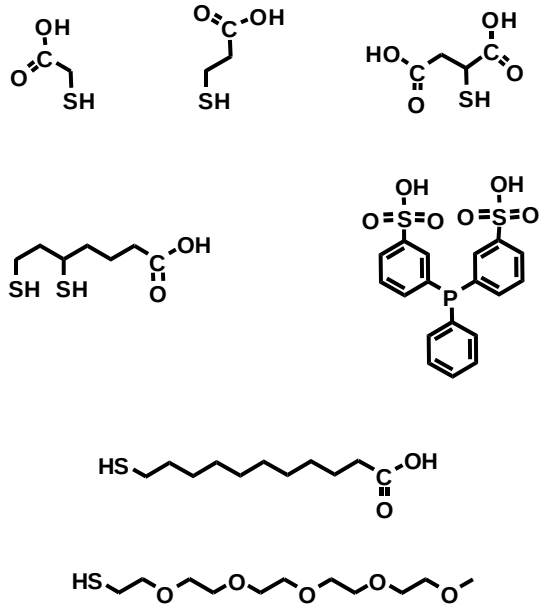

Figure 1.15: Capping ligands used to stabilize nanoparticles in the aqueous phase. From the left to the right the hydrophilic molecules represented in here are: thioglycolic acid (mercaptoacetic acid), mercaptopropionic acid, mercaptosuccinic acid, dihydrolipid acid, *bis*-sulfonated triphenylphosphine, mercaptoundecanoic acid and 2,5,8,11,14-pentaoxahexanedecane-16-thiol.[77]

The second methodology includes the modification of the nanoparticles with a silica shell. The latter can be considered as a polymer functionalized with polar groups, which insulate the hydrophilic QDs. This method uses a ligand exchange procedure in order to wrap a first silane layer to the quantum dot surface. By means of this layer, a cross-linked silica shell layer is deposited on the particle, which can once more be modified leading to nanoparticles of different materials like Au[78], CdSe/ZnS[79] or Fe.[80]

The third strategy maintains the already existing capping ligands on the particles' surface and uses an additional polymer coating that adsorbs by hydrophobic interactions of side-hydrocarbon chains and van-der-Waals forces between the molecules. The final coated particles bear physical and chemical surface characteristics, which are independent of the core material. Amphiphilic polymers provide a great number of contact points between the ligands and the polymeric sites preventing the release of the polymer from the particle surface. Acrylic acid- and maleic anhydride-based polymers are typical examples of the class of amphiphilic polymers.[81,82] Block copolymers can also be used as amphiphiles, building a coating *via* the micellar structures generated by their hydrophobic or hydrophilic segments inside the backbone when dispersed to the respective solvent.[83,84] The goal of synthesizing stable nanocrystals by converting in principle hydrophobic surfaces to hydrophilic ones as described previously, is to exploit and take advantage of the unique properties of the semiconductor quantum dots. Quantum dots are excellent inorganic dyes due to their precisely tuned emission wavelength upon change of their size, their extreme photostability and their resistance to bleaching over long period of time. These properties combined with the fact that quantum dots can be rendered biocompatible[85] expand their applicability to the biomedical field opening the way for *in vivo* imaging[86,87] and fluorescence labeling.[88] However, and despite the advances regarding the two aforementioned technologies, the issue of toxicity arising from the heavy metals and the capping agents incorporated in the nanocrystals should still be properly addressed in the future, in order to perhaps some day realize diagnostic treatments in human organisms, as well.[88] Furthermore, the broad absorption spectrum of the quantum dots as already illustrated in **Figure 1.13** gives the opportunity to excite them at almost all excitation wavelengths shorter than their emission maximum. This advantageous behavior of the nanocrystals can be useful when detection of different colors in a sample is needed and mediated *via* a single excitation wavelength and a single emission scan. As nanocrystals excited by light exhibit the tendency to suck the generated charge carriers, quantum dots are suitable for solar cell fabrication, as well. Moreover, the high stability and large quantum yield of the nanoparticulate material make quantum dots also good candidates in light-emitting diodes and as fluorescence markers in non-polar media.[70]

1.4 Polymer-Nanocrystal Composites/Hybrids

Nanocomposites based on semiconducting quantum dots and conjugated polymers represent a class of functional materials bearing optical, electronic and magnetic properties not observed in any of the two counterparts. Their promising synergistic properties like for example the spectral tunability and photostability, made nanocomposites desirable candidates in applications like light-emitting displays[89,90] and photovoltaics[91-93] and triggered a further interest in terms of preparing such composite systems and subsequently controlling and tuning their new-gained electronic and spectroscopic characteristics. According to the International Union of Pure and Applied Chemistry (IUPAC) composites are defined as 'multi-component materials comprising different phase domains in the solid or liquid state where at least one type of domain is a continuous phase'[94], while this definition is complemented by the statement of 'a physical distinction between the components and their interface'.[95] Hybrids, on the other side, are defined as 'materials, which consist of chemically different components whose distribution in the molecular level is accomplished by mixing the components or by interconnecting the counterparts *via* covalent, coordinative, ionic or hydrogen bonds.[96] Each of the counterparts retains its chemical identity and can exist independently even beyond the hybrids. The hybrids, where the components are kept together by means of a bond, can be subdivided into two classes, taking into consideration the type of linkage. Thus, hybrid materials with components interacting weakly through hydrogen bonds or van-der-Waals forces belong to class I, while hybrids, where the organic and inorganic blocks are linked strongly to each other, through covalent or ionic bonds are hybridic materials of the class II.[97]

1.4.1 Fabrication of Polymer-Nanocrysral Hybrids

Combination of semiconductor nanocrystals with functional conjugated polymers is a highly desirable approach as the resulting hybrid materials take over the properties of processability, mechanical strength and flexibility from the organic counterpart[98-100] and of broad absorption spectrum, photostability and high electron affinity from the inorganic part.[101,102] Efforts on the preparation of the polymer-nanocrystal hybrids have been recorded in a large number of publications over the past fifteen years[102-105], whereby the variety in the chemical configuration of the chosen components provided a basis for the development of different synthetic approaches, the most significant are summarized and described below.

1.4.1.1 Blending

Non-functionalized polymers are dissolved in trivial solvents and subsequently mixed with nanoparticles capped with initial ligands such as oleic acid, trioctylphosphine oxide, hexadecylamine. During the blending strategy neither polymers are derivatized nor nanocrystals are subjected to a ligand exchange procedure, restricting thus the applicability of the method. This limitation has its origin to the phenomenon of phase separation of the components in the micrometre scale[106] coming into sight due to the agglomeration tendency of the nanocrystals, when solvent is removed[107,108] and the tendency of the polymers to solidify and create semi-crystalline structures, whereby crystalline zones are separated from amorphous ones.[109]

1.4.1.2 Capping

Conjugated macrocompounds are functionalized with groups containing an anchoring function capable to tie on the nanocrystal surface and to perform an exchange with the initial ligands. The most popular anchoring groups are thiols but amines, phosphonic acids and carboxylic ones have been utilized as well.[110-113] Despite the importance of the capping ligands in terms of stabilization and prevention of particle aggregation, little knowledge is available regarding the strength of the nanocrystal-ligand bonds. A recent work on CdSe nanocrystals, however, showed binding energies between CdSe and ligands hexylthiolate ($C6S^-$), hexylamine ($C6NH_2$), hexylthiol (C6SH) and tributylphosphine oxide (TBPO) of 1283 kJ/mol, 313.6 kJ/mol, 86.8 kJ/mol and 34.7 kJ/mol, correspondingly.[114] These data prove an enhanced stability in case of the thiolate-CdSe bond. For instance, molecules containing the chelating carbodithiolate moiety are excellent binding ligands due to their strong chemical affinity for the nanocrystal surface and can quantitatively be exchanged with the initial ligands.[115] Prerequisite to achieve chemical binding is to firstly synthesize oligomers, polymers and quantum dots with compatible functional groups that allow the counterparts to react with each other without jeopardizing the stability and the photophysical characteristics of the components. For oligomers, the anchor functionalities are placed as termini- or as side groups (**Figure 1.16**, routes 1 and 2), which can be the case in polymers as well (**Figure 1.16**, routes 4 and 5). However, as the number of anchoring groups decreases along the high-molecular weight chain, their incorporation in the side-chains is preferred. Examples of the ligand exchange method for the preparation of hybrids include conjugated

oligo- and poly(thiophene)s functionalized with thiol[116], phosphonic acid[101] or alkylene carboxylate substituents.[117] Preparation of nanocomposites of quantum dots (CdSe) and dendritic oligo- and poly(thiophene)s containing phosphonic acid moieties as linking mediators was achieved as well (**Figure 1.16**, route 3).[111] Beyond the thiophene class of macrocompounds, oligomers or polymers belonging to the family of phenylenes and bearing oxide[118] or sulfide[119] type terminal groups were also bound to the surface of nanocrystals.

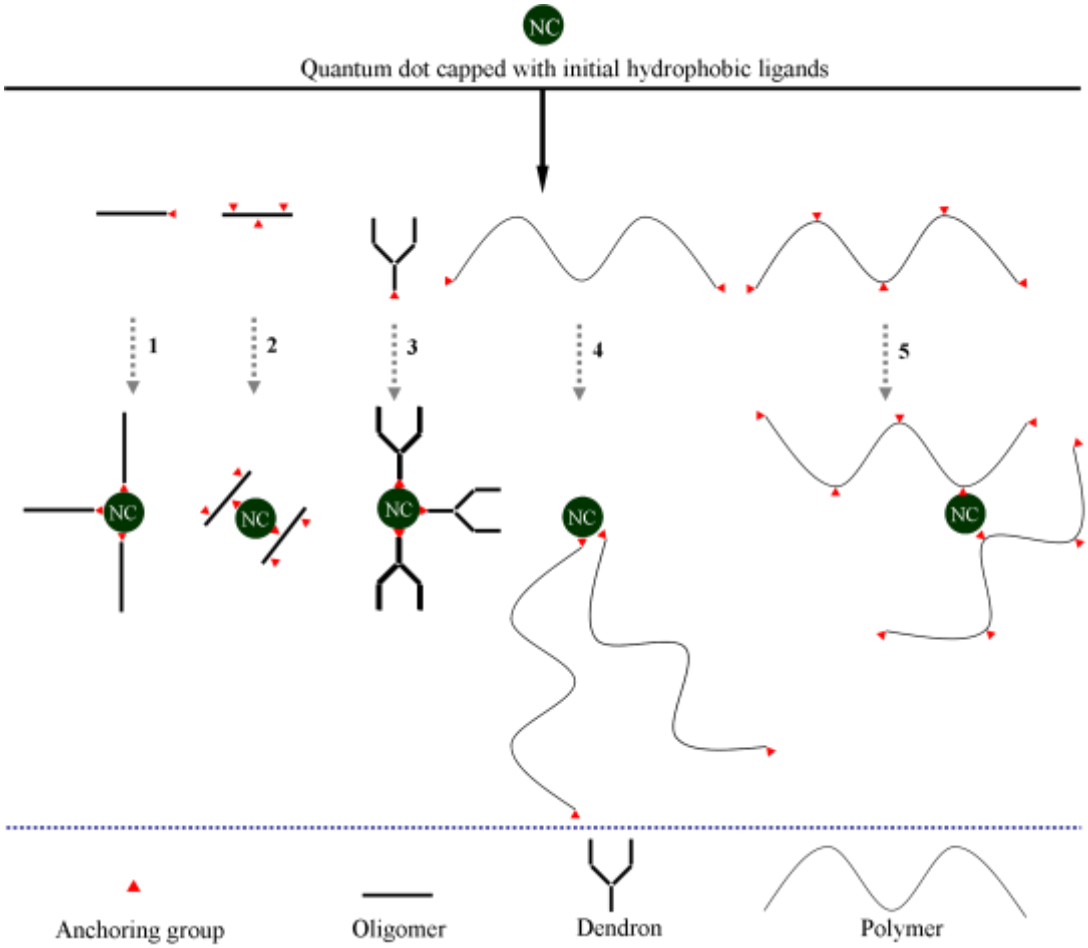

Figure 1.16: Schematic representation of the synthetic routes for the preparation of hybrid materials following a ligand exchange procedure of the initial hydrophobic ligands.[96]

A further success was the association of a triblock copolymer embracing fluorene and ethylmethacrylate building blocks with CdSe nanocrystals, in which case the coordination of the amphiphilic polymer over a great number of contact points on the quantum dot surface stabilized the formed hybrid.[120]

1.4.1.3 Covalent Grafting

Conjugated oligomers or polymers can be directly grafted-from or onto the surface of suitably functionalized nanocrystals. The 'grafting-from' approach works in the absence of the ligand-exchange process and reduces thus the preparation of the hybrids to one single step. For this purpose a bifunctional ligand (*p*-bromobenzyl-di-*n*-octylphosphine oxide, DOPO-Br) endowed with a phosphine oxide group in order to facilitate the surface-linkage and an arylbromide-functionality capable of participating in a surface-initiated polymerization was fabricated.[121] By means of this compound, CdSe nanocrystals capped with DOPO-Br were obtained and further used to uniformly grow *para*-phenylene vinylene chains on all directions by copolymerizing them with 1,4-divinyl- and 1,4-dibromo-benzene derivatives *via* a palladium-catalyzed Heck coupling. However, the lack of control over the reaction conditions leading to organic segments of different length attached around the core results in a control-loss over the HOMO-LUMO levels of the grafted molecules as well, rendering the composites of limited value. On the other side, the 'grafting-onto' strategy offers the possibility to manipulate the photophysics of the hybrids as predesigned polymers come this time into play. The initial ligands of the quantum dots are replaced by molecules, which possess an end-group capable to bind on the nanocrystal surface and an additional reactive group with the role of making a reaction with the side- or end-functionalized predesigned macromolecule feasible. Using again DOPO-Br as surface-linker the synthetic procedure will be now carried out as following: the trioctylphosphine oxide ligands attached on the nanocrystals are initially exchanged with pyridine ones, which from their side can be easily replaced by the DOPO-Br molecules. The latter can initiate a grafting reaction *via* a Heck coupling between its bromo-group and a terminal vinyl-group of poly(3-hexylthiophene).[122] Limitation regarding the 'grafting-onto' approach can arise from polymer chains of relative shortness, the use, however, of predetermined macrocompounds directly attached on the surface of the quantum dot reveal characteristical photophysical and spectroscopic properties different from a poly(3-hexylthiophene):QD blend.[123]

1.4.1.4 Non-covalent Interactions

The strong tendency of conjugated macrocompounds and nanocrystals to phase separate when incorporated in hybrid systems can be circumvented by allowing the components to interact non-covalently. Such interactions can be achieved by the molecular recognition approach, whereby a homogeneous distribution of the quantum dots in the polymer matrix is feasible. In

particular, a functionalized macromolecule for example poly(alkylthiophene) containing diaminopyrimidine side-groups is able to molecularly recognize surface-functionalized nanocrystals like 1-(6-mercaptohexyl)thymine capped CdSe *via* hydrogen bonding (**Figure 1.17**).[124] Electrostatic interactions have also been used for the preparation of hybrids and this approach is, based on the coming-together of quantum dots, stabilized for example by mercaptoundecanoic acid and a poly(thiophene) side-chain functionalized with a propyl trimethylammonium bromide-moiety.[125]

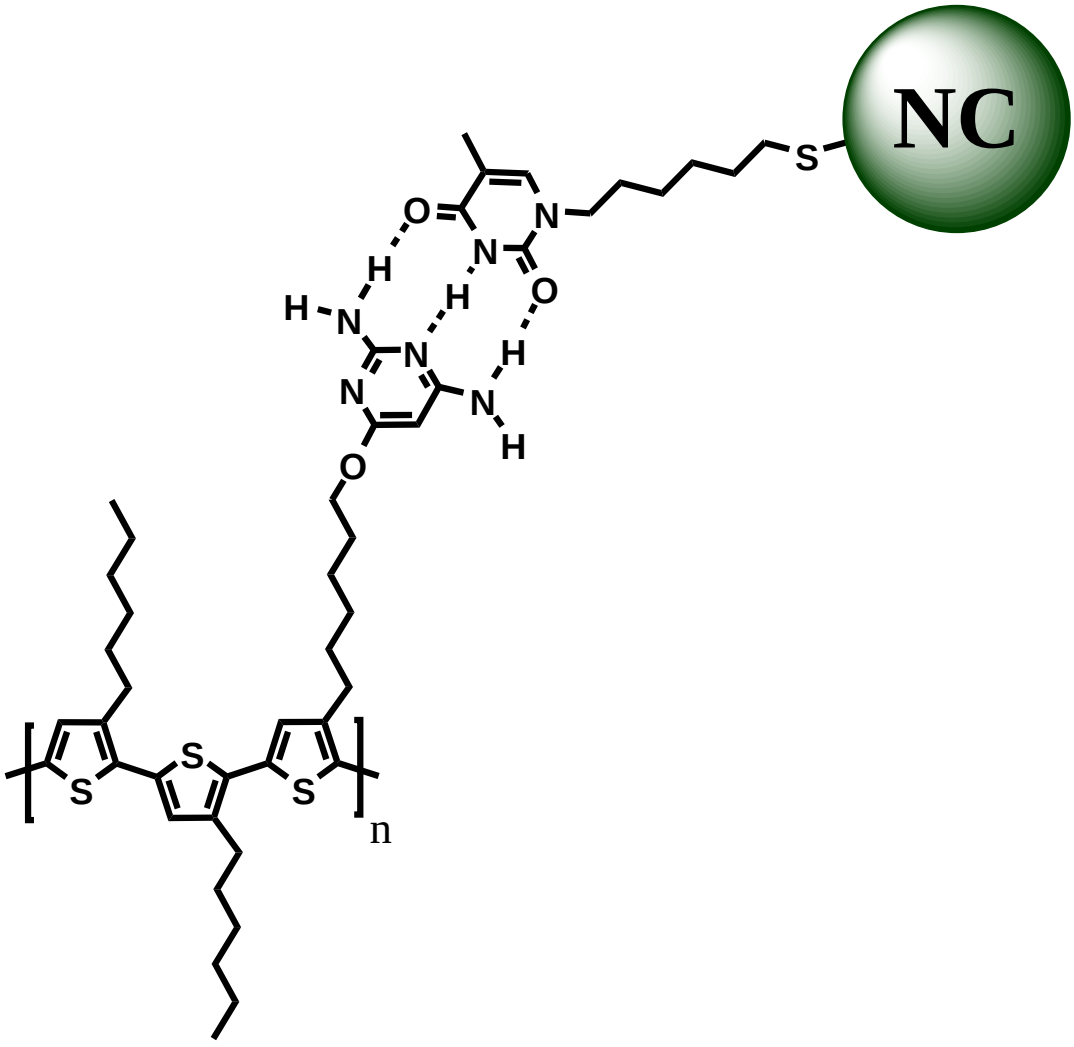

Figure 1.17: Schematic representation of the molecular recognition approach between a side-chain functionalized poly(thiophene) and 1-(6-mercaptohexyl)thymine capped CdSe nanocrysrals proceeding *via* establishment of three hydrogen bonds.[124]

Regarding the family of poly(fluorene)s, achieved hybrids upon this methodology include a water-soluble fluorene-phenylene copolymer interconnected with thioglycolic acid-capped

CdTe nanocrystals[126] and a dendritic fluorene derivative non-covalently bound on CdS nanocrystals.[127]

1.4.1.5 *In-situ* Growth

Nanocrystal precursors are dissolved in a polymer solution and grow within the polymer template overcoming thus the problem of finding a solvent, where both counterparts are processable. The polymer chains exhibit the property to stabilize the nanocrystals and passivate the surface, obtaining thus closely-associated blends. A typical example of this strategy is the *in-situ* grow of CdS nanorods in a poly(3-hexylthiophene) matrix, whereby the thiophene-sulfur enables the linkage to spherical particles, which subsequently nucleate and evolve into nanorods.[128] Nevertheless, growth of nanoparticles in a poly(thiophene)-based copolymer yielding a poly(thiophene)-ZnO hybrid has also been reported.[129]

1.4.2 Energy Transfer

Hybrids synthesized on the basis of conjugated polymers and semiconductor nanocrystals have contributed to the development of technologically relevant materials applicable in light-emitting and photovoltaic devices.[89,92] The spectroscopic characteristics of the resulting nanocomposites and their control through the synthetic concepts applied, remains a challenge for the scientific world as the phenomena having the most important influence over the photophysics of the hybrids, namely energy transfer and charge separation are not fully comprehensible. Förster resonant energy transfer (FRET) is a non-radiative dipole-dipole coupling mechanism taking place between optically active species (donor-acceptor) and is dominated by the spectral overlap between the emission spectrum of the donor and the absorption spectrum of the acceptor and their spatial alignment as well.[130] The FRET mechanism theory came into sight in 1948 by Theodor Förster, who was the first one describing the process of non-radiative energy transfer from a donor fluorophore to an acceptor fluorophore of the same type.[131] One year later, Förster extended his theory on donor species possessing a larger energetic level difference ΔE_D compared to the electronic transition of the acceptor molecule ΔE_A (**Figure 1.18**).[132]

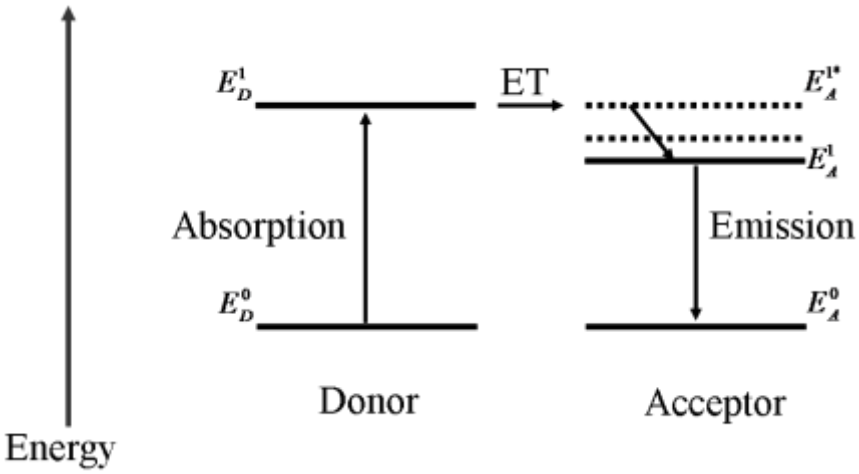

Figure 1.18: Schematic representation of the Förster resonant energy transfer mechanism.[130]

The term resonant means that the energy transfer from the donor to the acceptor proceeds *iso*energetically, in other words from the excited donor level E_D^1 only into a vibronically excited state of the acceptor E_A^{1*}. However, excess of energy is dispersed in less than a picosecond leaving the acceptor in the E_A^1 state. This rapid energy vanishment, which takes place at a much faster pace, compared to the time interval needed for the resonant energy transfer, renders the FRET mechanism an 'one way' process. Fluorescence results, in the end, from the acceptor. Förster described the energy transfer rate by means of **Equation 2** assuming the donor-acceptor dyad as point-like molecules:

$$R_{ET} = \frac{9c^4\kappa^2}{8\pi n^4 \tau_r} \frac{1}{d^6} \int_0^\infty \frac{f_D(\omega)\sigma_A(\omega)}{\omega^4} d\omega \qquad (2)$$

where c is the speed of light,

n the refractive index of the medium hosting the dyad,

κ^2 a parameter dependent on the mutual orientation of the two dipoles of the acceptor and donor,

τ_r the radiative lifetime of the donor,

d the distance between the donor and the acceptor,

$f_D(\omega)$ the integral normalized fluorescence spectrum of the donor,

$\sigma_A(\omega)$ the absorption cross section of the acceptor molecules and

ω the angular frequency.

The efficiency of the FRET mechanism, representing the number of quanta transferred from the donor to the acceptor divided by all the quanta absorbed by the donor, may be calculated as well using **Equation 3**[133]:

$$E = 1\text{-}F_{DA}/F_D \qquad (3)$$

where F_{DA},F_D are the donor intensities in the presence and absence of the acceptor both normalized to the same donor concentration. The energy transfer efficiency depends on the distance separating the donor-acceptor pair, the overlap of the fluorescence spectrum of the donor with the absorption spectrum of the acceptor and the relative orientation of the donor and acceptor dipoles.[133] However, the Förster theory can only be implemented for donor and acceptor molecules, whose pure dipole-dipole interactions predominate and can, therefore, occur over longer distances. For significantly smaller distances, stronger electric and magnetic interactions between the donor-acceptor pair should be the case, allowing for example dipole-quadrupole interactions and the so-called Dexter energy transfer to occur. The Dexter ET is a non-radiative process taking place at sub-nanometer distances, which render an overlap of donor and acceptor electron orbitals feasible.[134] Otherwise, like the Förster mechanism, the Dexter theory involves a double electron transfer between donor and acceptor, whereby the latter fluoresces after energy transfer from the former (**Figure 1.19**). Except singlet-singlet ET the Dexter mechanism enables diffusion of triplet excitons as well.

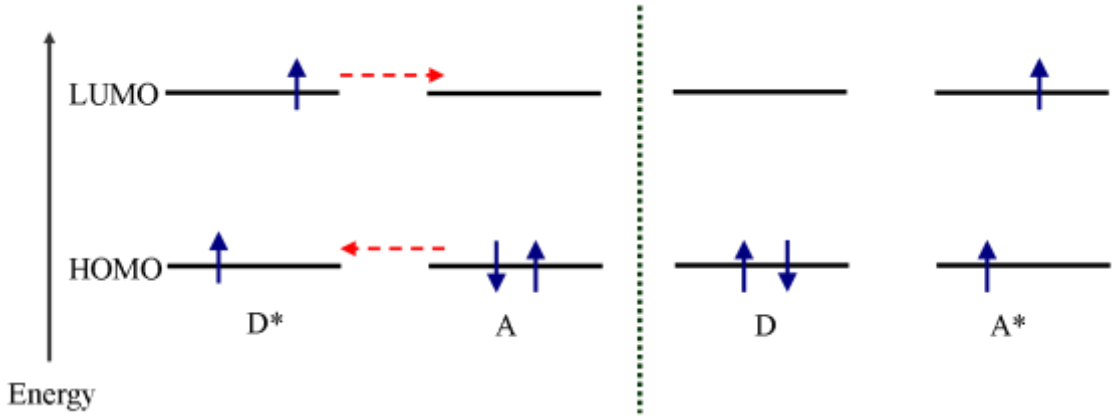

Figure 1.19: Schematic diagram of the Dexter mechanism where the asterisk stands for excited states of the donor (D) and the acceptor (A) and the red arrows reveal the electronic configuration rearrangements.[135]

The energy transfer rate, unlike the six-power dependence of FRET, is described by an exponential function of the separation distance between the donor-acceptor dyad and is mathematically represented in **Equation 4**:

$$K_{Dexter} = K\,J\,e^{\frac{-2R_{DA}}{L}} \qquad (4)$$

where J is the normalized overlap integral of the absorption and emission spectra,

R_{DA} the distance between donor and acceptor,

L the sum of van-der-Waals radius and

K an experimental factor related to specific orbital interactions.

Beside the energy transfer, the conductive pathway of charge transfer is an equivalently significant electronic process. Such a transfer takes place in the interface of a donor-acceptor pair, when the energy level of the LUMO of the acceptor is significantly lower than the LUMO of the excited donor (**Figure 1.20**). The electron-hole separation, made possible when their binding energy has been surmounted, allows an electron transfer to take place from the donor to the acceptor and discloses the phenomenon of charge transfer. Its outcome is positively and negatively charged donor and acceptor molecules, respectively.

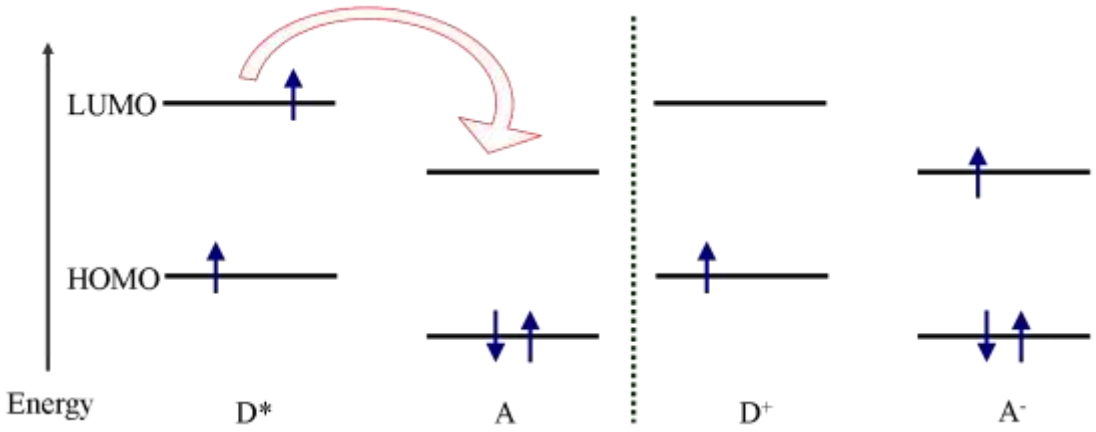

Figure 1.20: Schematic representation of the charge transfer process, where the asterisk stands for excited states and the plus-minus symbols for positively and negatively charged species of the donor (D) and the acceptor (A).[135]

The charge separation process drew the attention of scientists and conjugated polymer/nanocrystal systems became due to their special band-gaps, which are suitable for charge separation across their interface, the subject of intensive studies.[136-138] Nevertheless, the non-radiative energy transfer *via* Förster or Dexter mechanism has been observed in such hybrids as well[139-141], revealing even a competing character to the charge transfer process.[138] The latter antagonism renders the occurrence and explanation of the energy and charge transfer mechanisms even more complex. This complexity is further substantiated by a possible simultaneous existence of both energy transfer processes, whereby spatial and energetic parameters establish the dominant one. Furthermore, in solid-state systems, except from the energy-level alignment, additional phenomena must be taken into consideration like aggregation of nanocrystals or stacking of the polymer chains.[138] A recent investigation in hybrid organic-inorganic nanocomposites based on a poly(fluorene)-CdSe/ZnS system shed light on the significance of the temperature on the exciton diffusion during the energy transfer process revealing a decrease in the transfer efficiency from 30% at room temperature to 5% efficiency at low temperature. The characteristic transfer distances found in this system (10-40 Å) were notably smaller compared to the dipole-dipole couplings with Förster radii of about 50-70 Å. As a result the exciton has to approach close enough to the surface of the quantum dot before it can be transferred non-radiatevely. The expected weaker coupling strength implies a coupling between polymer and quantum dot, which is far-away from the dipole-dipole approach of the Förster theory and closer to a Dexter or multipole-multipole interaction.[142] Thus, it is due to the competition not only between energy transfer and charge separation but also between the Förster and Dexter mechanisms, a long way towards the direction of tailoring and optimizing the opto-electronic properties of organic-inorganic nanocomposites as a deep knowledge regarding the underlying electronic processes is still required.

1.5 Conjugated Polymer Nano/Micro(particle)s

As particle is designated every entity in the sub-micrometer regime representing a distinct discontinuous phase surrounded by a continuous free-flowing medium like for example water or positioned at the top of a surface.[143] Due to the progress in polymer chemistry and in colloid physico-chemistry, nanoparticles of conjugated polymers dispersed in a continuous phase were possible to be prepared and used as protection, binding or polish ingredients in industrial products like paper, metal or wood.[144] Polymer particles could further be

implemented in important biological, medical or analytical applications including cell labeling, drug delivery and materials for chromatography columns.[145-147] Polymer nanoparticles can be categorized into the two main classes of nanospheres and nanocapsules according to their structural configuration (**Figure 1.21**).[148]

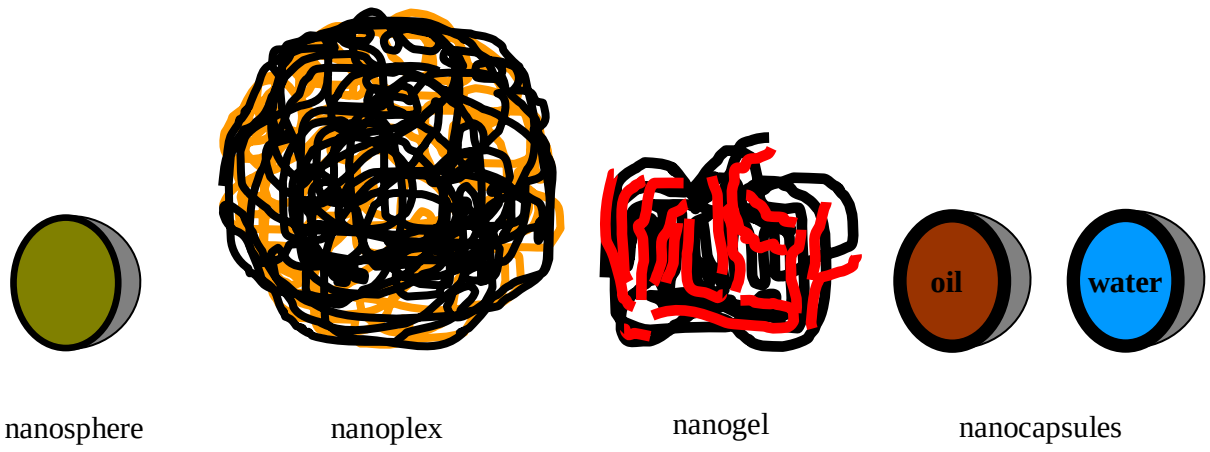

Figure 1.21: Structural configuration of polymer nanoparticles.[148]

Nanospheres have a matrix-type structure whose entire mass is solid. Their size can vary from tenths to hundreds of nanometers, fine nanoparticles, however, have sizes between 1 and 100 nm. Nanospheres are usually shaped spherically, though different forms are found in the literature as well.[149] Due to their ability to self-assembly, polymers can build polyelectrolyte complexes (nanoplexes) or spherical supramolecular conglomerates (nanogels) from their polymer solutions both also considered as spheres (**Figure 1.21**). Nanocapsules, on the other hand, possess a reservoir-like structure, in which a solid shell surrounds a solid or semisolid core at room temperature. From the material point of view, the core can be composed either of oil supplying the nanoparticle with a high loading capacity of liposoluble compounds or water enabling encapsulation of water-soluble compounds. The coating shell is achieved by means of precipitation of a predesigned polymer at the surface of emulsion droplets[150-152] or by polymerization occurring at the interface of the dispersed and continuous phase of the emulsion[153-155] and is made of amphiphilic block copolymers of different structures like buckles or brushes.[148]

The motivation towards the synthesis of conjugated polymer nano- or microspheres was the desire to overcome the difficulties arising in terms of insolubility and processability of conjugated polymers, when not equipped with appropriate functionalized side-chains. The first reports regarding this endeavor came up in the 1980s by the works of Vincent[156],

Liedberg[157] and Aldissi[158] who prepared poly(acetylene), poly(pyrole) and poly(aniline) microparticles, correspondingly. The efforts to synthesize particles of conjugated polymers was further extended to the families of poly(thiophene)s[159,160], poly(phenylene ethynylene)s[161], poly(arylenevinylene)s[162,163] and poly(fluorene)s[162,164]. Nano- and microparticles of all these classes of macrocompounds are in general achievable either by the methodology of post-polymerization dispersion of preformed polymers or by the strategy of polymerization in heterophase systems. The post-polymerization dispersion, known also as secondary dispersion technique, uses solutions of conjugated polymers in an organic solvent and proceeds to the creation of particles either by solvent removal from emulsified droplets (emulsion polymerization) or by polymer precipitation, when adding the polymer solution into a continuous phase miscible with the initial organic solvent (precipitation technique).[143] Emulsion polymerization is a simple and the most common method used for the synthesis of conjugated polymer nanoparticles, giving particles of high molecular weight and monodispersity. The method is based on the dissolution of polymer into a water immiscible organic solvent, whereby the resulting solution is mixed with an aqueous surfactant solution. The heterophase system is subjected to high shear by means for example of a sonotrode in order to create stable sub-micrometer droplets of a precursor material. The size of the droplets can vary from 30-500 nm and can be adjusted by the surfactant and the polymer concentration. In a subsequent step, the organic solution was removed affording a dispersion of polymer particles in water. Destabilization of the particles caused by Ostwald ripening[165] or coalescence is prevented through appropriate surfactants and hydrophobic agents, respectively.

The precipitation technique, known also as reprecipitation or nanoprecipitation, proceeds by dissolving a polymer in a good solvent and, subsequently, injecting its dilute solution to an excess of a non-solvent (e.g. water), which is miscible with the good solvent (**Figure 1.22**).[166-168] Particle formation is assisted by sonication and the main driving force being responsible for their formation is the hydrophobic effect. Mixing of the solvent with the non-solvent affects the solvent quality negatively and the hydrophobic polymer chains try to minimize their contact points to water as far as possible. This environmental circumstance induces the polymer precipitation and its folding to spheres as the spherical shape exhibits the minimum exposure to the aqueous medium, representing the thermodynamically favorable lowest surface per volume conformation.[145,166] The precipitation technique does not require the utilization of surfactants and hydrophobic agents as emulsion polymerization does and the nanoparticle size can be tuned *via* the concentration

of the polymer solution. Furthermore, the acquirement of nanoparticle dispersions is not only limited to aqueous systems but can be extended to a purely organic system by mixing for example a tetrahydrofuran solution of a fluorene-based copolymer with cyclohexane.[169]

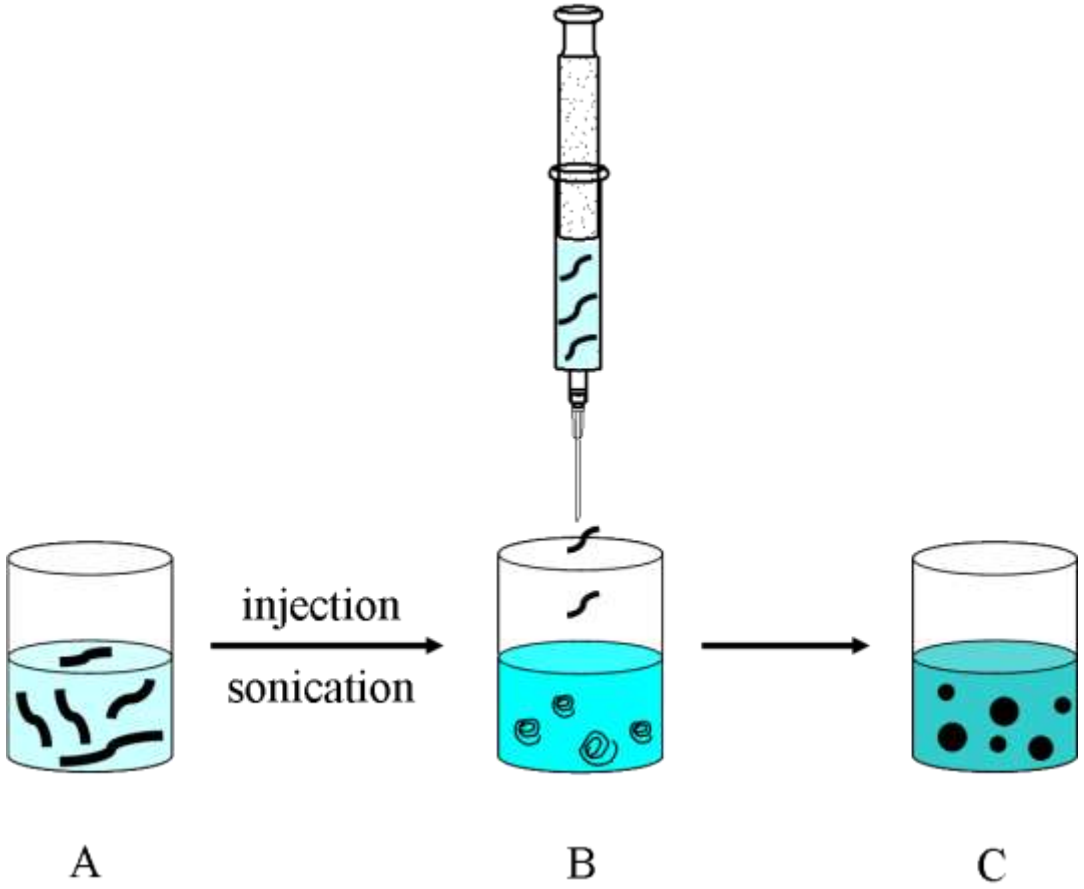

Figure 1.22: The principle of the preparation of nano/microparticles by means of the precipitation technique. A: Polymer solution in a good solvent; B: Injection of the polymer solution in a non-solvent, while sonicating and subsequent removal of the good solvent; C: Dispersion of the formed polymer nano/microparticles in the non-solvent.[145]

The polymerization in heterophase systems, the second of the two main particle synthetic approaches, involves the generation of polymer particles during the polymerization of appropriate monomers in a dispersing medium, which is a non-solvent for the resulting polymer. Preparatively, this methodology includes aqueous oxidative polymerizations or transition-metal-catalyzed coupling reactions. Different types of heterophase polymerization exist, which can be divided into the dispersion and emulsion polymerization.[143] The dispersion polymerization is based on a reaction medium, where the monomer is soluble but the formed polymer not, while the nano/microparticles are retained as colloidal dispersions

preventing deposition by use of steric stabilizers linked on the particle surface. The emulsion polymerization uses monomers with a low solubility in the dispersing medium, which build a separate phase of droplets. Reaction starts in the dispersing medium by means of catalysts and the subsequent chain growth has as a result the nucleation of particles, which are stabilized by surfactants or lyophilic molecules covalently incorporated in the polymers. Two variations of the emulsion polymerization are available, the so-called miniemulsion and microemulsion polymerizations. In the miniemulsion, monomer droplets are resistant enough to shear forces and build, after polymerization in the droplet, stable emulsions of polymer nanoparticles with sizes varying from 30 to 500 nm. In the microemulsion, a microemulsion of the monomer is the initiation step of the polymerization and is indicated by the formation of a single transparent phase without application of shear.[170] Microemulsion is, in particular, suitable for the preparation of extremely small particles with sizes below 20 nm.

Nano- or microparticles of conjugated polymers obtained by one of the afore-described procedures possess a high degree of dispersion retaining simultaneously a low viscosity even at high polymer loads. They become thus highly attractive materials, easy to be synthesized, handled and processed, offering the feasibility to prepare organic-inorganic composites as well.[171,172] Hybrid systems containing donor polymers and acceptor dye molecules captivated the attention of scientists since several years and the investigation of their energy transfer mechanisms was pursued.[173-175] The combination, however, of donor and acceptor nanoparticles in form of physical mixtures towards the acquirement of hybridic materials is a rather recently developed approach. Nanocomposites obtained by precipitation or miniemulsion techniques involved different conjugated polymers playing the roles of the donor-acceptor pair[176], different CdTe nanocrystals as donor-acceptor pair[177] or nanometal particles in conjunction to other nanometal particles or a fluorescent dye in the roles of donor and acceptor, correspondingly.[178] These densely packed dyadic systems were checked in terms of their energy transfer abilities allowing a fine-tuning of the chromaticity coordinates and the achievement of higher fluorescence brightness. Nonetheless, the exploitation of the advantages arising from the confined nano-environment of the nanoparticle, which allows the inorganic part to grow inside the particle or on the outside particle surface, has not reached its zenith yet and remains thus an enticing and promising challenge for the scientific community.

1.6 References

[1] W. R. Salaneck, R. H. Friend, J. L. Brèdas, *Phys. Rep.* **1999**, 319, 231.
[2] A. J. Heeger, *Rev. Mod. Phys.* **2001**, 73, 681.
[3] G. Odian, *Principles of Polymerization*, John Wiley & Sons, New Jersey, **2004**.
[4] M. H. Harun, E. Saion, A. Kassim, N. Yahya, E. Mahmud, *J. Advancem. Sci. Arts* **2007**, 2, 63.
[5] H. A. Pohl, E. H. Engelhardt, *J. Phys. Chem.* **1962**, 66, 2085.
[6] B. S. Wildi, J. E. Katon, *J. Polym. Sci. Part A: General Papers* **1964**, 2, 4709.
[7] M. Goehring, *Q. Rev. Chem. Soc.* **1956**, 10, 437.
[8] P. L. Kronick, H. Kaye, E. F. Chapman, S. B. Mainthia, M. M. Lahes, *J. Chern. Phys.* **1962**, 36, 2235.
[9] H. Shirakawa, E. J. Louis, A. G. MacDiarmid, C. K. Chiang, A. J. Heeger, *J. Chem. Soc. Chem. Commun*. **1977**, 474, 578.
[10] T. C. Clarke, R. H. Geiss, J. F. Kwak, G. B. Street, *J. Chem. Soc. Chem. Commun.* **1978**, 338, 489.
[11] J. L. Brèdas, R. R. Chance, R. Silbey. *Physical Review B* **1982**, 26, 5843.
[12] A. J. Heeger, N. S. Sariciftci, E. B Namdas, *Semiconducting and Metallic Polymers*, Oxford University Press, New York, **2010**.
[13] M. Okada, K. Tanaka, A. Takata, T. Yamabe, *Synth. Met.* **1993**, 59, 223.
[14] J. H. Burroughes, D. D. C. Bradley, A. R. Brown, R. N. Marks, K. Mackay, R. H. Friend, P. L. Burns, A. B. Holmes, *Nature* **1990**, 347, 539.
[15] D. R. Baigent, N. C. Greenham, J. Grüner, R. N. Marks, R. H. Friend, S. C. Moratti, A. B. Holmes, *Synth. Met.* **1994**, 67, 3.
[16] D. Bradley, *Curr. Opin. Solid State Mater. Sci.* **1996**, 1, 789.
[17] A. C. Show, H. J. Tzu, H. L. Hsin, *J. Chin. Chem. Soc.* **2010**, 57, 439.
[18] J. Svoboda, M. Bláha, J. Sedláček, J. Vohlídal, H. Balcar, I. Mav-Golež, M. Žigon, *Acta Chim. Slov.* **2006**, 53, 407.
[19] K. J. Ivin, J. C. Mol, *Olefin Metathesis and Metathesis Polymerization*, Academic Press, San Diego, **1997**.
[20] N. Toshima, S. Hara, *Prog. Polym. Sci.* **1995**, 20, 155.
[21] A. Kraft, A. C. Grimsdale, A. B. Holmes, *Angew. Chem. Int. Ed*. **1998**, 37, 402.
[22] A. G. Macdiarmid, J. C. Chiang, A. F. Richter, A. J. Epstein, *Synth. Met*. **1987**, 18, 285.
[23] A. Sarkar, S. Okada, H. Matsuzawa, H. Matsuda, H. Nakanishi, *J. Mater. Chem.* **2000**, 10, 819.
[24] M. Knaapila, M. J. Winokur, *Adv. Polym. Sci.* **2008**, 212, 227.
[25] A. C. Grimsdale, K. Müllen, *Adv. Polym. Sci.* **2006**, 199, 1.
[26] M. Knaapila, R. Stepanyan, B. P. Lyons, M. Torkkeli, A. P. Monkman, *Adv. Funct. Mater.* **2006**, 16, 599.
[27] D. Neher, *Macromol. Rapid Commun*. **2001**, 22, 1365.
[28] A. F. Diaz, *Chem. Scr*. **1981**, 17, 145.
[29] R. J. Waltman, J. Bargon, *J. Electroanal. Chem.* **1985**, 194, 49.
[30] J. Rault-Berthelot, J. Simonet, *J. Electroanal. Chem.* **1985**, 182, 187.
[31] M. Fukuda, K. Sawada, K. Yoshino, *Jpn. J. Appl. Phys.* **1989**, 28, L1433.
[32] J. A. Mikroyannidis, V. P. Barberis, V. Cimrova´, *J. Polym. Sci. Part A: Polym. Chem.* **2007**, 45, 1016.
[33] S. H. Jin, M. Y. Kim, D. S. Koo, Y. I. Kim, *Chem. Mater.* **2004**, 16, 3299.
[34] X. M. Liu, C. He, J. Huang, J. Xu, *Chem. Mater.* **2005**, 17, 434.
[35] M. C. Stefan, A. E. Javier, I. Osaka, R. D. McCullough, *Macromolecules* **2009**, 42, 30.

[36] Q. Pei, Y. Yang, *J. Am. Chem. Soc.* **1996**, 118, 7416.
[37] M. Ranger, D. Rondeau, M. Leclerc, *Macromolecules* **1997**, 30, 7686.
[38] M. Helgesen, F. C. Krebs, *Macromolecules* **2010**, 43, 1253.
[39] X. Zhang, H. Tian, Q. Liu, L. Wang, Y. Geng, F. Wang, *J. Org. Chem.* **2006**, 71, 4332.
[40] M. L. Keshtov, V. A. Vasnev, G. D. Markova, V. A. Barachevskii, A. R. Khokhlov, *Polymer Science Ser. B* **2011**, 53, 345.
[41] M. Grell, W. Knoll, D. Lupo, A. Meisel, T. Miteva, D. Neher, H. G. Nothofer, U. Scherf, A. Yasudo, *Adv. Mater*. **1999**, 11, 671.
[42] A. D. Schlüter, *J. Polym. Sci. Part A: Polym. Chem*. **2001**, 39, 1533.
[43] S. Sinha, C. Rothe, R. Güntner, U. Scherf, A. P. Monkman, *Phys. Rev. Lett.* **2003**, 90, 127402.
[44] S. King, C. Rothe, A. Monkman, *J. Chem. Phys.* **2004**, 121, 10803.
[45] H. D. Burrows, J. S. de Melo, C. Serpa, L. G. Arnaut, A. P. Monkman, I. Hamblett, S. Navaratnam, *J. Chem. Phys.* **2001**, 115, 9601.
[46] S. M. King, C. Rothe, D. Dai, A. P. Monkman, *J. Chem. Phys*. **2006**, 124, 234903.
[47] M. Leclerc, *J. Polym. Sci. Part A: Polym. Chem.* **2001**, 39, 2867.
[48] Y. Yang, Q. Pei, *J. Appl. Phys.* **1997**, 81, 3294.
[49] M. Kreyenschmidt, G. Klaerner, T. Fuhrer, J. Ashenhurst, S. Karg, W. D. Chen, V. Y. Lee, J. C. Scott, R. D. Miller, *Macromolecules* **1998**, 31, 1099.
[50] E. W. J. List, R. Güntner, P. Scanducci de Freitas, U. Scherf, *Adv. Mater*. **2002**, 14, 374.
[51] M. Gaal, E. J. W. List, U. Scherf, *Macromolecules* **2003**, 36, 4236.
[52] D. Sainova, T. Miteva, H. G. Nothofer, U. Scherf, I. Glowacki, J. Ulanski, H. Fujikawa, D. Neher, *Appl. Phys. Lett*. **2000**, 76, 1810.
[53] D. Marsitzky, R. Vestbery, P. Blainey, B. T. Tang, C. J. Hawker, K. R. Carter, *J. Am. Chem. Soc*. **2001**, 123, 6965.
[54] S. Setayesh, A. C. Grimsdale. T. Weil, V Enkelmann, K. Müllen, F. Meghdadi, E. J. W. List, G. Leising, *J. Am. Chem. Soc*. **2001**, 123, 946.
[55] M. R. Craig, M. M. de Kok, J. W. Hofstraat, A. P. H. J. Schenning, E. W. Meister, *J. Mater. Chem.* **2003**, 13, 2861.
[56] S. Y. Cho, A. C. Grimsdale, D. J. Jones, S. E. Watkins, A. B Holmes, *J. Am. Chem. Soc.* **2007**, 129, 11910.
[57] J. Kido, K. Hongawa, K. Okuyama, K. Nagai, *Appl. Phys. Lett*. **1994**, 64, 815.
[58] X. Gong, J. C. Ostrowski, G. C. Bazan, D. Moses, A. J. Heeger, M. S. Liu, A. K. Y. Jen, *Adv. Mater*. **2003**, 15, 45.
[59] M. Grell, D. D. C. Bradley, M. Inbasekaran, E. P. Woo, *Adv. Mater.* **1997**, 9, 798.
[60] J. Teetsov, M. A. Fox, *J. Mater. Chem*. **1999**, 9, 2117.
[61] A. C. Grimsdale, K. Müllen, *Adv. Polym. Sci.* **2008**, 212, 1.
[62] A. Henglein, *Ber. Bunsenges. Phys. Chem.* **1982**, 86, 301.
[63] A. Henglein, *Ber. Bunsenges. Phys. Chem.* **1982**, 86, 241.
[64] M. McDowell, A. E. Wright, N. I. Hammer, *Materials* **2010**, 3, 614.
[65] A. J. Nozik, *Fundamentals and Applications of Quantum-confined Structures*, Imperial College Press, London UK, **2008**, 147.
[66] S. V. Gaponenko, *Optical Properties of Semiconductor Nanocrystals*, Cambridge University Press, **1998**.
[67] L. E. Brus, *J. Chem. Phys.* **1984**, 80, 4403.
[68] C. B. Murray, D. J. Norris, M. G. Bawendi, *J. Am. Chem. Soc.* **1993**, 115, 8706.
[69] H. S. Mansur, *WIREs Nanomedicine and Nanobiotechnology* **2010**, 2, 113.

[70] D. Neß, J. Niehaus, *Semiconductor Nanoparticles-A Review*, Strem Chemicals Inc. **2011**, XXV, 2, 39.
[71] I. Medintz, E. L. Uyeda, E. R. Goodman, H. Mattousi, *Nat. Mater.* **2005**, 4, 435.
[72] C. You, A. Chompoosor, V. M. Rotello, *Nanotoday* **2007**, 2, 34.
[73] C. Kittel, *Einführung in die Festkörperphysik 12. Auflage*, Oldenbourg Verlag, München Wien, **1999**.
[74] D. V. Talapin, R. Koeppe, S. Go1tzinger, A. Kornowski, J. M. Lupton, A. L. Rogach, O. Benson, J. Feldmann, H. Weller, *Nano Lett.* **2003**, 3, 1677.
[75] R. Xie, U. Kolb, J. Li, T. Basche, A. Mews, *J. Am. Chem. Soc*. **2005**, 127, 7480.
[76] W. R. Algar, U. J. Krull, *Chem. Phys. Chem.* **2007**, 8, 561.
[77] R. A. Sperling, W. J. Parak, *Phil. Trans. R. Soc A* **2010**, 368, 1333.
[78] L. M. Liz-Marzán, M. Giersig, P. Mulvaney, *Langmuir* **1996**, 12, 4329.
[79] D. Gerion, F. Pinaud, S. C. Williams, W. J. Parak, D. Zanchet, S. Weiss, A. P. Alivisatos, *J. Phys. Chem. B* **2001**, 105, 8861.
[80] M. Ohmori, E. Matijevic, *J. Colloid Interf. Sci.* **1993**, 160, 288.
[81] B. A. Kairdolf, A. M. Smith, S. Nie, *J. Am. Chem. Soc.* **2008**, 130, 12866.
[82] T. Pellegrino, L. Manna, S. Kudera, T. Liedl, D. Koktysh, A. L. Rogach, S. Keller, J. Rädler, G. Natile, W. J. Parak, *Nanoletters* **2004**, 4, 703.
[83] M. Möller, J. P. Spatz, A. Roescher, *Adv. Mater.* **1996**, 8, 337.
[84] J. F. Berret, A. Sehgal, M. Morvan, O. Sandre, A. Vacher, M. Airiau, *J. Colloid Inter. Sci.* **2006**, 303, 315.
[85] Y. Zhang, A. Clapp, *Sensors* **2011**, 11, 11036.
[86] M. N. Rhyner, A. M. Smith, X. H. Gao, H. Mao, L. Yang, S. Nie, *Nanomed.* **2006**, 1, 2.
[87] Z. Liu, W. B. Cai, L. N. He, N. Nakayama, K. Chen, X. Sun, X. Chen, H. Dai, *Nat. Nanotechnol.* **2007**, 2, 47.
[88] U. Resch-Genger, M. Grabolle, S. Cavaliere-Jaricot, R. Nitschke, T. Nann, *Nat. Methods* **2008**, 5, 763.
[89] V. L. Colvin, M. C. Schlamp, A. P. Alivisatos, *Nature* **1994**, 370, 354.
[90] T. W. F. Chang, S. Musikhin, L. Bakueva, L. Levina, M. A. Hines, P. W. Cyr, E. H. Sargent, *Appl. Phys. Lett.* **2004**, 84, 4295.
[91] W. U. Huynh, X. G. Peng, A. P. Alivisatos, *Adv. Mater.* **1999**, 11, 923.
[92] W. U. Huynh, J. J. Dittmer, A. P. Alivisatos, *Science* **2002**, 295, 2425.
[93] S. A. McDonald, G. Konstantatos, S. G. Zhang, P. W. Cyr, E. J. D. Klem, L. Levina, E. H. Sargent, *Nat. Mater*. **2005**, 4, 138.
[94] W. J. Work, K. Horie, M. Hess, R. F. T. Stepto, *Pure Appl. Chem*. **2004**, 76, 1985.
[95] C. Sanchez, P. Gómez-Romero, *Functional Hybrid Materials*, Wiley Weinheim, **2004**.
[96] P. Reiss, E. Couderc, J. De Girolamo, A. Pron, *Nanoscale* **2011**, 3, 446.
[97] P. Judenstein, C. Sanchez, *J. Mater. Chem.* **1996**, 6, 511.
[98] B. J. Schwartz, *Annu. Rev. Phys. Chem.* **2003**, 54, 141.
[99] Y. H. Lin, C. Y. Jiang, J. Xu, Z. Q. Lin, V. V. Tsukruk, *Soft Matter* **2007**, 3, 432.
[100] J. Xu, J. Xia, S. W. Hong, Z. Q. Lin, F. Qiu, Y. L. Yang, *Phys. Rev. Lett*. **2006**, 96, 066104.
[101] D. J. Milliron, A. P. Alivisatos, C. Pitois, C. Edder, J. M. J. Frechet, *Adv. Mater.* **2003**, 15, 58.
[102] Z. Lin, *Chem. Eur. J.* **2008**, 14, 6294.
[103] A. Watt, E. Thomsen, P. Meredith, H. Rubinsztein-Dunlop, *Chem. Commun*. **2004**, 2334.
[104] N. I. Hammer, T. Emrick, M. D. Barnes, *Nanoscale Res. Lett*. **2007**, 2, 282.

[105] Y. Yuan, M. Krüger, *Polymers* **2012**, 4, 1.
[106] E. Holder, N. Tessler, A. L. Rogach, *J. Mater. Chem*. **2008**, 18, 1064.
[107] C. B. Murray, C. R. Kagan, M. G. Bawendi, *Annu. Rev. Mater. Sci*. **2000**, 30, 545.
[108] A. L. Rogach, D. V. Talapin, E. V. Shevchenko, A. Kornowski, M. Haase, H. Weller, *Adv. Funct. Mater.* **2002**, 12, 653.
[109] M. Brinkmann, J. C. Wittmann, *Adv. Mater*. **2006**, 18, 860.
[110] H. Skaff, T. Emrick, *Chem. Commun.* **2003**, 52.
[111] J. Locklin, D. Patton, S. X. Deng, A. Baba, M. Millan, R. C. Advincula, *Chem. Mater.* **2004**, 16, 5187.
[112] Y. Liu, M. Kim, Y. Wang, Y. A. Wang, X. Peng, *Langmuir* **2006**, 22, 6341.
[113] T. Ren, P. K. Mandal, W. Erker, Z. Liu, Y. Avlasevich, L. Puhl, K. Müllen, T. Basché, *J. Am. Chem. Soc.* **2008**, 130, 17242.
[114] P. Schapotschnikow, B. Hommersom, T. J. H. Vlugt, *J. Phys. Chem. C* **2009**, 113, 12690.
[115] C. Querner, P. Reiss, J. Bleuse, A. Pron, *J. Am. Chem. Soc.* **2004**, 126, 11574.
[116] B. C. Sih, M. Wolf, *J. Phys. Chem. C* **2007**, 111, 17184.
[117] G. Zotti, B. Vercelli, A. Berlin, M. Pasini, T. L. Nelson, R. D. McCullough, T. Virgili, *Chem. Mater.* **2010**, 22, 1521.
[118] P. K. Sudeep, K. T. Early, K. D. McCarthy, M. Y. Odoi, M. D. Barnes, T. Emrick, *J. Am .Chem. Soc*. **2008**, 130, 2384.
[119] K. B. Chen, M. H. Chen, S. H. Yang, C. H. Hsieh, C. S. Hsu, C. C. Chen, H. J. Chien, *J. Polym. Sci. Part A: Polym. Chem*. **2006**, 44, 5378.
[120] C. Fang, X. Y. Qi, Q. L. Fan, L. H. Wang, W. Huang, *Nanotechnology* **2007**, 18, 035704.
[121] H. Skaff, K. Sill, T. Emrick, *J. Am. Chem. Soc*. **2004**, 126, 11322.
[122] Q. Zhang, T. P. Russell, T. Emrick, *Chem. Mater*. **2007**, 19, 3712.
[123] J. Xu, J. Wang, M. Mitchell, P. Mukherjee, M. Jeffries-EL, J. W. Petrich, Z. Q. Lin, *J. Am. Chem. Soc.* **2007**, 129, 12828.
[124] J. De Girolamo, P. Reiss, A. Pron, *J. Phys. Chem. C* **2007**, 111, 14681.
[125] S. B. Wang, C. Li, G. Q. Shi, *Sol. Energy Mater. Sol. Cells* **2008**, 92, 543.
[126] A. A. Lutich, A. Poschl, G. X. Jiang, F. D. Stefani, A. S. Susha, A. L. Rogach, J. Feldmann, *Appl. Phys. Lett*. **2010**, 96, 083109.
[127] C. H. Chou, H. S. Wang, K. H. Wei, J. Y. Huang, *Adv. Funct. Mater.* **2006**, 16, 909.
[128] H. C. Liao, S. Y. Chen, D. M. Liu, *Macromolecules* **2009**, 42, 6558.
[129] X. M. Peng, L. Zhang, Y. W. Chen, F. Li, W. H. Zhou, *Appl. Surf. Sci*. **2010**, 256, 2948.
[130] A. L. Rogach, T. A. Klar, J. M. Lupton, A. Meijerink, J. Feldmann, *J. Mater. Chem.* **2009**, 19, 1208.
[131] T. Förster, *Annalen der Physik* **1948**, 2, 55.
[132] T. Förster, *Zeitschrift für Naturforschung* **1949**, 4a, 321.
[133] A. P Demchenko, *Förster Resonance Energy Transfer: Introduction to Fluorescence Sensing*, Springer, Berlin, **2008**.
[134] D. L. Dexter, *J. Chem. Phys.* **1953**, 21, 836.
[135] O. V. Mikhnenko, *Singlet and Triplet Excitons in Organic Semiconductors*, PhD Thesis, **2011**.
[136] Y. Wang, N. Herron, *J. Lumin*. **1996**, 70, 48.
[137] N. C. Greenham, X. Peng, A. P. Alivisatos, *Phys. Rev. B* **1996**, 54, 17628.
[138] A. A. Lutich, G. Jiang, A. S. Susha, A. L. Rogach, F. D. Stefani, J. Feldmann, *Nano Lett.* **2009**, 9, 2636.

[139] T. W. F. Chang, S. Musikhin, L. Bakueva, L. Levina, M. A. Hines, P. W. Cyr, E. H. Sargent, *Appl. Phys. Lett*. **2004**, 84, 4295.
[140] M. Anni, L. Manna, R. Cingolani, D. Valerini, A. Creti′, M. Lomas-Colo, *Appl. Phys. Lett*. **2004**, 85, 4169.
[141] T. Stöferle, R. F. Mahrt, *Proc. SPIE* **2009**,73930C, 7393.
[142] T. Stöferle, U. Scherf, R. F. Mahrt, *Nano Lett*. **2009**, 9, 453.
[143] J. Pecher, S. Mecking, *Chem. Rev*. **2010**, 110, 6260.
[144] K. Takamura, D. Urban, *Polymeric Dispersions and Their Industrial Applications*, Wiley-VCH, Weinheim, **2002**.
[145] D. Tuncel, H. V. Demir, *Nanoscale* **2010**, 2, 484.
[146] J. A. Champion, Y. K. Katare, S. Mitragotri, *J. Controlled Release* **2007**, 121, 3.
[147] D. Dendukuri, P. S. Doyle, *Adv. Mater.* **2009**, 21, 4071.
[148] C. Vauthier, K. Bouchemal, *Pharmaceutical Research* **2009**, 26, 1025.
[149] C. Vauthier, P. Couvreur, *Handbook of Pharmaceutical Controlled Release Technology* ed. D. L. Wise, Marcel Dekker, New York, **2000**, 413.
[150] N. Ammoury, H. Fessi, J. P. Devissaguet, F. Puisieux, S. Benita, *J. Pharm. Sci*. **1990**, 79, 763.
[151] D. Quintanar-Guerrero, É. Allémann, É. Doelker, H. Fessi, *Pharm. Res*. **1998**, 15, 1056.
[152] D. Moinard-Chécot, Y. Chevalier, S. Briançon, L. Beney, H. Fessi. *J. Colloid Interface Sci.* **2008**, 317, 458.
[153] H. Vranckx, M. Demoustier, M. Deleers, *J. Pharm. Pharmacol.* **1996**, 42, 345.
[154] M. Wohlgemuth, W. Mächtle, C. Mayer, *J. Microencapsulation* **2000**, 17, 437.
[155] K. Bouchemal, S. Briançon, H. Fessi, Y. Chevalier, I. Bonnet, E. Perrier, *Mater. Sci. Eng. C* **2006**, 26, 472.
[156] J. Edwards, R. Fisher, B. Vincent, *Macromol. Chem. Rapid Commun.* **1983**, 4, 393.
[157] R. B. Bjorklund, B. Liedberg, *J. Chem. Soc. Chem. Commun.* **1986**, 16, 1293.
[158] S. P. Armes, M. Aldissi, *J. Chem. Soc. Chem. Commun.* **1989**, 2, 88.
[159] N. Kurokawa, H. Yoshikawa, N. Hirota, K. Hyodo, H. Masuhara, *Chem. Phys. Chem.* **2004**, 5, 1609.
[160] S. J. Lee, J. M. Lee, I. W. Cheong, H. Lee, J. H. Kim, *J. Polym. Sci. Part A: Polym. Chem.* **2008**, 46, 2097.
[161] E. Hittinger, A. Kokil, C. Weder, *Angew. Chem. Int. Ed.* **2004**, 43, 1808.
[162] T. Kietzke, B. Stiller, K. Landfester, R. Montenegro, D. Neher, *Synth. Met.* **2005**, 152, 101.
[163] H. Yabu, A. Tajima, T. Higuchi, M. Shimomura, *Chem. Commun.* **2008**, 38, 4588.
[164] I. O. Huyal, T. Ozel, D. Tuncel, H. V. Demir, *Opt. Express* **2008**, 16, 13391.
[165] D. F. Evans, H. Wennerström, *The Colloidal Domain*, Wiley-VCH, Weinheim Germany, **1999**.
[166] C. Wu, C. Szymanski, J. McNeill, *Langmuir* **2006**, 22, 2956.
[167] C. Wu, C. Szymanski, Z. Cain, J. McNeill, *J. Am. Chem. Soc*. **2007**, 129, 12904.
[168] C. Wu, B. Bull, C. Szymanski, K. Christensen, J. McNeill, *ACS Nano*, **2008**, 2, 2415.
[169] Y. L. Chang, R. E. Palacios, F. R. F. Fan, A. J. Bard, P. F. Barbara, *J. Am. Chem. Soc.* **2008**, 130, 8906.
[170] C. Stubenrauch (ed.), *Microemulsions: Background, New Concepts, Applications, Perspectives*, Wiley, Chichester U.K., **2009**.
[171] A. Ethrirajan, K. Landfester, *Chem. Eur. J*. **2010**, 16, 9398.
[172] I. O. Ozel, T. Ozel, H. V. Demir, D. Tuncel, *Opt. Express* **2010**, 18, 671.

[173] K. Tada, H. Harada, M. Onoda, H. Nakayama, K. Yoshino, *Synth. Met*. **1999**, 102, 981.
[174] J. Cabanillas-Gonzalez, A. M. Fox, J. Hill, D. D. C. Bradley, *Chem. Mater*. **2004**, 16, 4705.
[175] H. V. Demir, S. Nizamoglu, T. Ozel, E. Mutlugun, I. O. Huyal, E. Sari, E. Holder, N. Tian, *N. J. Phys.* **2007**, 9, 1367.
[176] C. Wu, H. Peng, Y. Jiang, J. McNeill, *J. Phys. Chem. B* **2006**, 110, 14148.
[177] N. Cicek, S. Nizamoglu, T. Ozel, E. Mutlugun, D. U. Karatay, V. Lesnyak, T. Otto, N. Gaponik, A. Eychmüller, H. V. Demir, *Appl. Phys. Lett*. **2009**, 94, 061105.
[178] S. Saini, S. Bhowmick, V. B. Shenoy, B. Bagchi, *J. Photochem. Photobiol. Chem.* **2007**, 190, 335.

2 Aim and Scope

2.1 Motivation and Objective

Organic-inorganic composite materials on the basis of conjugated polymers as hosts and colloidal quantum dots in the guest-role combine the inherent advantages of both counterparts and can find implementation in, for instance, light-emitting, photovoltaic or sensing technologies.[1-3] Poly(fluorene)s, one of the most widely-studied classes of conjugated polymers, have due to their high stability, high purity, efficient photoluminescence and feasibility to span the color emission in the entire visible spectrum, raised as promising materials for modern and high-tech applications.[4-6] Poly(fluorene)s have already been used as hosts for semiconductor quantum dots[7-11], the acquirement of profound knowledge in terms of the electronic energy transfer processes occurring at the interface of the organic-inorganic components within the composite systems is, however, still an up-to-date affair. The understanding of these underlying transfer processes is substantial in order to optimize such composite systems with regard to their opto-electronic properties. Recently acquired data brought the complexity of the occurring mechanisms into light, demonstrating the treatment of an energy transfer anticipated as a Förster one beyond the Förster theory but by means of the electron exchange Dexter mechanism.[12] The concurrent operation of both mechanisms and their competition to the charge transfer process in organic-inorganic composites, revealed the necessity for detailed microscopic understanding of the energy transfer processes. Towards the strategy of synthesizing organic-inorganic nanocomposites, the aim of this doctoral thesis was the development of poly(fluorene)-nanocrystal composite systems and the subsequent performance of energy transfer investigations in order to gain insight in a phenomenon, which still remains a subject of extensive research. For this purpose, in addition to fabricating composites by simply mixing the synthesized fluorene-based or fluorene-and carbazole-based copolymers with inorganic quantum dots, two more sophisticated approaches, namely, the ‘grafting-from’ and the ‘microparticle’ methodology were applied as well. The blending strategy was performed with copolymers possessing amino-functionalized side-chains, which render an interconnection with nanocrystals like CdTe feasible.[13,14] On the other side, the ‘grafting-from’ approach represents an innovative but simple way in order to grow oligo(fluorene) or poly(fluorene) moieties from the surface of nanocrystals *via* a facile polymerization protocol.[15] In this case, the goal is to create a direct linkage between the two counterparts and investigate the consequence of this environmental circumstance on

the energy transfer process. Last but not least, side-chains functionalized with amphiphilic end-groups were targeted for the backbone of fluorene-based copolymers following a random or an alternating pattern. The bringing-together of the copolymers with water-stable nanocrystals forming microparticulate composites in an aqueous medium *via* a precipitation methodology would be to the best of our knowledge the first time that such systems would be reported.[16]

2.2 References

[1] V. L. Colvin, M. C. Schlamp, A. P. Alivisatos, *Nature* **1994**, 370, 354.
[2] W. U. Huynh, J. J. Dittmer, A. P. Alivisatos, *Science* **2002**, 295, 2425.
[3] C. Sanchez, B. Lebeau, *MRS Bull.* **2001**, 26, 377.
[4] J. Cornil, I. Gueli, A. Dkhissi, J. C. Sancho-Garcia, E. Hennebicq, J. P. Calbert, V. Lemaur, D. Beljonne, J. L. Brèdas, *J. Chem. Phys.* **2003**, 118, 6615.
[5] W. Y. Wong, *Coord. Chem. Rev.* **2005**, 249, 971.
[6] M. J. Park, J. Lee, J. H. Park, S. K. Lee, J. I. Lee, H. Y. Chu, D. H. Hwang, H. K. Shim, *Macromolecules* **2008**, 41, 3063.
[7] H. V. Demir, S. Nizamoglum, T. Ozel, E. Mutlugun, I. O. Huyal, E. Sari, E. Holder, N. Tian, *New J. Phys.* **2007**, 9, 362.
[8] E. Holder, N. Tessler, A. L. Rogach, *J. Mater. Chem.* **2008**, 18, 1064.
[9] A. A. Lutich, G. Jiang, A. S. Susha, A. L. Rogach, F. D. Stefani, J. Feldmann, *Nano Lett.* **2009**, 9, 2636.
[10] Z. S. Guo, L. Zhao, J. Pei, Z. L. Zhou, G. Gibson, J. Brug, S. Lam, S. S. Mao, *Macromolecules* **2010**, 43, 1860.
[11] M. Anni, E. Alemanno, A. Cretí, C. Ingrosso, A. Panniello, M. Striccoli, M. L. Curri, M. Lomascolo, *J. Phys. Chem. A* **2010**, 114, 2086.
[12] T. Stöferle, R. F. Mahrt, *Proc. SPIE* **2009**,73930C, 7393.
[13] I. Kanelidis, V. Elsner, M. Bötzer, M. Butz, V. Lesnyak, A. Eychmüller, E. Holder, *Polymer* **2010**, 51, 5669.
[14] I. Kanelidis, Y. Ren, V. Lesnyak, J. C. Gasse, R. Frahm, A. Eychmüller, E. Holder, *J. Polym. Sci. Part A: Polym. Chem.* **2011**, 49, 392.
[15] I. Kanelidis, A. Vaneski, D. Lenkeit, S. Pelz, V. Elsner, R. M. Stewart, J. Rodríguez-Fernández, A. A. Lutich, A. S. Susha, R. Theissmann, S. Adamczyk, A. L. Rogach, E. Holder, *J. Mater. Chem.* **2011**, 21, 2656.
[16] I. Kanelidis, O. Altintas, J. C. Gasse, R. Frahm, A. Eychmüller, E. Holder, *Polym. Chem.* **2011**, 2, 2597.

3 Results and Discussion

3.1 Poly(fluorene)s Containing Amino-Side-Chains

3.1.1 Poly(fluorene)s Containing Aliphatic Amino-Functionalized Side-Chains

One strategy in order to design polymers with amino-functionalized side-chains is the application of different C-C coupling reactions[1,2] utilizing side-chain functionalized comonomers in order to firstly build up the polymers' backbones. Subsequently, the performance of a post-treatment on their side-chains enables the introduction of the desired functional groups.[3-5] In this work, a Yamamoto methodology[6-8] allows the incorporation of a monomer with bromo-functionalized side-chains as building block in the backbone, giving the opportunity for the further transformation of the bromo-atoms to an amino-based group. In particular, the attachment of two 6-bromohexyl chains at the carbon-9 position of the fluorene-ring is the first step towards the synthesis of the 2,7-dibromo-9,9'-*bis*(6-bromohexyl)-9*H*-fluorene (**2**) building block and the polymer design is completed by combination of the latter with 2,7-dibromo-9,9'-dioctyl-9*H*-fluorene (**3**) and (*E*)-1,2-*bis*(4-bromophenyl)ethene (**4**). 2,7-Dibromo-9,9'-*bis*(6-bromohexyl)-9*H*-fluorene (**2**)[9] and 2,7-dibromo-9,9'-dioctyl-9*H*-fluorene (**3**)[10] were synthesized according to a base-mediated alkylation facilitated by means of a phase-transfer catalyst (PCT) using an excess of the corresponding alkyl-chain (**Scheme 3.1**). (*E*)-1,2-*Bis*(4-bromophenyl)ethene (**4**)[11] was achieved by applying a McMurry reaction using 4-bromobenzaldehyde as starting material in the presence of $TiCl_4$ and zinc as reducing agent. The *E*-isomer was isolated after recrystallization from ethyl acetate (**Scheme 3.1**).

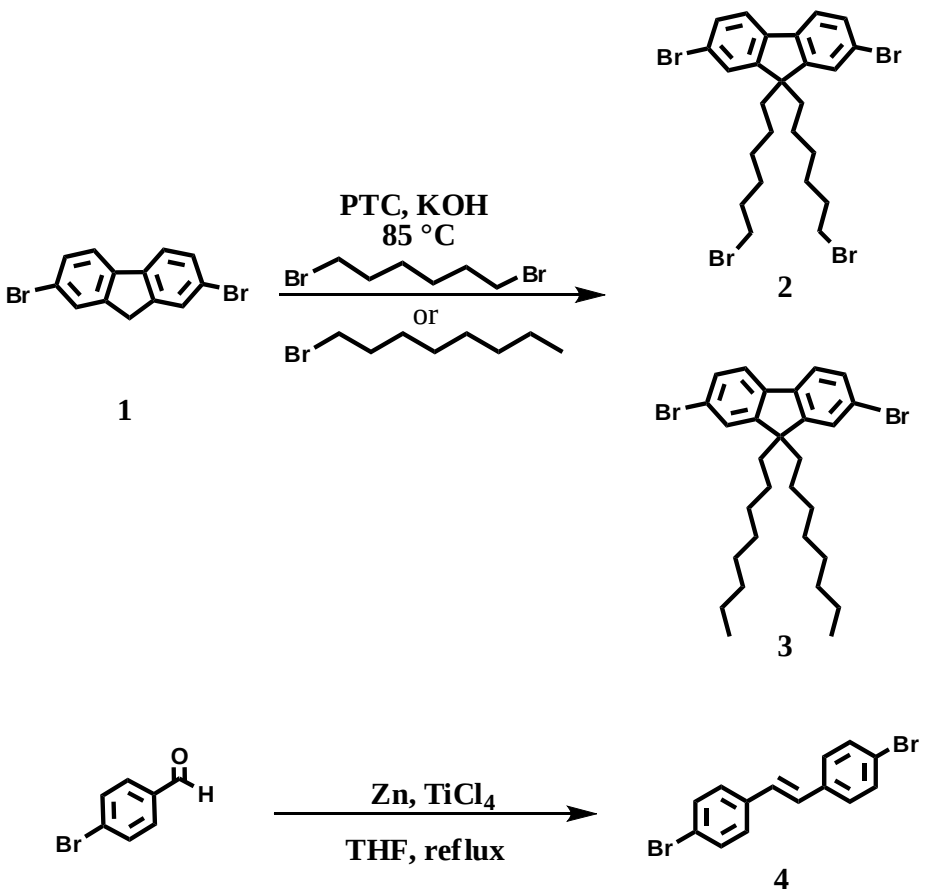

Scheme 3.1: Synthesis of 2,7-dibromo-9,9'-*bis*(6-bromohexyl)-9*H*-fluorene (**2**), 2,7-dibromo-9,9'-dioctyl-9*H*-fluorene (**3**) and (*E*)-1,2-*bis*(4-bromophenyl)ethene (**4**).

The monomers were fully characterized by means of NMR-, IR-, UV-, fluorescence-spectroscopy and mass spectrometry. The successful alkylation of comonomer **2** is confirmed by the pattern of the six methylene (-CH_2-) signals appearing at the ^{1}H-NMR spectrum (**Figure 3.1a**). The 3.29 ppm signal can be clearly assigned to the protons attached on the carbon connected to the bromo-atom. The five high-field shifted peaks observed at 0.56-1.95 ppm represent the five methylene-groups of the hexyl side-chains and as expected exhibit perfect integrations of two protons each. Detailed analytics of compounds **2-4** are available in the experimental part. As the scope of this work was the post-treatment of precursor polymers with bromo-functionalized side-chains, it was plausible to firstly try the success of such a reaction on monomer 2,7-dibromo-9,9'-*bis*(6-bromohexyl)-9*H*-fluorene (**2**), which when incorporated in the polymer backbone should be subjected to the same transformation reaction, as well. Thus, 2,7-dibromo-9,9'-*bis*(6-bromohexyl)-9*H*-fluorene (**2**) participated in a substitution reaction using di-*n*-propylamine as the nucleophile, whereby 6,6'-(2,7-dibromo-9*H*-fluorene-9,9'-diyl)*bis*(*N*,*N*'-dipropylhexan-1-amine) (**5**) was obtained in a 91% yield[12] (**Scheme 3.2**).

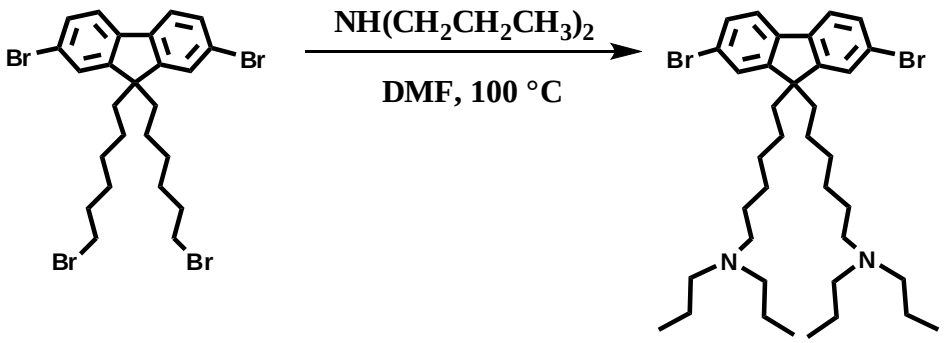

2 **5**

Scheme 3.2: Synthesis of 6,6'-(2,7-dibromo-9*H*-fluorene-9,9'-diyl)*bis*(*N,N'*-dipropylhexan-1-amine) (**5**).

^{1}H-NMR spectroscopy (**Figure 3.1b**) reveals a high-field shift (from 3.29 ppm to 2.91 ppm) of the protons, which now belong to a carbon with a nitrogen-atom attached on it. The resonances of these protons were found to overlap with the protons of two methylene-groups of the di-*n*-propylamine moiety ($CH_3CH_2C\boldsymbol{H_2}NHC\boldsymbol{H_2}CH_2CH_3$) directly linked to the nitrogen-atom. Moreover, the remaining methylene- and methyl-groups of di-*n*-propylamine ($C\boldsymbol{H_3}C\boldsymbol{H_2}CH_2NHCH_2C\boldsymbol{H_2}C\boldsymbol{H_3}$) provide an abundance of peaks in the aliphatic region compared to the forerunner compound **2**.

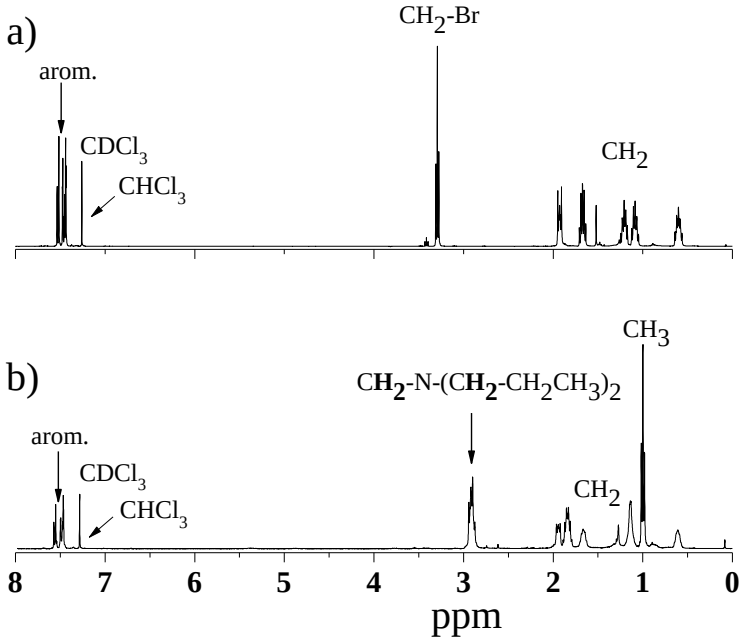

Figure 3.1: ^{1}H-NMR spectra of (a) bromo-functionalized compound **2** and (b) amino-functionalized derivative **5**. All spectra were recorded in $CDCl_3$.

Based on compounds **2**, **3** and **4** as building blocks and by applying a nickel(0)-catalyzed polycondensation, fluorene-based copolymers **P1a** and **P1b** with bromo-functional end-groups on their side-chains were synthesized, using different monomer feed ratios. Polymerizations were conducted in THF by means of $Ni(COD)_2$ as catalyst and 2,2´-bipyridine as the organometallic counterpart (**Scheme 3.3**). Building blocks **2**, **3** and **4** were used in proportions of 40:10:50% for polymer **P1a** and 35:15:50% in the case of polymer **P1b**. A reference polymer **Pref** comprising a 50:50% ratio of comonomers **2** and **4** was synthesized, as well. All polymers were extracted in ethanol by means of Soxhlet extractor in order to gain unimodal molecular weight distributions. The polymers' purification led to yields of 30% for the yellow solids, which were well-soluble in solvents of medium polarity like toluene, chloroform or dichloromethane. The moderate yields are a consequence of the complexity of the polymer backbone and the solubility provided through the side-chain functionalities, not disregarding the exhaustive purification steps of the polymers *via* several precipitations and/or extraction.[13,14] The post-functionalization was conducted in a 1:1 THF/DMF mixture at 85 °C reaction temperature by addition of di-*n*-propylamine at 0 °C and precipitation of the polymers from acetone. All polymers were fully characterized (see Experimental Section) and the successful incorporation of the bromo-ended side-chains could be monitored by means of ^{1}H-NMR spectroscopy, while the success of the post-functionalization was verified by elemental analysis. The ^{1}H-NMR spectra of the precursor polymers **P1a**-**b** showed a broadened peak pattern typical for polymers and the resonance at 3.31 ppm was indicative for the integration of 2,7-dibromo-9,9'-*bis*(6-bromohexyl)-9*H*-fluorene **2** in both polymer backbones. The substitution reaction of the bromo-atoms resulted in an effective post-functionalization of the 6-bromohexyl-chains with the di-*n*-propylamine group. For the obtained polymers **P2a** and **P2b** a signal assigned to the protons of the carbons linked to the nitrogen is not as pronounced as in the case of their forerunners and thus success of the post-functionalization was confirmed utilizing elemental analysis in order to detect the existence of nitrogen in the backbone. A nitrogen content of 8.3% and 9% was determined for polymers **P2a**-**b**, respectively and the successful post-functionalization was once more supported by the vibrational bands detected at 2050 cm^{-1} and 2348 cm^{-1} in the infrared spectra, assigned to the stretching vibration of positively charged quaternary ammonium ions. The aforementioned cations are probably accessible through the quaternization process of the tertiary amine di-*n*-propylamine, when combined with the long 6-bromohexyl-chains of the precursor polymers during the performance of the substitution reaction.

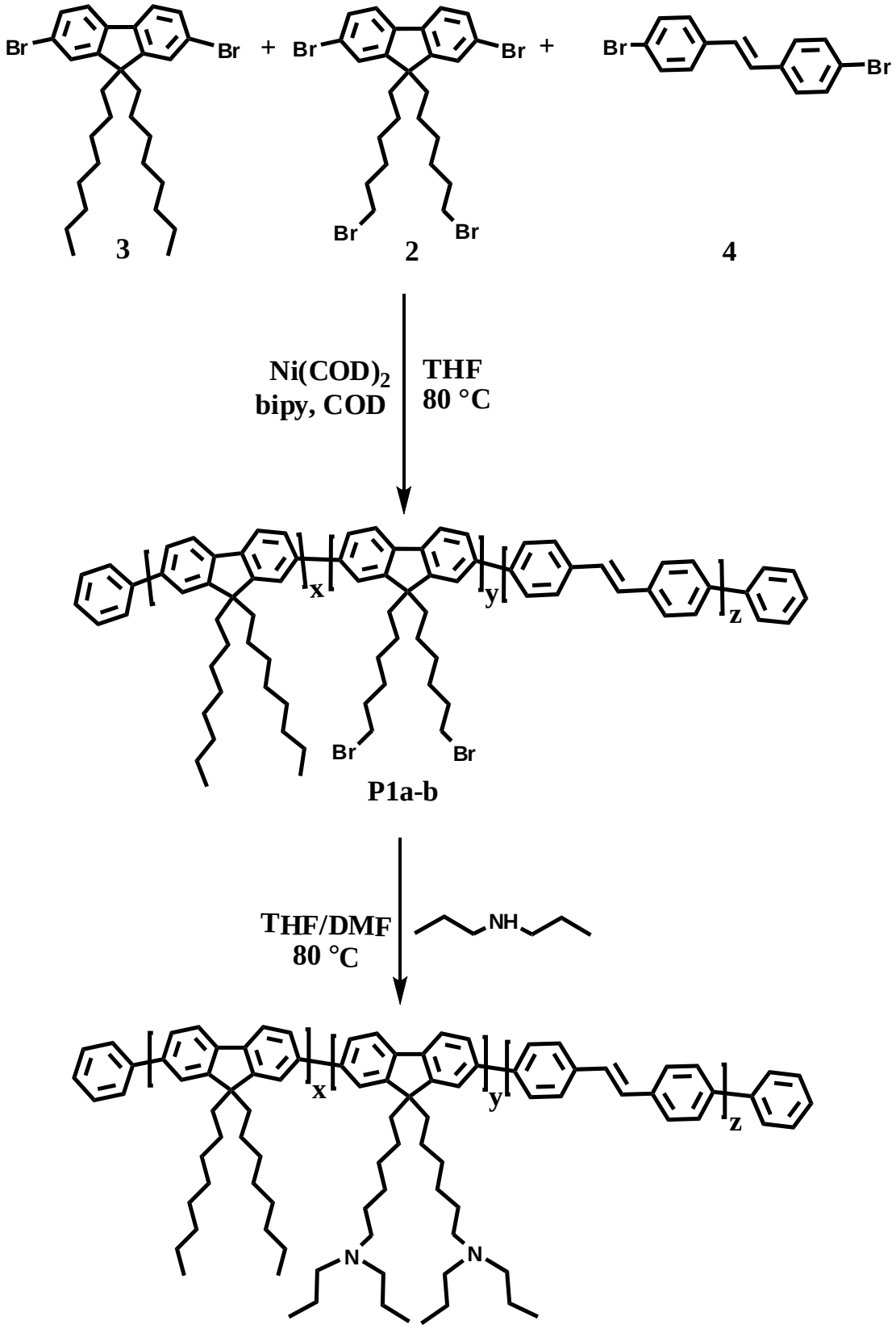

Scheme 3.3: Synthetic route of the bromo side-chain functionalized precursor polymers **P1a-b** and their amino side-chain post-functionalized successors **P2a-b**.

Determination of the molecular weights of all achieved compounds certified their polymeric nature and their homogeneity through the unimodal molecular weight distributions. Gel permeation chromatography analysis (GPC) detected weight average molecular weights (M_w) of the magnitude of 18000 g/mol for the precursors with polydisperities (PDI) of 2.49 for **P1a** and 2.75 for **P1b**. For the amino-functional polymers, molecular weights of 9000 g/mol were determined, while the PDI values were 2.28 and 1.90 for polymers **P2a** and **P2b**, correspondingly. The by-half reduced M_w values could most probably be assigned to the differentiation of the solubility behavior between precursor and final polymers assigned to the di-*n*-propylamine group, which through its increased polarity allows the dissolution of the higher molecular weight fractions upon precipitation from polar acetone.[5] Nevertheless, acetone seems to be the optimal work-up medium for the amine-functionalized copolymers as change to a more polar medium like methanol led to extremely reduced yields (10%). The optical properties of all polymers were investigated in solution and solid-state revealing blue-light emission and are detailed illustrated in **Table 3.1**.

Table 3.1: Optical properties of the copolymers **P1a-b**, **P2a-b** and **Pref** in $CHCl_3$ solutions and in thin films.

Polymers	**Abs_{sol}**[a)] **(log ε)** ——— [nm] ([L × mol^{-1} × cm^{-1}])	**Abs_{film}** ——— [nm]	**Em_{sol}**[a);b)] ——— [nm]	**Em_{film}**[b)] ——— [nm]	**Eg_{sol}**[a);c)] ——— [eV]	**Eg_{film}**[c)] ——— [eV]	**Φ_{sol}**[a);d)] ———
P1a	382 (5.86)	400	432/455	451/477	2.88	2.42	0.60
P1b	388 (5.80)	397	435/458	451/480	2.85	2.41	0.55
P2a	388 (5.39)	397	434/456	451/479	2.84	2.70	0.77
P2b	388 (5.37)	398	434/458	449/478	2.84	2.69	0.78
Pref	391 (6.06)	401	434/461	451/477	2.89	2.71	0.59

[a)]in chloroform solution (10^{-7} mol/L); [b)]$\lambda_{exc.}$ 390 nm; [c)]calculated from the absorption band-edge; [d)]determined according to Demas and Crosby[15] using **PF8** (Φ_{sol} 0.45)[16] as a reference. Note in literature, the Φ values for **PF8** vary over a wide range[17,18] also depending on the structural features of the investigated copolymer.[4,16]

As can be seen in **Figure 3.2a**, a red shift of 6 nm differentiates copolymer **P1a** from **P1b** regarding their absorption, while 3 nm is their discrepancy in terms of emission maxima.

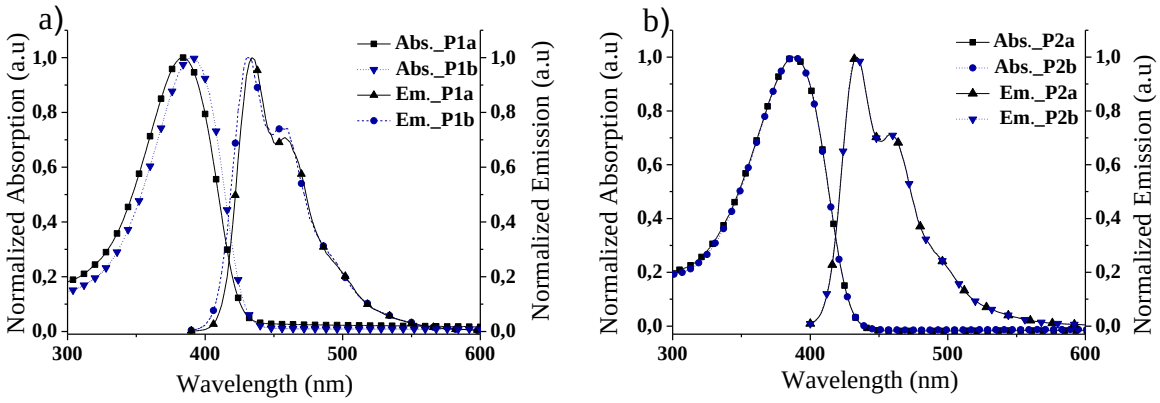

Figure 3.2: (a) Normalized absorption and emission spectra of copolymers **P1a** (black lines) and **P2b** (blue lines) in solution (chloroform, 10^{-7} mol/L). (b) Normalized absorption and emission spectra of copolymers **P2a** (black lines) and **P2b** (blue lines) in solution (chloroform, 10^{-7} mol/L).

The plots of the absorption and emission spectra of the post-functionalized polymers **P2a-b** exhibit an extreme coincidence (**Figure 3.2b**). The amino-functional polymers **P2a-b** possess quantum yield efficiencies of 0.77 and 0.78, correspondingly. These values increased compared to their forerunners. Their optical band-gaps (2.70 & 2.69) calculated from the absorption band-edge in films are enhanced compared to the precursors (2.42 & 2.41) but have similar values to the precursors in chloroform solutions (~2.84). The wide band-gap polymers **P2a-b** can become host candidates of low band-gap compounds such as semiconductor nanocrystals (NCs), while their amino-functionalities can create links on the surface of the NCs. The polymer-nanocrystal systems include except of **P2a-b** as the polymers, CdTe nanocrystals as the low band-gap compounds and the potential energy transfer behaviour of the systems was investigated and detailed reported in section **4.2.1**.

3.1.2 Poly(fluorene)s and Poly(carbazole)s Containing Arylamino-Functionalized Side-Chains

The 9-position in the fluorene and carbazole fused aromatic rings offers the opportunity to prepare monomers with bulky aryl-substituents. Incorporation of such monomers in the polymer backbone can help to overcome structural decomposition due to oxidation when heating is applied in the solid-state[19] and circumvent *inter*chain interactions thereby improving the polymer opto-electronic properties.[20-22] Triarylamine, a hole transporting chromophore, and aniline, which is a primary amine, are the two bulky substituents applied in

the here described poly(fluorene)s and poly(carbazole)s, synthesized by means of the palladium-mediated Suzuki cross-coupling reaction.[23] Four alternating copolymers were the result of the close collaboration with student Yi Ren. For the design of the fluorene-based copolymers, 4,4'-(2,7-dibromo-9*H*-fluorene-9,9'-diyl)dianiline **7** and 4,4'-(2,7-dibromo-9*H*-fluorene-9,9'-diyl)*bis*(*N,N'*-diphenylaniline) **8** were used as the monomers, while the poly(carbazole)s were based on 4-(3,6-dibromo-9*H*-carbazol-9-yl)aniline **10** and 4-(3,6-dibromo-9*H*-carbazol-9-yl)-*N,N'*-diphenylaniline **12** as monomers. The synthetic approaches of the aforementioned monomers, which in all four polymerizations were combined with comonomer 2,2'-(9,9'-dioctyl-9*H*-fluorene-2,7-diyl)*bis*(1,3,2-dioxaborinane) **DFB** are illustrated in **Scheme 3.4**.

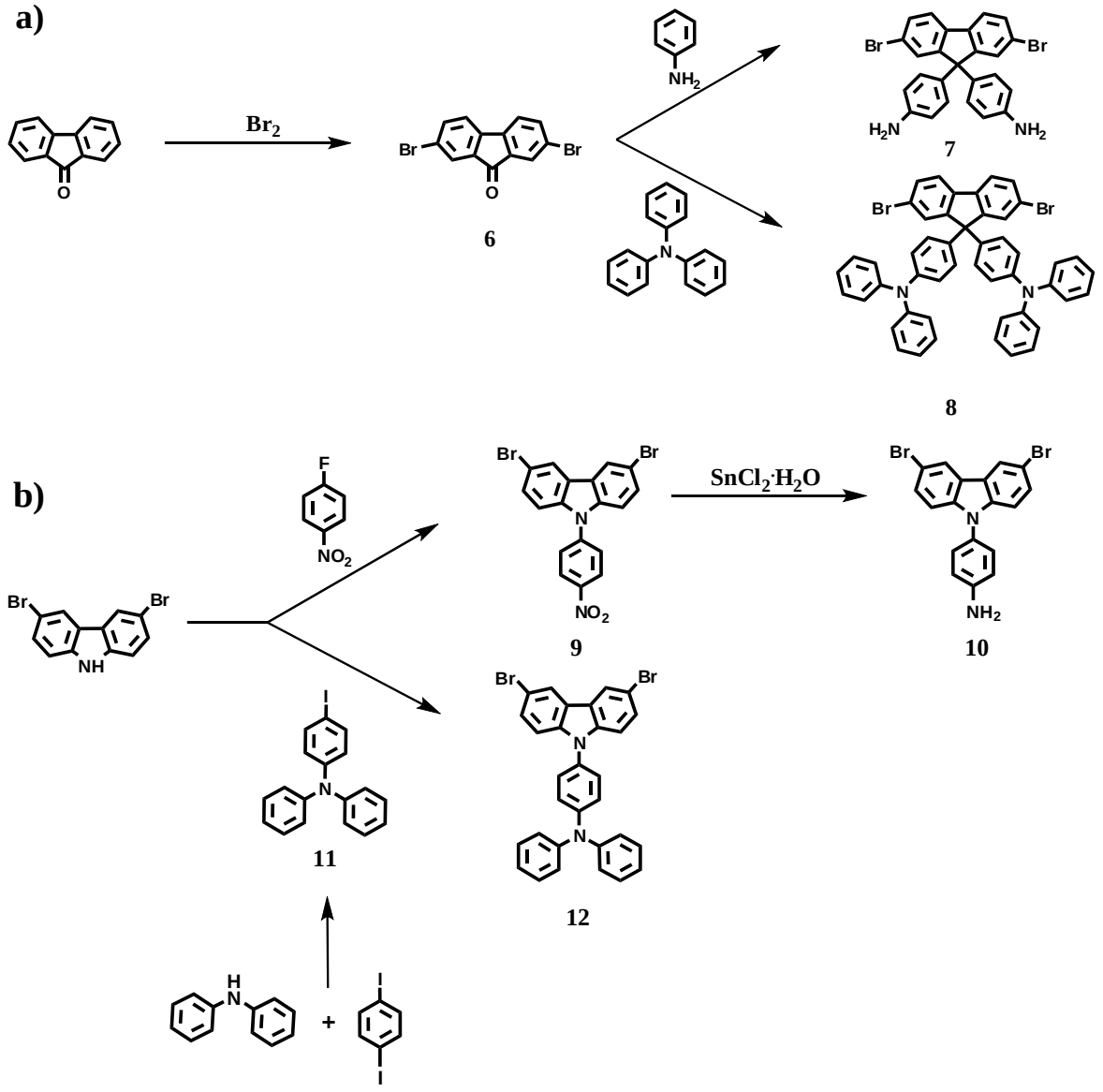

Scheme 3.4: The synthetic routes of (a) the fluorene-based monomers **7** and **8** and (b) the respective carbazole-based compounds **10** and **12**.

4,4'-(2,7-Dibromo-9*H*-fluorene-9,9'-diyl)*bis*(*N,N′*-diphenylaniline) **7** was synthesized by introducing two aniline-groups in the 9-position of 2,7-dibromo-9*H*-fluoren-9-one **6** through a condensation reaction using excess of the phenylamine.[24] A similar procedure facilitated by means of the methane sulfonic acid was utilized in case of the second fluorene-based arylamine namely 4-(2,7-dibromo-9*H*-fluorene-9,9'-diyl)*bis*(*N,N′*-diphenylaniline) **8**.[25] The basis for the fabrication of the corresponding carbazole monomers was 3,6-dibromo-9*H*-carbazole. The educt was subjected to a nucleophilic substitution upon addition of 1-fluoro-4-nitrobenzene in the presence of potassium carbonate giving compound **9**, which reduction by means of tin(II) chloride allowed the acquirement of 4-(3,6-dibromo-9*H*-carbazol-9-yl)aniline **10** as yellow crystalline solid.[26,27] An Ullman coupling reaction of educt 3,6-dibromo-9*H*-carbazole with 4-iodo-*N,N′*-diphenylaniline **11** in the presence of copper(I) iodide and [18]-crown-6 led to the desired 4-(3,6-dibromo-9*H*-carbazol-9-yl)-*N,N′*-diphenylaniline **12**.[28] Precursor 4-iodo-*N,N′*-diphenylaniline **11** was synthesized by means of an Ullmann reaction as well, coupling diphenylamine and 1,4-diiodobenzene under the presence of copper(II) sulfate and potassium carbonate at a reaction temperature of 220 °C.[29] The monomers were fully characterized by means of ^{1}H-, ^{13}C-, IR-, mass-, UV-, fluorescence-spectroscopy and elemental analysis. All analytical data and yields are listed in the Experimental Section. Using the above-mentioned compounds as building blocks and combining them with comonomer 2,2'-(9,9'-dioctyl-9*H*-fluorene-2,7-diyl)*bis*(1,3,2-dioxaborinane) **DFB**, four alternating copolymers were synthesized applying a Suzuki polymerization protocol.[30] **Scheme 3.5** shows illustratively the achieved polymers under the palladium(0)-catalyzed reaction conditions using *tetrakis*(triphenylphosphine)palladium(0) as catalyst, a water solution of K_2CO_3 of 2M concentration as base and refluxing toluene as the reaction medium.

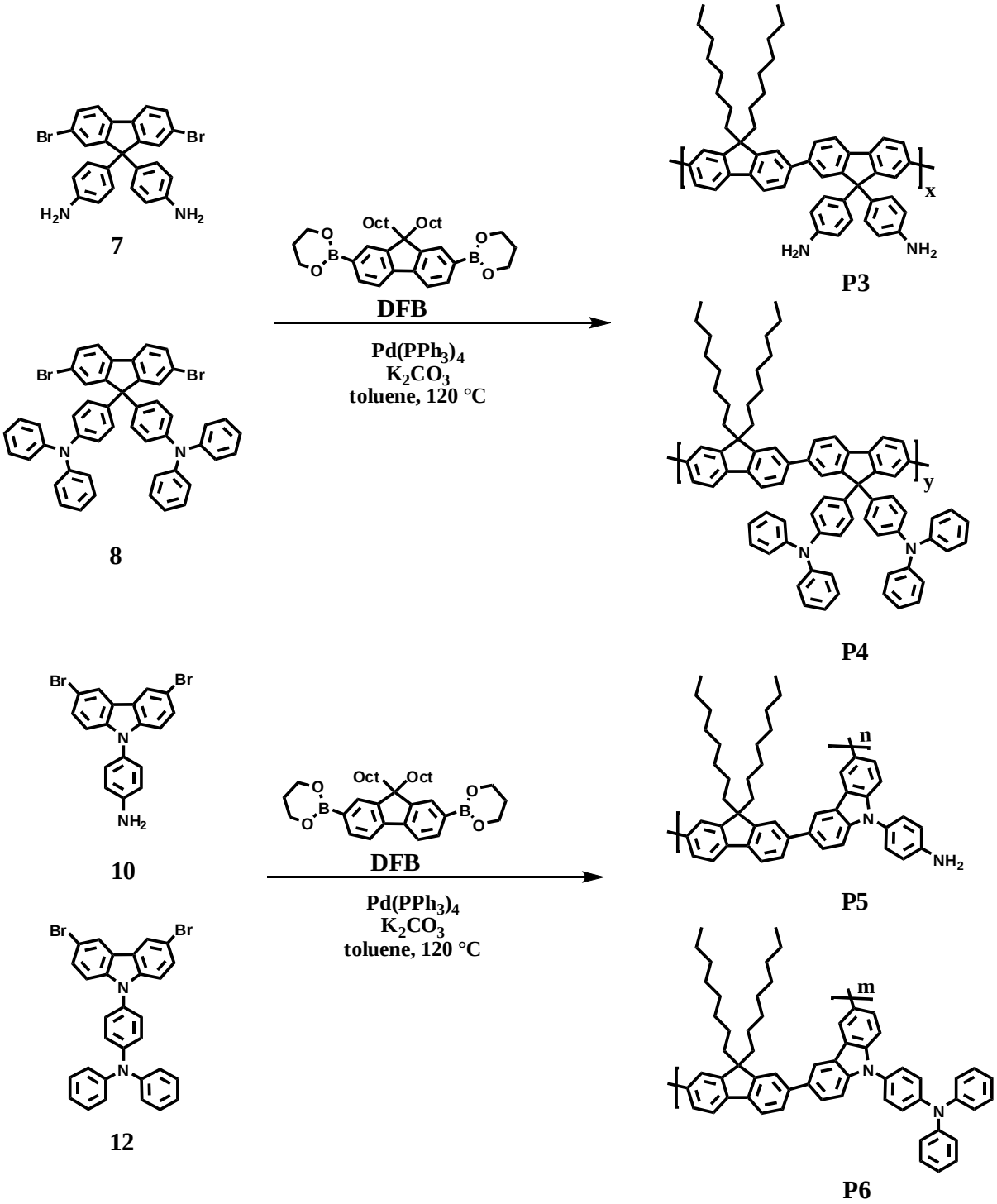

Scheme 3.5: Synthesis of the alternating arylamino-functionalized poly(fluorene)s **P3**, **P4** (upper) and their poly(carbazole) analogues **P5**, **P6** (below) prepared under Suzuki step-growth reaction conditions.

After firstly precipitating the polymers from methanol, the solids were further purified by extracting them with *iso*propanol and chloroform over a period of 3 days by means of a Soxhlet-apparatus. The chloroform fraction was once more precipitated from mixtures of methanol/ethyl acetate, methanol/tetrahydrofuran or acetone and these laborious purification

procedures resulted in yields of 30-36% for the yellowish solids with unimodal molecular weight distributions and solubility in solvents of medium polarity like toluene, chloroform or dichloromethane. Moderate yields are not an uncommon occasion in fluorene-based backbones and fluorene-carbazole systems furnished with bulky side-chains.[31-33]

Characterization of the copolymers by ^{1}H-NMR spectroscopy revealed the incorporation of comonomers **7** and **10** in the polymer structures as the resonance of the protons attached to their nitrogen-atoms appeared at 3.62 ppm for polymer **P3** and 3.94 ppm for polymer **P5**. As polymers **P4** and **P6** embrace building blocks with tertiary amines such a proton alignment is excluded and elemental analysis is now evidencing the successful coupling. For copolymer **P4** the nitrogen content amounts to 2.55%, while for copolymer **P6** elemental analysis showed an N-content of 3.09% elucidating once more the successful copolymerization. In order to prove the coincidence of the 1:1 comonomer feed ratio to the experimentally-incorporated one, NMR spectroscopy and elemental analysis were applied and compared to each other. The calculations performed by means of these two methodologies showed a preference for one repeating unit more regarding the **DFB** building block. Thus, the experimentally incorporated monomer ratio deviates from the exact 1:1 theoretical stoichiometry, with an excess of comonomer **DFB** compared to the values obtained for monomers **7**, **8**, **10** and **12** being in all cases available in the respective copolymers backbone **P3-P6**. The comparison between the two methodologies is listed in **Table 3.2**.

Table 3.2: Ratio of the monomers **7**,**8**,**10**,**12** to **DFB** in the polymer backbones according to NMR- and elemental analysis-based calculations, GPC characterization of **P3-P6** and their thermal properties.

Polymer	**Monomer ratio** (7,8,10,12/DFB) (molar %)		**M_n** ($g \times mol^{-1}$)	**M_w** ($g \times mol^{-1}$)	**PDI** Units	**$T_{d5\%}$** [c)] (°C)	**T_g** (°C)
P3	46/54[a)]	46/54[b)]	5700	17300	3.0	420	-
P4	48/52[a)]	47/53[b)]	5500	12900	2.4	440	150
P5	46/54[a)]	45/55[b)]	2900	5300	1.8	420	-
P6	46/54[a)]	46/54[b)]	2900	5300	1.8	420	128

[a)]calculated from ^{1}H-NMR; [b)]calculated from elemental analysis; [c)]@ 5% weight loss.

Moreover, polymers were investigated by means of gel permeation chromatography (**Table 3.2**), whereby their molecular weight distributions can be seen in **Figure 3.3**.

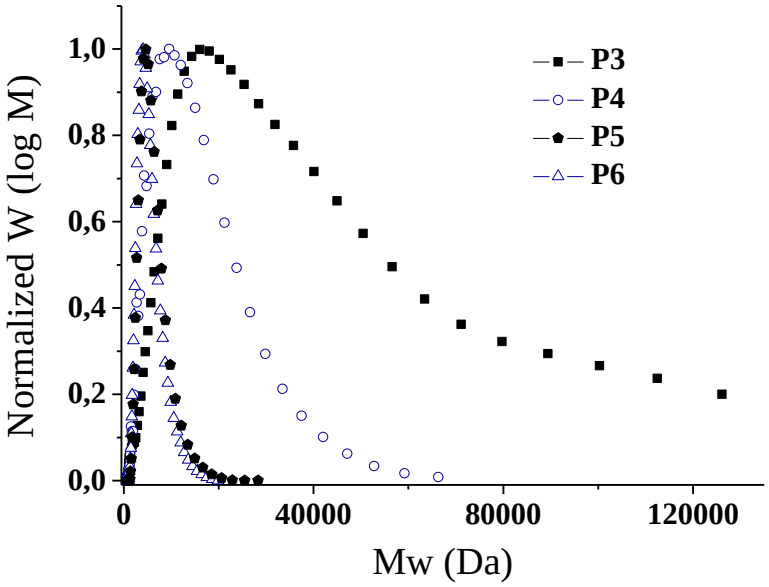

Figure 3.3: Molecular weight distributions of polymers **P3-P6** determined by gel permeation chromatography.

Carbazole monomers, when used as building blocks for polymer backbones, exhibit the tendency to impair the solubility of the coming-out polymers depending on the nature of the substituent attached on the carbazolic nitrogen.[34] Thus, the by-half reduced molecular weights of carbazole-based polymers **P5**, **P6** are not unusual, as literature research proves[32,35] and are influenced by the Suzuki-mediated reaction conditions as well.[8,32] Even preparation of homo-poly(carbazole)s is not excluded from this tendency.[36] A further aspect, which must be considered is that the precipitation of the polymers from acetone can induce a loss of high molecular weight fraction due to solubility matters.[5] Nevertheless, acetone seems to be the appropriate precipitation medium for amine-functionalized polymers as alcohol-based media like methanol reduce the acquired yields drastically even below 10%, due to the alcohol-solubility of the amino-functional side-chains.[37] Despite the moderate molecular weights, the polydispersities (PDI) of the polymers (**Table 3.2**) and their molecular weight distributions (**Figure 3.3**) argue for the homogeneity of the final macrocompounds. The thermal behaviour of the polymers is given in terms of 5% weight loss temperature (T_d) and glass temperature (T_g). As can be seen in **Table 3.2**, all four polymers exhibited propitious thermal stabilities indicated by T_d values @ 5% weight-loss of 420 °C or even higher, enabling their thin film processing from high boiling-point solvents. However, only for polymers **P4** and **P6** a glass transition temperature could be detected. In particular, polymer **P4** with the highest T_d (440 °C) and T_g (150 °C) values should be classified as the

material with the better long-term thermal stability. The characterization of the polymers was complemented by investigating their optical properties in solution and films. **Figure 3.4** illustrates the normalized absorption and emission spectra of the polymers, while **Table 3.3** gives an all-round overview of their absorption and emission maxima, their band-gap values and quantum efficiency yields. All of them exhibit blue-light emission with a red shift of about 5-12 nm for the solid-state experiments.

Table 3.3: Optical properties of copolymers **P3**-**P6**.

Polymer	**Abs_{sol}**[a] (nm) **log ε** ([L × mol^{-1} × cm^{-1}])	**Abs_{film}** (nm)	**Em_{sol}**[a;b] (nm)	**Em_{film}**[b] (nm)	**Eg_{sol}**[a;c] (eV)	**Eg_{film}**[c] (eV)	**Φ_{sol}**[a;d]
P3	385 (6.28)	387	418/442	424/448	2.93	2.84	0.32
P4	381 (6.34)	395	416/441	428/447	2.94	2.71	0.66
P5	343 (6.68)	350	401/420	411/425	3.10	2.76	0.84
P6	341 (6.10)	358	404/420	409/426	3.07	2.72	0.51

[a]in chloroform solution (10^{-6} mol/L); [b]$\lambda_{exc.}$ 380 nm for **P3**/**P4**, 360 nm for **P5**/**P6**; [c]calculated from the absorption band-edge; [d]determined according to Demas and Crosby by using **PF8** (Φ_{sol} 0.71) as a reference.[15,18]

The carbazole-based polymers **P5** and **P6** exhibited, as expected, wider band-gaps in solution (3.07 and 3.10 eV) compared to their fluorene analogues (2.93 and 2.94 eV) as the carbazole unit can raise the highest occupied molecular orbital (HOMO) energy level of the polymers.[38] In thin films, a slight reduction of the band-gaps was observed (2.71 to 2.84 eV). The wide band-gaps of the polymers can make them useful as hosts for low band-gap compounds like nanocrystals.[39] A further prerequisite, when quantum dots come into play is their spectral overlap with the corresponding polymers. CdTe nanocrystals having different emission maxima (see section **4.2.2**) possessing, however, absorption maxima, which overlap with the emission patterns of the polymers can be deployed for this purpose. Fulfilling the basic preconditions for energy transfer from the polymer backbones to the NC, solid-state measurements of the optical properties of bare NCs, polymers and NC-polymer systems were conducted and the results are detailed explained in the '**Energy and Electron Transfer Studies'** Section.

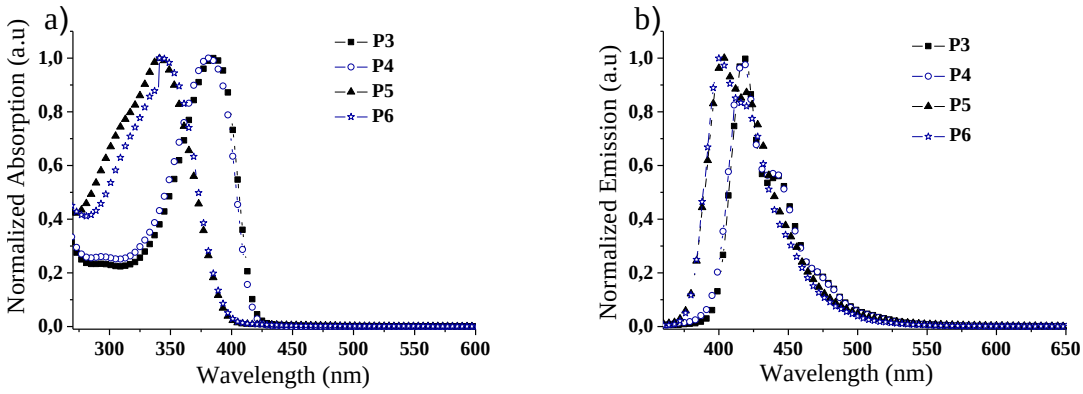

Figure 3.4: Normalized absorption (a) and emission (b) spectra of copolymers **P3-P6** in solution (chloroform, 10^{-6} mol/L).

In a final characterization step, the polymers' morphology was investigated by means of atomic force microscopy in the tapping mode. **Figure 3.5** shows the images of the four polymers, whereby the big spots of 5-16 µm in size are most probably induced by a dewetting process, while the smaller polymer spots are in the scale of 0.8-2 µm. The tailing of the latter and their repeating structures is assigned to artifacts arising due to material dragged from the cantilever over the scanned surface.

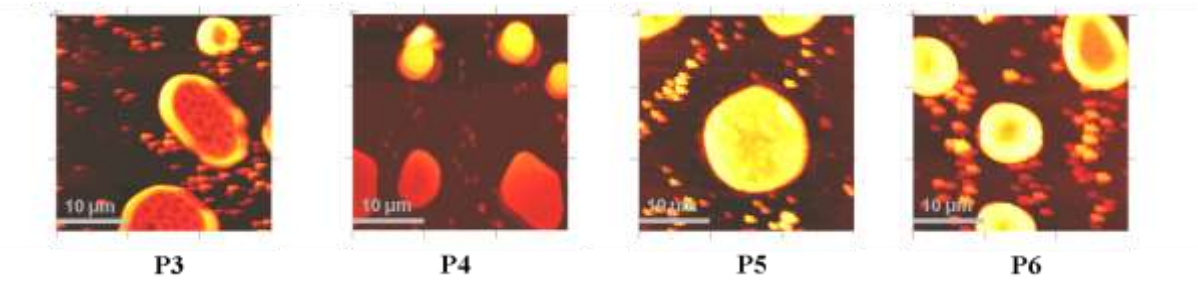

Figure 3.5: AFM images (tapping mode) of films of polymers **P3-P6** (concentrations of 0.5 mg/mL in THF) prepared on glass substrates by drop-casting. The AFM images have a scale of 30 × 30 µm.

3.2 Poly(fluorene)-CdSe Hybrids

The introduction of organic and inorganic components in hybrid structures is a new trend in material's design. The 'grafting-on' and 'grafting-from' procedures offer synthetic pathways towards this class of compounds. The former methodology renders possible the direct interconnection of pre-planned polymers like poly(thiophene)s with quantum dots[40], while the 'grafting-from' technique allows the growth of individual polymer chains such as

poly(*para*-phenylene vinylene)[41] or P3HT[42] from pre-designed and functionalized nanocrystals like CdSe. In this work, poly(fluorene) chains of different length were grafted from the surface of luminescent semiconductor CdSe nanocrystals. For this purpose an amino-functionalized fluorene ligand was synthesized[43,44] in order to be directly utilized at the synthesis stage of the CdSe nanocrystals and subsequently used as building block in a facile Yamamoto-mediated polymerization protocol obtaining two different kinds of inorganic-organic nanocomposites with varying fluorene chain-lengths. The desired amino-functionalized fluorene ligand **14** was synthesized by applying a typical Gabriel reaction[44] using 2,7-dibromo-9,9'-*bis*(6-bromohexyl)-9*H*-fluorene **2** as starting material (**Scheme 3.6**). Final product **14** and intermediate 2,2'-(6,6'-(2,7-dibromo-9*H*-fluorene-9,9'-diyl)*bis*(hexane-6,1-diyl))diisoindoline-1,3-dione **13** were fully characterized by means of ^{1}H-, ^{13}C-, IR-, UV-, fluorescence-spectroscopy, mass-spectrometry and elemental analysis.

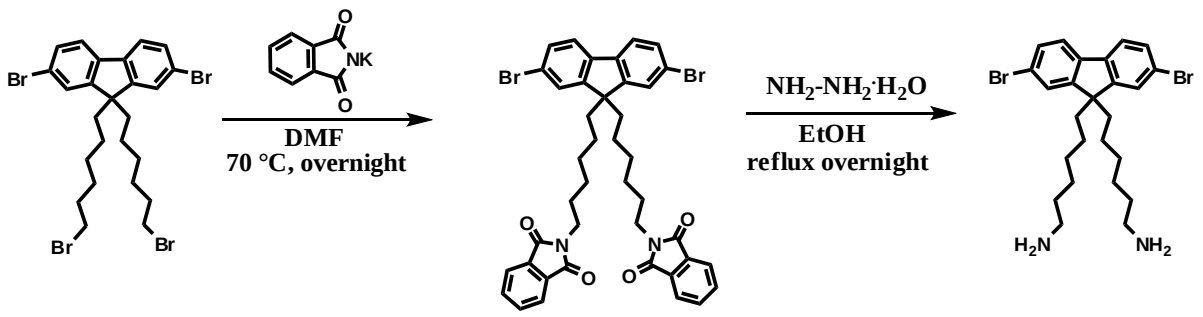

2 **13** **14**

Scheme 3.6: Synthesis of 6,6'-(2,7-dibromo-9*H*-fluorene-9,9'-diyl)dihexan-1-amine **14** by a Gabriel protocol *via* intermediate 2,2'-(6,6'-(2,7-dibromo-9*H*-fluorene-9,9'-diyl)*bis*(hexane-6,1-diyl))diisoindoline-1,3-dione **13**.

The next step was carried out by Alexander Vaneski in the group of Dr. Andrey Rogach in the Department for Physics and Center for Nanoscience at the Maximilian University of Munich, whereby compound **14** was introduced as co-ligand in order to synthesize CdSe nanocrystals allowing thus their surface functionalization and yielding the amino-fluorene modified CdSe nanocomposite **1** (**NC1**). As a reference, CdSe nanocrystals that have been surface endcapped with *n*-hexadecylamine and tetradecylphosphonic acid (**CdSe$_{ref}$**) were prepared as well, following the same synthetic approach.[41] Weakly bound surface ligands have been removed by dissolving CdSe **NC1s** and **CdSe$_{ref}$** in toluene followed by several precipitations from methanol. The two differently functionalized CdSe nanocrystals are depicted in **Figure 3.6**. The size comparison on the basis of the absorption spectra using the sizing curve of reference

[45] shows nanocrystals of 3.5 nm for **NC1** after heating for 5 min and nanocrystals of 4.8 nm for **CdSe$_{ref}$** after only 3 min reaction-time implying a slow-down of the growth kinetics, when the amino-functionalized fluorene ligand **14** is introduced in the synthesis of the CdSe NCs.

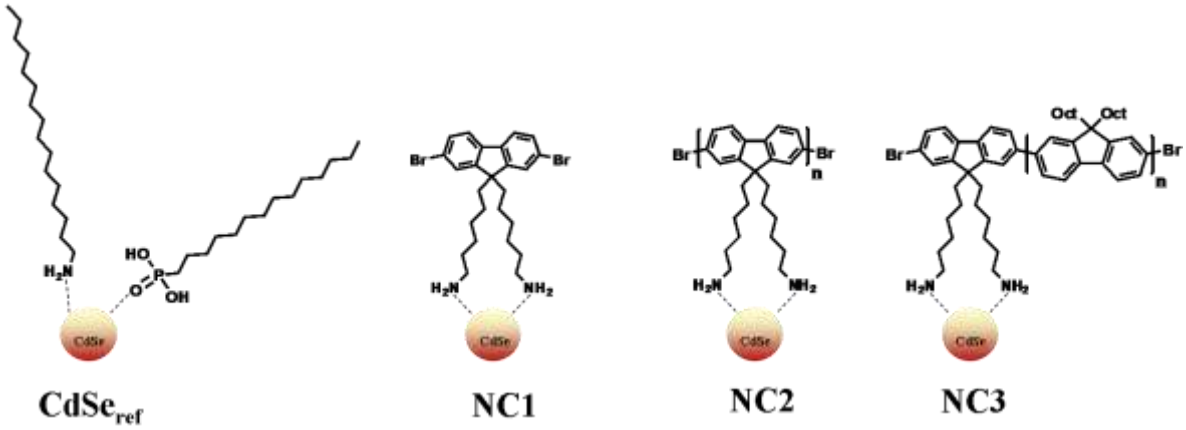

Figure 3.6: The reference CdSe NCs endcapped with *n*-hexadecylamine and tetradecylphosphonic acid (**CdSe$_{ref}$**) and the amino-fluorene modified CdSe NCs (**NC1**). **NC1** was used for the synthesis of CdSe-oligo(fluorene) nanocomposite **NC2** and CdSe-poly(fluorene) nanocomposite **NC3**.

The amino-fluorene modified CdSe nanocrystals were applied in a facile nickel(0)-mediated Yamamoto protocol[7] as single monomer in order to obtain an oligo(fluorene)-functionalized CdSe nanocrystal surface (**NC2**) or as comonomer together with 2,7-dibromo-9,9'-dioctyl-9*H*-fluorene, whereby longer chain-growth at the surface of CdSe NCs is induced (**NC3**). The visualization of the two aforementioned approaches in terms of achieved structures is illustrated in **Figure 3.6**. All nanocomposite materials were firstly investigated by means of UV-vis and fluorescence spectroscopy as shown in **Figure 3.7**. **Figure 3.7a** reveals the pattern of four well-resolved absorption maxima indicating the high purity of **NC1** and **CdSe$_{ref}$** further corroborated by the narrow emission bands with maxima at 580 nm and 610 nm, correspondingly. The monodispersity of **NC1** evidencing the high quality of the material as well can be pointed out by the high-resolution transmission electron microscopy-image (HRTEM), which shows crystallinity and lattice areas, which resemble the hexagonal CdSe phase (**Figure 3.8a**). **Figure 3.8b** shows once more the formation of the CdSe nanoparticles and the side-by-side packing of a monolayer on the TEM grid. TEM pictures were recorded in the Faculty of Engineering and Center for Nanointegration at the University of Duisburg-Essen by Dr. Ralf Theissmann. FT-IR measurements indicated the linkage of compound **14** on the surface of the CdSe nanocrystals *via* the band at 2359 cm^{-1} assigned to the stretching vibration of the surface-bound NH_2-group (**Figure 3.9a**).

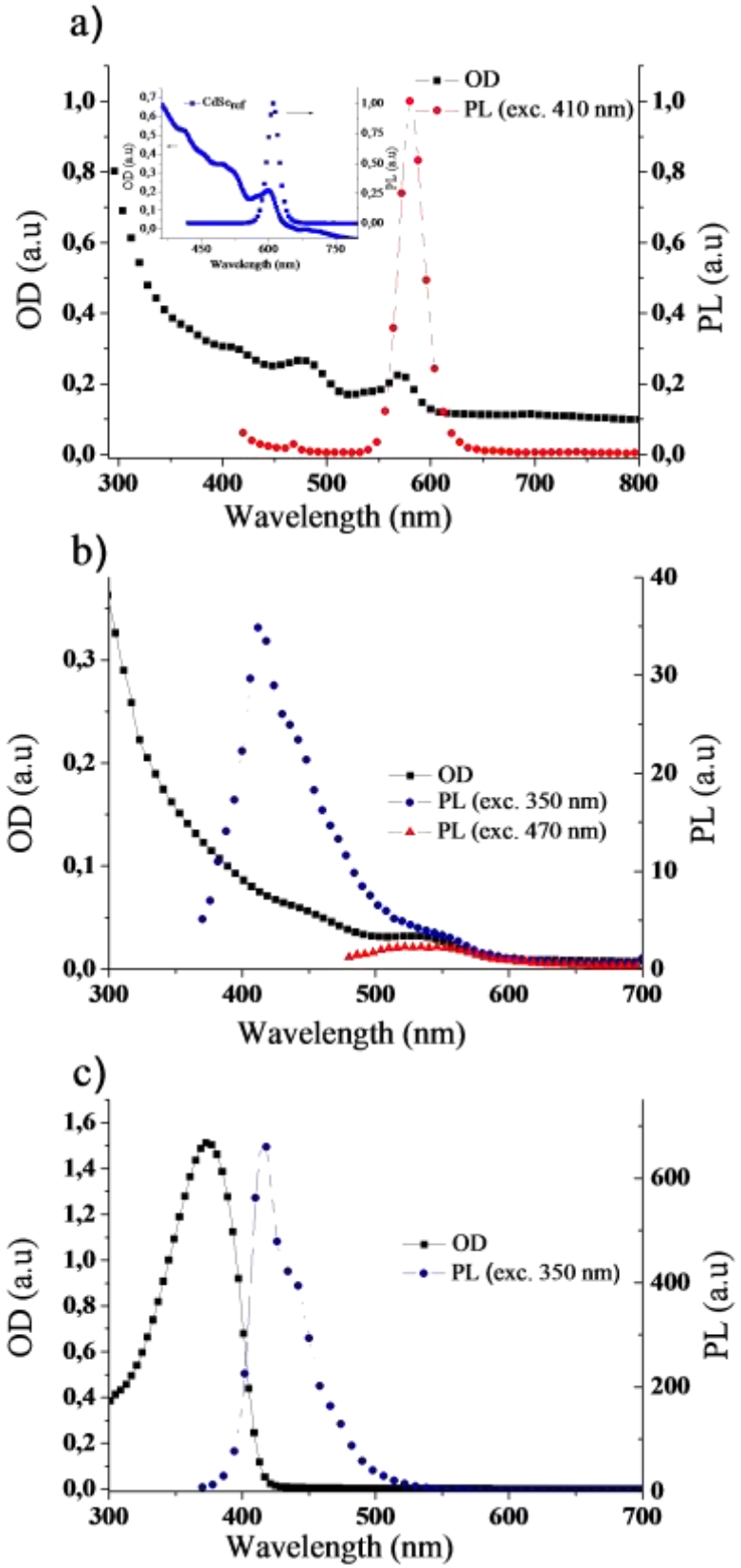

Figure 3.7: (a) Absorption (OD) and photoluminescence PL ($\lambda_{exc.}$ 410 nm) spectra of **NC1** compared to the spectra of **$CdSe_{ref}$** (inset). (b) Absorption and photoluminescence spectra of **NC2** taken at two different excitation wavelengths ($\lambda_{exc.}$ 350 & 470 nm). (c) Absorption and PL ($\lambda_{exc.}$ 350 nm) spectra of **NC3**.

In the case of **CdSe$_{ref}$**, the aforementioned band originating now from the surface-bound amino-group of the *n*-hexadecylamine ligand, appears much weaker (**Figure 3.9a**). Bringing this observation into connection with the strongly slowed-down growth kinetics upon introduction of **14** into the reaction mixture, a higher affinity of **14** towards the CdSe surface compared to *n*-hexadecylamine can be assumed. **NC1s** undergo a favourable capping of their CdSe surface attributed to the chelating character provided by the amines of ligand **14**.[46] In case of **CdSe$_{ref}$** nanocrystals the surface coverage operates only through the intrinsic ability of the *n*-hexadecylamines to coordinate with CdSe[47-49] leading thus to weakly bound amino-groups on their surface.

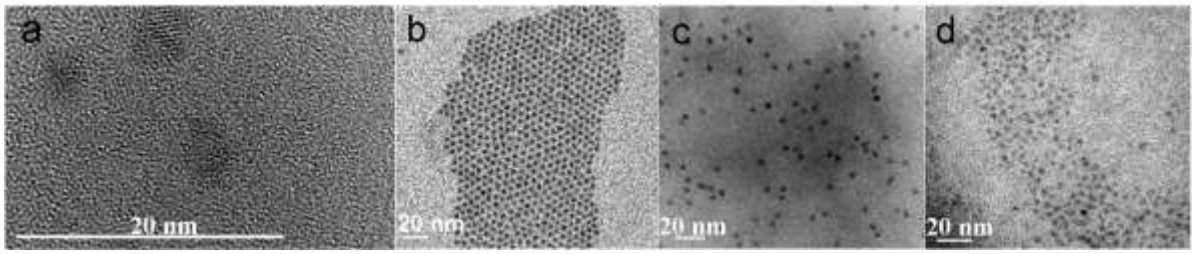

Figure 3.8: High-resolution transmission electron microscopy image of **NC1** with an image scale of 29 × 18 nm (a) and transmission electron microscopy images of **NC1** (b), **NC2** (c) **NC3** (c). The TEM images b and c have a scale of 190 × 175 nm, while d has a scale of 140 × 130 nm. The scale bar is 20 nm for all frames.

The CdSe nanocrystals with the amino-functionalized fluorene as endcapper were firstly subjected to a facile Yamamoto protocol[7] using **NC1** as the single starting material, $Ni(COD)_2$ as C-C coupling mediator and THF/toluene 1/1 (v/v) as the solvent mixture. After conventional work-up, purification *via* preparative size exclusion chromatography (Biobeads) gave nanocomposite **NC2** in a yield of 71%. The absorption pattern of **NC2** is predominated by the absorption features of the CdSe nanocrystals, whereas the emission maxima obtained at two different excitation wavelengths reveal the contribution of both parts i.e. oligo(fluorene) and CdSe part to the optical properties of the composite. The morphology investigated by TEM shows the formation of non-agglomerated nanoparticles. This observation excludes the possibility of *inter*-particle polymerisation, suggesting rather an *intra*-particle mechanism at the surface of the CdSe nanocrystals, through which oligomerization occurs. *Intra*-particle oligomerization is further supported by the predomination of the nanocrystals in the absorption spectrum of composite **NC2**, while its FT-IR spectrum (**Figure 3.9b**) exhibits a

pronounced band at 2359 cm^{-1} assigned to surface bound NH_2-groups implying the intactness of the links between the CdSe nanocrystals and the ligand **14** under the reaction conditions.

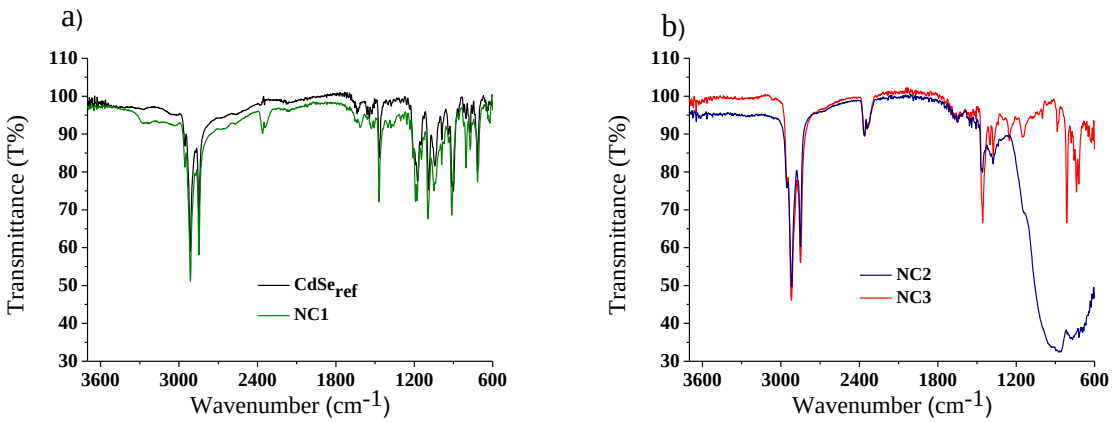

Figure 3.9: FT-IR spectra of (a) **$CdSe_{ref}$** and **NC1**, (b) nanocomposites **NC2** and **NC3**.

Applying the similar polymerization procedure and combining **NC1** with comonomer 2,7-dibromo-9,9'-dioctyl-9*H*-fluorene, nanocoposite **NC3** was prepared inducing a chain-growth polymerization at the surface of the CdSe nanocrystals. Purification by precipitation from methanol and size exclusion chromatography acquired a polymer-like material in a yield of 83%. The optical properties of the material are dominated by features typical for poly(fluorene)s with the emission of the CdSe nanocrystals being completely quenched (**Figure 3.7c**). The TEM image for nanocomposite **NC3** indicates, however, the presence of the inorganic part of the composite through the presence of CdSe cores (**Figure 3.8d**). FT-IR spectroscopy as the presence of the band at 2359 cm^{-1} proves (**Figure 3.9b**), shows once more that the NH_2-groups of compound **14** remain attached on the surface of the CdSe nanocrystals under the Yamamoto polymerization conditions allowing thus the grafting of the second comonomer from the amino-functionalized fluorene surface endcapper. In a further step, all three nanocomposites were characterized by means of gel permeation chromatography and atomic force microscopy. The latter measurements were carried out by Sylwia Adamzcyk from the group of Prof. Dr. Ullrich Scherf in the Department of Macromolecular Chemistry at the University of Wuppertal. The gel permeation chromatography analysis can be seen in **Figure 3.10**, where elugrams of **NC1-3** and the corresponding molecular weight distributions are illustrated in comparison to the internal standard butylated hydroxytoluene (BHT). **NC1** does not show any pronounced molecular weight distribution giving a peak at just 736 Da, a value much lower compared to the molecular weight of a II-VI nanocrystal estimated from the mass of the constituting elements for a given NC size.[50] This **NC1**-signal has an elution volume of 32.2 mL accompanied by a tail, which is most probably related to NCs aggregates

(**Figure 3.10a**). The formation of agglomerates hinders the penetration of the nanocrystals through the pores of the column gel. As the separation range of the column bears a limit of 1000 Da, the exclusion volume of the gel-particles is only available for the nanocrystals, which start to exit the column at an earlier elution time (22.74 mL, **Figure 3.10a**). The tailing of the elution ends up with an elution peak (32.2 mL), which is very close to the elution volume of the internal standard used for the GPC analysis, namely BHT (34.8 mL). Thus, an overlap of **NC1** and BHT can not be excluded as **Figure 3.10b** demonstrates. The afore-described observation implies that the GPC data, which represent values obtained relative to poly(methyl methacrylate) standards, can not be regarded as absolute in case of NCs, whose hydrodynamic volumes are much smaller than of the utilized polymer standards.

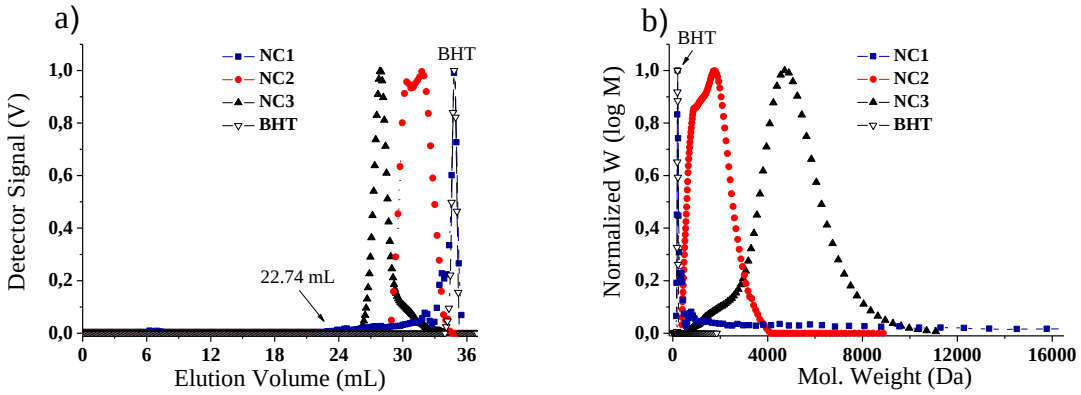

Figure 3.10: (a) Gel permeation chromatography elugrams of nanocomposites **NC1**, **NC2** and **NC3** compared to the internal standard butylated hydroxytoluene (BHT) and (b) the corresponding molecular weight distributions.

The signal of **NC2** (**Figure 3.10a**) shows a coexistence of two species with molecular weights in the range of 1700 Da as can be seen in **Figure 3.10b**. This molecular weight refers to the weight of oligomers formed at the NC surface and is evidence that the catalytic polymeriazation cycle breaks up after three repeating units of **14** undergo the *intra*-particle oligomerisation. The interruption of the Yamamoto cycle can be assigned to space limitations at the surface of the NCs. Furthermore, the molecular weight was investigated by means of MALDI-TOFMS and these measurements were carried out in the group of Prof. Dr. Oliver J. Schmitz in the Department of Analytical Chemistry at the University of Wuppertal. The resulting *m/z* values could be assigned to a fluorene trimer, a finding, which can be practically related to the molecular weight of the organic part of composite **NC2**. The coincidence of the MALDI-TOF measurement with the GPC findings supports the assumption of the catalytic termination after the coming-together of three fluorene units. In contrast to **NC2**, the elugram

of **NC3** indicates the successful polymerization, whereby a mass average molecular weight of 4738 g/mol is determined. The unimodality of the elugram on the other side speaks for a homogeneous and stable end-product (**Figure 3.10a**). MALDI-TOFMS analysis resulted this time in a vast number of signals, which could be assigned to fractions of the organic counterpart ranging from the dodecamer (*m/z*: 4663.9 g/mol) to the monomer (*m/z*: 387.4 g/mol). The MALDI-TOFMS results are consistent to the GPC analysis data and corroborate the claim of polymer chain-growth from the nanocrystal surface. As mentioned, the morphology of the nanocomposites was also investigated by means of atomic force microscopy (**Figure 3.11**).

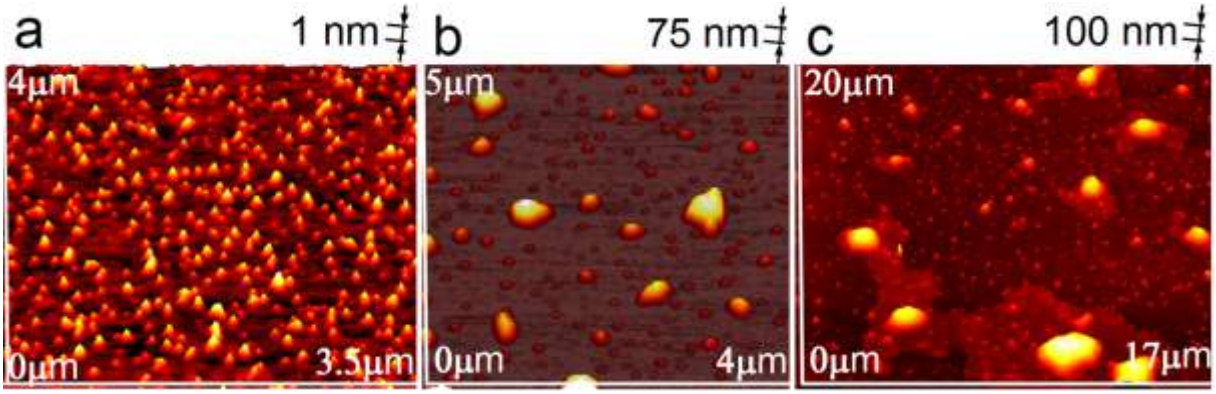

Figure 3.11: AFM images (tapping mode) of thin films of **NC1** (a), **NC2** (b) and **NC3** (c) dip-coated on glimmer from toluene (**NC1**) or chloroform (**NC2-3**) dispersions of 10 mg/mL concentration, after annealing at 180 °C for 4 hours.

The films for the AFM measurements were prepared by dip-coating nanocomposite **NC1** in toluene and nanocomposites **NC2** and **NC3** in chloroform on glimmer. The average surface roughness revealed by these measurements, represent values of only 0.7 nm for **NC1** and increased roughness of 25.5 and 70.0 nm for **NC2** and **NC3**, respectively. **NC1** seems to build equal-large spots, larger spots come up in the image of **NC2**, while nanocomposite **NC3** with the grafted poly(fluorene) chains consisting the major part of the composite, reveal clustered agglomerates of 200 nm in size, which formation is mediated *via* the tendency of the polymers to fold/aggregate.[51] A final discussion field is the possibility of energy or electron transfer in the described nanocomposite systems. Detailed investigations on this topic can be found in section **4.1**.

3.3 Poly(fluorene) Microparticles

The synthesis of water-soluble nano/micro-particles containing fluorescent polymers with molecules possessing both hydrophilic and hydrophobic properties (amphiphile) displays a new emerging trend for the polymer scientists.[52] Nanoprecipitation, one of the nanoparticles' preparation method, provides particles with sizes up to 50 nm, exhibiting high fluorescence brightness.[53,54] Poly(fluorene)s with phosphonate-groups can fulfill the criterion of amphiphilic character and are of particular interest due to their solubility in polar solvents[55] and their strong chemical affinity to semiconductor quantum dots.[56] In this chapter, the synthesis of two phosphonate-functionalized poly(fluorene)s is described based on a random and alternating backbone configuration and subsequent operative processing *via* a precipitation-sonication method that led to particles of micrometer-size. In a first step, the literature known monomers 2,7-dibromo-9,9'-*bis*(6-bromohexyl)-9*H*-fluorene (**2**)[10] and 2,7-dibromo-9,9'-dioctyl-9*H*-fluorene (**3**)[9] were combined using Yamamoto conditions[7], while the purchased 2,2'-(9,9'-dioctyl-9*H*-fluorene-2,7-diyl)*bis*(1,3,2-dioxaborinane) (**DFB**) was copolymerized with comomomer **2** following a Suzuki-mediated protocol.[8] 2,7-Dibromo-9,9'-*bis*(6-bromohexyl)-9*H*-fluorene (**2**) utilized in both synthetic approaches, was synthesized by a NaOH-mediated alkylation reaction in the presence of the phase-transfer catalyst tetra-butylammonium bromide yielding 69% of **2** as a white solid. The bromo side-chain-functionalized precursor copolymer, obtained according to the Ni(0)-mediated Yamamoto C-C coupling protocol[6], was prepared in THF as solvent by means of $Ni(COD)_2$ and 2,2´-bipyridine as the organometallic counterpart (**Scheme 3.7a**). For the Suzuki step-growth polymerization[30], the building blocks were allowed to react in toluene using equivalent volume of 2M Na_2CO_3 water-solution by means of *tetrakis*(triphenyl)phosphine palladium(0) as catalyst and aliquat 336 as phase-transfer mediator (**Scheme 3.7b**). The Yamomoto-synthesized copolymer **P7a** was obtained by using an equal molar feed-ratio of monomers **2** and **3** and a typical 1:1 stoichiometry between the monomer with the dibromo- and diboronic acid ester-functionalities was the case in the synthesis of the alternating Suzuki copolymer **P8a**. The polymers were purified by extracting them with ethanol, *iso*propanol and chloroform over intervals of 1 to 3 days with the aid of a Soxhlet apparatus. This can ensure the acquirement of homogeneous final products, later evidenced by the unimodality of their molecular-weight distributions (**Figure 3.12**). The precursor copolymers were well-soluble in solvents of medium to high polarity like chloroform, dichloromethane, or tetrahydrofuran.

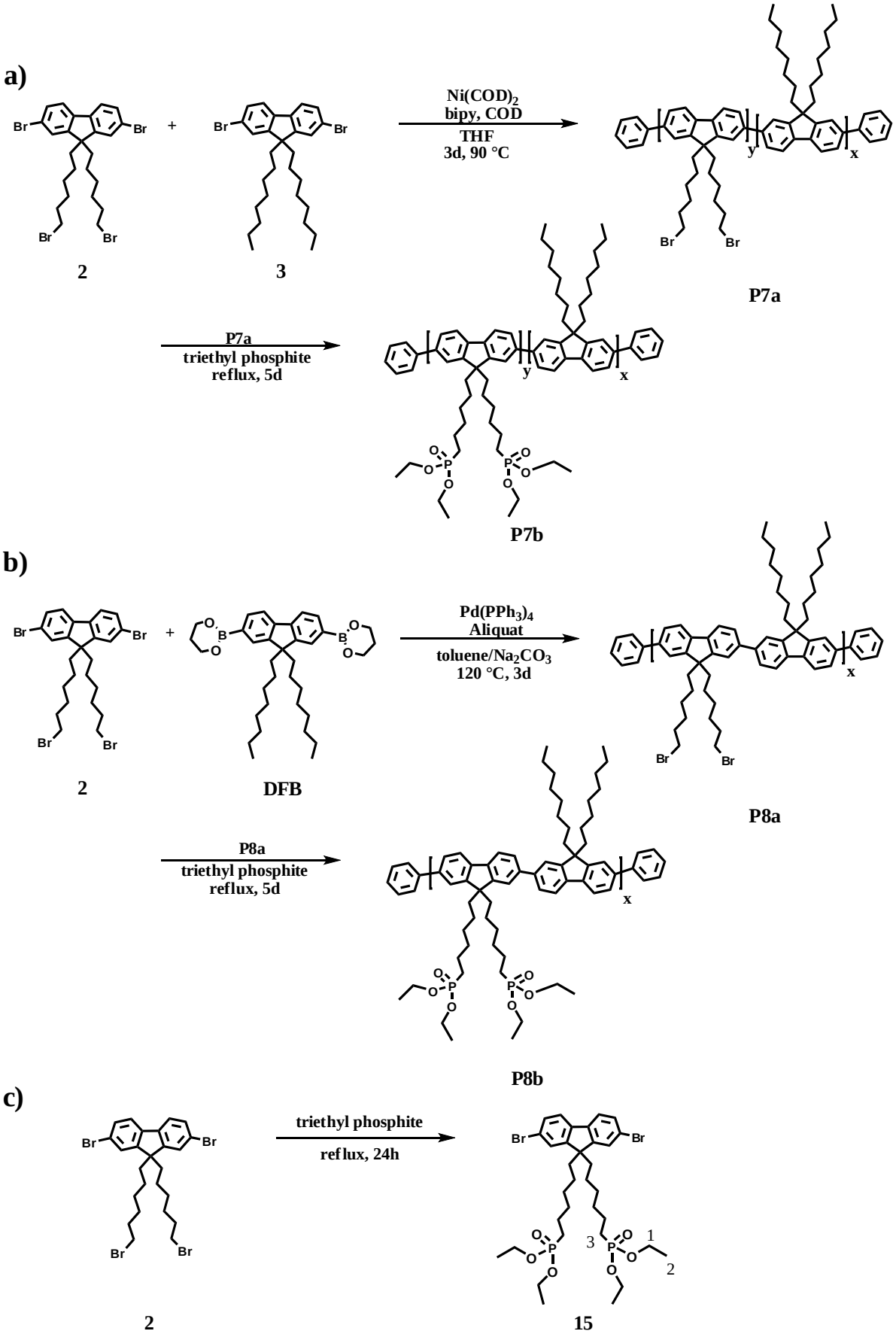

Scheme 3.7: Synthesis of copolymers **P7a-b** (a) and **P8a-b** (b) and of the phosphonate-functionalized fluorene **15** (c).

The post-fuctionalization proceeded by following an Arbuzov protocol, which was initially applied on compound 2,7-dibromo-9,9'-*bis*(6-bromohexyl)-9*H*-fluorene (**2**) by refluxing it in triethyl phosphite for 24 h (**Scheme 3.7c**).[57]

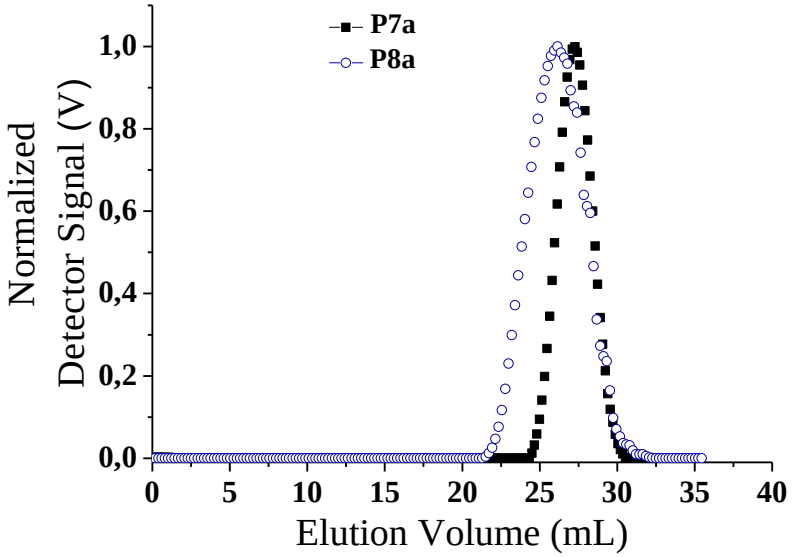

Figure 3.12: Gel permeation chromatography elugrams of copolymers **P7a**, **P8a**.

A colorless liquid was obtained in a yield of 81% and the successful reaction course gave the green light for trying the phosphonate modification on the precursor polymers with the bromo-functionalized side-chains **P7a** and **P8a**. The post-functionalization was conducted in triethyl phosphite at 165 °C reaction temperature and the acquisition of the copolymers by precipitation from *n*-hexane (**Schemes 3.7a-b**). The obtained copolymers **P7b**, **P8b** exhibited exceptional solubility in even more polar solvents like dimethylformamide, when compared to their forerunners. All copolymers were fully characterized by NMR-, IR-, UV-vis- and fluorescence spectroscopy, elemental analysis and as already mentioned gel permeation chromatography. The ^{1}H-NMR spectra in **Figure 3.13** recorded in deuterated chloroform ($CDCl_3$), illustrate an exemplarily comparison between precursor copolymer **P7a** and final end-product **P7b**. The resonance at 3.32 ppm (copolymers **P7a**, **P8a**) in **Figure 3.13a** is assigned to the protons of the carbon-atom with the attached bromo-function ($C_5H_{10}C\mathit{H}_2$-Br) and is evidence for the success of the applied protocols.

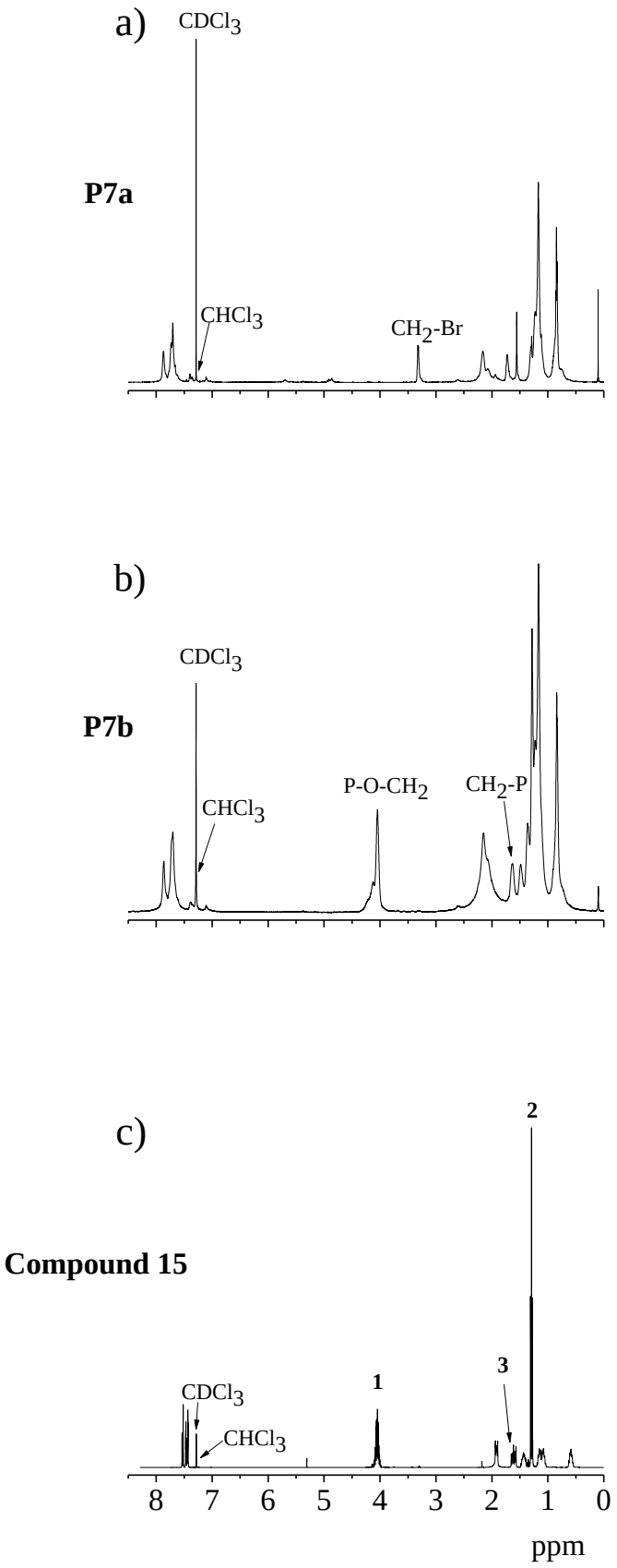

Figure 3.13: ^{1}H-NMR spectra of precursor copolymer **P7a** (a), post-functionalized target copolymer **P7b** (b) and 6-(2,7-dibromo-9*H*-fluoren-9-yl)hexyl phosphonate (**15**) (c).

The spectrum of the post-functionalized copolymer **P7b** brings into sight new signals, monitored at 1.64 ppm and 4.04 ppm. The 1.64 ppm signal is the high-field shifted signal of the protons attached on the carbon next to the phosphor-atom ($C_5H_{10}C\mathit{H}_2$-P), being previously linked to the bromo-functionality. The resonance at 4.04 ppm is the strongest indication for the success of the modification of the bromo-atoms to phosphonate-groups as this peak is assigned to the protons of the carbon linked directly to the oxygen-atom [(P-(O-CH_2)$_2$]. The two aforementioned resonances are observed in the spectrum of the analogue phosphonate monomer **15** designated with the numbers 1 and 3 in **Scheme 3.7c**. The peak of the methyl-group of the phosphonate-moiety is detected as well and labeled with the number 2 appearing at 1.20-1.22 ppm. ^{31}P-NMR spectroscopy with the peak at 32.48 ppm typical for phosphor incorporated in the phosphonate-group is a further proof for the success of the post-functionalization. Comparing this value to the chemical shift of the corresponding monomer **15** (32.41 ppm) an excellent coincidence is observed. ^{1}H-NMR spectroscopy allowed the determination of the percentage of each comonomer incorporated in the copolymer backbone and the results are presented in **Table 3.4**. In Yamamoto-mediated copolymer **P7a**, a predomination of comonomer **3** is recorded with 76% backbone incorporation, while the Suzuki-based copolymer **P8a** revealed an expected alternating backbone constitution of 44% of the 9,9'-*bis*(6-bromohexyl)-9*H*-fluorene **2** and 56% of the 9,9'-dioctyl-9*H*-fluorene derivative. The predomination of a specific building block in case of random copolymers like **P7a** is not uncommon[37] and can be attributed to the enhanced solubility of the comonomer with the octyl side-chains compared to the bromohexyl-chains keeping in mind that the fluorene cores with the bromo-atoms at the 2 and 7 positions possess the same inherent reactivity. In case of Suzuki-synthesized polymers like **P8a**, the building block with the diboron-ester functionality is favored by one to two repeating units more due to insufficient reactivity of the co-reactant with the bromo-functionalities.[58,59] Applying the ^{1}H-NMR-based calculations on the post-functionalized polymers, a 71% content of the dioctyl-fluorene-building block comes out in case of **P7b**, while copolymer **P8b** exhibited an alternating backbone pattern similar to the precursor **P8a** with comonomers **DFB** and **15** being integrated by a 54:46% ratio, correspondingly. Gel permeation chromatography analysis illustrated homogenous precursor polymers (**Figure 3.12**) and detected number average molecular weight of 15100 g/mol (PDI: 2.28) for copolymer **P7b** and 9100 g/mol (PDI: 2.26) for copolymer **P8b**. Deviations of the molecular weights between precursor and final copolymers are recorded, a phenomenon attributed to the rather different dissolution behavior of the two copolymer classes. The post-functionalized copolymers possessed the ability *via* their

phosphonate-groups attached on their side-chains to dissolve significantly better in dimethylformamide, which was the solvent used during the performance of the GPC measurements.

Table 3.4: Actual percentages of monomers **2**, **3** and **15** in the backbone of the precursor and final polymers calculated by means of ^{1}H-NMR spectroscopy.

Polymer	Monomer **2**	Monomer **3**	**15**
	y(%)	x(%)	y(%)
P7a	24	76	-
P8a	44	56	-
P7b	-	71	29
P8b	-	54	46

The enhanced polarity of these groups induced through the presence of the electronegative oxygen atoms, play a crucial role for the increased dissolution efficiency of the copolymers **P7b**, **P8b**. On the other side, the bromo-atoms present as end-groups in the side-chains of the precursors **P7b**, **P8b** make polymeric chains with higher molecular weights less soluble.[60] Moreover, the different work-up techniques applied on precursor and final polymers should not be neglected, when discussing the lower molecular weights of the former.[61] Precursor copolymers were purified by Soxhlet extraction and the usage of chloroform as extraction medium can lead to a partial fractionation resulting in losses of the less soluble but higher in molecular weight fraction. Precipitation from *n*-hexane in the case of the post-functionalized copolymers made such a fractionation unlikely. Regarding now the almost quantitative post-functionalization process confirmed by the ^{1}H-NMR calculations and the fact that molecular weight and PDI values should be treated as rough estimates due to the different hydrodynamic volumes of conjugated copolymers and poly(methyl)methacrylate standards, the amphiphilic character of the phosphonate-groups and their larger total weight compared to the previous bromo-functionalities seem to be the reasons for the enhancement of the molecular weights. The copolymers were furthermore characterized in terms of their optical properties and the results are listed in **Table 3.5**. **Figures 3.14a-b** illustrate the UV-vis and fluorescence spectra of the final polymers in solution and films, correspondingly, exhibiting a blue-light emission with a maximum at 416 nm and quantum yields up to 0.54 (**Table 3.5**). An advantageous precipitation method allows shifting their blue emission to white by preparation of water-stable dispersions, whereby microparticles possessing high quantum yields of up to 0.84 were obtained (**Table 3.5**). The precipitation method involves the dissolution of copolymers **P7b**,

P8b in tetrahydrofuran and injection of the solution in vibrating water by means of ultrasonic bath. The sonication process is sustained for 1 h at room temperature and is illustratively depicted in **Scheme 3.8**.

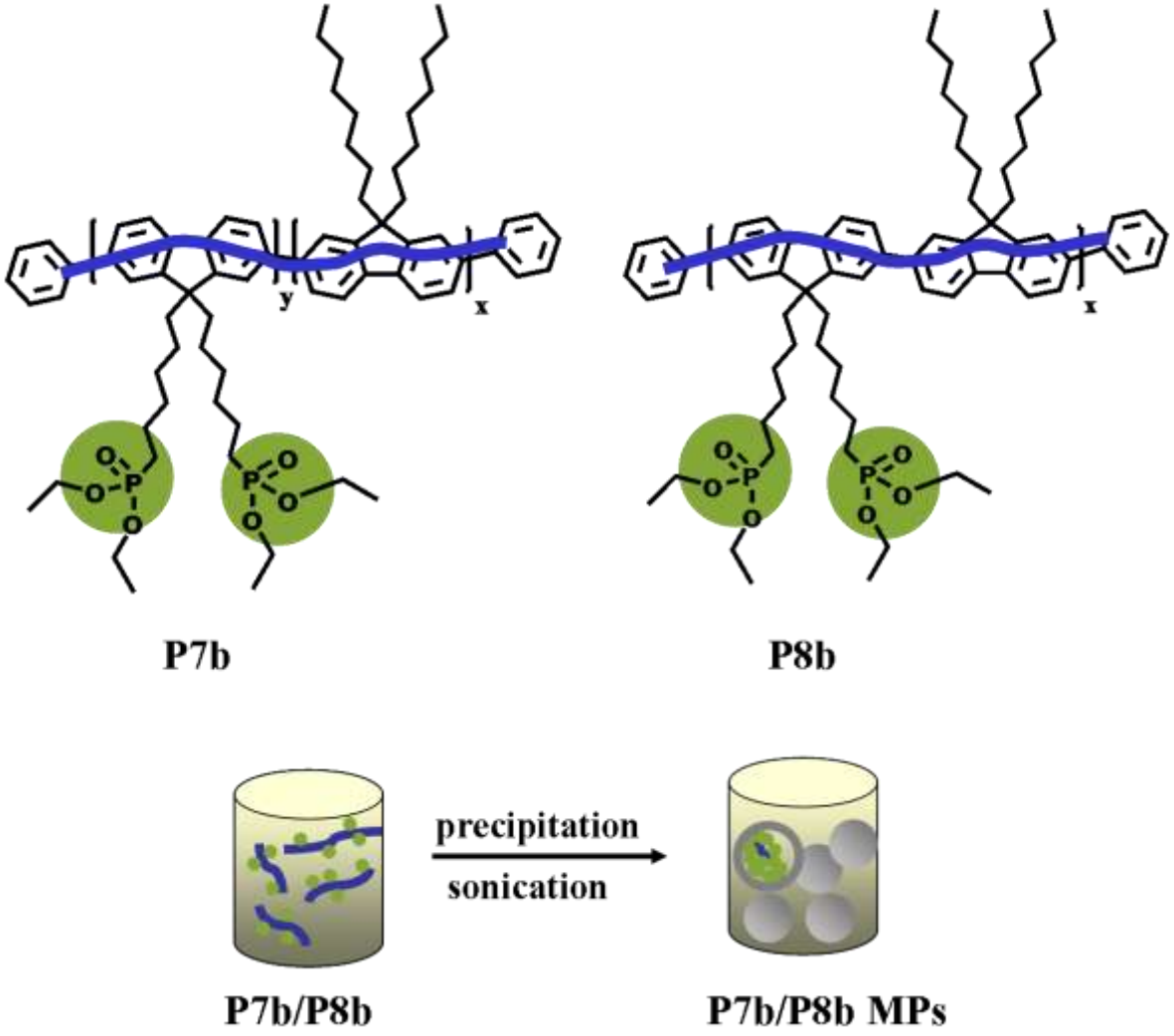

Scheme 3.8: Schematic representation of the formation of the copolymer microparticles **P7b MPs** and **P8b MPs**.

In principle, when using this method, we are dealing with a solvent exchange process, whereby the target polymers are firstly dissolved in a 'good' solvent (THF) and rapidly mixed by means of sonication with an excess of a 'poor' solvent (water). Important is that the chosen pair of 'good' and 'bad' solvent is miscible to each other. The discrepancy in the solubility, however, causes a collapse of the copolymer chains due to aggregation of the organic molecules forming thus hydrophobic copolymer particles (**Scheme 3.8**). The sudden change of solvent quality induces densely packed structures of particulate spheres designated as microparticles (**MPs**). The differentiation of their optical properties compared to the linear

analogues **P7b/P8b** can be seen in **Figures 3.14a-c**. In particular, the microparticles of the copolymer **P7b** exhibit a different fluorescence pattern compared to the **P8b MPs**, a differentiation, which may have to do with the fact that copolymer **P7b** was synthesized by application of a Yamamoto-mediated step-growth mechanism consisting the different optical behaviour dependent on the catalysis applied for the backbone design.

Table 3.5: Optical properties of copolymers **P7**,**8a-b** and microparticles **P7**,**8b MPs**.

Polymers	**Abs_{sol}**[a] (**log ε**)[e] ——— [nm]	**Abs_{film}** ——— [nm]	**Em_{sol}**[a;b] ——— [nm]	**Em_{film}**[b] ——— [nm]	**Eg_{sol}**[a;c] ——— [eV]	**Eg_{film}**[c] ——— [eV]	**Φ_{sol}**[a;d] ———
P7a	382 (5.44)	380	418/439	425/446	2.92	2.89	0.33
P8a	380 (5.20)	381	417/440	429/449	2.95	2.88	0.16
P7b	381 (4.98)	388	416/440	431/448	2.93	2.85	0.54
P8b	382 (5.71)	411	416/441	432/453	2.93	2.58	0.52
P7b MPs	380 (2.69)	397	432/455/530	-	2.86	2.59	0.61
P8b MPs	382 (2.45)	400	436/464/493	-	2.83	2.60	0.84

[a]in chloroform solution (10^{-6} mol/L) for copolymers **P7**,**8a-b** and in water solutions (10^{-4} mol/L) for polymer particles **P7**,**8b MPs**; [b]$\lambda_{exc.}$ 390 nm; [c]calculated from the absorption band-edge; [d]determined according to Demas and Crosby[15] by using **PF8** as reference; [e]log ε in $L \times mol^{-1} \times cm^{-1}$.

P7b MPs possessed an extra band at 530 nm, which complements the blue-emitting one at 432 nm and could be assigned to increased *inter*chain interactions leading to a small fraction of red-shifted agglomerated species[62] (**Figure 3.14c**). The outcome of this experiment is visualized in **Figure 3.15a**, where a white-light emitting dispersion, which remains stable for over a period of three weeks, is depicted. On the other side, the **P8b MPs** exhibit bands, which are sharper compared to **P8b** expanding, however, on the same wavelengths (**Figure 3.14c**). The lack of a band at 530 nm renders the dispersion capable of emitting only in the wavelengths of the blue region of the color spectrum (**Figure 3.15b**).

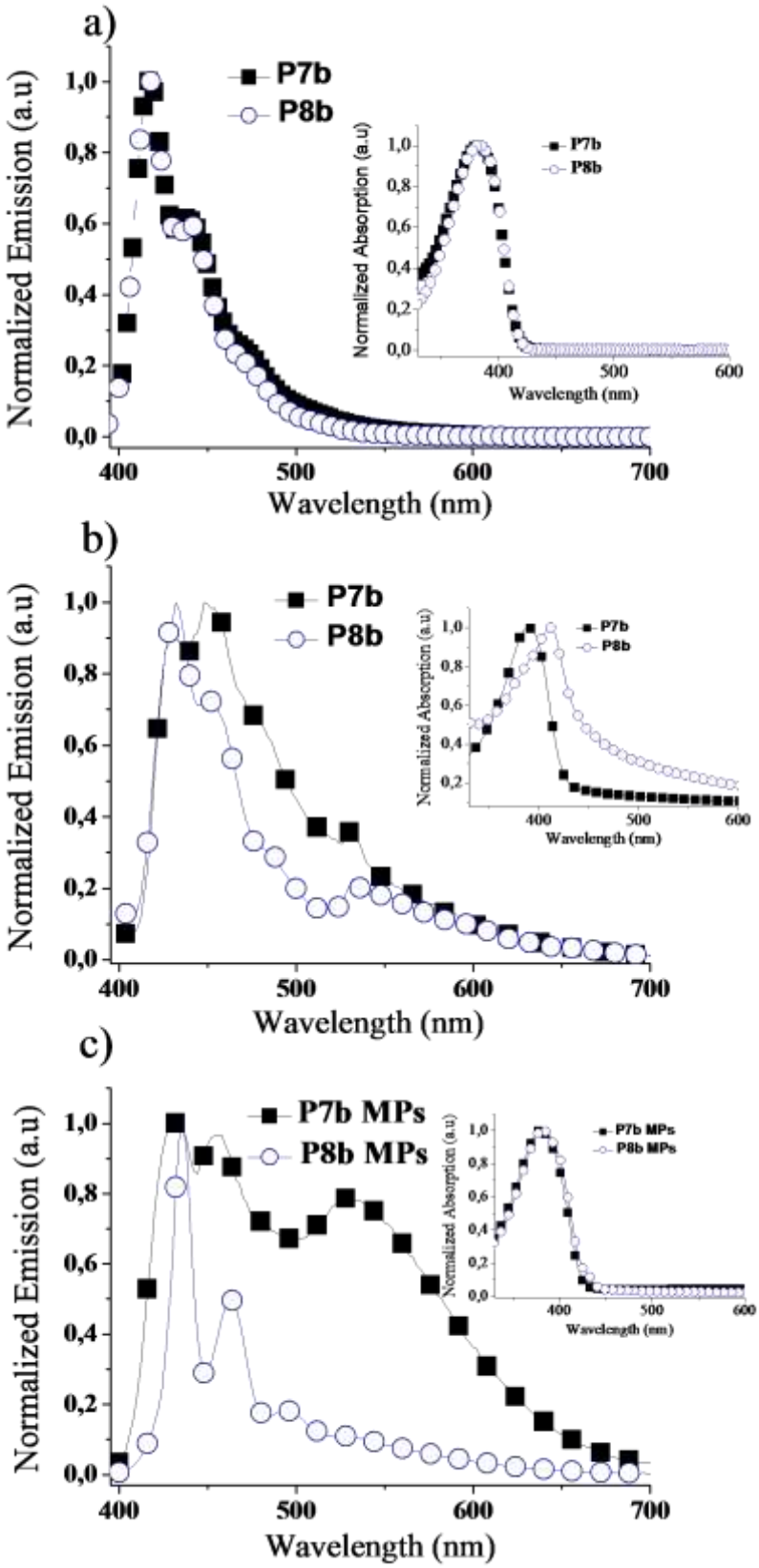

Figure 3.14: Normalized emission and absorption (inset) spectra of copolymers **P7**,**8b** in solution (chloroform, 10^{-6} mol/L) (a), films (drop-cast from chloroform, 1 mg/mL) (b) and as copolymer microparticles (**P7**,**8b MPs**) prepared *via* a precipitation-sonication procedure (water, 10^{-4} mol/L) (c).

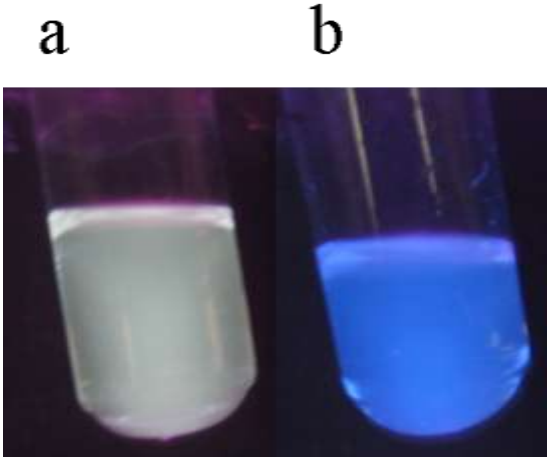

Figure 3.15: Photographs of the polymer microparticles **P7b MPs** (a) and **P8b MPs** (b), both illuminated with UV-vis irradiation under an excitation wavelength of $\lambda_{exc.}$ 366 nm.

The microparticles of the copolymers seem to possess electronic states, which might be brought in connection to a keto-defect circumstance. In order to clear up with this assumption, the microparticles were compared to fluorenone-containing poly(fluorene)s (**PFOs**). The additional peak arising at about 530-560 nm for the **PFOs** in different surroundings[63] can not distinctly exclude the possibility of the backbone oxidation during the Yamamoto catalysis, which becomes pronounced into sight when water is the medium used for the performance of the fluorescence measurements. Therefore, the photophysical properties of the microparticles seem to be affected by the solubility of the copolymers and the structural configuration of their backbone. The shifting in case of **P7b MPs** can be thus traced back to *intra*chain energy tranfer or *inter*chain excimer emission facilitated by the closer coming-together of the polymer chains[64], not the case for the alternating configuration of the **P8b** microparicles. This get-together tendency of the **P7b MPs** is evidenced by the formation of larger agglomerates compared to the **P8b MPs** and discussed later on, when describing the dynamic light scattering measurements (DLS).

The surface morphology of the copolymer microparticles was investigated by means of atomic force microscopy and the AFM images in **Figure 3.16a** are recorded in tapping mode showing the raw height data in top view and false color representation. In order to acquire more information about the surface morphology, the recorded AFM images are also represented with slope shading (**Figure 3.16b**) an option provided by the software, whereby a calculation of the raw data is implemented adding a perspective illumination from the right to the images[65-67]. The **P8b MPs** exhibited the tendency to build well-defined homogeneous

microparticle aggregates (500 nm in diameter), which agglomerate in even larger clusters (2500 nm in size). The particle formation occurred less pronounced in case of polymer **P7b**, where only partly microparticle clusters are built (900 nm in size, top-right side of the image). The average surface roughness of the copolymer microparticles **P8b** (264 nm) is by a factor of three lower compared to the average surface roughness of the **P7b MPs** (817 nm). This event can be a further reason for the differentiation in the appearance of the microparticles on the AFM pictures.

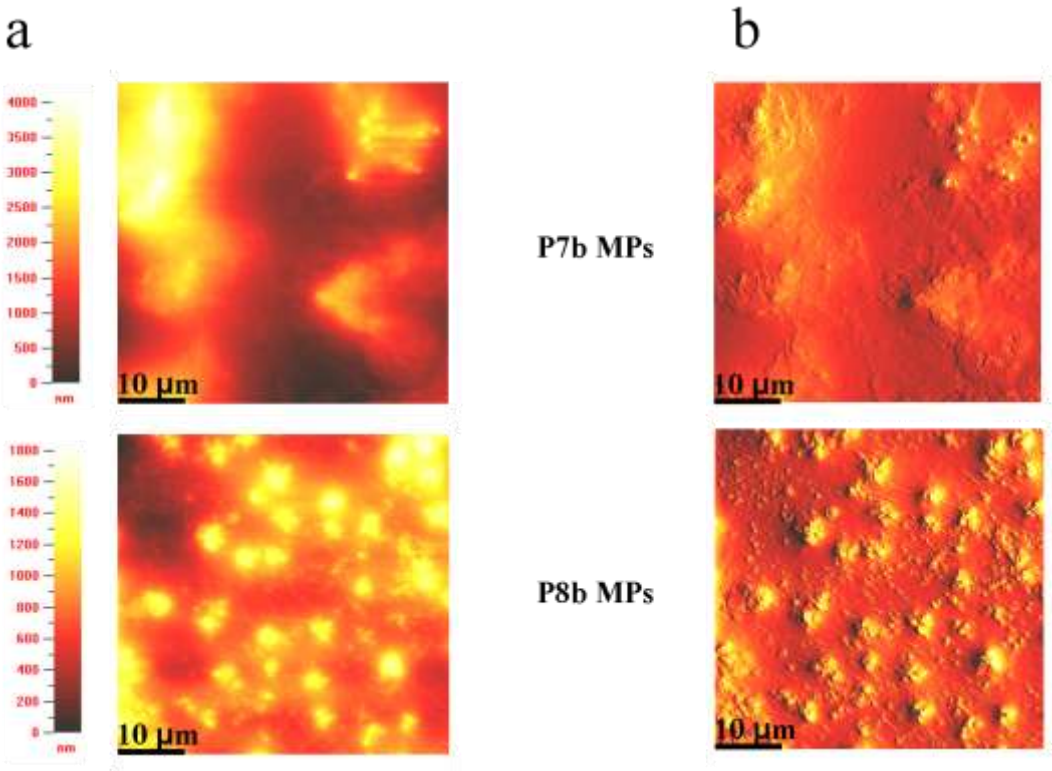

Figure 3.16: AFM images of the copolymer microparticles **P7**,**8b MPs** (a) False color representation of the raw height data acquired in the tapping mode. (b) Contour plot calculated from the raw data with slope shading. The films were prepared by drop-casting copolymer microparticles (10^{-2} mol/L) from water on glass substrates. The AFM images have a scale of 50 × 50 µm.

The particle size profile of **P7**,**8b MPs** is complemented by dynamic light scattering measurements. The **P7b MPs** revealed a particle distribution of 540.1 nm in diameter and a standard deviation of 343.6 nm, while the **P8b MPs** showed particles of 324.5 nm in diameter with a standard deviation of 143.3 nm. These values are reasonably comparable to the AFM ones, taking the respective standard deviations and the existing diversity of the preparation

conditions of the samples into consideration. The different molecular weights and the tightly packed structures leading to *inter*chain interactions[62] in case of the solid state AFM measurements may be the reasons for the differences in the microparticles' size.

Completing the analytical characterization of the copolymer microparticles, the precipitation-sonication method was extended to the direction of combining the copolymers with water-soluble CdTe nanocrystals in order to create composite systems. The successful outcome of these experiments is discussed in section **3.4**, while the possibility of energy transfer in those systems is scrutinized in the chapter of '**Energy and Electron Transfer Studies'**.

3.4 Poly(fluorene)-CdTe Composites

Incorporation of phosphonate side-chains in the backbone of polymers is of particular interest due to the amphiphilic properties accompanying the phosphonate-groups[68], the possibility to design well-soluble polymers[56] and their tendency to interact with inorganic compounds like quantum dots.[69] These characteristics can be essential in biological systems and in processing modern multi-layer devices.[70] Towards this direction and in the frame of this work two copolymers with phosphonate-functionalized side-chains were synthesized by applying a post treatment of precursor polymers under assistance of an Arbuzov protocol.[57] In a first step, the precursor polymers were synthesized by comprising 2,7-dibromo-9,9'-*bis*(6-bromohexyl)-9*H*-fluorene (**2**) and 2,7-dibromo-9,9'-dioctyl-9*H*-fluorene (**3**) in order to obtain the Yamamoto-based copolymer **P7a**, while 2,7-dibromo-9,9'-*bis*(6-bromohexyl)-9*H*-fluorene was combined with 2,2'-(9,9'-dioctyl-9*H*-fluorene-2,7-diyl)*bis*(1,3,2-dioxaborinane) (**DFB**) in order to end up with the Suzuki-mediated copolymer **P8a**. Post-functionalization using triethyl phosphite acquired the desired final products **P7b** and **P8b** after precipitation from *n*-hexane (**Scheme 3.9**). Applying a precipitation-sonication process allows the bringing-together of the phosphonate-functionalized copolymers with CdTe quantum dots (**Scheme 3.9**).

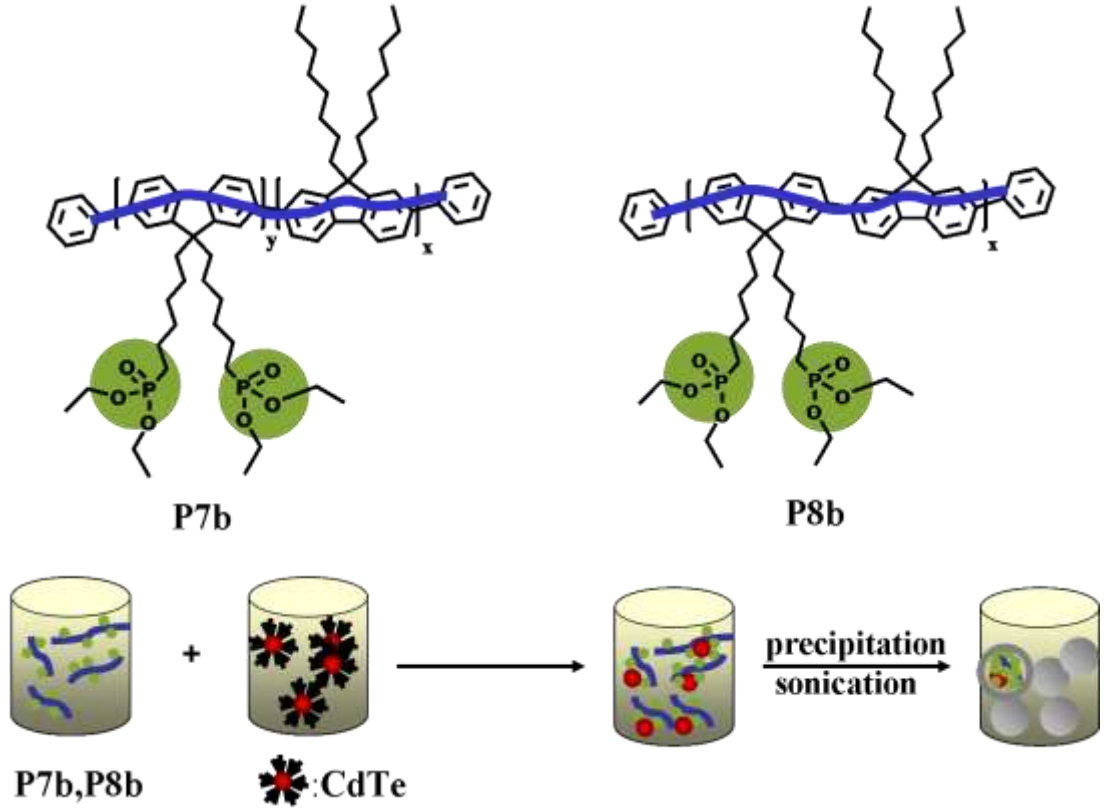

Scheme 3.9: Schematic representation of the structural configuration of final copolymers **P7b**, **P8b** (top) and their composites with CdTe nanocrystals *via* the precipitation-sonication method (bottom).

The in-here used nanocrystals synthesized by Dr. Vladimir Lesnyak in the group of Prof. Dr. Eychmüller (Technical University of Dresden, Physical Chemistry/Electrochemistry Department) represent two classes of CdTe quantum dots, both water-stable and endcapped with thioglycolic acid (TGA) possessing, however, different emission maxima at 534 nm (green CdTe) and 631 nm (red CdTe). The experiments to ally polymers and nanocrystals *via* a precipitation-sonication method resulted in microparticulate dispersions, which remained stable without deposition signs or diminution of their illumination. The resulting particulate material is designated as microparticles (**MPs**) and this is the case for the polymer-CdTe systems and the bare polymers as well. Details about the theoretical background of the precipitation-sonication methodology are cited in chapter **3.3**. The significance of the aforementioned processing is revealed, when sonication is eliminated during the preparation of these dispersions. Experiments performed excluding the use of an ultrasonic bath led to solutions with a blue tinge under UV-vis irradiation, even after addition of green or red-light emitting CdTe nanocrystals (**Figures 3.17a-b**). Increased concentration of for example red

CdTe nanocrystals (from 1×10^{-5} mol/L to 6×10^{-5} mol/L) induced a color change but the absence of sonication produced solutions with weak fluorescence.

As the optical properties of the nanocrystals remain unaltered, when injecting them in sonicating water, their combination with polymers **P7**,**8b** is possible. The implementation of sonication allows an intensification of the polymer-nanocrystal system emission color, when both counterparts are subjected to the sonication procedure (**Figure 3.17c**).

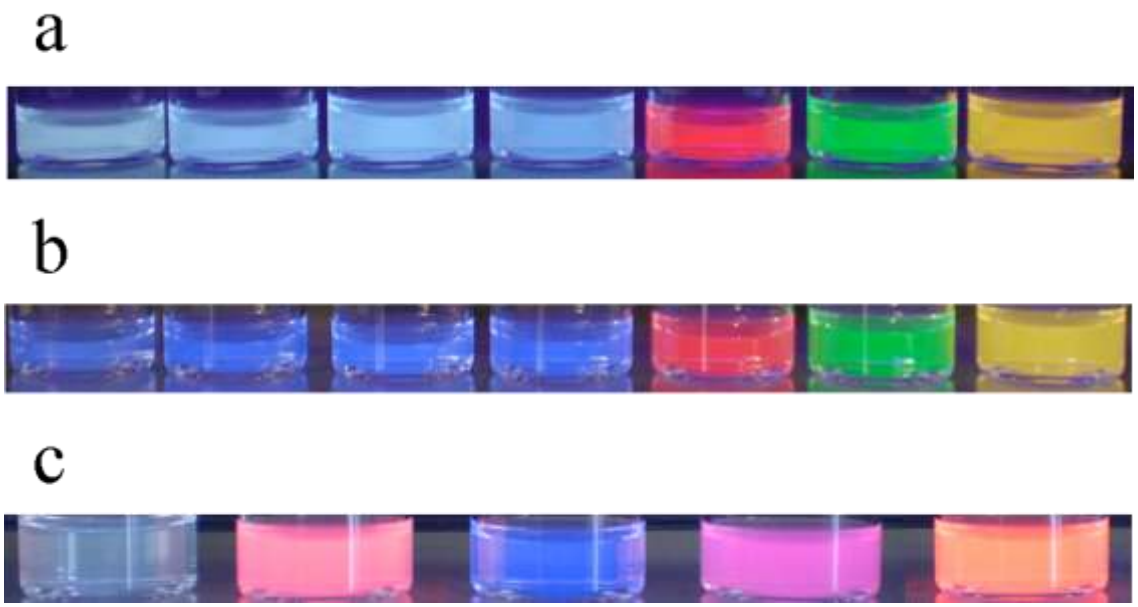

Figure 3.17: Photographs of **P7b**, **P7b**+$CdTe_{green}$, **P7b**+$CdTe_{red}$, **P7b**+$CdTe_{green+red}$, $CdTe_{red}$, $CdTe_{green}$, $CdTe_{green+red}$ (a) **P8b**, **P8b**+$CdTe_{green}$, **P8b**+$CdTe_{red}$, **P8b**+$CdTe_{green+red}$, $CdTe_{red}$, $CdTe_{green}$, $CdTe_{green+red}$ (b) **P7b MPs**, **P7b MPs**+$CdTe_{red}$, **P8b MPs**, **P8b MPs**+$CdTe_{red}$, $CdTe_{red}$ (c) (in that order left to right, under illumination of UV-vis irradiation at $\lambda_{exc.}$ 366 nm). Dispersions in **3.17c** are prepared by the precipitation-sonication method, not the case for the solutions in **3.17a-b**.

CdTe nanocrystals added in non-sonicated aqueous polymer solutions do not cause color changes as **Figures 3.17a-b** prove and a pronounced color changeover is the case only for sonicated systems (**Figure 3.17c**), rendering these systems applicable in multi-layer colored or white OLED devices even when processed from water. The stability of the composites was tested through centrifugation experiments of their dispersions followed by fluorescence emission measurements of the resulting supernates and precipitates. The conditions of the centrifugation experiments are listed in **Table 3.6**. Independently from the time and velocity of the centrifugation, a coexistence of polymers and nanocrystals in the supernates is

evidenced and designated with the + symbol in **Table 3.6**. The fluorescence measurements bringing into light this claim are depicted in **Figure 3.18**.

Table 3.6: Experimental parameters of the centrifugation trials.

P7b MPs+CdTe			**P8b MPs**+CdTe		
Time (min)	**Velocity** (rpm)	**Composite-Configuration**[a)]	**Time** (min)	**Velocity** (rpm)	**Composite-Configuration**[a)]
1	1600	+	1	1600	+
1	3000	+	1	3000	+
1	6000	+	1	6000	+
1	10000	+	1	10000	+
1	13000	+	1	13000	+
3	13000	+	3	13000	+

[a)]The + symbol is representative for the composite nature of the **P7b MPs**+CdTe and **P8b MPs**+CdTe systems in the supernates resulting after the performance of the centrifugation trials.

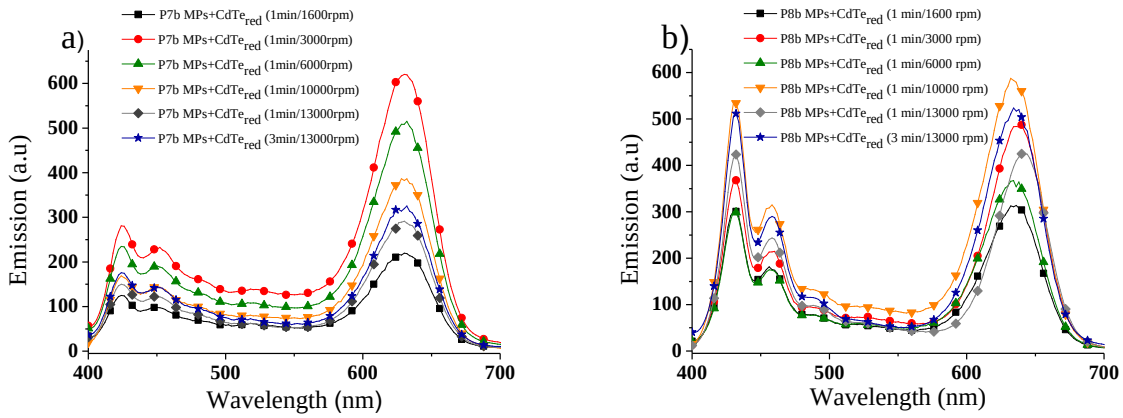

Figure 3.18: Fluorescence spectra of the supernates of the **P7b MPs**+CdTe (a) and **P8b MPs**+CdTe (b) systems, which were prepared by the precipitation-sonication procedure, followed by centrifugation at different time intervals and velocities. ($C_{\mathbf{P7b,P8b}}$: 10^{-4} mol/L and C_{CdTe}: 6×10^{-5} mol/L, $\lambda_{exc.}$ 380 nm).

The precipitates may bear weaker intensities exhibit, however, in both systems fluorescence spectra that are similar to the supernates. A decrease of the nanocrystals concentration by a factor of six (C_{CdTe}: 1×10^{-5} mol/L) in these systems led to the phenomenon of polymer leaching in the supernate and the nanocrystal sedimentation in the precipitate, which in terms

of fluorescence spectroscopy means pronounced polymer and CdTe bands in the spectra of supernate and precipitate, correspondingly. The composite configuration of the achieved polymer-nanocrsytal systems is once more verified by application of dynamic light scattering measurements performed at the Technical University of Dresden, Physical Chemistry/Electrochemistry Department in the group of Prof. Dr. Eychmüller under the assistance of Jan Poppe. The unimodal and symmetric particle distribution of the **P7b MPs**+CdTe and **P8b MPs**+CdTe systems can be seen in **Figure 3.19**. This observation indicates materials, which keep the two counterparts closely together. The fact that floating of CdTe aggregates is missing, as the size distribution profiles elucidate, can qualify these systems even for the class of hybrid materials.

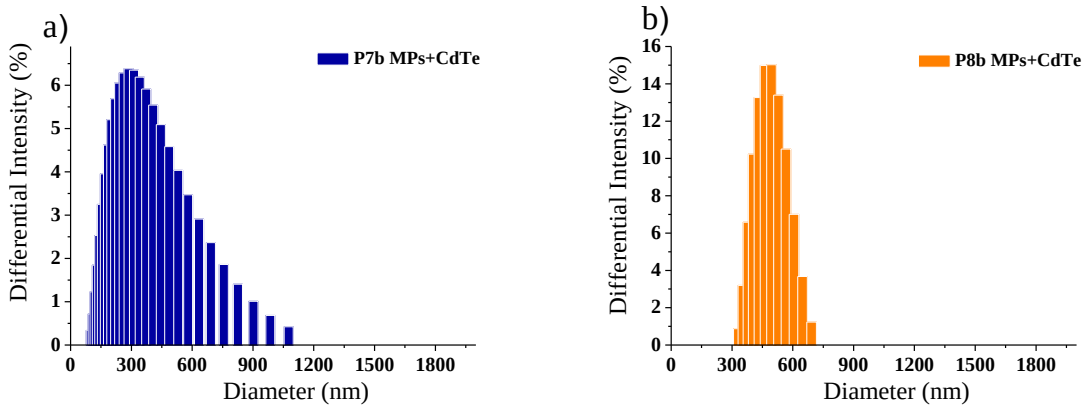

Figure 3.19: Dynamic light scattering measurements of the **P7b MPs**+CdTe (a) and **P8b MPs**+CdTe (b) composite systems illustrated as intensity distribution plots. The dispersions of the composites were prepared in water using 10^{-3} mol/L polymer and 1×10^{-4} mol/L CdTe concentration.

According to DLS, the composites of copolymer **P7b** and the CdTe nanocrystals build particles of 353.9 nm in average diameter and standard deviation of 186.9 nm exhibiting a parabolic distribution, while the composites consisting of copolymer **P8b** and the CdTe nanocrystals show a normal distribution profile (**Figure 3.19b**) with an average diameter of 488 nm and an expected smaller standard deviation of 79.9 nm. The surface morphology of the composites was investigated by means of atomic force microscopy in the tapping mode. The AFM images illustrate the raw height data in top view (**Figure 3.20a**) and the surface appearance with slope shading (**Figure 3.20b**), which is a calculation provided by the software, where a perspective illumination from the right is implemented on the images improving thus the contour visualization.[65-67]

The AFM measurements, in case of the **P7b MPs**+$CdTe_{red}$ composite system revealed formation of nanocrystal aggregates, which stand out from the polymer surface, while an alignment of the nanocrystals around the polymer chains was observed in case of **P8b MPs**+$CdTe_{red}$.

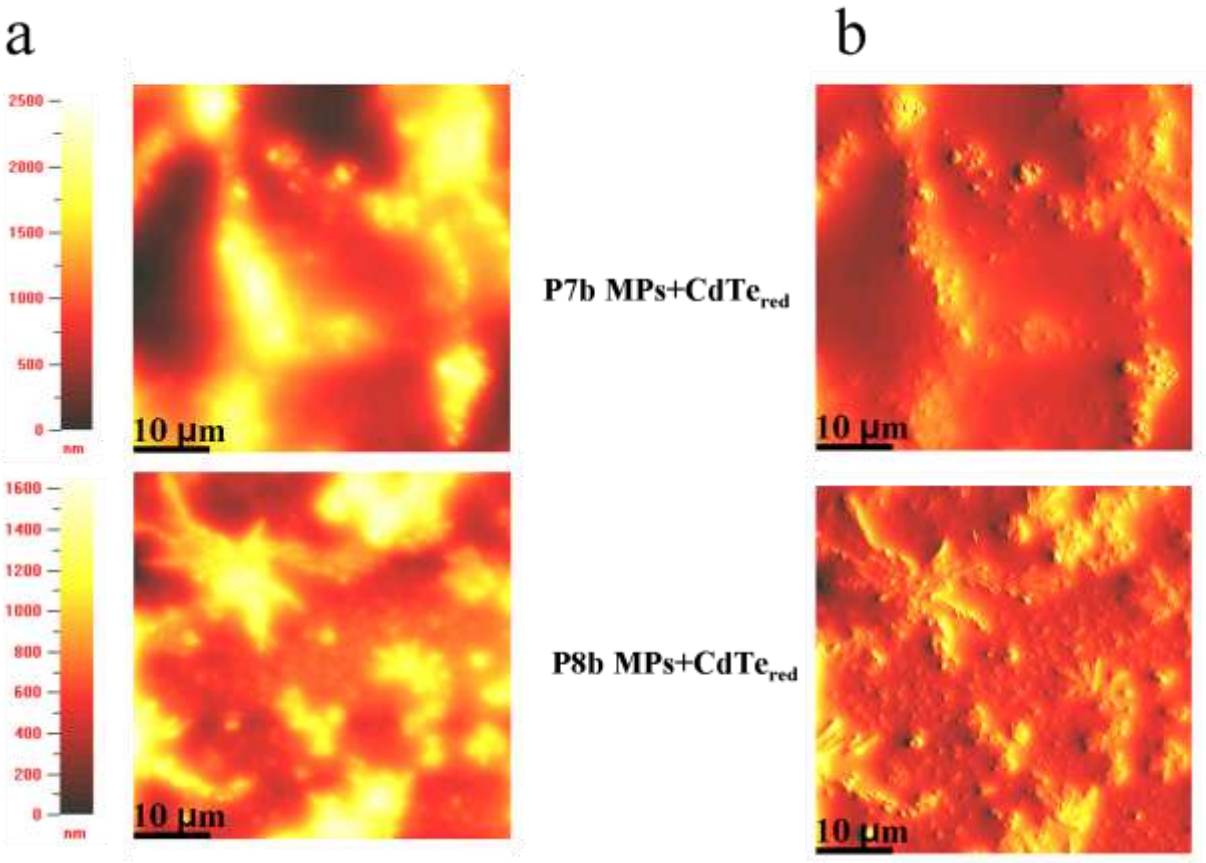

Figure 3.20: AFM images of **P7b MPs**+$CdTe_{red}$ and **P8b MPs**+$CdTe_{red}$ composites prepared from water dispersions *via* the precipitation-sonication method. (a) False color representation of the raw height data acquired in the tapping mode. (b) Contour plot calculated from the raw data with slope shading. The films were prepared by drop-casting microparticulate copolymer-$CdTe_{red}$ dispersions (10^{-2} mol/L copolymer and 10^{-3} mol/L nanocrystal concentration) from water on glass substrates. The AFM images have a scale of 50 × 50 µm.

The combination of the polymers with the nanocrystals provided average surface roughness of 499 nm in case of the **P7b MPs**+CdTe system (817 nm for the bare **P7b MPs**) and a 278 nm surface roughness in case of the **P8b MPs**+CdTe system (264 nm for the bare **P8b MPs**). A tendency to a smoother surface can be identified, when combining the CdTe nanocrystals with the **P7b** microparticles compared to the surface of the bare **P7b** microparticles, whereas the

surface characteristic is not immensely influenced for the **P8b MPs**+CdTe system allowing thus the monitoring of the postulated coming-together of the nanocrystals around the polymer chains. In terms of their optical properties, these composite systems are discussed in the chapter of '**Energy and Electron Transfer Studies**' elucidating a dependence of the realized energy transfer process on the preparation method of the composite dispersions.

3.5 References

[1] M. Leclerc, F. Martinez Diaz, G. Wegner, *Macromol. Chem. Rapid Commun.* **1989**, 190, 3105.
[2] T. Yamamoto, W. Yamada, M. Takagi, K. Kizu, T. Maruyama, N. Ooba, S. Tomaru, T. Kurihara, T. Kaino, K. Kubota, *Macromolecules* **1994**, 27, 6620.
[3] F. Huang, Y. Zhang, M. S. Liu, *Adv. Funct. Mater.* **2009**, 19, 2457.
[4] F. Huang, H. Wu, D. Wang, W. Yang, Y. Cao, *Chem. Mater*. **2004**, 16, 708.
[5] Z. S. Guo, L. Zhao, J. Pei, Z. L. Zhou, G. Gibson, J. Brug, S. Lam, S. S. Mao, *Macromolecules* **2010**, 43, 1860.
[6] L. Kinder, J. Kanicki, P. Petroff, *Synth. Met*. **2004**, 146, 181.
[7] A. Tsami, X. H. Yang, F. Galbrecht, T. Farrell, H. Li, S. Adamczyk, R. Heiderhoff, L. J. Balk, D. Neher, E. Holder, *J. Polym. Sci. Part A: Polym. Chem*. **2007**, 45, 4773.
[8] A. Tsami, X. H. Yang, T. Farrell, D. Neher, E. Holder, *J. Polym. Sci. Part A: Polym. Chem.* **2008**, 46, 7794.
[9] E. P. Woo, M. Inbasekaran, W. R. Shiang, Roof GR. WO//05184, **1997**.
[10] B. Liu, B. S. Gaylord, G. C. Bazan, *J. Am. Chem. Soc*. **2003**, 125, 6705.
[11] K. Jeong, S. Kim, U. Shin, *J. Am. Chem. Soc.* **2005**, 127, 17672.
[12] M. Stork, B. S. Gaylord, A. J. Heeger, G. C. Bazan, *Adv. Mater*. **2002**, 14, 361.
[13] U. Asawapirom, U. Scherf, *Macromol. Rapid Commun*. **2001**, 22, 746.
[14] L. Y. Wang, K. C. Li, H. C. Lin, *Polymer* **2010**, 51, 75.
[15] J. N. Demas, G. A. Crosby, *J. Phys. Chem*. **1971**, 75, 991.
[16] J. Liu, G. Tu, Q. Zhou, Y. Cheng, Y. Geng, L. Wang, D. Ma, X. Jing, F. J. Wang, *Mater. Chem.* **2006**, 16, 1431.
[17] A. A. Lutich, G. Jiang, A. S. Susha, A. L. Rogach, F. D. Stefani, J. Feldmann, *Nano Lett*. **2009**, 9, 2636.
[18] M. Ranger, D. Rondeau, M. Leclerc, *Macromolecules* **1997**, 30, 7686.
[19] S. Xiao, M. Nguyen, X. Gong, X. Cao, H. Wu, D. Moses, A. J. Heeger, *Adv. Funct. Mater.* **2003**, 13, 25.
[20] Y. Chen, Y. Araki, J. Doyle, A. Strevens, O. Ito, W. Blau, *J. Chem. Mater.* **2005**, 17, 1661.
[21] D. Marsitzky, R. Vestberg, P. Blainey, B. T. Tang, C. J. Hawker, K. R. Carter, *J. Am. Chem. Soc.* **2001**, 123, 6965.
[22] C. H. Chou, C. F. Shu, *Macromolecules* **2002**, 35, 9673.
[23] J. Sakamoto, M. Rehahn, G. Wegner, A. D. Schlüter, *Macromol. Rapid Commun.* **2009**, 30, 653.
[24] C. Chou, H. S. Lin, K. Dinakaran, M. Chiu, K. Wei, *Macromolecules* **2005**, 38, 745.
[25] C. Ego, A. C. Grimsdale, F. Uckert, G. Yu, G. Srdanov, K. Müllen, *Adv. Mater*. **2002**, 14, 809.
[26] A. Kulasi, H. Yi, A. Iraqi, *J. Polym. Sci. Part A: Polym. Chem.* **2007**, 45, 5957.

[27] Y. Chen, G. Huang, C. Hsiao, S. Chen, *J. Am. Chem. Soc.* **2006**, 128, 8549.
[28] A. Klapars, J. Anitilla, X. Huang, S. Buchwald, *J. Am. Chem. Soc*. **2001**, 123, 7727.
[29] C. Wang, L. O. Pålsson, A. S. Batsanov, M. R. Bryce, *J. Am. Chem. Soc.* **2006**, 128, 3789.
[30] U. Giovanella, M. Pasini, S. Destri, W. Porzio, C. Botta, *Synth. Met*. **2008**, 158, 113.
[31] L. R. Tsai, C. W. Li, Y. Chen, *J. Polym. Sci. Part A: Polym. Chem*. **2008**, 46, 5945.
[32] J. S. Park, M. Song, S. H. Jin, J. W. Lee, C. W. Lee, Y. S. Gal, *Macromol. Chem. Phys.* **2009**, 210, 1572.
[33] Y. Zhu, A. R. Rabindranath, T. Beyerlein, B. Tieke, *Macromolecules* **2007**, 40, 6981.
[34] J. F. Morin, M. Leclerc, D. Ades, A. Siove, *Macromol. Rapid Commun*. **2005**, 26, 761.
[35] J. Huang, Y. Niu, W. Yang, Y. Mo, M. Yuan, Y. Cao, *Macromolecules* **2002**, 35, 6080.
[36] Z. Fu, Z. Bo, *Macromol. Rapid Commun*. **2005**, 26, 1704.
[37] I. Kanelidis, V. Elsner, M. Bötzer, M. Butz, V. Lesnyak, A. Eychmüller, E. Holder, *Polymer* **2010**, 51, 5669.
[38] Y. Zou, Y. Zhou, G. Wu, Y. Li, C. Pan, *J. Appl. Polym. Sci.* **2009**, 111, 978.
[39] E. Holder, N. Tessler, A. Rogach, *J. Mater. Chem.* **2008**, 18, 1064.
[40] J. Liu, T. Tanaka, K. Sivula, A. P. Alivisatos, J. M. J Frechet, *J. Am. Chem. Soc*. **2004**, 126, 6550.
[41] H. Skaff, K. Sill, T. Emrick, *J. Am. Chem. Soc*. **2004**, 126, 11322.
[42] S. Dayal, N. Kopidakis, D. C. Olson, D. S. Ginley, G. Rumbles, *J. Am. Chem. Soc*. **2009**, 131, 17726.
[43] H. J. Egelhaaf, E. Holder, P. Herman, H. A. Mayer, D. Oelkrug, E. Lindner, *J. Mater. Chem.* **2001**, 11, 2445.
[44] V. Marin, E. Holder, R. Hoogenboom, U. S. Schubert, *Macromol. Rapid Commun.* **2004**, 25, 793.
[45] W. W. Yu, L. Qu, W. Guo, X. Peng, *Chem. Mater.* **2003**, 15, 2854.
[46] C. Querner, A. Benedetto, R. Demadrille, P. Rannou, P. Reiss, *Chem. Mater*. **2006**, 18, 4817.
[47] J. Liu, T. Tanaka, K. Sivula, A. P. Alivisatos, J. M. J Frechet, *J. Am. Chem. Soc*. **2004**, 126, 6550.
[48] D. V. Talapin, A. L. Rogach, A. Kornowski, M. Haase, H. Weller, *Nano Lett*. **2001**, 1, 207.
[49] C. Bullen, P. Mulvaney, *Langmuir* **2006**, 22, 3007.
[50] N. N. Mamedova, N. A. Kotov, A. L. Rogach, J. Studer, *Nano Lett.* **2001**, 1, 281.
[51] M. Grell, D. D. C. Bradley, G. Ungar, J. Hill, K. S. Whitehead, *Macromolecules* **1999**, 32, 5810.
[52] Z. Chen, X. Li, *WO 2007/027159 A1*, **2007**.
[53] C. F. Wu, B. Bull, C. Szymanski, K. Christensen, J. McNeill, *ACS Nano* **2008**, 2, 2415.
[54] J. B. Yu, C. F. Wu, S. P. Sahu, L. P. Fernando, C. Szymanski, J. McNeill, *J. Am. Chem. Soc.* **2009**, 131, 18410.
[55] C. J. Qin, H. Tong, L. X. Wand, *Sci. Chin. Ser. B Chem.* **2009**, 52, 833.
[56] X. Peng, M. C. Schlamp, A. V. Kadavanich, A. P. Alivisatos, *J. Am. Chem. Soc.* **1997**, 119, 7019.
[57] C. Qin, Y. Cheng, L. Wang, X. Jing, F. Wang, *Macromolecule*s **2008**, 41, 7798.
[58] J. Langecker, M. Rehahn, *Macromol. Chem. Phys*. **2008**, 209, 258.
[59] I. Kanelidis, Y. Ren, V. Lesnyak, J. C. Gasse, R. Frahm, A. Eychmüller, E. Holder, *J. Polym. Sci. Part A: Polym. Chem.* **2011**, 49, 392.

[60] M. Svensson, F. Zhang, S. C. Veenstra, W. J. H. Verhees, J. C. Hummelen, J. M. Kroon, O. Inganäs, M. R. Andersoon, *Adv. Mater*. **2003**, 15, 988.
[61] R. Gütner, U. Asawapirom, M. Forster, C. Schmitt, B. Stiller, B. Tiersch, A. Falcou, H. G. Nothofer, U. Scherf, *Thin Solid Films* **2002**, 417, 1.
[62] C. Wu, J. McNeill, *Langmuir* **2008**, 24, 5855.
[63] S. Shekhar, E. Aharon, N. Tian, F. Galbrecht, U. Scherf, E. Holder, G. L. Frey, *Chem. Phys. Chem.* **2009**, 10, 576.
[64] Q. Pei, Y. Yang, *J. Am. Chem. Soc.* **1996**, 118, 7416.
[65] E. J. Houser, D. B. Chrisey, M. Bercu, N. D. Scarisoreanu, A. Purice, D. Colceag, C. Constantinescu, A. Moldovan, M. Dinescu, *Appl. Surface Sci.* **2006**, 252, 4871.
[66] H. L. Hing, S. J. Shee, M. A Kaswandi, A. H. Abd Aziz, A. Z. Sahalan, *Proc. MST Conf.* **2010**, 12.
[67] S. S. Stewart-Clark, Y. M. Lvov, *J. Coat. Technol. Res.* **2011**, 8, 275.
[68] C. Edder, J. M. J. Frechet, *Org. Lett.* **2003**, 5, 1879.
[69] B. Zhang, C. Qin, J. Ding, L. Chen, Z. Xie, Y. Cheng, L. Wang, *Adv. Funct. Mater.* **2010**, 20, 2951.
[70] N. Tian, A. Thiessen, R. Schiewek, O. J. Schmitz, D. Hertel, K. Meerholz, E. Holder, *J. Org. Chem.* **2009**, 74, 2718.

4 Energy and Electron Transfer Studies

4.1 CdSe

CdSe nanocrystals were firstly used in a synthesis, where the synthesized amino-functionalized fluorene **14** played the role of one co-ligand. The obtained fluorene-surface-functionalized CdSe nanocrystals (**NC1**) synthesized in the group of Dr. Andrey Rogach (Department for Physics and Center for Nanoscience, Maximilian University of Munich) have been used as starting material in straight-forward Yamamoto protocols in order to obtain oligo(fluorene) capped CdSe NCs (**NC2**) and upon combination of **NC1** with 2,7-dibromo-9,9'-dioctyl-9*H*-fluorene, CdSe nanocrystals surrounded by poly(fluorene) chains (**NC3**). The investigation of the optical properties by means of photoluminescence spectroscopy for the three nanocomposites in comparison to reference nanocrystals (**$CdSe_{ref}$**) endcapped with *n*-hexadecylamine and tetradecylphosphonic acid revealed (section **3.2**, **Figure 3.7**) neither for **NC2** nor for **NC3** reliable signatures of energy transfer from the polymer part to the nanocrystals. On the other hand, quenching of the nanocrystal emission is observed (**Figures 3.7b-c**), a phenomenon attributed to the short separation distances between the organic and inorganic components provided through their direct chemical binding. The direct linkage of CdSe NCs and fluorene-moieties favours efficient charge separation, which is a process competitive to the energy transfer from the organic to the inorganic counterpart included in organic-inorganic composites.[1] A deeper insight in the photophysics of the in-here synthesized nanocomposites was gained by conducting time-resolved photoluminescence measurements. The latter experiments were carried out in the groups of Dr. Andrey Rogach and Prof. Dr. Feldmann in the Department for Physics and Center for Nanoscience at the Maximilian University of Munich. **Figure 4.1** visualizes the time-resolved PL measurements in terms of photoluminescence decay. The photoluminescence kinetics of CdSe NCs in composites **NC1** and **NC3** are in the frame of experimental error differ, however, clearly from **$CdSe_{ref}$**. As **Figure 4.1** reveals, the nanocrystals in the composites **NC1** and **NC3** exhibit significantly faster photoluminescence decays compared to the reference CdSe nanocrystals. This observation is a further argument supporting, together with the photoluminescence quenching, the hypothesis of a charge separation process between CdSe nanocrystals and fluorene counterparts rendering these hybrid materials promising for photovoltaic devices.[2]

a)

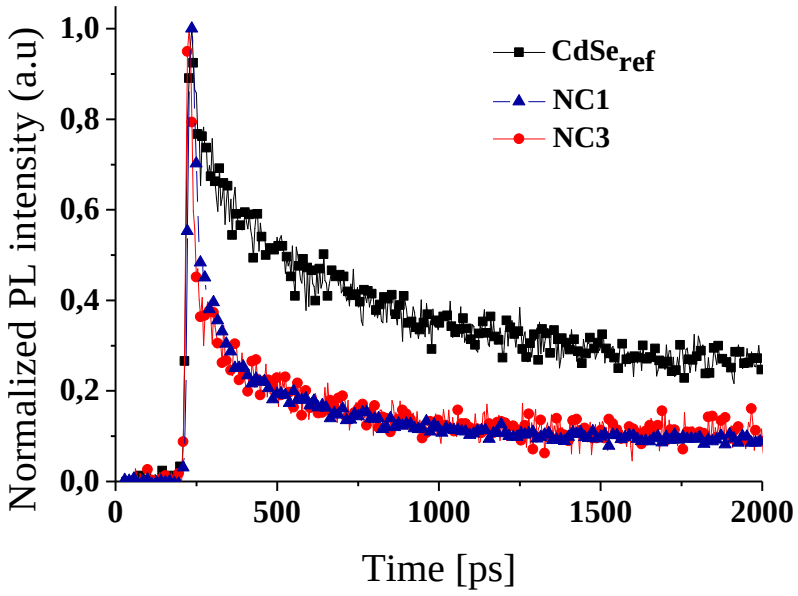

b)

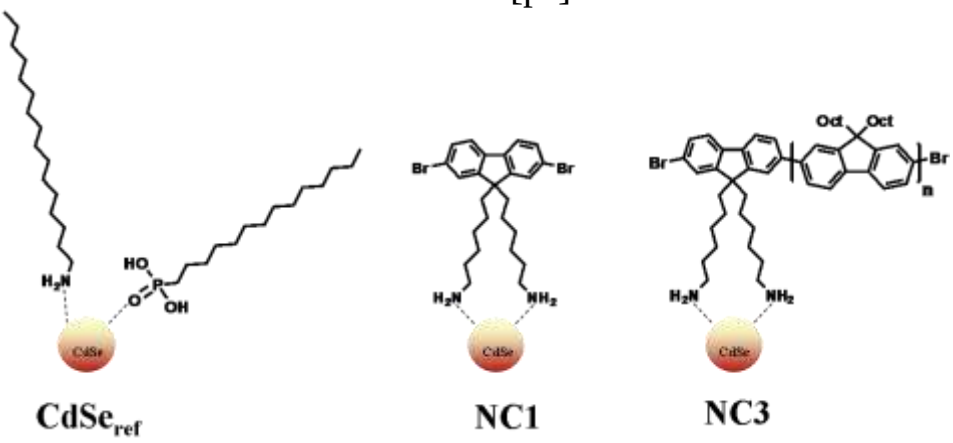

Figure 4.1: (a) Time-resolved photoluminescence spectra of CdSe nanocrystals embraced in the samples of the reference nanocrystals **$CdSe_{ref}$** and the nanocomposites **NC1** and **NC3** and (b) the corresponding structural configurations of the materials.

Regarding the fact that measurements of nanocomposites **NC1** and **NC3** comprise and coincide to experimental errors, it seems that the opto-electronic properties of these composites are not influenced by the polymerization conditions but depend on the chemical linkages proceeding on the surface of the nanocrystals between fluorenes and CdSe.

4.2 CdTe

4.2.1 CdTe and Poly(fluorene)s Containing Aliphatic Amino-Side-Chains

Two fluorene-based wide band-gap copolymers (**P2a-b**) equipped with aliphatic amino-end-groups and prepared from their side-chain bromo-functionalized precursors (**P1a-b**), which were synthesized according to a Ni(0) mediated Yamamoto polymerization, were applied as hosts for low band-gap CdTe nanocrystals. A reference polymer **Pref**, where the building block with amine-functionality was excluded, was synthesized as well (**Figure 4.2**).[3]

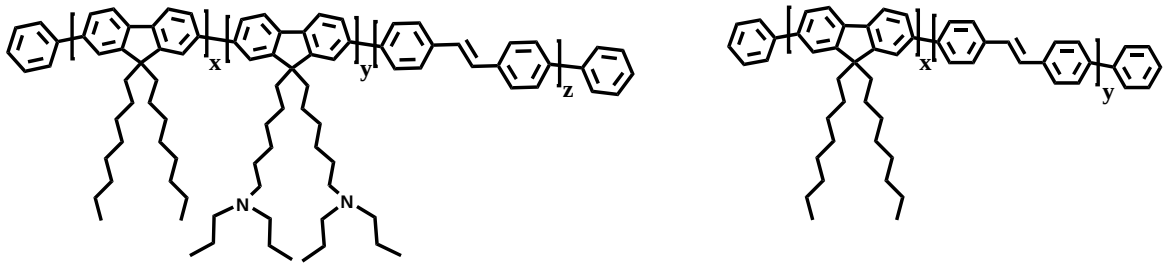

P2a-b **Pref**

Figure 4.2: Configuration of the amino-functionalized copolymers **P2a** (x/y/z: 40/10/50) and **P2b** (x/y/z: 35/15/50) and the reference copolymer **Pref** (x/y: 50/50), where x,y,z represent the feed ratio of the initial building blocks in %.

The CdTe nanocrystals were endcapped with 4-bromobenzenethiol and prepared in the group of Prof. Dr. Eychmüller (Technical University of Dresden, Physical Chemistry/Electrochemistry Department) by Dr. Vladimir Lesnyak using a literature approach.[4] The detailed synthesis is described in the experimental part (section **6.5.1**). The average particle diameter of the CdTe/HS-C_6H_4-Br NCs is 2.9 nm and their optical properties are shown in **Figure 4.3**.

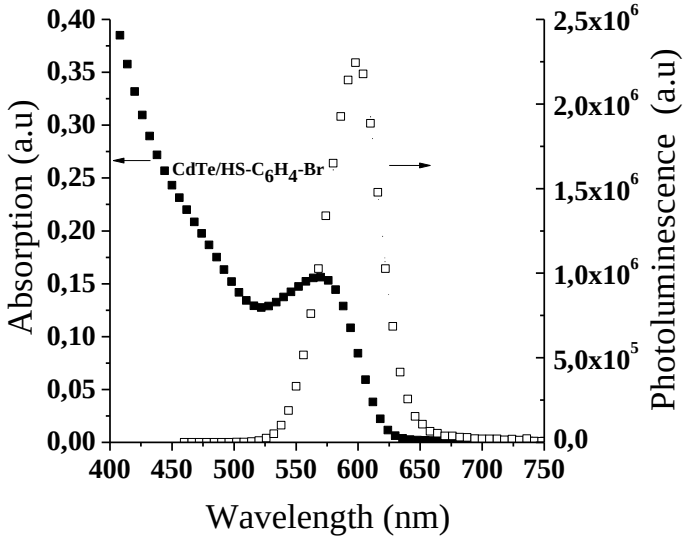

Figure 4.3: Absorption and emission spectra of the CdTe/HS-C_6H_4-Br nanocrystals in dimethylformamide (DMF). The particle concentration in DMF was 9×10^{-4} M (40 mg/mL).

The next step was the preparation of CdTe-polymer composites by a respective procedure explained in the experimental part (section **6.5.2**). Subsequently, solid-state measurements of the optical properties of the copolymers solely and the CdTe-polymer systems were conducted in terms of relative emission intensities (**Figure 4.4a**). The bare copolymers **Pref**, **P2a** and **P2b** showed efficient blue-light emission at an excitation wavelength of 410 nm. The addition of the CdTe nanocrystals in order to create the CdTe-polymer systems quenched the polymer emission without initiating an energy transfer process onto the added nanocrystals. The sequence of the quenching effect (QE) assigned to the polymer backbone band follows the order $QE_{\mathbf{Pref}} < QE_{\mathbf{P2a}} < QE_{\mathbf{P2b}}$. In concrete terms, the signal of the nanocomposite comprising **Pref** and CdTe NCs is quenched by a factor of 8.4 compared to the bare **Pref**, while the intensities of the composites based on copolymers **P2a** and **P2b** were lowered by a magnitude of 12.5 and 24.7, correspondingly, and in respect to their neat copolymer bands, as well. By normalizing the fluorescence measurements on the basis of the polymer emission, the 610 nm band, which was not pronounced during the relative emission intensities measurements, becomes obvious and is assigned to the CdTe nanocrystals (**Figure 4.4b**). This band exhibited an intensity enhancement (IE) following the order: $IE_{\mathbf{P2b}+CdTe} > IE_{\mathbf{Pref}+CdTe} > IE_{\mathbf{P2a}+CdTe}$. The larger fluorescence deactivation of **P2b** compared to polymers **P2a** and **Pref** in their composites with CdTe nanocrystals and the corresponding higher intensity enhancement of the NC band in the **P2b**+CdTe composite, may thus be brought in connection to the content of the amino-groups in the copolymer side-chains. In this way, the enhanced

nitrogen content in case of **P2b** can possibly influence the surface states of the CdTe NCs.[5,6]

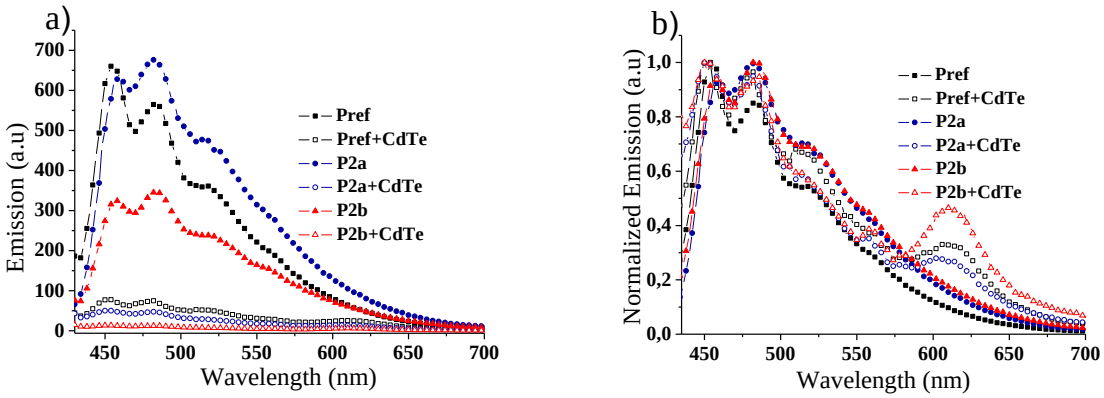

Figure 4.4: Emission (a) and normalized emission (b) spectra of copolymers **Pref**, **P2a**, **P2b** (1 mg/mL in THF) and their composites with CdTe ($\lambda_{exc.}$ 410 nm) drop-casted from THF and a DMF/THF (1/3) mixture, respectively.

The deactivation process can be monitored on the pictures of **Figure 4.5** and can be most probably assigned to collisional quenching, a phenomenon, for which bromobenzene, an efficient quencher of many fluorophores, is particularly known.[7]

Figure 4.5: Images of copolymer **P2b**, CdTe NCs and **P2b**+CdTe composite system (1:1 v/v) in that order from the left to the right without (left) and under UV-vis irradiation at an excitation wavelength of 366 nm (right).

4-Bromobenzenethiol (HS-C_6H_4-Br), the endcapper used for the synthesis of the CdTe nanocrystals in order to stabilize and functionalize their surface, belongs to the class of bromobenzenes and can thus suppress the polymer emission by a direct contact with the polymer in solid films. Furthermore, the solvent used for the maintenance of the nanocrystals namely *N*,*N*-dimethylformamide is also known for its quenching properties and can contribute to the appearing fluorescence drop. It seems that the deactivation and intensity enhancement processes in these composite systems exhibit a dependence on the bromo-functionalized stabilizing ligands of the nanocrystals and the nitrogen content of the copolymers as well.[3] The polymer with the highest nitrogen amount incorporated in the backbone (**P2b**) showed a double and triple order luminescence decrease compared to **P2a** and **Pref**, rendering the emission deactivation a possible nitrogen-content depending process. The electron-rich amine

end-groups of the fluorene-based copolymers **P2a-b** may thus provide detection capabilities of nanocrystals decorated with electron deficient ligands and can become candidates as fluorescent-based sensor materials. On the other hand, the dependence on the bromo-functionalities embraced in the nanocrystal-surface endcappers can render the resulting luminescence diminishment promising for sensing bromo-containing aromatic compounds.

4.2.2 CdTe and Poly(fluorene)s/Poly(carbazole)s Containing Arylamino Side-Chains

Two alternating poly(fluorene)s designed with 4,4'-(2,7-dibromo-9*H*-fluorene-9,9'-diyl) dianiline or 4,4'-(2,7-dibromo-9*H*-fluorene-9,9'-diyl)*bis*(*N*,*N′*-diphenylaniline) as building blocks (**P3** & **P4**) and their corresponding poly(carbazole)s based on comonomers 4-(3,6-dibromo-9*H*-carbazol-9-yl)aniline or 4-(3,6-dibromo-9*H*-carbazol-9-yl)-*N*,*N′*-diphenylaniline (**P5** & **P6**) were prepared by copolymerizing them with 2,2'-(9,9'-dioctyl-9*H*-fluorene-2,7-diyl)*bis*(1,3,2-dioxaborinane) following a classical Suzuki protocol (**Figure 4.6**).[8,9]

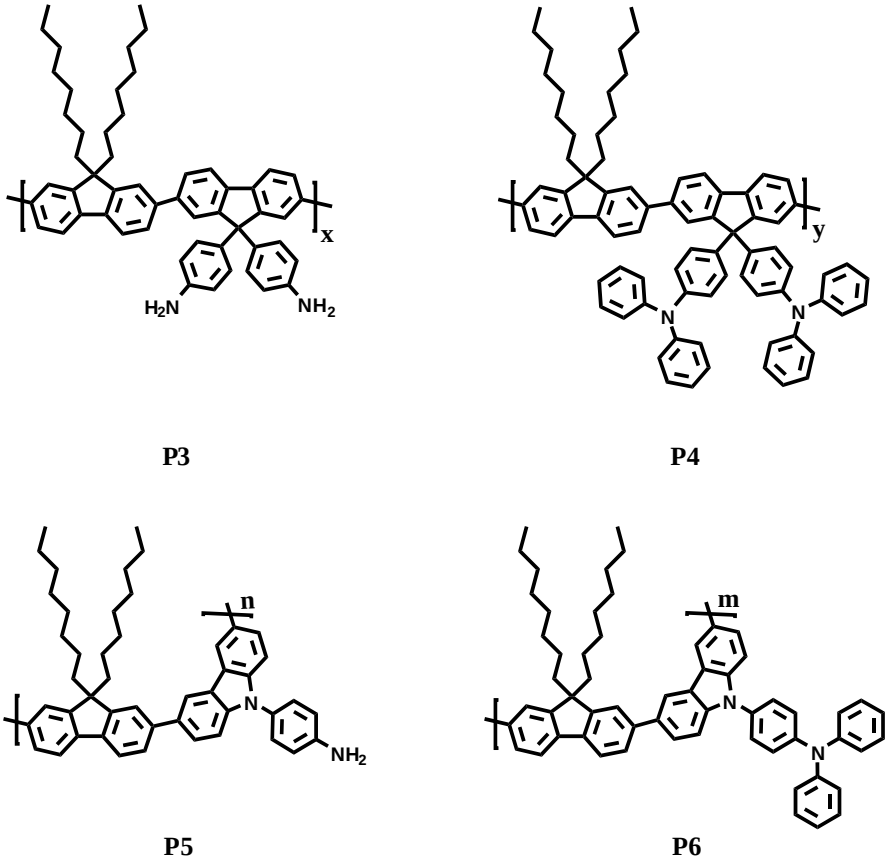

Figure 4.6: The fluorene- (**P3** & **P4**) and carbazole-based (**P5** & **P6**) alternating arylamino-functionalized copolymers.

The wide band-gaps of the polymers and their nitrogen containing side-chains can facilitate their function as linkers to a variety of nanoparticles like the semiconductor low band-gap CdTe nanocrystals. The CdTe nanocrystals used in our experiments were endcapped with 4-bromobenzenethiol (HS-C_6H_4-Br) and synthesized by Dr. Vladimir Lesnyak from the group of Prof. Dr. Eychmüller (Technical University of Dresden, Physical Chemistry/Electrochemistry Department).[4] The emission color of the obtained CdTe nanocrystals varied from green (CdTe A) to orange-red (CdTe E), whereby their optical properties, morphology and appearance in solution are given in **Figures 4.7a**, **4.7b** and **4.7c**, respectively.

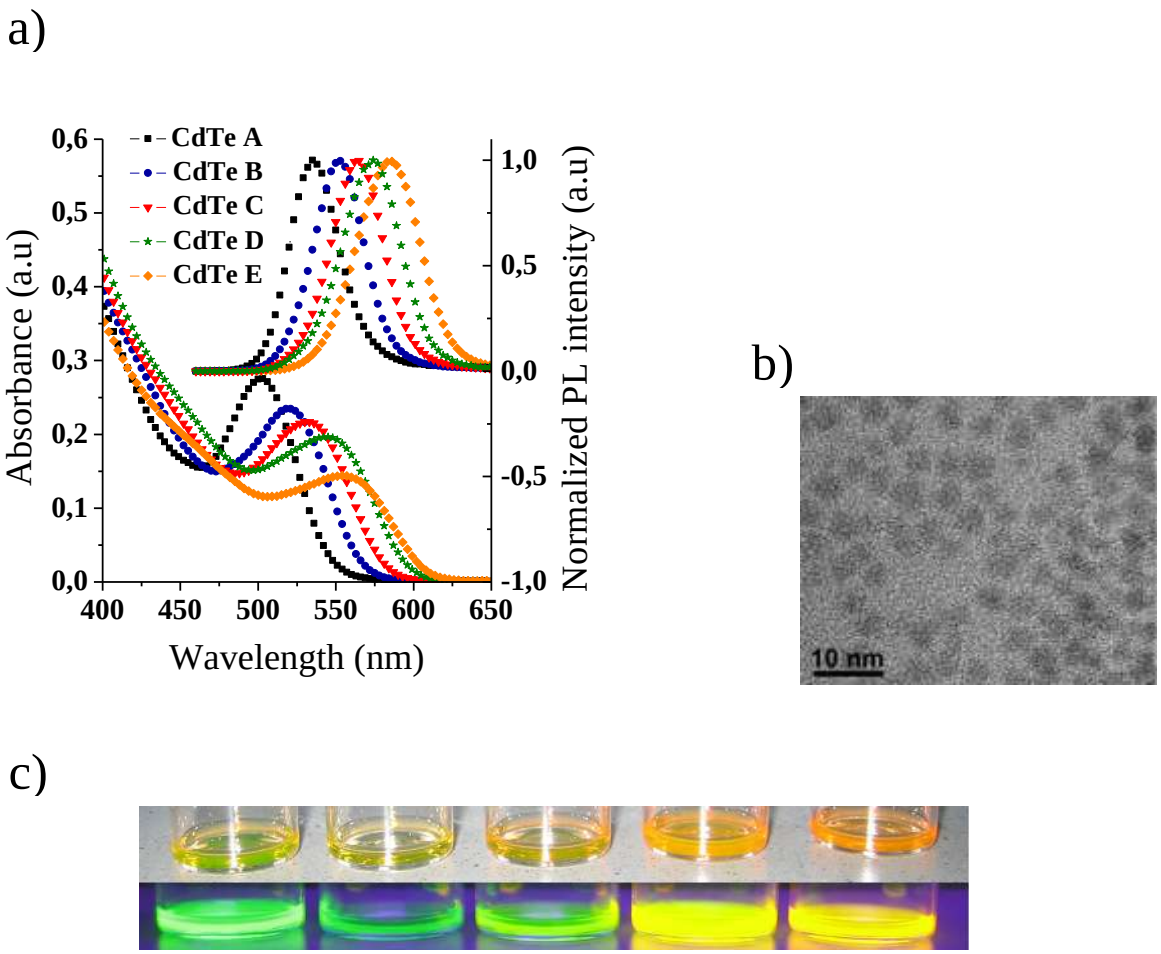

Figure 4.7: (a) Absorption and emission spectra of CdTe/HS-C_6H_4-Br NCs emitting light from green (CdTe A) to orange-red (CdTe E) color. The particle concentration in DMF varied from 10^{-3} M to 7.3×10^{-4} M. (b) TEM image of CdTe/HS-C_6H_4-Br NCs emitting orange light (CdTe E). (c) Photographs of CdTe NCs A, B, C, D, E in DMF (in this sequence from the left to the right): daylight (top) and under illumination of UV light at an excitation wavelength of 366 nm (bottom).

Copolymers and nanocrystals exhibit overlapping emission and absorption spectra and the band-gap alignment of the copolymers is suitable to play the role of the host. Solid-state measurements of the optical properties of polymers, nanocrystals and their composites were conducted in order to investigate possible energy transfer from the polymers onto the CdTe nanocrystals.[8]

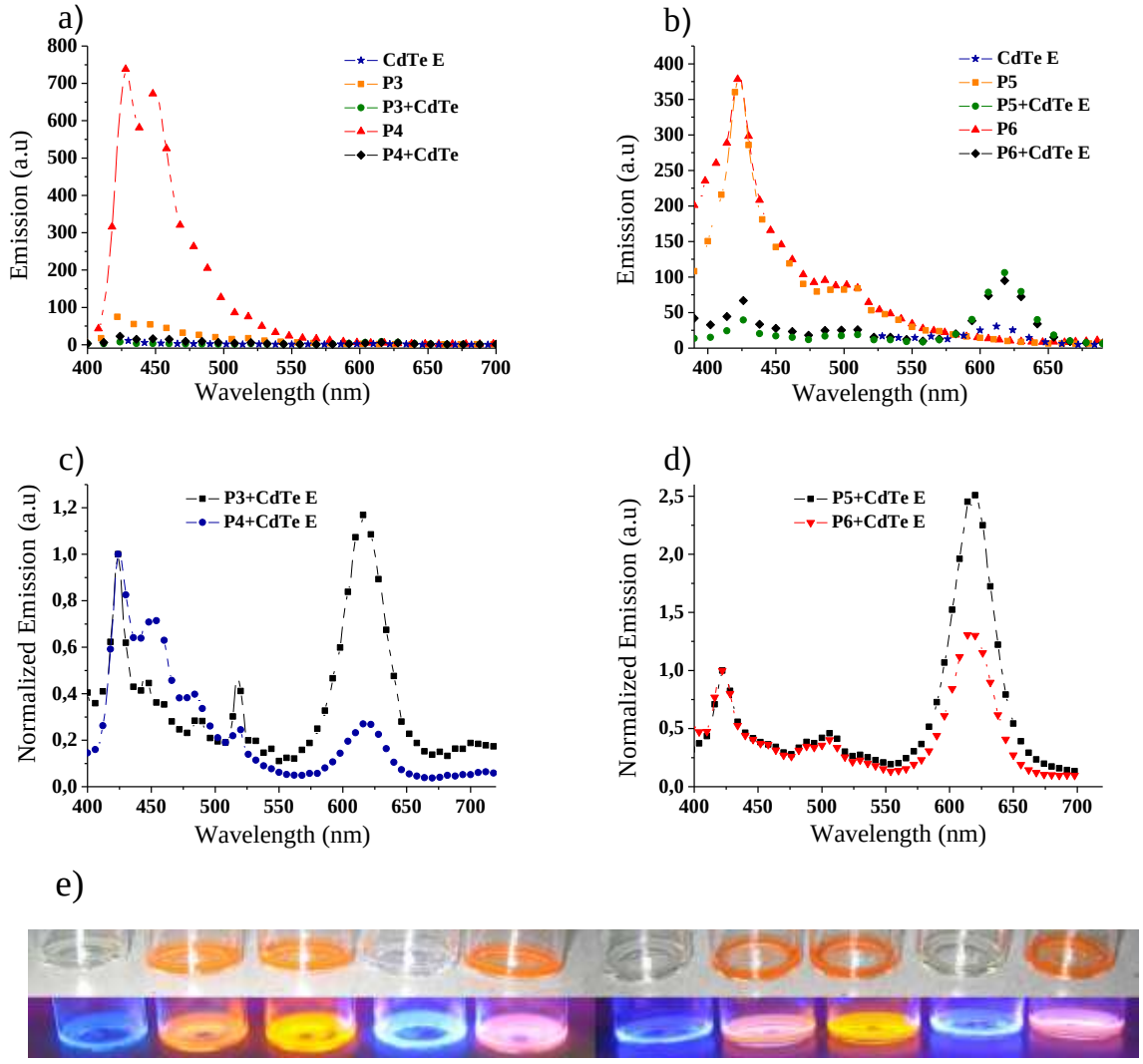

Figure 4.8: (a) Emission spectra of films of polymers **P3**, **P4**, CdTe E nanocrystals and their composites ($\lambda_{exc.}$ 380 nm). (b) Emission spectra of films of polymers **P5**, **P6**, CdTe E nanocrystals and their composites ($\lambda_{exc.}$ 370 nm). (c,d) Normalized emission spectra of the composites of polymers **P3**-**P6** with CdTe E nanocrystals. Polymer films were drop-casted from THF, while nanocrystal and composite films from a DMF/THF (1/3) mixture. (e) Photographs: Left: **P3**, **P3**+CdTe E, CdTe E, **P4**, **P4**+CdTe E, in that order left to right. Right: **P5**, **P5**+CdTe E, CdTe E, **P6**, **P6**+CdTe E in that order left to right without and under illumination of UV light ($\lambda_{exc.}$ 366 nm).

Figures 4.8a and **4.8b** visualize the aforementioned measurements, which reveal an insufficient tendency for energy transfer from the polymers to the nanocrystals, probably due to 4-bromobenzenethiol (HS-C_6H_4-Br) used for the nanocrystal surface functionalization and known for its polymer-emission quenching properties. On the other side, the intolerability of the nanocrystals in solvents like chloroform or hexane makes their storage obligatorily feasible in *N*,*N*-dimethylformamide, a solvent known for its quenching ability, as well. However, the normalized emission spectra of the composites (**Figures 4.8c**, **4.8d**), when viewed in conjunction to the photographs of polymer, CdTe and composite solutions (**Figure 4.8e**), reveal a potential for tuning the emission color of the host-guest system. The pictures in **Figure 4.8e** make the color shift visible, whereby a color change from blue to red is observed in the case of copolymer **P3** and to reddish-white in the case of **P4**. The composites prepared by carbazole-based copolymers **P5** and **P6** exhibited a reddish-white color change, when compared to the blue-emitting polymers and the orange-red emitting CdTe E nanocrystals. The morphology of the achieved composites were investigated by means of atomic force microscopy in the tapping mode and the measured films were prepared by mixing DMF solutions of the CdTe E nanocrystals (8 mg/mL) with THF solutions of the polymers (1 mg/mL) in a 1:1 (v/v) ratio by drop-casting on glass substrates. The AFM experiments were carried out in the group of Prof. Dr. Frahm at the University of Wuppertal and supported by Jan-Christoph Gasse. **Figure 4.9a** illustrates the formation of CdTe nanoparticle clusters with a domain size of ~ 200 nm as revealed by AFM. The formed CdTe nanocrystal aggregates seem to be over-coated with a layer of the individual polymer as the comparison of the composite images with the bare CdTe nanocrystals shows (**Figure 4.9b**). The roughness of the film surfaces is considerable for the polymer-nanocrystal systems and traversing from composites built with polymer **P3**-**P6** the average roughness values recorded were as following: 146.6 nm, 322.8 nm, 254.5 nm and 165.7 nm.

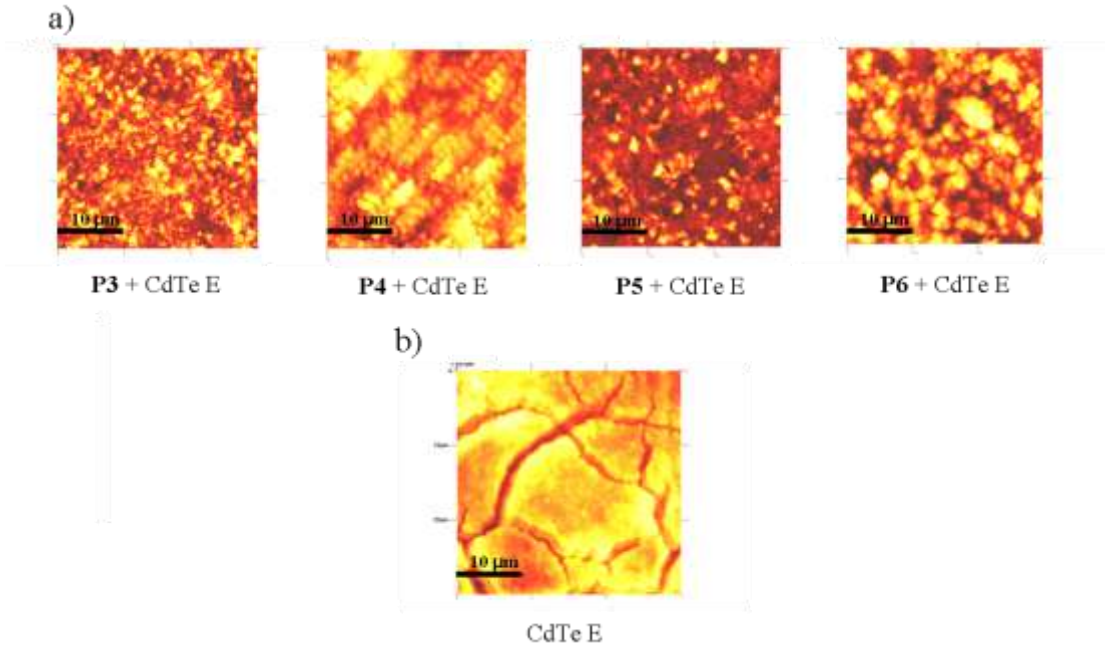

Figure 4.9: AFM images (tapping mode) of (a) films of composites prepared by mixing DMF solutions of the CdTe E nanocrystals (8 mg/mL) with THF solutions of the polymers (1 mg/mL) in a 1:1 (v/v) ratio and (b) film of the CdTe E nanocrystals (4 mg/mL concentration in DMF) on glass substrates obtained by drop-casting the respective solutions. The AFM images have a scale of 30 × 30 μm.

The quite large roughness is an attribute of the drop-wise addition of the prepared AFM solutions on the glass substrates as the lack of spinning hinders the formation of perfectly homogeneous films. CdTe E nanocrystals exhibit a more uniform film compared to the films of the composites with a roughness of 319.9 nm. The larger packed regions (10-21 μm) leading to larger aggregation phenomena, may be the result of the breaking-down of the film due to shrinkage by solvent evaporation. As the fluorescence solid-state measurements pointed out, an appropriate combination of copolymers and CdTe nanocrystals renders the accomplishment of white-light emission possible.[8] For this purpose, the blue-emitting copolymers **P3**-**P6** were brought together with a yellow-emitting CdTe species. The latter was prepared by mixing the orange-red emitting CdTe NCs E with the green emitting CdTe NCs B (section **6.5.3**). The approach towards white-light emission in solution was revealed by the emission bands at ~ 425 nm and ~ 545 nm as is shown in **Figure 4.10a**. The complementary yellow band appearing at 545 nm is essential for the achievement of white light.

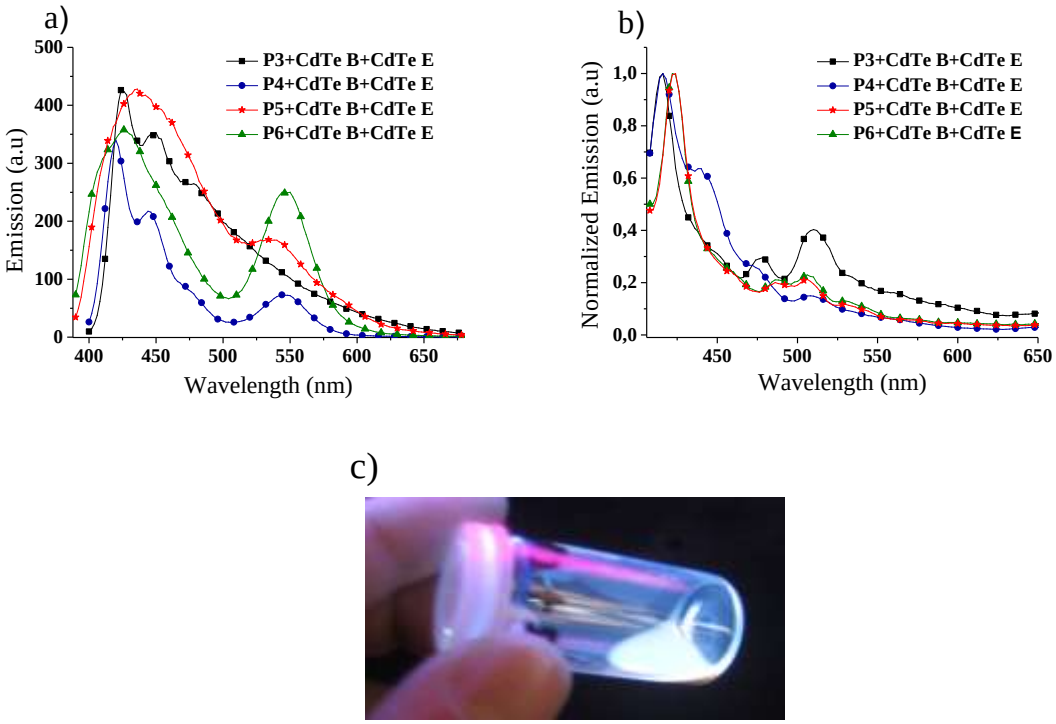

Figure 4.10: (a) Emission spectra of copolymers **P3**, **P4**+CdTe ($\lambda_{exc.}$ 380 nm) and copolymers **P5**, **P6**+CdTe ($\lambda_{exc.}$ 370 nm) in DMF solutions. (b) Normalized emission spectra of copolymers **P3**, **P4**+CdTe ($\lambda_{exc.}$ 380 nm) and copolymers **P5**, **P6**+CdTe ($\lambda_{exc.}$ 370 nm) in films drop-casted from DMF. (c) Exemplary photograph of white-light emission under illumination of UV light ($\lambda_{exc.}$ 366 nm) of the composite of copolymer **P4**+CdTe NCs B and E.

The corresponding solid-state measurements are seen in **Figure 4.10b**, showing a blue shift of both bands coming up now at ~ 420 nm and ~510 nm, respectively. Figure **4.10c** illustrates exemplarily the achieved favorable white-light emission for the composite system of polymer **P4** with CdTe nanocrystals B and E in DMF solution. Thus, following a fine color-tuning process, white-light emission within organic-inorganic composites was achieved. The emission colors of the host-guest systems can be varied according to the operator's desire, implying the interconnection of the amino-functionalized copolymers to CdTe semiconductor NCs as indicated by the tuning of the emission color of the host-guest systems.

4.2.3 CdTe and Poly(fluorene)s Containing Phosphonate-Functionalized Side-Chains

Two phosphonate-functionalized fluorene-based copolymers (**P7b**, **P8b**) were prepared by post-modifying the bromo-functionalized precursors (**P7a**, **P8a**) under assistance of an

Arbuzov protocol (**Figure 4.11**). The latter were synthesized using nickel(0)- and palladium(0)-mediated polymerizations.[10]

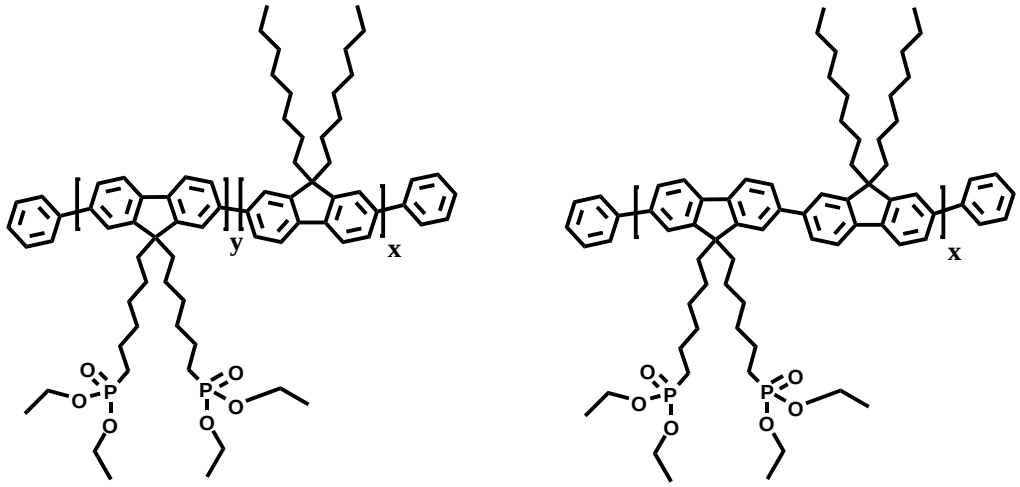

P7b **P8b**

Figure 4.11: Phosphonate-functionalized copolymers **P7b** and **P8b**.

Incorporating the final polymers in a precipitation-sonication methodology, microparticles (**P7b**/**P8b MPs**) were targeted building water-stable dispersions (section **3.3**). Combination of the polymers with water-stable CdTe nanocrystals under the precipitation-sonication conditions gave the opportunity to end up with composites, which maintained their stability and their intact emission brightness as centrifugation experiments of their dispersions evidenced (section **3.4**).[10] The CdTe nanocrystals used in our experiments were endcapped with thioglycolic acid (HS-CH_2-COOH) and synthesized by Dr. Vladimir Lesnyak in the group of Prof. Dr. Eychmüller (Technical University of Dresden, Physical Chemistry/Electrochemistry Department) following a standard aqueous synthetic approach.[4] The composite nature of the systems in the dispersions was confirmed by means of centrifugation experiments. The investigation of the resulting supernates by fluorescence spectroscopy brought polymer and nanocrystal bands into light, indicating coexistence of the two counterparts (section **3.4**, **Figure 3.18**). The **P7b**/**P8b MPs**+CdTe dispersions were subjected to dynamic light scattering measurements as well, giving unimodal particle size distribution profiles. AFM measurements performed in the group of Prof. Dr. Frahm at the University of Wuppertal allowed the observation of a coming-closer of the nanocrystals around the chains of the polymer (section **3.4**, **Figure 3.20**), being a further indication for a successful preparation of composite materials *via* the precipitation-sonication method. The fact that the polymers seem to play the role of the host for the semiconductor CdTe

nanocrystals and their emission overlaps the absorption spectrum of the quantum dots, renders the investigation of the energy transfer feasibility in these composite systems of great interest. Therefore, UV-vis and fluorescence spectroscopy experiments were conducted implying the significance of the precipitation-sonication method, when it has to do with the disclosure of the energy transfer process.[10] **Figure 4.12** illustrates the absorption spectra of the **P7b**/**P8b**+CdTe systems under assistance of sonication or excluding this treatment.

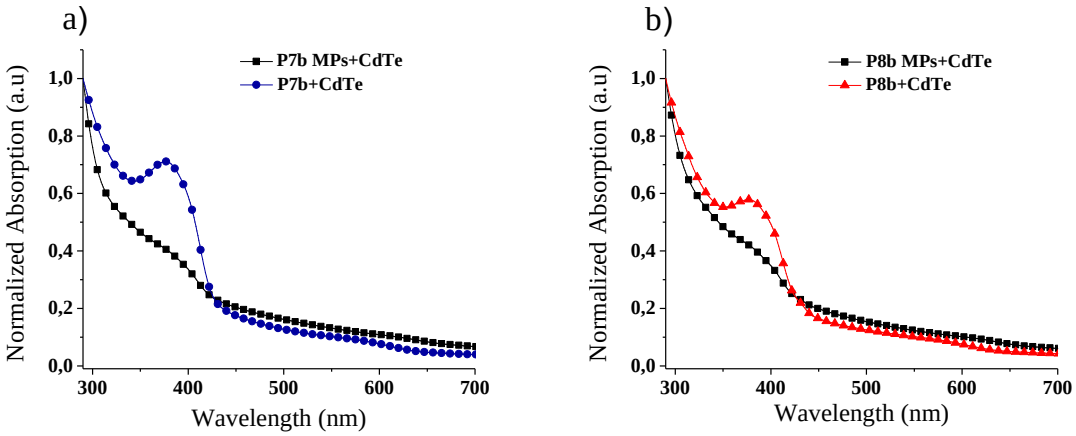

Figure 4.12: Normalized UV-vis spectra of the copolymer-CdTe water dispersions prepared *via* the precipitation-sonication process (**P7b**/**P8b MPs**+CdTe) and compared to non-sonicated systems (**P7b**/**P8b**+CdTe).

All UV-vis spectra are dominated by the CdTe absorption pattern. The higher absorbance of the non-sonicated systems (**P7b**/**P8b**+CdTe) can be attributed to scattering effects induced by nanocrystal aggregates, which cover the polymer absorption band. On the other side, the absorption of the sonicated systems (**P7b**/**P8b MPs**+CdTe) can be considered as a further indication of their composite-like nature due to the fact that polymer microparticles and nanocrystals seem both to participate and establish optical properties of the supposed composite material. The predomination of the nanocrystal absorption pattern is also connected to their higher electron affinity compared to conjugated polymers.[11] The fluorescence spectra of the aforementioned systems are illustrated in **Figure 4.13**, indicating, at a first glance, the emergence of a CdTe emission band (645 nm) exclusively for both sonicated systems. The absence of this peak at the non-sonicated systems can not be attributed to concentration effects but may be solely traced back to the use of the ultrasonic bath, which facilitates closer coming-together of polymers and nanocrystals and may thus support energy transfer due to exciton diffusion from **P7b** to the inorganic dye.[12]

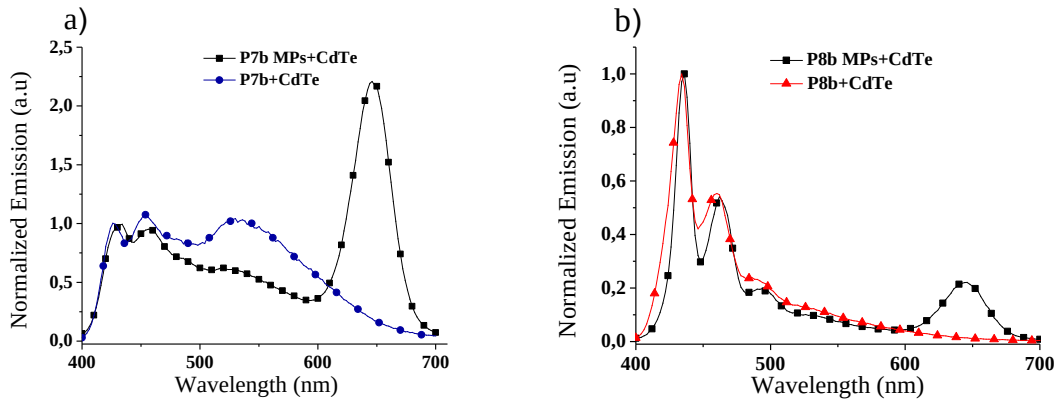

Figure 4.13: Normalized fluorescence spectra of the copolymer-CdTe water dispersions prepared *via* the precipitation-sonication process (**P7b**/**P8b MPs**+CdTe) and compared to non-sonicated systems (**P7b**/**P8b**+CdTe). Fluorescence spectra were normalized regarding the polymer emission maximum ($\lambda_{exc.}$ 390 nm, $C_{\mathbf{P7b,P8b}}$: 10^{-4} mol/L and C_{CdTe}: 6×10^{-5} mol/L).

The inadequate transfer in case of the **P8b MPs**+CdTe system can be an issue of marginal inorganic dye concentration for this kind of copolymer. The fact that polymer **P8b** builds moderate agglomerates in solution (particles of 324.5 nm in diameter) compared to the high aggregation of **P7b** (particles of 540.1 nm in diameter) as elucidated by dynamic light scattering measurements, can lead to pronounced *inter*- and *intra*-forces between nanocrystals and polymers in case of the latter. Bearing in mind that an excimer-like state is responsible for the observed photoluminescence behavior, weaker *inter*chain interactions are expected in case of polymer **P8b** due to the moderate folding and packing of the chains and this might be the reason for the intensity differentiation between the two composite systems.[11]

4.3 References

[1] A. A. Lutich, G. Jiang, A. S. Susha, A. L. Rogach, F. D. Stefani, J. Feldmann, *Nano Lett.* **2009**, 9, 2636.

[2] I. Kanelidis, A. Vaneski, D. Lenkeit, S. Pelz, V. Elsner, R. M. Stewart, J. Rodríguez-Fernández, A. A. Lutich, A. S. Susha, R. Theissmann, S. Adamczyk, A. L. Rogach, E. Holder, *J. Mater. Chem.* **2011**, 21, 2656.

[3] I. Kanelidis, V. Elsner, M. Bötzer, M. Butz, V. Lesnyak, A. Eychmüller, E. Holder, *Polymer* **2010**, 51, 5669.

[4] A. L. Rogach, T. Franzl, T. A. Klar, J. Feldmann, N. Gaponik, V. Lesnyak, A. Shavel, A. Eychmüller, Y. P. Rakovich, J. F. Donegan, *J. Phys. Chem. C* **2007**, 111, 14628.

[5] M. Agrawal, J. Rubio-Retama, N. E. Zafeiropoulos, N. Gaponik, S. Gupta, V. Cimrova, V. Lesnyak, E. Lopez-Cabarcos, S. Tzavalas, R. Rojas-Reyna, A. Eychmüller, M. Stamm, *Langmuir* **2008**, 24, 9820.
[6] M. Soreni-Harari, N. Yaacobi-Gross, D. Steiner, A. Aharoni, U. Banin, O. Millo, N. Tessler, *Nano Lett.* **2008**, 8, 678.
[7] J. R. Lakowicz, *Principles of Fluorescence Spectroscopy 3rd ed*. Springer Science & Business Media, LCC: New York, **2006**.
[8] I. Kanelidis, Y. Ren, V. Lesnyak, J. C. Gasse, R. Frahm, A. Eychmüller, E. Holder, *J. Polym. Sci. Part A: Polym. Chem.* **2011**, 49, 392.
[9] U. Giovanella, M. Pasini, S. Destri, W. Porzio, C. Botta, *Synth. Met.* **2008**, 158, 113.
[10] I. Kanelidis, O. Altintas, J. C. Gasse, R. Frahm, A. Eychmüller, E. Holder, *Polym. Chem.* **2011**, 2, 2597.
[11] F. Guo, P. Xie, *Chin. J. Chem.* **2009**, 27, 1427.
[12] Q. Pei, Y. Yang, *J. Am. Chem. Soc.* **1996**, 118, 7416.

5 Summary and Conclusions

Conjugated polymers containing functional monomers as building blocks that can interact *via* their end-functionalities with other multi-functional or optically active species such as nanoparticles or semiconductor nanocrystals are of increasing interest in the modern light-emitting and display technology. Poly(fluorene)s (PFs) constitute a significant class of conjugated polymers, exhibiting desirable properties like good processability, high quantum yield and rather large band-gaps. Poly(fluorene)s can be obtained applying several C-C coupling reactions like the reductive nickel-mediated Yamamoto polymerization or the palladium-proceeded Suzuki polycondensation. Attachment of bulky moieties like triarylamine in their C-9 position can not only suppress the disturbing keto-defect emission overcoming in that way stability matters and improving the opto-electronic properties of the resulting polymers but can also facilitate their linking to nanocrystalline surfaces. Moreover, incorporation of carbazole-based building blocks in their backbone can contribute in addition to the blue-light emission to a higher hole-transporting mobility and to a raise of the energy level of the highest occupied molecular orbital (HOMO) rendering these polymers appropriate hosts for other semiconducting species. Furthermore, following the new trend in the materials' design of embracing organic and inorganic components in hybrid structures, fluorene derivatives combined with inorganic semiconductor nanocrystals (NCs) are in the focus due to the easy processing and mechanical flexibility of the former and the size-dependent optical properties of the latter. Poly(fluorene)s in the form of nanoparticles attracted currently the attention of the researchers especially in combination with biocompatible quantum dots, as well. The trend is corroborated by the advantages accompanying the family of PFs, namely the high fluorescence, the good processability and the facile side-chain modification. In the last case, groups with amphiphilic character like phosphonates can play a significant role, not only due to the fact that they can render the polymers water-soluble, but also because of their strong chemical affinity to quantum dots allowing the preparation of nanocomposite systems.

Within the framework of this thesis and bearing in mind the aforementioned interesting features of the fluorene chemistry, fluorene- and carbazole-based building blocks were synthesized and incorporated in Yamamoto or Suzuki polymerizations, targeting to post-modified copolymers, polymer microparticles or hybrids. Their combinative interplay with

inorganic quantum dots allowed the acquirement of composite materials and the subsequent investigation of the complicated phenomena of the energy and electron transfer.

Using a facile Yamamoto protocol two random bromo-side-chain functionalized fluorene-based copolymers were obtained by applying 2,7-dibromo-9,9'-*bis*(6-bromohexyl)-9*H*-fluorene, (*E*)-1,2-*bis*(4-bromophenyl)ethene and 2,7-dibromo-9,9'-dioctyl-9*H*-fluorene as comonomers in varying contents. The bromo-groups of the precursors were modified utilizing di-*n*-propylamine and the final amino-functionalized copolymers **P2a-b** (**Figure 5.1**) revealed wide band-gaps of 2.84 eV and favorable quantum yields of up to 0.78 in solution. The use of the polymers as hosts for CdTe nanocrystals allowed the monitoring of the deactivation and intensity enhancement process of the polymer and the CdTe emission, when both counterparts considered within a composite system. The quenching of the amino-functional copolymers emission upon addition of the CdTe NCs illustrated the polymer-CdTe interconnection. Moreover, the deactivation and intensity enhancement processes in these composite systems exhibited a dependence on the bromo-functionalized stabilizing ligands of the nanocrystals and the nitrogen content of the copolymers, as well.

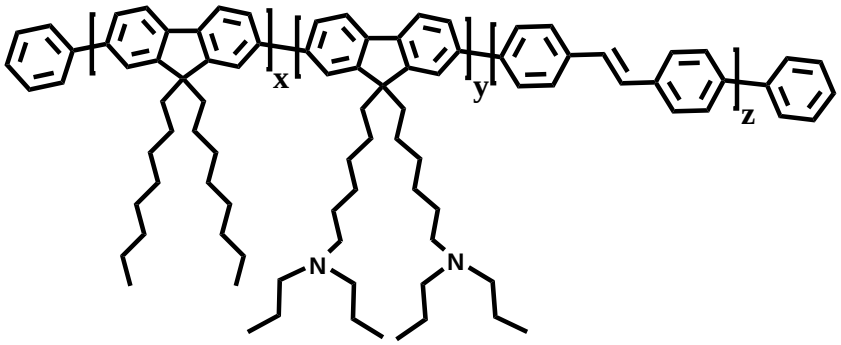

P2a-b

Figure 5.1: Chemical structure of the random amino-functionalized copolymers **P2a** (x/y/z: 40/10/50) and **P2b** (x/y/z: 35/15/50) synthesized *via* Yamamoto (x,y,z represent the feed ratio of the initial building blocks in %).

Alternating copolymers were synthesized in Suzuki copolymerizations applying 4,4'-(2,7-dibromo-9*H*-fluorene-9,9'-diyl)dianiline, 4,4'-(2,7-dibromo-9*H*-fluorene-9,9'-diyl)*bis*(*N*,*N*′-diphenylaniline), 4-(3,6-dibromo-9*H*-carbazol-9-yl)aniline and 4-(3,6-dibromo-9*H*-carbazol-9-yl)-*N*,*N*′-diphenylaniline, each of them in combination with 2,2'-(9,9'-dioctyl-9*H*-fluorene-2,7-

diyl)*bis*(1,3,2-dioxaborinane). The resulting arylamino-functionalized copolymers **P3**-**P6** (**Figure 5.2**) revealed blue-light emission and wide optical band-gaps of at least 2.93 eV for the fluorene-based (**P3**, **P4**) and 3.07 eV for the carbazole-based polymers (**P5**, **P6**). Their wide band-gaps can make them useful as hosts for low band-gap compounds like CdTe nanocrystals, which possess absorption maxima, which overlap with the emission patterns of the polymers. Solid-state measurements of the optical properties of polymers, different CdTe nanocrystals and their composites revealed an inadequate tendency for energy transfer from the polymers to the nanocrystals but simultaneously a potential for tuning the emission color of the host-guest system. The appropriate combination of copolymers and CdTe nanocrystals rendered the accomplishment of white-light emission possible and in principle the emission colors of the host-guest systems could be varied according to the operator's desire.

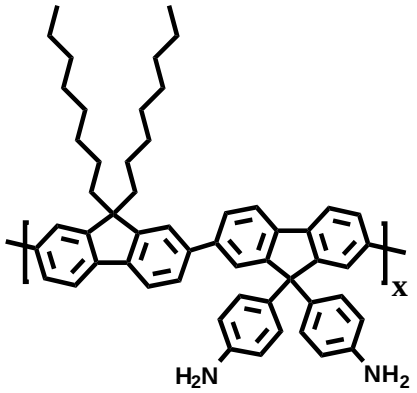

P3

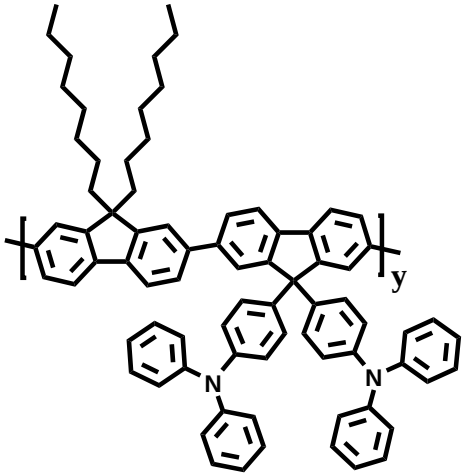

P4

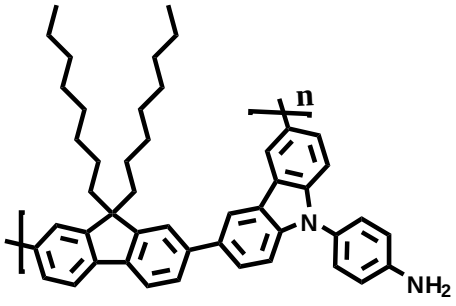

P5

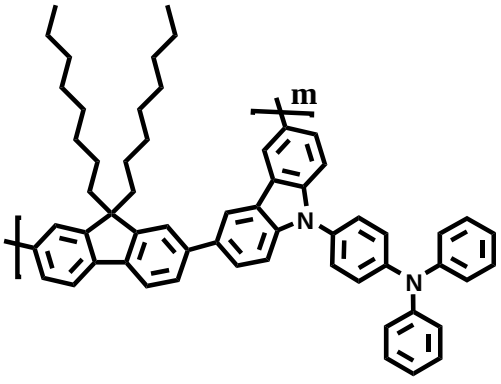

P6

Figure 5.2: The alternating fluorene- (**P3**, **P4**) and carbazole-based (**P5**, **P6**) arylamino-functionalized copolymers synthesized *via* Suzuki.

Utilizing either a Yamamoto or a Suzuki protocol, two bromo-functionalized fluorene-based copolymers were once more synthesized using this time 2,7-dibromo-9,9'-*bis*(6-bromohexyl)-9*H*-fluorene and 2,7-dibromo-9,9'-dioctyl-9*H*-fluorene or 2,2'-(9,9'-dioctyl-9*H*-fluorene-2,7-diyl)*bis*(1,3,2-dioxaborinane) as comonomers in a 1:1 stoichiometry for both protocols, respectively. These precursor copolymers were subjected to a post-functionalization using triethyl phosphite and the final copolymers **P7**,**8b** (**Figure 5.3**) could be processed from polar solvents like tetrahydrofuran or dimethylformamide giving them thus the opportunity to participate in a precipitation-sonication procedure, whereby water-stable dispersions of polymer microparticles (**P7b MPs**, **P8b MPs**) were obtained possessing very high quantum yields of up to 0.84 (**Figure 5.4**). The microparticles revealed bright and stable emission with colors ranging from blue in the organic solvents to even white emission in water, optical properties, which are dependent on the catalysis method applied for the preparation of each copolymer. Their size profile was investigated by means of atomic force microscopy and complemented by dynamic light scattering.

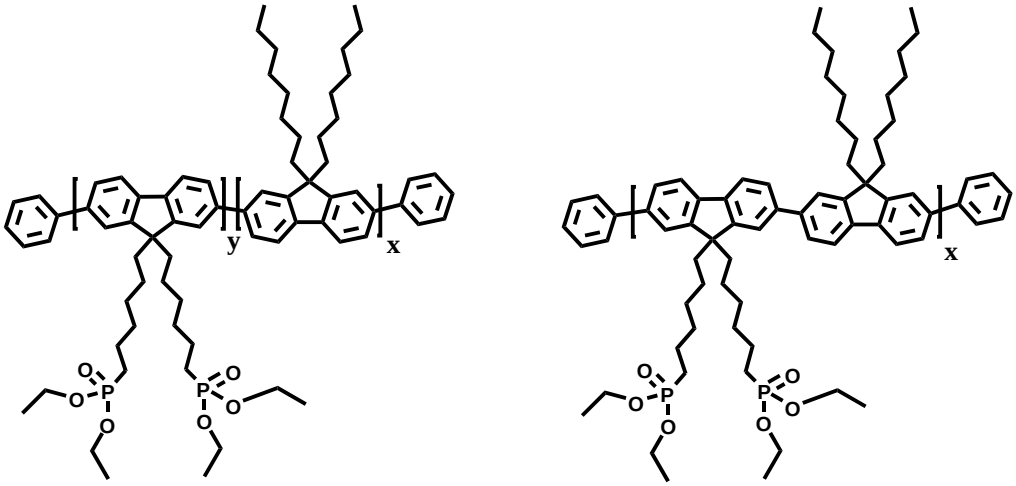

P7b **P8b**

Figure 5.3: Structural configuration of the phosphonate-functionalized copolymers **P7b** and **P8b**.

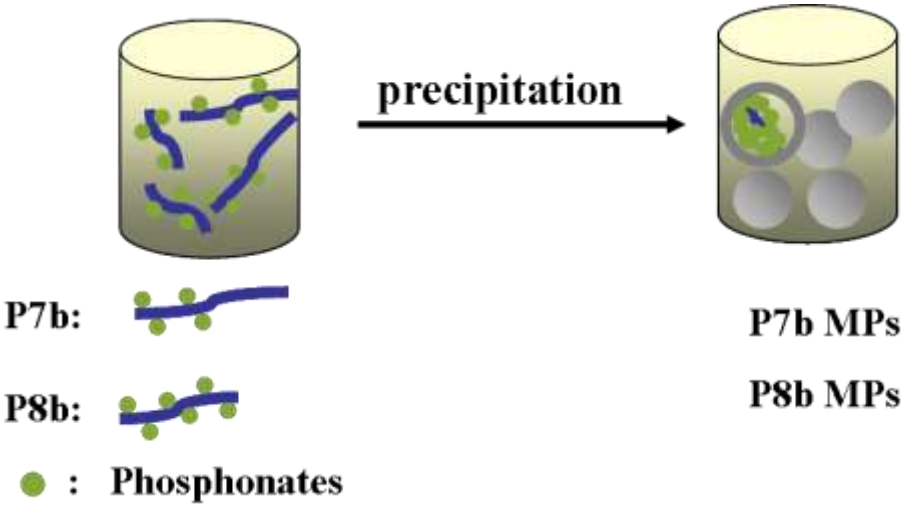

Figure 5.4: Schematic representation of the preparation of the polymer microparticles **P7b MPs** and **P8b MPs**.

The precipitation-sonication method was further extended to the direction of combining the copolymers with water-soluble CdTe nanocrystals capped with thioglycolic acid in order to create composite systems. The resulting particulate composites exhibited exceptional optical properties and long-term stability with emission colors different from the original colors of each counterpart, separately. The stability of the composites was tested through centrifugation experiments and the subsequent acquired fluorescence spectra of the supernates evidenced the composite configuration of the systems. The latter was further supported by DLS measurements, which revealed unimodal particle distribution profiles. Investigation of the energy transfer feasibility in these composite systems brought into light a dependence of the observed energy transfer process on the preparation method of the composite dispersions as in sonicated systems contrary to non-sonicated ones a closer coming-together between polymers and nanocrystals may take place supporting thus energy transfer.

Towards the synthesis of organic-inorganic composites, 6,6'-(2,7-dibromo-9*H*-fluorene-9,9'-diyl)dihexan-1-amine was firstly synthesized and used directly in the synthesis stage of CdSe nanocrystals. In this way, monodisperse, crystalline, strongly-emitting CdSe nanocrystals surface-modified by amino-fluorene moieties (**NC1**) have been obtained and could be used as starting material in a straight-forward Yamamoto protocol in order to end up with oligo(fluorene) capped CdSe nanocrystals (**NC2**) *via* a 'grafting-from' approach. Combining **NC1** with 2,7-dibromo-9,9'-dioctyl-9*H*-fluorene as second comonomer, a longer grafted chain at the surface of CdSe nanocrystals was achieved resulting in CdSe NCs surrounded by

poly(fluorene) moieties (**NC3**). Nanocomposites **NC1-3** (**Figure 5.5**) were characterized in detail by optical and FT-IR spectroscopy, TEM, AFM, and GPC. Concretely, FT-IR data confirmed the linkage of the amine-functionalized fluorene derivative on the surface of the CdSe nanocrystals and its intactness under the reaction conditions. The TEM images provided through the presence of non-agglomerated CdSe cores in all three nanocomposites a further indication for the hybrid nature of the systems. GPC measurements were consistent to MALDI-TOFMS findings related to the organic parts of **NC2** and **NC3**. Photoluminescence spectroscopy of the three nanocomposites in comparison to reference nanocrystals (**$CdSe_{ref}$**) endcapped with *n*-hexadecylamine and tetradecylphosphonic acid revealed a quenching of the CdSe emission. The effect is ascribed to the charge separation between CdSe nanocrystals and fluorene moieties, a process competitive to the energy transfer and facilitated by the direct linkage of the two counterparts in the organic-inorganic composites. Charge separation is further supported by the significantly faster photoluminescence decay times of the CdSe nanocrystals in the composites **NC1** and **NC3**, when compared to the reference CdSe nanocrystals, rendering the opto-electronic properties of these composites independent from the polymerization conditions. The high control over their properties makes these materials suitable candidates for photovoltaic and opto-electronic applications.

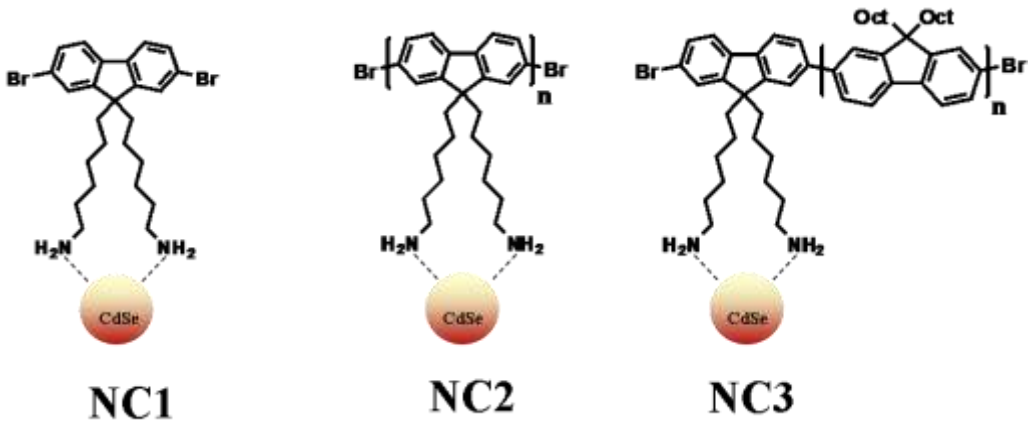

Figure 5.5: CdSe-fluorene-based nanocomposites **NC1-3**.

6 Experimental Section

6.1 Materials and Instrumentation

Starting materials were purchased from ABCR, Acros, Aldrich, Alfa Aesar, Fluka and Merck and were utilized directly without further manipulations. Polymerizations were performed in dry solvents under an argon atmosphere. Ultraviolet-visible measurements were performed on a Jasco V-550 spectrophotometer, while fluorescence spectroscopic measurements were performed on a Cary Eclipse Fluorescence Spectrophotometer by means of 1 cm cuvettes. UV-vis and fluorescence of CdTe/HS-C_6H_4-Br nanocrystals was performed in the Technical University of Dresden, Physical Chemistry/Electrochemistry Department using a Cary 50 spectrophotometer (Varian Inc., Palo Alto, USA) and a FluoroMax-4 spectrofluorometer (HORIBA Jobin Yvon Inc., Edison, NJ, USA), correspondingly. For infrared studies a JASCO FT/IR-4200 Fourier-Transform-Spectrometer was utilized. Mass spectra were obtained using a Bruker micrOTOF instrument equipped with an electrospray ionization source (ESI-MS) and a Shimadzu Biotech Axima matrix-assisted laser-desorption/ionization time-of-flight mass spectrometer (MALDI-TOFMS). For the electron impact ionization (EI) mass spectra, the device MAT 311A from Varian was utilized. MALDI-TOF samples were prepared by drop-casting their THF solutions without the addition of a matrix. Gel permeation chromatography analysis was carried out on a Jasco AS950 and a Jasco AS2055 apparatus. The Jasco AS950 device used Jasco UV-2070, Jasco RI-930 and Viscotek T60 as detectors (column MZSD of particle size 5 μm, eluent chloroform) and molecular weights were determined based on a calibration of polystyrene standards. The Jasco AS2055 apparatus utilized a Jasco UV/VIS-2070/75 and a Jasco RI-2031 detector [GRAM columns, dimethylformamide (DMF) as eluent with ammonium hexafluorophosphate 5 mM as salt], while for the determination of the molecular weights a calibration based on poly(methyl methacrylate) standards was applied. ^{1}H- and ^{13}C-NMR spectroscopy was carried out on Bruker ARX 400 and 600 Fourier Transform Nuclear Resonance Spectrometer using TMS as internal standard and $CDCl_3$ as deuterated solvent. Elemental analyses were performed by means of the Vario Elemental EL analyzer. Thermal gravimetric analysis was performed under argon by means of a Mettler Toledo TGA/DSC 1 model, applying a heating correspondingly cooling rate of 10 K/min. Transmission electron microscopy (TEM) was performed in the Technical University of Dresden, Physical Chemistry/Electrochemistry Department on a EM208 microscope (Philips) and in the Faculty of Engineering and Center

for Nanointegration at the University of Duisburg-Essen on a JEOL JEM-1011 electron microscope (accelerating voltage of 100 kV). In the case of the EM208 microscope, the specimens were prepared by dropping diluted nanocrystal solutions onto copper grids coated with a hydrophilic collodion film prepared from collodion solution (Fluka). Atomic force microscopy was performed on a Q-Scope^{TM} 250 (Quesant Instrument Corporation) and a diInnova microscope from Veeco using in both cases the tapping mode. In the first case, a scan head was utilized of 1 nm lateral resolution, 9 μm maximal vertical range, 0.1 nm vertical resolution and a four-quadrant photodiode. For the Q-Scope device samples were drop-casted from THF, water or DMF solutions on glass substrates, while for the diInnova instrument the samples were dip-coated on glimmer from chloroform or toluene dispersions of 10 mg/mL concentration, after annealing at 180 °C for 4 hours. The silicon cantilevers used were between 215-235 μm in length and had a resonance frequency of approximate 84 kHz, while the tip height was between 15-20 μm. Time-resolved photoluminescence measurements were done with a streak camera (Hahamatsu C5680) combined with the spectrometer (Cromex, 40gr/mm grating) and were carried out in the Department for Physics and Center for Nanoscience at the Maximilian University of Munich. The frequency doubled output of the mode-locked titanium-sapphire laser (150 fs, 100 kHz) was used as an excitation source at 400 nm. Dynamic light scattering measurements were carried out in the Technical University of Dresden, Physical Chemistry/Electrochemistry Department on a Delsa Nano C Particle Analyzer of the Beckman Coulter Company by means of the software Delsa Nano Beckman Coulter Inc. Centrifugations were conducted on a Biofuge 13 centrifuge of the manufacturer Heraeus Sepatech, while for the sonication experiments an ultrasonic bath of the company Bandelin Sonorex was utilized. For the purification of the monomers by means of column chromatography silica gel of particle size 50-200 mesh was utilized as the stationary phase, while thin layer chromatography (TLC) was performed on TLC aluminium sheets bearing a 0.2 mm silica gel layer with fluorescent indicator. Biobeads used for the fractionation and isolation of copolymers and hybrids were purchased from Bio-Rad Laboratories possessing spherical beads of 200-400 mesh.

6.2 Monomers

6.2.1 2,7-Dibromo-9*H*-fluorene (1)

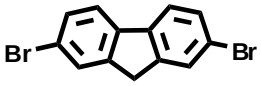

According to references [1] and [2], a white solid was obtained after recrystallizing from ethanol and toluene (3.2 g, 34%). UV-vis: λ_{max} (log ε [L × mol^{-1} × cm^{-1}]) 279 nm (4.00), 301 nm (3.61), 312 nm (3.68). Emission: λ_{max} 328 nm. IR (cm^{-1}): 2955 (w, C-H, stretching), 2915 (m, C-H, stretching), 2847 (w, C-H, stretching), 1451 (m, C-H, scissor), 1397 (w, C-H, deformation), 811 (s, aromatic C-H, out-of-plane deformation). GC-MS (*m/z*): Calcd. $C_{13}H_8Br_2$ 323.9; Found 324. ^{1}H-NMR ($CDCl_3$): δ (ppm) = 3.86 (s, 2H, CH_2), 7.50 (d, 2H, arom.), 7.59 (d, 2H, arom.), 7.66 (d, 2H, arom.). ^{13}C-NMR ($CDCl_3$): δ (ppm) = 144.8, 139.7, 130.2, 128.3, 121.2, 121.0 (arom.), 36.6 ().

6.2.2 2,7-Dibromo-9,9'-*bis*(6-bromohexyl)-9*H*-fluorene (2)

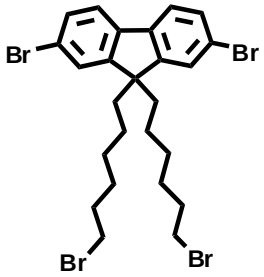

Following references [2-5] a white solid was acquired (6.78 g, 69%). UV-vis: λ_{max} (log ε [L × mol^{-1} × cm^{-1}]) 283 nm (4.47), 316 nm (4.31). Emission: λ_{max} 329 nm. IR (cm^{-1}): 2925 (m, CH_2, stretching), 2850 (m, CH_2, stretching), 1568 (w, C=C, stretching), 1460 (m, CH_2, scissor), 1446 (s, C-H, deformation), 810 (s, aromatic C-H, out-of-plane deformation). ESI-MS (*m/z*): Calcd. $C_{25}H_{30}AgBr_4$ 758; Found 758.8. ^{1}H-NMR ($CDCl_3$): δ (ppm) = 0.56-0.64 (m, 4H, CH_2), 1.04-1.12 (m, 4H, CH_2), 1.17-1.24 (m, 4H, CH_2), 1.64-1.71 (m, 4H, CH_2), 1.91-1.95 (m, 4H, CH_2), 3.29 (t, 4H, CH_2-Br), 7.41-7.56 (m, 6H, arom.). ^{13}C-NMR ($CDCl_3$): δ (ppm) = 152.1, 139.05, 130.06, 126.1, 121.5, 121.1 (arom.), 55.5 (), 39.9, 33.7, 32.5, 28.9, 27.7, 23.4 (aliph.).

6.2.3 2,7-Dibromo-9,9'-dioctyl-9*H*-fluorene (3)

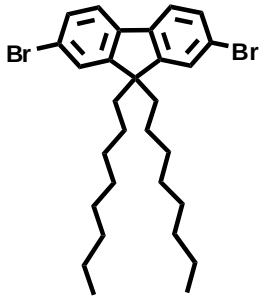

A yellowish solid (2.49 g, 54%) was obtained by following references [2] and [6]. UV-vis: λ_{max} (log ε [L × mol^{-1} × cm^{-1}]) 283 nm (4.31), 315 nm (4.18). Emission: λ_{max} 328 nm. IR (cm^{-1}): 2947 (m, C-H, stretching), 2911 (s, C-H, stretching), 2847 (m, C-H, stretching), 1565 (w, C=C, stretching), 1465 (m, CH_2, scissor), 1443 (m, C-H, deformation), 1372 (w, CH_3, deformation), 1253 (w, C-C, skeletal), 1131 (w, C-C, rocking), 883 (m, aromatic C-H, out-of-plane deformation), 808 (s, aromatic C-H, out-of-plane deformation). GC-MS (*m/z*): Calcd. $C_{29}H_{40}Br_2$ 548; Found 548. ^{1}H-NMR ($CDCl_3$): δ (ppm) = 0.61 (s, 4H, CH_2), 0.84 (t, 6H, CH_3), 1.06-1.12 (m, 16H, CH_2), 1.20-1.24 (t, 4H, CH_2), 1.90-1.94 (m, 4H, CH_2), 7.46 (m, 4H, arom.), 7.50-7.53 (m, 2H, arom.). ^{13}C-NMR ($CDCl_3$): δ (ppm) = 152.4, 139.4, 130.5, 126.4, 121.6, 121.2 (arom.), 55.7 (), 40.1, 31.7, 29.8, 29.15, 29.13, 23.6, 22.6, 14.0 (aliph.).

6.2.4 (*E*)-1,2-*Bis*(4-bromophenyl)ethene (4)

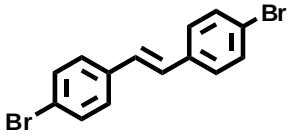

A white solid (4.33 g, 48%) was isolated by a synthetic approach described in references [2] and [7]. UV-vis: λ_{max} (log ε [L × mol^{-1} × cm^{-1}]) 308 nm (4.65), 323 nm (4.69). Emission: λ_{max} 368 nm. IR (cm^{-1}): 3100-3000 (s, C-H, stretching). ESI-MS (*m/z)*: Calcd. $C_{14}H_{10}Br_2$ $(M+H)^+$ 335.91; Found 336. ^{1}H-NMR ($CDCl_3$): δ (ppm) = 7.01 (s, 2H), 7.37 (d, 4H), 7.49 (d, 4H). ^{13}C-NMR ($CDCl_3$): δ (ppm) = 135.8, 131.8, 128.1, 127.9, 121.6.

6.2.5 6,6'-(2,7-Dibromo-9*H*-fluorene-9,9'-diyl)*bis*(*N*,*N'*-dipropylhexan-1-amine) (5)

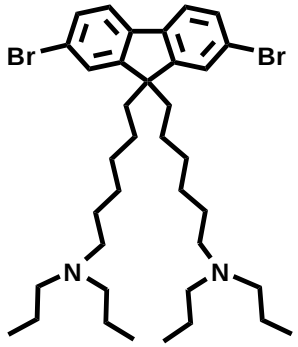

By means of literature procedures [2] and [8] a brown solid was acquired (0.26 g, 91%). UV-vis: λ_{max} (log ε [L × mol^{-1} × cm^{-1}]) 280 nm (5.74), 310 nm (4.04). Emission: λ_{max} 329 nm. IR (cm^{-1}): 2922 (m, CH_2, stretching), 2855 (m, CH_2, stretching), 2506 (w, $^{+}$HN-C, stretching), 1447 (s, CH_2, deformation), 1249 (m, C-N, stretching), 1055 (s, C-N, stretching), 973 (m, C-C, skeleton), 818 (s, C-H, out-of-plane deformation). ESI-MS (*m/z*): Calcd. $C_{37}H_{59}Br_3N_2$ 770.2; Found 773.2. ^{1}H-NMR ($CDCl_3$): δ (ppm) = 0.67 (s, 4H, CH_2), 0.99 (t, 12H, CH_3), 1.14 (m, 8H, CH_2), 1.66 (m, 4H, CH_2), 1.87 (m, 8H, CH_2), 1.96 (m, 4H, CH_2), 2.91 (q, 12H, N-CH_2), 7.46-7.49 (d, 4H, arom.), 7.55-7.57 (d, 2H, arom.). ^{13}C-NMR ($CDCl_3$): δ (ppm) = 151.9, 139.0, 130.4, 126.0, 121.5, 121.3 (arom.), 55.4 (), 54.0 (C-N), 52.3 (C-N), 39.7, 28.9, 26.2, 23.2, 22.9, 16.8, 11.2 (aliph.).

6.2.6 2,7-Dibromo-9*H*-fluoren-9-one (6)

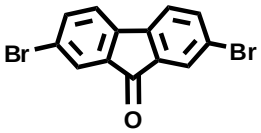

2,7-Dibromo-9*H*-fluoren-9-one was obtained as a yellow solid (24.77 g, 76%) from 9*H*-fluoren-9-one (38.99 g, 17.40 mmol) by addition of bromine (2 mL, 38.99 mmol) in water.[9,10] UV-vis: λ_{max} (log ε [L × mol^{-1} × cm^{-1}]) 299 nm (2.59), 311 nm (2.50). Emission: λ_{max} 387 nm, 399 nm. IR (cm^{-1}): 3407 (w, C=O, stretching), 3080 (w, C-H, stretching), 3055 (w, C-H, stretching), 1720 (s, C=O, stretching), 1051 (m, C-Br, stretching). GC-MS (*m/z*): Calcd. $C_{13}H_6Br_2O$ 337.9; Found 338. ^{1}H-NMR ($CDCl_3$): δ = 7.40 (d, 2H), 7.65 (dd, 2H), 7.79 (d, 2H). ^{13}C-NMR ($CDCl_3$): δ = 190.8, 142.2, 137.4, 135.3, 127.8, 123.3, 121.8. Anal. Calcd. for $C_{13}H_6Br_2O$: C, 46.20; H, 1.79. Found: C, 46.42; H, 2.79.

6.2.7 4,4'-(2,7-Dibromo-9*H*-fluorene-9,9'-diyl)dianiline (7)

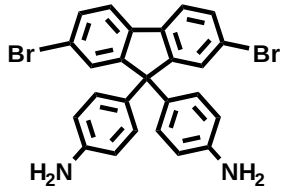

4,4'-(2,7-Dibromo-9*H*-fluorene-9,9'-diyl)dianiline was prepared from 2,7-dibromo-9*H*-fluoren-9-one (4.2 g, 12.4 mmol), aniline hydrochloride (2 g, 15.3 mmol) and aniline (10 mL, 109 mmol) following literature approaches.[10,11] The product **7** was isolated after column chromatography (*n*-hexane/ethyl acetate 4:1) as a grey solid (4.30 g, 70%). UV-vis: λ_{max} (log ε [L × mol^{-1} × cm^{-1}]) 293 nm (6.20), 319 nm (6.18). Emission: λ_{max} 335 nm. IR (cm^{-1}): 3457-3339 (w, N-H, stretching), 3030 (w, C-H, stretching), 1616 (s, N-C, deformation), 1049 (s, C-Br, skeleton). ESI-MS (*m/z)*: Calcd. $C_{25}H_{18}Br_2N_2$ 506.2; Found 507. ^{1}H-NMR ($CDCl_3$): δ (ppm) = 3.64 (s, 4H, NH_2), 6.58 (d, 4H, arom.), 6.96 (d, 4H, arom.), 7.47 (dd, 2H, arom.), 7.49 (d, 2H, arom.), 7.57 (d, 2H, arom.). ^{13}C-NMR ($CDCl_3$): δ (ppm) = 154.1, 145.3, 137.8, 134.4, 130.5, 129.2, 128.9, 121.7, 121.4, 115.0 (arom.), 64.4 (). Anal. Calcd. for $C_{25}H_{18}Br_2N_2$: C, 59.31; H, 3.58; N, 5.53. Found: C, 59.32; H, 3.53; N, 5.52.

6.2.8 4,4'-(2,7-Dibromo-9*H*-fluorene-9,9'-diyl)*bis*(*N,N'*-diphenylaniline) (8)

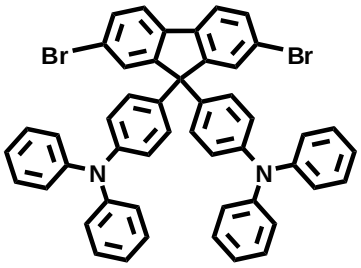

The compound was prepared from 2,7-dibromo-9*H*-fluoren-9-one (2.46 g, 7.28 mmol), triphenylamine (25 g, 102 mmol) and methane sulfonic acid (1.4 g, 14.56 mmol) according to references [10] and [12]. Compound **8** was isolated as a white solid (4.8 g, 81%). UV-vis: λ_{max} (log ε [L × mol^{-1} × cm^{-1}]) 295 nm (3.19), 308 nm (3.23). Emission: λ_{max} 388 nm, 399 nm. IR (cm^{-1}): 3030 (w, C-H, stretching), 1270 (s, C-N, stretching). ESI-MS (*m/z)*: Calcd. $C_{49}H_{34}Br_2N_2$ 810.1; Found 810.6. ^{1}H-NMR ($CDCl_3$): δ (ppm) = 6.95 (d, 4H), 7.01-7.06 (m, 4H), 7.11 (dd, 8H), 7.24-7.30 (m, 12H), 7.51 (dd, 2H), 7.56 (d, 2H), 7.60 (d, 2H). ^{13}C-NMR ($CDCl_3$): δ (ppm) = 153.4, 147.5, 146.7, 137.9, 137.6, 130.8, 129.3, 129.2, 129.1, 128.6, 124.6, 124.4, 123.0, 122.9, 122.8, 122.7, 121.7, 121.5 (arom.), 64.6 (). Anal. Calcd. for $C_{49}H_{34}Br_2N_2$: C, 72.60; H, 4.23; N, 3.46. Found: C, 72.28; H, 3.95; N, 3.23.

6.2.9 3,6-Dibromo-9-(4-nitrophenyl)-9*H*-carbazole (9)

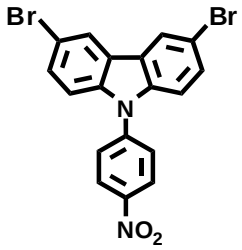

3,6-Dibromo-9-(4-nitrophenyl)-9*H*-carbazole (yellow crystals, 4.3 g, 76%) was prepared from 3,6-dibromo-9*H*-carbazole (4.09 g, 12.6 mmol), potassium carbonate (8.71 g, 62.02 mmol) and 1-fluoro-4-nitrobenzene (7.11 g, 50.42 mmol) in DMF (80 mL) following approaches cited in the literature.[10,13,14] UV-vis: λ_{max} (log ε [L × mol^{-1} × cm^{-1}]) 374 nm (2.44). Emission: λ_{max} 388 nm, 398 nm. IR (cm^{-1}): 1498 (s, N=O, asymmetric stretching), 1325 (s, N=O, symmetric stretching), 1054 (m, C-Br, skeleton). ESI-MS (*m/z)*: Calcd. $C_{18}H_{10}Br_2N_2O_2$ 446.1; Found 446. ^{1}H-NMR ($CDCl_3$): δ (ppm) = 7.33 (d, 2H), 7.56 (d, 2H), 7.74 (d, 2H), 8.21 (s, 2H), 8.50 (d, 2H). ^{13}C-NMR ($CDCl_3$): δ (ppm) = 146.4, 142.8, 138.9, 129.9, 126.8, 125.7, 124.7, 123.6, 114.3, 111.2. Anal. Calcd. for $C_{18}H_{10}Br_2N_2O_2$: C, 48.46; H, 2.26; N, 6.28. Found: C, 48.41; H, 1.46; N, 6.29.

6.2.10 4-(3,6-Dibromo-9*H*-carbazol-9-yl)aniline (10)

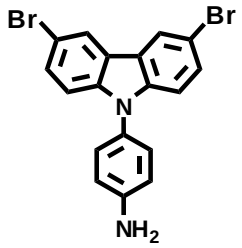

Addition of tin(II) chloride (3.16 g, 14.01 mmol) in a 3,6-dibromo-9-(4-nitrophenyl)-9*H*-carbazole (1.25 g, 2.80 mmol) ethanol solution gave the desired product.[10,13,14] After recrystallization from toluene white crystals of compound **10** were obtained (1.02 g, 87%). UV-vis: λ_{max} (log ε [L × mol^{-1} × cm^{-1}]) 346 nm (2.04), 358 nm (2.05). Emission: λ_{max} 387 nm, 398 nm. IR (cm^{-1}): 3443-3357 (m, N-H, stretching), 3048 (m, C-H, stretching), 1619 (s, C-N, deformation), 1271 (s, C-N, stretching), 1051 (m, C-Br, skeleton). ESI-MS (*m/z*): Calcd. $C_{18}H_{12}Br_2N_2$ 416.1; Found 416. ^{1}H-NMR ($CDCl_3$): δ (ppm) = 6.88 (d, 2H), 7.17-7.29 (m, 4H), 7.50 (dd, 2H), 8.20 (d, 2H). ^{13}C-NMR ($CDCl_3$): δ (ppm) = 146.4, 140.4, 129.1, 128.3, 127.0, 123.5, 123.0, 115.9, 112.5, 111.5. Anal. Calcd. for $C_{18}H_{10}Br_2N_2$: C, 51.96; H, 2.91; N, 6.73. Found: C, 52; H, 2.55; N, 6.73.

6.2.11 4-Iodo-*N*,*N′*-diphenylaniline (11)

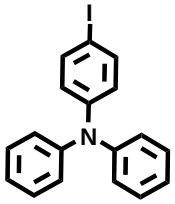

4-Iodo-*N*,*N′*-diphenylaniline was obtained as a white solid (2.2 g, 42%) from 1,4-diiodobenzene (8.8 g, 26 mmol), diphenylamine (2.4 g, 14.10 mmol), copper(II) sulfate (0.176 g, 0.705 mmol) and potassium carbonate (1.95 g, 14.1 mmol) and the synthesis was proceeded according to references [10] and [15]. UV-vis: λ_{max} (log ε [L × mol^{-1} × cm^{-1}]) 307 nm (2.72). Emission: λ_{max} 387 nm, 398 nm. IR (cm^{-1}): 3059 (w, C-H, stretching), 3030 (w, C-H, stretching), 1583 (s, C=C, stretching), 1060 (s, C-I, skeleton). GC-MS (*m/z)*: Calcd. $C_{18}H_{14}NI$ 371.21; Found 371. ^{1}H-NMR ($CDCl_3$): δ (ppm) = 6.86 (d, 2H), 7.07 (dd, 2H), 7.11 (dd, 4H), 7.29 (dd, 4H), 7.53 (d, 2H). ^{13}C-NMR ($CDCl_3$): δ (ppm) = 147.7, 147.2, 138.0, 129.3, 125.2, 124.5, 123.3 (arom.), 84.7 (C-I). Anal. Calcd. for $C_{18}H_{14}NI$: C, 58.24; H, 3.80; N, 3.77. Found: C, 58.67; H, 3.13; N, 3.81.

6.2.12 4-(3,6-Dibromo-9*H*-carbazol-9-yl)-*N*,*N′*-diphenylaniline (12)

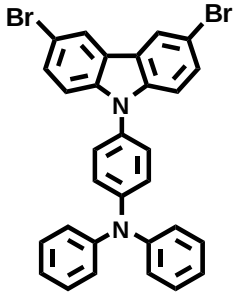

4-(3,6-Dibromo-9*H*-carbazol-9-yl)-*N*,*N′*-diphenylaniline was obtained from 4-iodo-*N*,*N′*-diphenylaniline (0.557 g, 1.50 mmol), 3,6-dibromo-9*H*-carbazole (0.4 g, 1.23 mmol), copper(I) iodide (0.05 g, 0.263 mmol), [18]-crown-6 (0.03 g, 0.114 mmol) and potassium carbonate (0.8 g, 5.80 mmol) in 5 mL DMSO.[10,16] Purification by column chromatography (petrol ether/ethyl acetate 15:1) gave a white solid of compound **12** as isolated product (0.402 g, 57%). UV-vis: λ_{max} (log ε [L × mol^{-1} × cm^{-1}]) 305 nm (3.00). Emission: λ_{max} 387 nm, 399 nm. IR (cm^{-1}): 3055 (w, C-H, stretching), 3038 (w, C-H, stretching), 1585 (s, C=C, stretching), 1054 (s, C-Br, skeleton). ESI-MS (*m/z)*: Calcd. $C_{30}H_{20}Br_2N_2$ 568.3; Found 568. ^{1}H-NMR ($CDCl_3$): δ (ppm) = 7.13 (t, 2H), 7.23-7.27 (m, 14H), 7.53 (dd, 2H), 8.21 (d, 2H).

^{13}C-NMR ($CDCl_3$): δ (ppm) = 147.7, 147.3, 140.1, 130.0, 129.5, 127.6, 125.0, 123.8, 123.7, 123.5, 123.1, 112.8, 111.6. Anal. Calcd. for $C_{30}H_{20}Br_2N_2$: C, 63.40; H, 3.55; N, 4.93. Found: C, 63.21; H, 3.38; N, 4.87.

6.2.13 2,2'-(6,6'-(2,7-Dibromo-9*H*-fluorene-9,9'-diyl)*bis*(hexane-6,1-diyl))diisoindoline-1,3-dione (13)

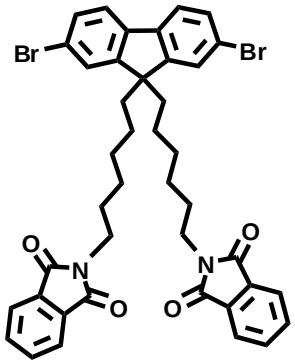

Compound **13** was obtained from 2,7-dibromo-9,9'-*bis*(6-bromohexyl)-9*H*-fluorene (1 g, 1.54 mmol) and potassium phthalimide (1.426 g, 7.7 mmol) in 30 mL DMF.[4,17] The resulting yellowish oil was purified by column chromatography (silica, *n*-hexane/ethyl acetate 3:1) yielding a white solid (0.74 g, 62%). UV-vis: λ_{max} (log ε [L × mol^{-1} × cm^{-1}]) 283 nm (4.55), 313 nm (4.36). Emission: λ_{max} 328 nm. IR (cm^{-1}): 2920 (m, CH_2, stretching), 2854 (m, CH_2, stretching), 1700 (s, C=O, stretching), 1400 (m, C-H, deformation), 1050 (m, C-N, stretching), 720 (s, C-C, skeleton). ESI-MS (*m/z)*: Calcd. $C_{41}H_{38}Br_2N_2O_4$ $(M+H)^{+2}$ 392.3; Found 393. ^{1}H-NMR ($CDCl_3$): δ (ppm) = 0.56-0.59 (m, 4H, CH_2), 0.84-0.91 (m, 4H, CH_2), 1.22-1.29 (m, 4H, CH_2), 1.48-1.54 (m, 4H, CH_2), 1.87-1.91 (m, 4H, CH_2), 3.55-3.58 (t, 4H, N-CH_2), 7.41-7.51 (m, 6H, arom.), 7.66-7.83 (m, 6H, arom.). ^{13}C-NMR ($CDCl_3$): δ (ppm) = 168.3 (C=O), 157.7, 152.2, 139.0, 133.7, 132.1, 130.2, 126.1, 123.1, 121.5, 121.2 (arom.), 55.5 (), 40.0, 37.8, 31.8, 29.4, 28.4, 26.4, 23.5, 20.9 (aliph.). Anal. Calcd. for $C_{41}H_{38}Br_2N_2O_4$: C, 62.93; H, 4.89; N, 3.58. Found: C, 62.98; H, 4.77; N 3.24.

6.2.14 2,7-Dibromo-9,9'-*bis*(6-aminohexyl)-9*H*-fluorene (14)

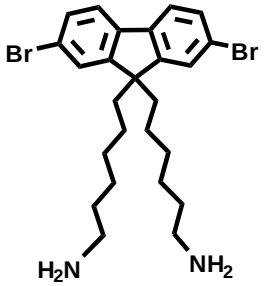

2,2'-(6,6'-(2,7-Dibromo-9*H*-fluorene-9,9'-diyl)*bis*(hexane-6,1-diyl))diisoindoline-1,3-dione (0.74 g, 0.95 mmol) was dissolved in 99.8% pure ethanol (30 mL) and hydrazine monohydrate (0.2 mL, 4.13 mmol) was added.[4,17] Compound **14** was isolated as a brownish solid (0.39 g, 49%). UV-vis: λ_{max} (log ε [L × mol^{-1} × cm^{-1}]) 283 nm (3.78), 313 nm (3.52). Emission: λ_{max} 324 nm. IR (cm^{-1}): 3352 (w, N-H, stretching), 2920 (s, CH_2, stretching), 2850 (s, CH_2, stretching), 1568 (m, N-H, scissoring), 1448 (s, C-H, deformation), 1056 (m, C-N, stretching), 1003 (m, C-C, skeleton), 808 (s, N-H, out-of-plane bending), 724 (m, C-C, skeleton). ESI-MS (*m/z)*: Calcd. $C_{25}H_{34}Br_2N_2$ $(M+H)^+$ 523.1; Found 523.1. ^{1}H-NMR ($CDCl_3$): δ (ppm) = 0.56-0.63 (m, 4H, CH_2), 0.83-0.89 (m, 4H, CH_2), 1.07 (t, 4H, CH_2), 1.25 (m, 4H, CH_2), 1.89-1.93 (m, 4H, CH_2), 2.55 (t, 4H, N-CH_2), 7.43-7.52 (m, 6H, arom.). ^{13}C-NMR ($CDCl_3$): δ (ppm) = 152.4, 139.0, 130.2, 127.2, 126.1, 121.1 (arom.), 55.6 ( ), 42.1, 40.0, 33.6, 29.6, 26.4, 23.6 (aliph.). Anal. Calcd. for $C_{25}H_{34}Br_2N_2$: C, 57.48; H, 6.56; N, 5.36. Found: C, 57.49; H, 7.14; N, 4.48.

6.2.15 Tetraethyl-6,6'-(2,7-dibromo-9*H*-fluorene-9,9'-diyl)*bis*(hexane-6,1-diyl)diphosphonate (15)

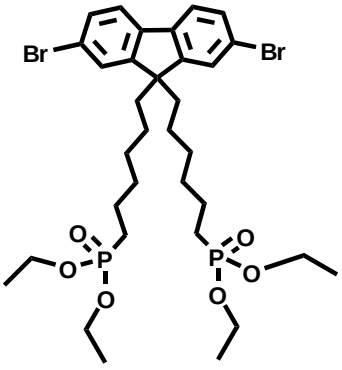

The compound was synthesized according to the literature approaches [5] and [18] and was prepared from 2,7-dibromo-9,9'-*bis*(6-bromohexyl)-9*H*-fluorene (2 g, 4.098 mmol) upon

reflux overnight in 5 mL of triethyl phosphite. Excess of triethyl phosphite was removed by batch distillation and the crude product was purified by column chromatography (ethyl acetate) yielding a colorless liquid (2.53 g, 81%). UV-vis: λ_{max} (log ε [L × mol^{-1} × cm^{-1}]) 283 nm (4.49), 304 nm (4.21), 316 nm (4.33). Emission: λ_{max} 328 nm. IR (cm^{-1}): 3461 (w, P=O, stretching overtone), 2980 (w, CH_2, stretching), 2930 (m, CH_2, stretching), 2855 (w, CH_2, stretching), 1648 (w, C=C, stretching), 1569 (w, C=C, stretching), 1451 (m, CH_3, deformation), 1393 (m, O-CH_2, wagging), 1232 (s, P=O, stretching), 1024 (s, P-O/=C-H, stretching/in-plane deformation), 951 (s, P-O/=C-H, bending/out-of-plane deformation). GC-MS (*m/z*): Calcd. $C_{22}H_{28}Br_2NO_3P$: 545.24; Found 545.03. ^{1}H-NMR ($CDCl_3$): δ (ppm) = 0.48-0.51 (m, 4H, CH_2), 0.98-1.01 (m, 4H, CH_2), 1.04-1.08 (m, 4H, CH_2), 1.20-1.22 (m, 6H, CH_3), 1.34-1.35 (m, 4H, CH_2), 1.50-1.56 (m, 4H, CH_2P=O), 1.82-1.85 (m, 4H, Ar-CH_2), 3.95-3.99 (m, 8H, O-CH_2), 7.34-7.35 (d, 2H, arom.), 7.38-7.39 (m, 2H, arom.), 7.44-7.45 (d, 2H, arom.). ^{13}C-NMR ($CDCl_3$): δ (ppm) = 152.2, 139.0, 130.2, 126.0, 121.5, 121.2 (arom.), 61.3 (CH_2-O), 55.5 (♡), 40.1, 30.2 (CH_2-P), 30.1, 29.3, 25.9, 25.0, 16.4 (aliph.). ^{31}P-NMR ($CDCl_3$): δ (ppm) = 32.41. Anal. Calcd. for $C_{33}H_{50}Br_2O_6P_2$: C, 51.84; H, 6.59. Found: C, 51.93; H, 6.63.

6.3 Copolymers

6.3.1 Random Poly(fluorene)s Containing Bromo-Functional Side-Chains P1a & P1b

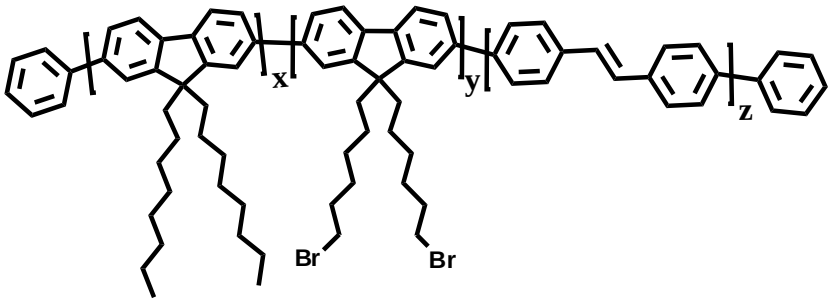

P1a/P1b [2,19]

	Feed Ratio (%)		
Polymer	**x**	**y**	**z**
P1a	40	10	50
P1b	35	15	50

*General Procedure for the Synthesis of **P1a** and **P1b***

Compounds **2**, **3**, and **4**, $Ni(COD)_2$, 2,2'-bipyridine and 1,5-cyclooctadiene (COD) were added in a Schlenk tube. Subsequently, THF (20 mL) was added and the reaction system was allowed to stir for 3 days at 80 °C. 3 Hours before stopping the reaction, 0.05 mL of bromobenzene were added and after cooling down to room temperature the reaction solution was extracted with chloroform and washed with 2 N HCl (2 × 100 mL), saturated $NaHCO_3$ solution (1 × 100 mL) and water (2 × 100 mL). The organic phase was dried over Na_2SO_4 and the solvent removed under reduced pressure. The residue was dissolved in chloroform (1-2 mL), precipitated from methanol (300 mL) and the yellow solid further extracted with ethanol.

P1a: **2** (0.049 g, 0.077 mmol), **3** (0.168 g, 0.307 mmol), **4** (0.13 g, 0.384 mmol), $Ni(COD)_2$ (0.506 g, 1.84 mmol), 2,2'-bipyridine (0.263 g, 1.68 mmol) and 1,5-cyclooctadiene (0.181 g, 1.68 mmol). **P1a** was obtained as a yellow solid (107 mg, 31%). UV-vis: λ_{max} (log ε [L × mol^{-1} × cm^{-1}]) 382 nm (5.86). Emission: λ_{max} 432 nm, 455 nm. IR (cm^{-1}): 2926 (s, CH_2, stretching), 2847 (m, CH_2, stretching), 1459 (m, C-H, deformation), 1256 (m, C-C, skeletal), 1056 (m, =C-H, in-plane deformation), 810 (s, =C-H, out-of-plane deformation), 739 (m, C-Br, stretching). GPC (g/mol): M_n = 7450, M_w = 18600, PDI 2.49. ^{1}H-NMR ($CDCl_3$): δ (ppm) = 0.84 (dist. t, CH_3), 1.15-1.28 (m, CH_2, aliph.), 2.13 (s, CH_2, aliph.), 3.31 (s, CH_2-Br), 7.68-7.85 (d, arom.). Anal. Calcd. for $(C_{29}H_{40})_x(C_{25}H_{30}Br_2)_y(C_{14}H_{10})_z$: C, 89.14; H, 7.58; Br, 3.26. Found: C, 78.36; H, 8.43.

P1b: **2** (0.074 g, 0.114 mmol), **3** (0.147 g, 0.268 mmol), **4** (0.13 g, 0.384 mmol). Yellow solid (104 mg, 30%). UV-vis: λ_{max} (log ε [L × mol^{-1} × cm^{-1}]) 389 nm (5.80). Emission: λ_{max} 435 nm, 458 nm. IR (cm^{-1}): 2918 (m, CH_2, stretching), 2851 (m, CH_2, stretching), 1453 (m, C-H, deformation), 1252 (m, C-C, skeletal), 1021 (m, =C-H, in-plane deformation), 956 (w, =C-H, in-plane deformation), 807 (s, =C-H, out-of-plane deformation), 731 (m, C-Br, stretching). GPC (g/mol): M_n = 6600, M_w = 18100, PDI 2.75. ^{1}H-NMR ($CDCl_3$): δ (ppm) = 0.84 (t, CH_3), 1.14-1.22 (m, CH_2, aliph.), 1.55 (s, CH_2, aliph.), 2.13 (s, CH_2, aliph.), 3.31 (s, CH_2-Br), 7.68-7.84 (m, arom.). Anal. Calcd. for $(C_{29}H_{40})_x(C_{25}H_{30}Br_2)_y(C_{14}H_{10})_z$: C, 87.72; H, 7.38; Br, 4.88. Found: C, 79.87; H, 6.47.

6.3.2 Random Poly(fluorene)s Containing Amino-Functional Side-Chains P2a & P2b

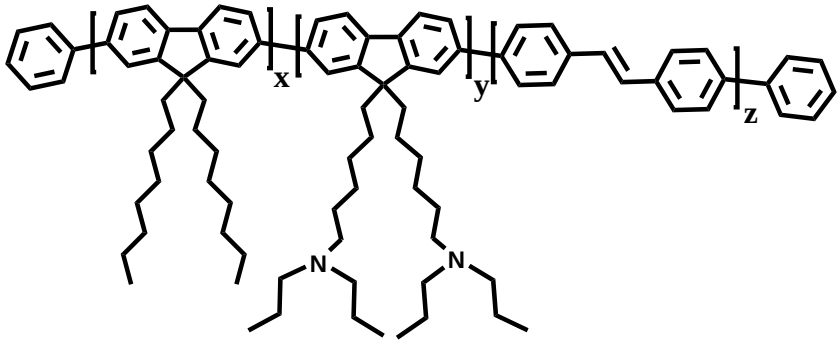

P2a/P2b[2,8,20]

*General Procedure for the Synthesis of **P2a** and **P2b***

Copolymers **P1a/P1b** were dissolved in a DMF/THF 1:1 mixture (15 mL each) and excess of di-*n*-propylamine was added. The system was vigorously stirred for 6 days at 85 °C. Solvent was removed by batch distillation and the residue dissolved in $CHCl_3$ (1 mL) and precipitated from acetone (300 mL).

P2a: Polymer **P1a** (59 mg), di-*n*-propylamine (0.8 mL). **P2a** was obtained as a brown solid (23 mg, 39%). UV-vis: λ_{max} (log ε [L × mol^{-1} × cm^{-1}]) 388 nm (5.39). Emission: λ_{max} 434 nm, 456 nm. IR (cm^{-1}): 2972 (s, CH_2, stretching), 2919 (s, CH_2, stretching), 2050 and 1999 (w, N-H^+, stretching), 1461 (m, C-H, deformation), 1386 (m, C-C, skeletal), 1163 (w, C-N, stretching), 955 (w, =C-H, in-plane deformation), 808 (m, =C-H, out-of-plane deformation), 711 (m, C-C, skeletal). GPC (g/mol): M_n = 3780, M_w = 8620, PDI 2.28. ^{1}H-NMR ($CDCl_3$): δ (ppm) = 0.84 (dist. t, CH_3), 0.91 (t, C*H*$_3$-$(CH_2)_2$-N, aliph.), 1.14-1.28 (m, CH_2, aliph.), 1.62 (s, CH_2, aliph.), 2.12 (s, CH_2, aliph.), 7.73-7.86 (d, arom.). Anal. Calcd. for $(C_{29}H_{40})_x(C_{37}H_{59}N_2)_y(C_{14}H_{10})_z$: C, 91.35; H, 7.08; N, 0.52. Found: C, 83.95; H, 9.67; N, 0.56.

P2b: Polymer **P1b** (60 mg), di-*n*-propylamine (0.9 mL). **P2b** appeared as a yellow solid (18 mg, 30%). UV-vis: λ_{max} (log ε [L × mol^{-1} × cm^{-1}]) 388 nm (5.37). Emission: λ_{max} 434 nm, 458 nm. IR (cm^{-1}): 2919 (s, CH_2, stretching), 2843 (m, CH_2, stretching), 2348 (w, N-H^+, stretching), 1454 (s, C-H, deformation), 1249 (w, C-C, skeletal), 1075 (w, C-N, stretching), 1005 (w, =C-H, in-plane deformation), 966 (m, =C-H, in-plane deformation), 818 (s, =C-H,

out-of-plane deformation). GPC (g/mol): M_n = 4810, M_w = 9150, PDI 1.90. ^{1}H-NMR ($CDCl_3$): δ (ppm) = 0.84 (dist. t, CH_3), 0.91 (t, C*H*$_3$-$(CH_2)_2$-N), 1.14-1.28 (m, CH_2, aliph.), 1.63 (s, CH_2, aliph.), 2.12 (s, CH_2, aliph.), 7.68-7.86 (m, arom.). Anal. Calcd. for $(C_{29}H_{40})_x(C_{37}H_{59}N_2)_y(C_{14}H_{10})_z$: C, 91.03; H, 8.14; N 0.81. Found: C, 83.34; H, 8.92; N, 0.70.

6.3.3 Alternating Poly(fluorene)s Containing Amino-Functional Side-Chains P3 & P4

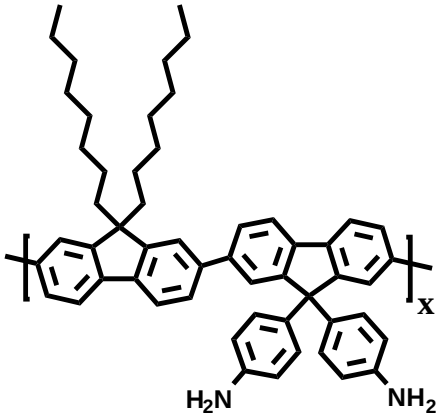

P3[10,12,21]

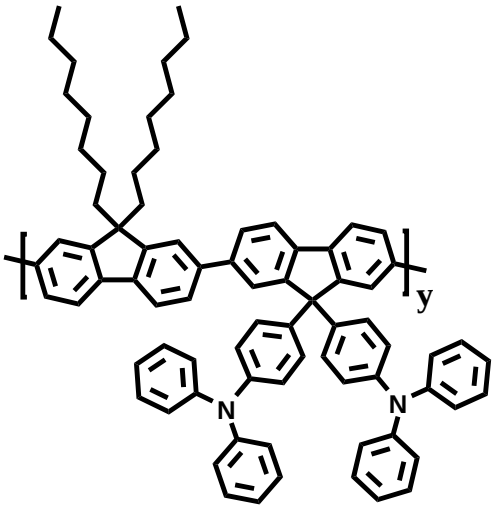

P4[10,12,21]

*General Procedure for the Synthesis of **P3** and **P4***

Copolymers **P3** and **P4** were synthesized by adding comonomers **7** or **8** together with 2,2'-(9,9'-dioctyl-9*H*-fluorene-2,7-diyl)*bis*(1,3,2-dioxaborinane) and $Pd(PPh_3)_4$ in a Schlenk tube. Subsequently, freeze-pump degassed toluene (3 mL) and Na_2CO_3 solution (1 mL) were added and the reaction system was allowed to stir for 3 days at 120 °C. After cooling down to room temperature, the reaction solution was extracted with chloroform and washed with saturated NaEDTA solution (1 × 50 mL), brine (1 × 100 mL) and water (1 × 50 mL). The organic phase was dried over $MgSO_4$ and the solvent removed under reduced pressure. The residue was dissolved in chloroform (1-2 mL) and precipitated from methanol. The polymers were further purified by Soxhlet extraction using *iso*propanol or chloroform as a solvent and once more polymer **P3** was precipitated from methanol-ethyl acetate and methanol-THF mixtures (400 mL), while polymer **P4** was precipitated from acetone (400 mL).

P3: **7** (0.0254 g, 0.5 mmol), 2,2'-(9,9'-dioctyl-9*H*-fluorene-2,7-diyl)*bis*(1,3,2-dioxaborinane) (0.28 g, 0.5 mmol), $Pd(PPh_3)_4$ (0.05 g, 0.043 mmol). **P3** was precipitated from methanol, Soxhlet extracted with *iso*propanol and chloroform, while the chloroform fraction was precipitated from a 1:1 (v:v) methanol/ethyl acetate and 3:1 (v:v) methanol/THF mixture yielding a yellow solid (99 mg, 30%). UV-vis: λ_{max} (log ε [L × mol^{-1} × cm^{-1}]) 385 nm (6.28). Emission: λ_{max} 418 nm. IR (cm^{-1}): 2919 (s, CH_2, stretching), 2847 (m, CH_2, stretching), 1616 (m, C=C, stretching), 1511 (s, =CH, stretching), 1461 (m, C-H, deformation), 1278 (m, C-C, skeletal vibration), 1185 (m, C-N, stretching), 815 (s, =C-H, out-of-plane deformation). GPC (g/mol): M_n = 5660, M_w = 17300, PDI 3.06. ^{1}H-NMR ($CDCl_3$): δ (ppm) = 0.78 (b, 6H, CH_3), 0.9-1.3 (b, 20H, aliph.), 1.99 (b, 4H, aliph.), 3.62 (s, 4H, NH_2), 6.58 (m, 8H, arom.), 7-7.9 (m, 12H, arom.). Anal. Calcd. for $(C_{56}H_{64}N_2)_x$: C, 87.91; H, 8.43; N, 3.66. Found: C, 87.99; H, 8.74; N, 3.35. TGA: $T_{d5\%}$: 420 °C.

P4: **8** (0.406 g, 0.5 mmol), 2,2'-(9,9'-dioctyl-9*H*-fluorene-2,7-diyl)*bis*(1,3,2-dioxaborinane) (0.28 g, 0.5 mmol), $Pd(PPh_3)_4$ (0.05 g, 0.043 mmol). **P4** was precipitated from methanol, Soxhlet extracted with *iso*propanol-chloroform mixture, while the chloroform fraction was once more precipitated from acetone. A yellow solid was obtained (171 mg, 33%). UV-vis: λ_{max} (log ε [L × mol^{-1} × cm^{-1}]) 381 nm (6.34). Emission: λ_{max} 416 nm. IR (cm^{-1}): 2919 (m, CH_2, stretching), 2847 (w, CH_2, stretching), 1587 (m, C=C, stretching), 1490 (s, =CH, stretching), 1447 (m, C-H, deformation), 1271 (s, =CH, in-plane deformation), 1178 (w, C-N, stretching), 1024 (w, =C-H, in-plane deformation), 808 (s, =C-H, out-of-plane deformation), 747 (m, C-C, skeleton). GPC (g/mol): M_n = 5520, M_w = 12900, PDI 2.47. ^{1}H-NMR ($CDCl_3$): δ (ppm) = 0.9 (b, 6H, CH_3), 1.02-1.30 (m, 16H, aliph.), 1.96 (b, 4H, aliph.), 2.06 (b, 4H, aliph.), 6.93-7.27 (m, 28H, arom.), 7.50-7.95 (m, 12H, arom.). Anal. Calcd. for $(C_{80}H_{80}N_2)_x$: C, 89.84; H, 7.54; N, 2.62. Found: C, 88.92; H, 6.84; N, 2.55. TGA: $T_{d5\%}$: 440 °C. DSC: T_g: 150 °C.

6.3.4 Alternating Poly(carbazole)s Containing Amino-Functional Side-Chains P5 & P6

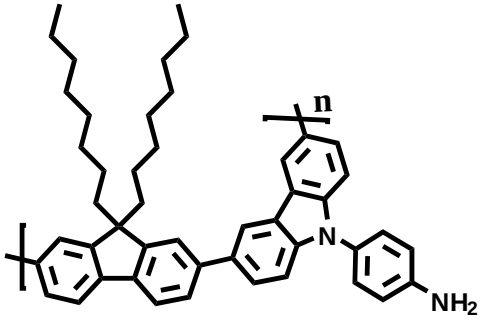

P5[10,12,21]

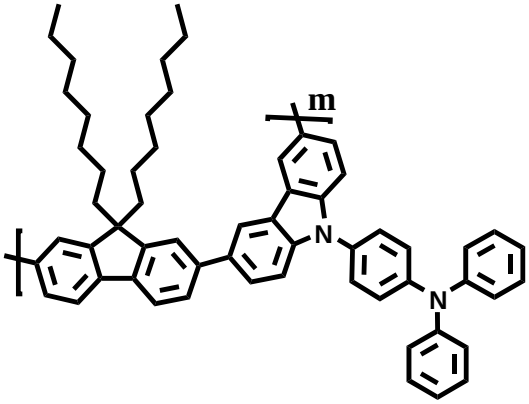

P6[10,12,21]

*General Procedure for the Synthesis of **P5** and **P6***

Copolymers **P5** and **P6** were synthesized by adding comonomers **10** or **12** together with 2,2'-(9,9'-dioctyl-9*H*-fluorene-2,7-diyl)*bis*(1,3,2-dioxaborinane) and $Pd(PPh_3)_4$ in a Schlenk tube. Subsequently, freeze-pump degassed toluene (3 mL) and Na_2CO_3 solution (1 mL) were added and the reaction system was allowed to stir for 3 days at 120 °C. After cooling down to room temperature, the reaction solution was extracted with chloroform and washed with saturated NaEDTA solution (1 × 50 mL), brine (1 × 100 mL) and water (1 × 50 mL). The organic phase was dried over $MgSO_4$ and the solvent removed under reduced pressure. The residue was dissolved in chloroform (1-2 mL) and precipitated from methanol. The polymers were further purified by Soxhlet extraction using *iso*propanol or chloroform as a solvent and once more polymer **P5** was precipitated from methanol-ethyl acetate and methanol-THF mixtures (400 mL), while polymer **P6** was precipitated from acetone (400 mL).

P5: **10** (0.209 g, 0.5 mmol), 2,2'-(9,9'-dioctyl-9*H*-fluorene-2,7-diyl)*bis*(1,3,2-dioxaborinane) (0.28 g, 0.5 mmol), $Pd(PPh_3)_4$ (0.05 g, 0.043 mmol). **P5** was precipitated from methanol, Soxhlet extracted with *iso*propanol-chloroform mixture, while the chloroform fraction was once more precipitated from a 1:1 (v:v) methanol/ethyl acetate and a 3:1 (v:v) methanol/THF mixture. A yellow solid was obtained (109 mg, 34%). UV-vis: λ_{max} (log ε [L × mol^{-1} × cm^{-1}]) 343 nm (6.68). Emission: λ_{max} 401 nm. IR (cm^{-1}): 2969 (w, CH_2, stretching), 2922 (m, CH_2, stretching), 2855 (w, CH_2, stretching), 2359 (s, N-H, stretching), 1619 (m, C=C, stretching),

1511 (s, =CH, stretching), 1454 (s, C-H, deformation), 1274 (m, C-C, skeletal), 1174 (m, C-N, stretching), 1131 (w, =CH, in-plane deformation), 955 (w, =C-H, in-plane deformation), 801 (s, =C-H, out-of-plane deformation). GPC (g/mol): M_n = 2890, M_w = 5340, PDI 1.85. ^{1}H-NMR ($CDCl_3$): δ (ppm) = 0.8 (b, 6H, CH_3), 1.0-1.30 (m, 24H, aliph.), 2.12 (b, 4H, aliph.), 3.94 (dist. s, 2H, NH_2), 6.95 (s, 4H, arom.), 7.3-7.9 (m, 10H, arom.), 8.55 (m, 2H, arom.). Anal. Calcd. for $(C_{47}H_{52}N_2)_x$: C, 87.26; H, 8.41; N, 4.33. Found: C, 85.44; H, 6.98; N, 3.87. TGA: $T_{d5\%}$: 420 °C. DSC: T_g: 152 °C.

P6: **12** (0.285 g, 0.5 mmol), 2,2'-(9,9'-dioctyl-9*H*-fluorene-2,7-diyl)*bis*(1,3,2-dioxaborinane) (0.28 g, 0.5 mmol), $Pd(PPh_3)_4$ (0.05 g, 0.043 mmol). **P6** was precipitated from methanol, Soxhlet extracted with *iso*propanol-chloroform mixture, while the chloroform fraction was once more precipitated from acetone. A yellow solid was obtained (143 mg, 36%). UV-vis: λ_{max} (log ε [L × mol^{-1} × cm^{-1}]) 341 nm (6.10). Emission: λ_{max} 404 nm. IR (cm^{-1}): 2980 (m, CH_2, stretching), 2915 (m, CH_2, stretching), 1587 (m, C=C, stretching), 1501 (s, =CH, stretching), 1457 (m, C-H, deformation), 1274 (m, C-C, skeletal), 1178 (m, C-N, stretching), 808 (s, =C-H, out-of-plane deformation). GPC (g/mol): M_n = 2920, M_w = 5290, PDI 1.81. ^{1}H-NMR ($CDCl_3$): δ (ppm) = 0.8 (b, 6H, CH_3), 1.0-1.50 (m, 24H, aliph.), 2.16 (b, 4H, aliph.), 7.31-7.90 (m, 24H, arom.), 8.55 (m, 2H, arom.). Anal. Calcd. for $(C_{59}H_{60}N_2)_x$: C, 88.67; H, 7.82; N, 3.51. Found: C, 85.60; H, 4.47; N, 3.09. TGA: $T_{d5\%}$: 420 °C. DSC: T_g: 128 °C.

6.3.5 Random and Alternating Poly(fluorene)s Containing Bromo-Functional Side-Chains P7a & P8a

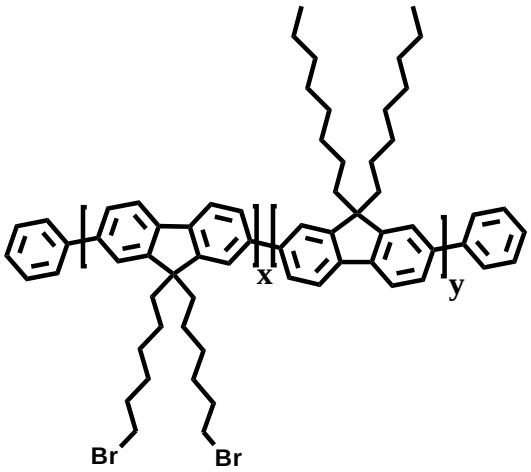

P7a[5,19]

Synthetic Procedure

2, **3**, $Ni(COD)_2$, 2,2'-bipyridine and 1,5-cyclooctadiene were added together in a Schlenk tube. Subsequently, THF (10 mL) was added to the reaction system and stirring was allowed for 3 days at 80 °C. 3 Hours before stopping the reaction, 0.05 mL of bromobenzene were added and after cooling down to room temperature the reaction solution was taken with chloroform and washed with 2 N HCl (2 × 100 mL), saturated $NaHCO_3$ solution (1 × 100 mL) and water (2 × 100 mL). The organic phase was dried over Na_2SO_4 and the solvent removed under reduced pressure. The residue was dissolved in chloroform (1-2 mL), precipitated from methanol (300 mL) and the yellow solid further extracted with ethanol, *iso*propanol and chloroform. The chloroform fraction was concentrated under vacuum and precipitated from acetone.

P7a: **2** (0.15 g, 0.265 mmol), **3** (0.175 g, 0.265 mmol), $Ni(COD)_2$ (0.355 g, 1.3 mmol), 2,2'-bipyridine (0.185 g, 1.15 mmol) and 1,5-cyclooctadiene (0.123 g, 1.15 mmol). **P7a** was obtained yielding a yellow solid (118 mg, 36%). UV-vis: λ_{max} (log ε [L × mol^{-1} × cm^{-1}]) 382 nm (5.44). Emission: λ_{max} 418 nm, 439 nm. IR (cm^{-1}): 2922 (s, CH_2, stretching), 2851 (m, CH_2, stretching), 1453 (m, C-H, deformation), 1252 (w, C-C, skeletal), 1096 (w, =C-H, in-plane deformation), 882 (w, =C-H, out-of-plane deformation), 813 (s, =C-H, out-of-plane deformation). GPC (g/mol): M_n = 5500, M_w = 6700, PDI 1.22. ^{1}H-NMR ($CDCl_3$): δ (ppm) =

0.84 (t, CH_3), 1.17 (s, CH_2, aliph.), 1.55 (s, CH_2, aliph.), 1.73 (s, CH_2, aliph.), 2.16 (s, CH_2, aliph.), 3.32 (s, CH_2-Br), 7.70-7.73 (dist. d, 8H, arom.), 7.87 (s, 4H, arom.). Anal. Calcd. for $(C_{29}H_{40})_x(C_{25}H_{30}Br_2)_y$: C, 75.43; H, 8.27. Found: C, 77.94; H, 9.89.

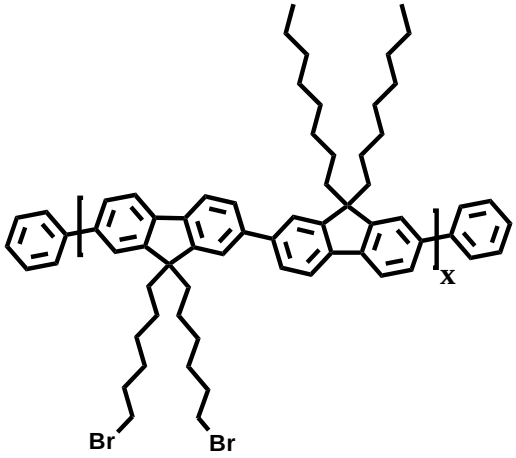

P8a[5,22]

Synthetic Procedure

Compound **2**, **DFB**, *tetrakis*(triphenylphosphine)palladium(0) and aliquat 336 were added in a Schlenk tube. Subsequently, 2M Na_2CO_3 solution and toluene were added in a 1:1 mixture and the system was allowed to stir for 3 days at 120 °C. Bromobenzene was added to the system and further stirred for 3 hours. 3 Hours before stopping the reaction phenylboronic acid was added and after cooling down to room temperature the reaction solution was taken with chloroform and washed with 2 N HCl (2 × 100 mL), saturated $NaHCO_3$ solution (1 × 100 mL) and water (2 × 100 mL). The organic phase was dried over Na_2SO_4 and the solvent removed by means of reduced pressure. The residue was dissolved in chloroform (1-2 mL), precipitated from methanol (300 mL) and the brown solid further extracted with ethanol, *iso*propanol and chloroform. The chloroform fraction was evaporated under vacuum and reprecipitated from acetone.

P8a: **2** (0.15 g, 0.23 mmol), 2,2'-(9,9'-dioctyl-9*H*-fluorene-2,7-diyl)*bis*(1,3,2-dioxaborinane) (0.128 g, 0.23 mmol), *tetrakis*(triphenylphosphine)palladium(0) (0.021 g, 0.0184 mmol). Yellowish solid (110 mg, 39%). UV-vis: λ_{max} (log ε [L × mol^{-1} × cm^{-1}]) 380 nm (5.20). Emission: λ_{max} 417 nm, 440 nm. IR (cm^{-1}): 2922 (s, CH_2, stretching), 2851 (m, CH_2, stretching), 1734 (w, C=C, stretching), 1605 (w, C=C, stretching), 1451 (m, C-H, deformation), 1249 (m, C-C, skeletal), 1024 (m, =C-H, in-plane deformation), 811 (s, =C-H,

out-of-plane deformation). GPC (g/mol): M_n = 7700, M_w = 12600, PDI 1.64. ^{1}H-NMR ($CDCl_3$): δ (ppm) = 0.82-0.84 (q, CH_3), 1.17 (s, CH_2, aliph.), 1.56 (s, CH_2, aliph.), 1.73 (s, CH_2, aliph.), 2.16 (s, CH_2, aliph.), 3.32 (s, CH_2-Br), 7.70-7.72 (dist. d, 8H, arom.), 7.87 (s, 4H, arom.). Anal. Calcd. for $(C_{54}H_{70}Br_2)_y$: C, 73.79; H, 8.03. Found: C, 74.39; H, 9.20.

6.3.6 Poly(fluorene)s Containing Phosphonate Side-Chains P7b & P8b

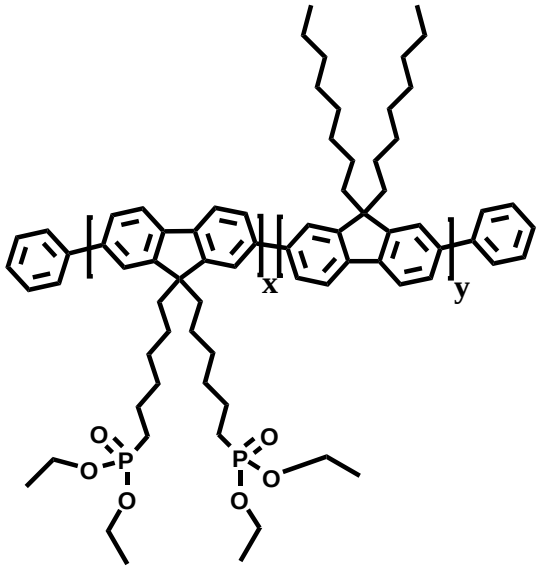

P7b[5,18]

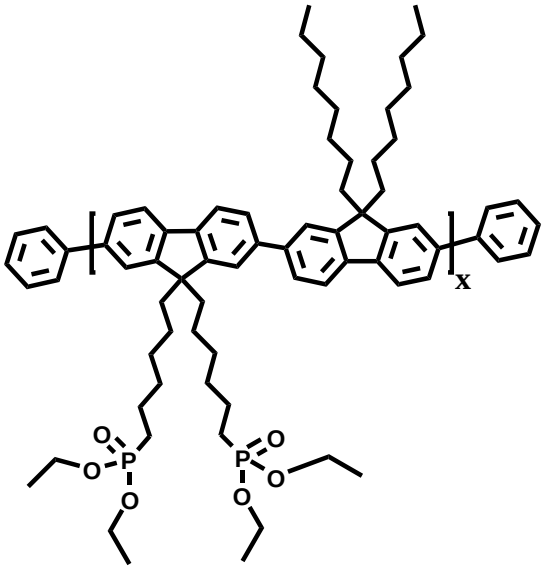

P8b[5,18]

*General Procedure for the Synthesis of **P7b** and **P8b***

Precursors **P7a**/**P8a** were dissolved in triethyl phosphite (10 mL) and vigorously stirred for 5 days under reflux. Excess of triethyl phosphite was removed by batch distillation and the residue dissolved in $CHCl_3$ (1 mL) and precipitated from cold *n*-hexane (300 mL).

P7b: Polymer **P7a** (53 mg), triethyl phosphite (10 mL). Yellow solid (39 mg, 74%). UV-vis: λ_{max} (log ε [L × mol^{-1} × cm^{-1}]) 381 nm (4.98). Emission: λ_{max} 416 nm, 440 nm. IR (cm^{-1}): 2922 (s, CH_2, stretching), 2851 (m, CH_2, stretching), 2152 (w, P=O, stretching), 1453 (m, C-H/P-OC_2H_5, deformation/stretching), 1397 (w, P-OC_2H_5, wagging), 1233 (m, P=O, stretching), 1020 (s, P-OC_2H_5/=C-H, stretching/in-plane deformation), 953 (s, P-OC_2H_5/=C-H, bending/out-of-plane deformation), 812 (s, =C-H, out-of-plane deformation). GPC (g/mol): M_n = 15100, M_w = 34400, PDI 2.28. ^{1}H-NMR ($CDCl_3$): δ (ppm) = 0.84 (dist. t, CH_3), 1.16-1.28 (m, CH_2), 1.36 (s, CH_2), 1.48 (s, CH_2), 1.64 (s, CH_2), 2.15 (s, CH_2), 4.04 (dist. s, CH_2-O-P), 7.70 (s, arom.), 7.86 (s, arom.). ^{31}P-NMR ($CDCl_3$): δ (ppm) = 32.48. Anal. Calcd. for $(CHCl_3)(C_{29}H_{40})_x(C_{33}H_{50}O_6P_2)_y$: C, 71.60; H, 8.81. Found: C, 70.42; H, 9.39.

P8b: Polymer **P8a** (70 mg), triethyl phosphite (8 mL). **P8b** was obtained as a greenish solid (43 mg, 61%). UV-vis: λ_{max} (log ε [L × mol^{-1} × cm^{-1}]) 382 nm (5.71). Emission: λ_{max} 416 nm, 441 nm. IR (cm^{-1}): 2922 (s, CH_2, stretching), 2851 (m, CH_2, stretching), 2152 (w, P=O, stretching), 1453 (m, C-H/P-OC_2H_5, deformation/stretching), 1396 (w, P-OC_2H_5, wagging), 1229 (m, P=O, stretching), 1160 (w, =C-H/P-OC_2H_5, in-plane deformation/rocking), 1025 (s, P-OC_2H_5/=C-H, stretching/in-plane deformation), 954 (s, P-OC_2H_5/=C-H, bending/out-of-plane deformation), 814 (m, =C-H, out-of-plane deformation). GPC (g/mol): M_n = 9100, M_w = 20600, PDI 2.26. ^{1}H-NMR ($CDCl_3$): δ (ppm) = 0.84 (dist. t, CH_3), 1.16 (s, CH_2), 1.36 (t, CH_2), 1.48 (s, CH_2), 1.64 (s, CH_2), 2.15 (s, CH_2), 4.04 (dist. s, CH_2-O-P), 7.71 (s, arom.), 7.86 (s, arom.). ^{31}P-NMR ($CDCl_3$): δ (ppm) = 32.48. Anal. Calcd. for $(CHCl_3)(C_{54}H_{90}O_6P_2)_y$: C, 69.72; H, 8.73. Found: C, 69.45; H, 9.11.

6.3.7 Reference Copolymer

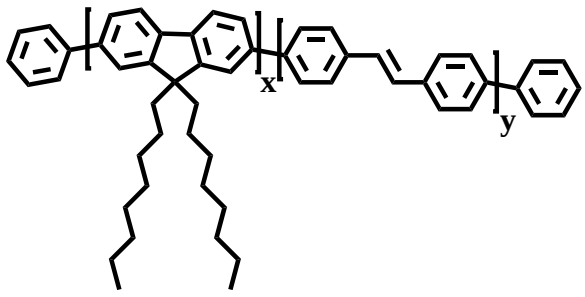

Pref[2,19]

3 (0.324 g, 0.59 mmol), **4** (0.2 g, 0.59 mmol). **Pref** yielded a yellow solid (73 mg, 13%). UV-vis: λ_{max} (log ε [L × mol^{-1} × cm^{-1}]) 391 nm (6.06). Emission: λ_{max} 434 nm, 461 nm. IR (cm^{-1}): 2918 (s, CH_2, stretching), 2844 (m, CH_2, stretching), 1453 (m, C-H, deformation), 1249 (w, C-H, deformation), 810 (s, =C-H, out-of-plane deformation). GPC (g/mol): M_n = 12200, M_w = 27100, PDI 2.2. ^{1}H-NMR ($CDCl_3$): δ (ppm) = 0.73-0.75 (t, CH_3), 1.06 (m, CH_2, aliph.), 1.27 (s, CH_2, aliph.), 1.60 (s, CH_2, aliph.), 2.1 (s, CH_2, aliph.), 7.60-7.76 (m, arom.). Anal. Calcd. for $(C_{29}H_{40})_x(C_{14}H_{10})_z$: C, 91.98; H, 8.01. Found: C, 80.68; H, 8.29.

6.4 Hybrids

6.4.1 Fluorene-CdSe Nanocomposite 1 as Monomer

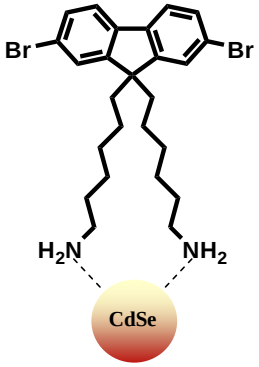

NC1[4,23]

The synthesis of **NC1** was performed in the groups of Dr. Andrey Rogach and Prof. Dr. Feldmann in the Department for Physics and Center for Nanoscience at the Maximilian University of Munich and is described below: 0.21 g (0.79 mmol) $Cd(CH_3COO)_2 \times 2\ H_2O$, 2.75 g (11.51 mmol) *n*-hexadecylamine, 0.75 g (2.71 mmol) tetradecylphosphonic acid and 0.94 g (0.18 mmol) 2,7-dibromo-9,9'-*bis*(6-aminohexyl)-9*H*-fluorene **14** were heated under argon to 270 °C. After formation of a transparent solution, 0.4 g of selenium in 4 g of *tris*-*n*-octylphosphine were added *via* a septum. After 5 minutes of heating under argon at 270 °C, the reaction was stopped and NCs have been purified by several cycles of precipitation with methanol and redissolution in toluene.

IR (cm^{-1}): 2955 (w, CH_2, stretching), 2911 (s, CH_2, stretching), 2843 (s, CH_2, stretching), 2359 (w, NH_2 surface-bound, stretching), 1637 (w, P-OH, deformation), 1540 (w, N-H, scissoring), 1468 (m, C-H, deformation), 1175 (m, C-N, stretching), 1088 (m, P=O, stretching), 1041 (m, C-C, skeleton), 897 (m, C-C, skeleton), 711 (m, C-C, skeleton).

6.4.2 Oligo(fluorene)-CdSe Nanocomposite 2

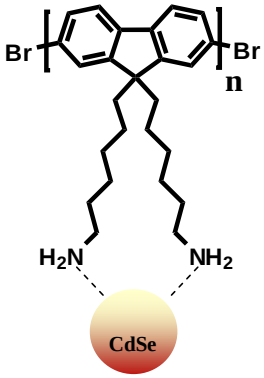

NC2[4,24]

Nanocomposite **NC1** (0.052 g, 46.1 × 10^{-7} mmol), $Ni(COD)_2$ (0.005 g, 0.018 mmol), 2,2'-bipyridine (0.003 g, 0.19 mmol) and 1,5-cyclooctadiene (0.01 mL, 0.08 mmol) were added together in a Schlenk tube. Subsequently, a THF/toluene 1:1 mixture (20 mL in total) was added to the reaction system and was allowed to stir for 3 days at 90 °C. 3 Hours before stopping the reaction, 0.05 mL of bromobenzene were added and after cooling down to room temperature the reaction solution was taken with chloroform and washed with 2 N HCl (1 × 100 mL), saturated $NaHCO_3$ solution (1 × 50 mL) and water (2 × 100 mL). The organic phase was dried over Na_2SO_4 and the solvent removed under reduced pressure. The residue was isolated as red-particle like material (0.037 g, 71%). UV-vis: λ_{max} (log ε [L × mol^{-1} × cm^{-1}]): 540 nm (3.07). Emission: λ_{max} 413 nm, 545 nm. IR (cm^{-1}): 2915 (s, CH_2, stretching), 2851 (m, CH_2, stretching), 2351 (w, NH_2 surface-bound, stretching), 2330 (w, NH_2 surface-bound, stretching), 1461 (w, C-H, deformation), 880 (s, N-H, out-of-plane bending). ^{1}H-NMR ($CDCl_3$): δ (ppm) = 0.90 (t, CH_2), 1.28 (s, aliph.), 1.52-1.62 (m, CH_2), 1.64-1.71 (m, CH_2), 1.88-1.95 (m, CH_2), 2.76 (s, N-CH_2). GPC (g/mol): M_n = 1276, M_w = 1736, PDI 1.36. MALDI-TOFMS (*m/z*): 1166.6 (trimer-Br).

6.4.3 Poly(fluorene)-CdSe Nanocomposite 3

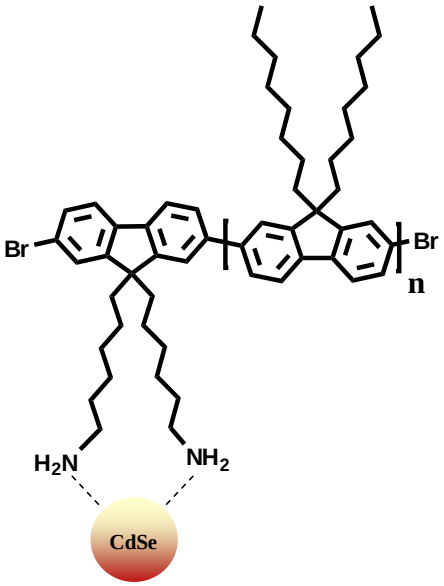

NC3[4,24]

Nanocomposite **NC1** (0.06 g, 0.109 mmol) with 2,7-dibromo-9,9'-dioctyl-9*H*-fluorene **3** (0.052 g, 9.2×10^{-7} mmol), $Ni(COD)_2$ (0.072 g, 0.26 mmol), 2,2'-bipyridine (0.037 g, 0.24 mmol) and 1,5-cyclooctadiene (0.03 mL, 0.24 mmol) were added together in a Schlenk tube. Subsequently, a THF/toluene 1:1 mixture (20 mL in total) was added to the reaction system and was allowed to stir for 3 days at 90 °C. 3 Hours before stopping the reaction, 0.05 mL of bromobenzene were added and after cooling down to room temperature the reaction solution was taken with chloroform and washed with 2 N HCl (1 × 100 mL), saturated $NaHCO_3$ solution (1 × 50 mL) and water (2 × 100 mL). The organic phase was dried over Na_2SO_4 and the solvent removed under reduced pressure. The residue was dissolved in chloroform (1-2 mL) precipitated from methanol (300 mL) and further purified over size exclusion chromatography (Biobeads). Red particle-like material (0.1 g, 83%). UV-vis: λ_{max} (log ε [L × mol^{-1} × cm^{-1}]): 375 nm (4.54). Emission: λ_{max} 414 nm, 438 nm. IR (cm^{-1}): 2919 (s, CH_2, stretching), 2851 (m, CH_2, stretching), 2359 (w, NH_2 surface-bound, stretching), 2334 (w, NH_2 surface-bound, stretching), 1451 (m, C-H, deformation), 1145 (m, C-N, stretching), 815 (m, arom. C-H, out-of-plane deformation), 739 (m, C-C, skeletal). ^{1}H-NMR ($CDCl_3$): δ (ppm) = 0.89 (m, CH_3), 0.97-0.99 (d, CH_2), 1.07 (s, CH_2), 1.28 (s, CH_2), 1.46 (s, CH_2), 3.83 (t, N-CH_2, 1-*n*-hexyldecylamine), 4.33 (m, P-CH_2, tetradecylphosphonic acid), 7.46 (d, arom.), 7.48 (d, arom.), 7.53-7.57 (qui., arom.), 7.74 (s, arom.). GPC (g/mol): M_n = 3718, M_w = 4738, PDI 1.27. MALDI-TOFMS (*m/z*): 387.4 (monomer), 778.0 (dimer), 830 (monomer-ligand-Br), 1166.6 (trimer), 1556.2 (tetramer), 1943.6 (pentamer), 2332.9 (hexamer), 2722.0 (heptamer),

3109.2 (octamer), 3497.1 (nonamer), 3888.0 (decamer), 4275.6 (undecamer), 4663.9 (dodecamer).

6.4.4 $CdSe_{ref}$ Nanocrystals

The synthesis was carried out in the groups of Dr. Andrey Rogach and Prof. Dr. Feldmann in the Department for Physics and Center for Nanoscience at the Maximilian University of Munich.[25] Briefly, 0.21 g (0.79 mmol) $Cd(CH_3COO)_2 \times 2\ H_2O$, 2.75 g (11.51 mmol) *n*-hexadecylamine and 0.75 g (2.71 mmol) tetradecylphosphonic acid were heated under argon at 270 °C. After formation of a transparent solution 0.4 g of selenium in 4 g of *tris*-*n*-octylphosphine were added *via* a septum. After 3 minutes of heating under argon at 270 ^{o}C, the reaction was stopped and nanocrystals have been purified by several cycles of precipitation with methanol and redissolution in toluene.
IR (cm^{-1}): 2955 (w, CH_2, stretching), 2911 (s, CH_2, stretching), 2843 (s, CH_2, stretching), 2375 (vw, NH_2 surface-bound, stretching), 1637 (w, P-OH, deformation), 1540 (w, N-H, scissoring), 1471 (m, C-H, deformation), 1172 (m, C-N, stretching), 1090 (m, P=O, stretching), 1044 (m, C-C, skeleton), 901 (m, C-C, skeleton), 715 (m, C-C, skeleton).

6.5 Synthesis of CdTe Nanocrystals and Nanocrystal-Polymer Composites

6.5.1 CdTe/HS-C_6H_4-Br Nanocrystals

The synthesis was carried in the group of Prof. Dr. Eychmüller in the Physical Chemistry/Electrochemistry Department at the Technical University of Dresden.[25,26] Briefly, 0.53 g (2.3 mmol) of $Cd(OOCH_3)_2$ and 0.57 g (3 mmol) of 4-bromobenzenethiol were dissolved in 120 mL of DMF. This solution was deaerated by bubbling with argon for 30 min. Under stirring, H_2Te gas generated by the reaction of 0.67 g (1.5 mmol) of Al_2Te_3 with an excess of 0.5 M H_2SO_4 solution, was injected into the reaction mixture with a slow argon flow. The molar ratio of Cd^{2+}/Te^{2-}/HS-C_6H_4-Br was 1:2:1.3. Formation and growth of the NCs proceeded upon reflux under open-air conditions during an interval of 10 hours. The colloid obtained was purified by reprecipitation and removal of approximately 90% of the solvent under vacuum allowed a further precipitation by addition of excess of methanol. The precipitate was separated by centrifugation and dissolved in DMF yielding a nanocrystal concentration of 9×10^{-4} M (40 mg/mL).

A set of CdTe nanocrystals (CdTe A-E) with varying emission colors were also prepared following the same experimental procedure. Formation and growth of the NCs proceeded upon reflux under open-air conditions, however, colloidal fractions containing NCs of different sizes emitting green (2.1 nm) to orange (2.9 nm) were taken during the reaction after 20 min, 1 h, 2 h, 4 h and 6 h of reflux, respectively. The colloids obtained were purified by reprecipitation and after removal of the solvent the nanoparticles were precipitated by addition of methanol. The precipitates were separated by centrifugation and dissolved in DMF yielding nanocrystal concentrations varying from 1×10^{-3} M to 7.3×10^{-4} M.

6.5.2 CdTe/HS-C_6H_4-Br-Polymer Composites

Solutions of copolymers **Pref**, **P2a** and **P2b** in THF were prepared in a concentration of 1 mg/mL. The CdTe nanocrystals capped with 4-bromobenzenethiol (HS-C_6H_4-Br) and bearing a particle concentration of 9×10^{-4} M (40 mg/mL) in DMF were diluted in THF by a 1:3 ratio (v:v). Subsequently, 1:1 mixtures (v:v) of the respective copolymers and surface functionalized CdTe NCs were prepared. The solutions were heated up to 60 °C and subsequently, drop-casted (~100 µL) on glass substrates. After vaporization of the solvents by means of a fume hood, fluorescence excitation measurements were conducted.

6.5.3 CdTe/HS-C_6H_4-Br-Polymer Composites for White-Light Emission

Copolymers **P3-P6** were mixed with yellow-emitting CdTe nanocrystals, which were prepared by combining green (CdTe B) and orange-red emitting (CdTe E) nanocrystals. The CdTe B to CdTe E ratio varied from 2.5-2.8 and addition to the blue-emitting polymer-solutions resulted after fine tuning in white-light emitting DMF solutions. Films were prepared by drop-casting the aforementioned solutions on glass substrates. The batch concentrations used for the preparation of the solutions were 1.08×10^{-4} M for CdTe B nanocrystals, 2.4×10^{-5} M for CdTe E nanocrystals and 1 mg/mL for the polymers.

6.5.4 CdTe/HS-CH_2-COOH Nanocrystals

The CdTe nanocrystals were endcapped with thioglycolic acid (HS-CH_2-COOH) and synthesized by Dr. Vladimir Lesnyak in the group of Prof. Dr. Eychmüller (Technical University of Dresden, Physical Chemistry/Electrochemistry Department) following a standard aqueous synthetic approach.[25] The obtained nanocrystals were water-stable and

represent two different species exhibiting emission maxima at 534 (green CdTe) and 631 nm (red CdTe).

6.5.5 CdTe/HS-CH_2-COOH-Polymer Composites

THF solutions of copolymers **P7b/P8b** (0.1 mg/mL) were prepared and filtered through a micropore syringe filter (0.45 μm). A volume of 2 mL of the stock solutions was injected in 50 mL distilled water. After removal of THF under vacuum, the dispersions were filtered through a paper filter (90 mm of diameter). CdTe water solutions (100 μL) of 5.58×10^{-5} mol/L concentration for green-light emitting nanocrystals and 1×10^{-5} to 6×10^{-5} mol/L concentration for red-light emitting species were injected in the polymer dispersions of 10 mL in volume and 10^{-4} mol/L in concentration. The fluid systems were sonicated for 1 hour at room temperature. As a control experiment, nanocrystals or polymers solely with the aforementioned concentrations were injected in water and sonicated for 1 hour at room temperature. For solutions, which were not subjected to the ultrasonic bath procedure, concentrations of 10^{-4} mol/L for the copolymers (10 mL in volume), 1×10^{-5} mol/L for the red CdTe (100 μL) and 5.58×10^{-5} mol/L for the green CdTe (100 μL) nanocrystals were used, respectively (section **3.4**, **Figures 3.17 a-b**).

6.5.6 Centrifugation Experiments for the CdTe/HS-CH_2-COOH-Polymer Composites

Dispersions of the composites **P7b MPs**+CdTe and **P8b MPs**+CdTe were prepared according to the precipitation-sonication method (see **6.5.5**). The polymers concentration was 10^{-4} mol/L, while the CdTe concentration varied from 1×10^{-5} to 6×10^{-5} mol/L. Each time 1 mL of the dispersions was subjected to centrifugation applying different time intervals and centrifugation velocities (see section **3.4**, **Table 3.6**). Subsequently, the optical characterization of the supernates and the precipitates were investigated by means of fluorescence spectrophotometry.

6.6 References

[1] M. Ranger, M. Leclerc, *Chem. Commun*. **1997**, 1597.

[2] I. Kanelidis, V. Elsner, M. Bötzer, M. Butz, V. Lesnyak, A. Eychmüller, E. Holder, *Polymer* **2010**, 51, 5669.

[3] E. P. Woo, M. Inbasekaran, W. R. Shiang, Roof GR. WO//05184, **1997**.

[4] I. Kanelidis, A. Vaneski, D. Lenkeit, S. Pelz, V. Elsner, R. M. Stewart, J. Rodríguez-Fernández, A. A. Lutich, A. S. Susha, R. Theissmann, S. Adamczyk, A. L. Rogach, E. Holder, *J. Mater. Chem*. **2011**, 21, 2656.

[5] I. Kanelidis, O. Altintas, J. C. Gasse, R. Frahm, A. Eychmüller, E. Holder, *Polym. Chem*. **2011**, 2, 2597.

[6] B. Liu, B. S. Gaylord, G. C. Bazan, *J. Am. Chem. Soc*. **2003**, 125, 6705.

[7] K. Jeong, S. Kim, U. Shin, *J. Am. Chem. Soc.* **2005**, 127, 17672.

[8] M. Stork, B. S. Gaylord, A. J. Heeger, G. C. Bazan, *Adv. Mater*. **2002**, 14, 361.

[9] Z. Zhang, H. Zhang, J. B. Han, X. Ji, P. Zhang, 200910074090.8, **2009**.

[10] I. Kanelidis, Y. Ren, V. Lesnyak, J. C. Gasse, R. Frahm, A. Eychmüller, E. Holder, *J. Polym. Sci. Part A: Polym. Chem.* **2011**, 49, 392.

[11] C. Chou, H. S. Lin, K. Dinakaran, M. Chiu, K. Wei, *Macromolecules* **2005**, 38, 745.

[12] C. Ego, A. C. Grimsdale, F. Uckert, G. Yu, G. Srdanov, K. Müllen, *Adv. Mater*. **2002**, 14, 809.

[13] A. Kulasi, H. Yi, A. Iraqi, *J. Polym. Sci. Part A: Polym. Chem.* **2007**, 45, 5957.

[14] Y. Chen, G. Huang, C. Hsiao, S. Chen, *J. Am. Chem. Soc.* **2006**, 128, 8549.

[15] C. Wang, L. O. Pålsson, A. S. Batsanov, M. R. Bryce, *J. Am. Chem. Soc*. **2006**, 128, 3789.

[16] A. Klapars, J. Anitilla, X. Huang, S. Buchwald, *J. Am. Chem. Soc*. **2001**, 123, 7727.

[17] V. Marin, E. Holder, R. Hoogenboom, U. S. Schubert, *Macromol. Rapid Commun.* **2004**, 25, 793.

[18] C. Qin, Y. Cheng, L. Wang, X. Jing, F. Wang, *Macromolecules* **2008**, 41, 7798.

[19] L. Kinder, J. Kanicki, P. Petroff, *Synth. Met*. **2004**, 146, 181.

[20] F. Huang, Y. Zhang, M. S. Liu, *Adv. Funct. Mater.* **2009**, 19, 2457.

[21] U. Giovanella, M. Pasini, S. Destri, W. Porzio, C. Botta, *Synth. Met.* **2008**, 158, 113.

[22] A. Tsami, X. H. Yang, T. Farrell, D. Neher, E. Holder, *J. Polym. Sci. Part A: Polym. Chem.* **2008**, 46, 7794.

[23] H. Skaff, K. Sill, T. Emrick, *J. Am. Chem. Soc*. **2004**, 126, 11322.

[24] A. Tsami, X. H. Yang, F. Galbrecht, T. Farrell, H. Li, S. Adamczyk, R. Heiderhoff, L. J. Balk, D. Neher, E. Holder, *J. Polym. Sci. Part A: Polym. Chem*. **2007**, 45, 4773.

[25] A. L. Rogach, T. Franzl, T. A. Klar, J. Feldmann, N. Gaponik, V. Lesnyak, A. Shavel, A. Eychmüller, Y. P. Rakovich, J. F. Donegan, *J. Phys. Chem. C* **2007**, 111, 14628.

[26] N. Gaponik, D. V. Talapin, A. L. Rogach, K. Hoppe, E. V. Shevchenko, A. Kornowski, A. Eychmüller, H. Weller, *J. Phys. Chem. B* **2002**, 106, 7177.

7 Acknowledgements

In the first place, I would like to thank my supervisor **Prof**. **Dr**. **Elisabeth Holder** for her constant support and continuous motivation. Her guidance and encouragement were crucial for the accomplishment of this work.

Prof. **Dr**. **Alexander Eychmüller** is acknowledged for being the second referee and giving me the opportunity to collaborate with him sharing experiences and ideas while working in the frame of the project 'Hybrid polymer/nanocrystals structures: fabrication and studies of energy transfer, charge generation and transport'. In terms of materials he is acknowledged for providing the CdTe nanocrystals.

Prof. **Dr**. **Ullrich Scherf**, **Prof**. **Dr**. **Fabian Mohr** and **Prof**. **Dr**. **Hans-Josef Altenbach** are acknowledged for also being my examiners in the PhD defense.

Prof. **Dr**. **Ullrich Scherf** is further acknowledged for granting access to the tools of the Macromolecular Chemistry at the University of Wuppertal.

Prof. **Dr**. **Ronald Frahm** is acknowledged for his smooth art of co-operation and for granting access to the atomic force microscope, while many thanks go to **Jan-Christoph Gasse** for the performance of AFM measurements but above all for his willingness to help-out and discuss.

Prof. **Dr**. **Andrey Rogach** and **Prof**. **Dr**. **Jochen Feldmann** are acknowledged for the co-operation in the frame of the project 'Hybrid polymer/nanocrystals structures: fabrication and studies of energy transfer, charge generation and transport' and in terms of materials for the CdSe nanocrystals.

Prof. **Dr**. **Oliver Schmitz** is acknowledged for his help with MALDI-TOFMS analysis.

I would further like to thank **Dr**. **Vladimir Lesnyak** not only for synthesizing the CdTe nanocrystals but also for our co-operative work and his interesting suggestions.

I would like to express my thanks to my labor colleagues and collaboration partners **Yi Ren**, **Ozcan Altintas**, **Victoria Elsner**, **Monique Bötzer**, **Maren Butz**, **Daniel Lenkeit** and

Simon Pelz for the fruitful co-operation in terms of compound synthesis and successful publishing.

My thanks are also given to **Aleksandar Vaneski**, **Raphaela M**. **Stewart**, **Jessica Rodríguez-Fernández**, **Dr**. **Andrey A**. **Lutich** and **Dr**. **Andrei S**. **Susha** for the synthesis of CdSe nanocrystals as well as for TEM, absorption, photoluminescence and photoluminescence decay measurements.

Dr. **Ralf Theissmann** is acknowledged for conducting transmission electron microscopy measurements.

A special thank goes to **Sylwia Adamczyk** for some atomic force microscopy measurements and **Anke Helfer** for gel permeation chromatography analysis, thermal gravimetric analysis and differential scanning calorimetry measurements.

Ralf Radon is acknowledged for elemental analysis measurements, while **Andreas Siebert** for conducting ^{1}H-, ^{13}C- and ^{31}P-NMR spectroscopy.

My thanks also go to **Jürgen Dönecke**, **Melanie Dausend** and **Ilka Polanz** for their contribution by means of GC-MS and LC-MS experiments.

A particular thank-you goes to **Jan Poppe** for supporting and assisting the dynamic light scattering measurements.

A large hug and big thanks go of course to my labor mates **Nan Tian**, **Jinming Zhang** known also as ‘Kakaka’, **Cüneyt Karakus**, the man with the endless number of nicknames and the incredible whistling abilities, **Eike Heuser** known also as the ‘White Brasilian’, **Daniel Lenkeit** our ‘Captain’ and **Monique Bötzer** famous also as ‘the fastest mouse of Mexico’. It has been a joy working with all of you guys.

Furthermore, I would like to express my thanks to all members of the **Scherf group** for their helpful manner and the convenient working atmosphere.

My heartfelt thanks go to my dear **parents** and **grandparents** for their permanent support and encouragement. The same holds true for my beloved **sister**.

I would also like to express my gratefulness to my loyal friend **Vassilios** and my lovely friend **Hana** for accompanying and supporting me through the hard times, for sharing the good moments with me and rejoicing over every small success.

Finally, the **Deutsche Forschungsgemeinschaft** (DFG) is acknowledged for financial support within the grant application HO3911/2-1: "Hybrid polymer/nanocrystals structures: fabrication and studies of energy transfer, charge generation and transport".

8 List of Publications

8.1 Related to the PhD Thesis

1) Synthesis and characterization of amino-functional, blue light-emitting copolymers and their composites with CdTe nanocrystals.
I. Kanelidis, V. Elsner, M. Bötzer, M. Butz, V. Lesnyak, A. Eychmüller, E. Holder, *Polymer* **2010**, 51, 5669.

2) Arylamino-functionalized fluorene- and carbazole-based copolymers: Color-tuning their CdTe nanocrystal composites from red to white.
I. Kanelidis, Y. Ren, V. Lesnyak, J. C. Gasse, R. Frahm, A. Eychmüller, E. Holder, *J. Polym. Sci. Part A: Polym. Chem.* **2011**, 49, 392.

3) Inorganic-organic nanocomposites of CdSe nanocrystals surface-modified with oligo- and poly(fluorene) moieties.
I. Kanelidis, A. Vaneski, D. Lenkeit, S. Pelz, V. Elsner, R. M. Stewart, J. Rodríguez-Fernández, A. A. Lutich, A. S. Susha, R. Theissmann, S. Adamczyk, A. L. Rogach, E. Holder, *J. Mater. Chem*. **2011**, 21, 2656.

4) Microparticles of phosphonate-functionalized copolymers and their composites with CdTe nanocrystals prepared by sonication-precipitation.
I. Kanelidis, O. Altintas, J. C. Gasse, R. Frahm, A. Eychmüller, E. Holder, *Polym. Chem*. **2011**, 2, 2597.

5) Synthesis and characterization of random and alternating phosphonate-functionalized copolymers and their water-stable hybrid particles with CdTe nanocrystals.
I. Kanelidis, V. Lesnyak, J. C. Gasse, R. Frahm, A. Eychmüller, E. Holder, *Polym. Prepr.* **2011**, 52, 791.

6) Grafting oligo- and polyfluorenes from the surface of CdSe nanocrystals.
I. Kanelidis, A. Vaneski, D. Lenkeit, S. Pelz, V. Elsner, R. M. Stewart, J. Rodríguez-Fernández, A. A. Lutich, A. S. Susha, R. Theissmann, A. L. Rogach, E. Holder, *Macromol. Rapid Commun.* **2011**, 32, F79.

8.2 Further Publications

1) Phosphorescent, light-emitting copolymers: Synthesis and characterization.
N. Tian, **I**. **Kanelidis**, A. Thiessen, D. Hertel, K. Meerholz, E. Holder, *Macromol. Biosci.* **2009**, 9, F68.

2) Synthesis and characterization of near-infrared absorbing composites of conjugated macroligands on the surface of PbS nanoparticles.
I. **Kanelidis**, J. Zhang, L. Liebscher, S. G. Hickey, A. Eychmueller, E. Holder, *Polym. Prepr.* **2011**, 52, 789.

3) Metal-containing polymers: A perfect duo for applications using light interactions.
E. Holder, **I**. **Kanelidis**, J. Zhang, V. Lesnyak, A. Eychmuller, *POLY-602*, **2011**.